Protein-protein Interactions of the Androgen Receptor in Living Cells

Martin E. van Royen

Protein-protein Interactions of the Androgen Receptor in Living Cells

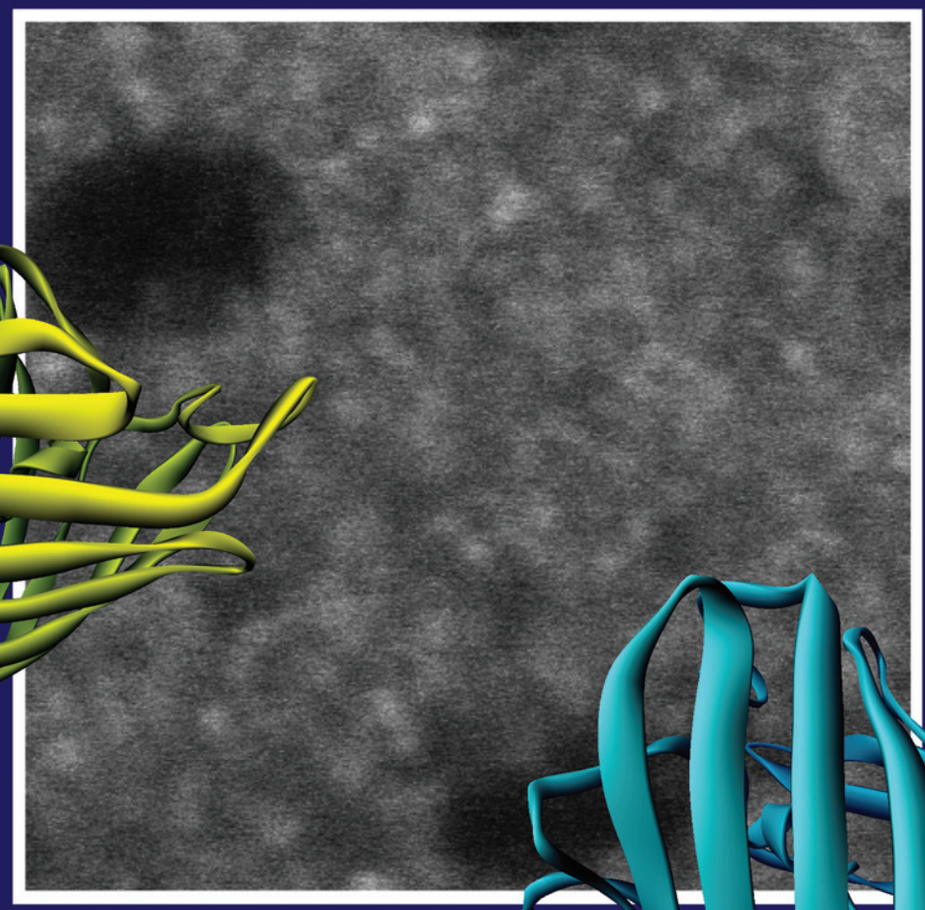

Martin E. van Royen

Protein-protein Interactions of the Androgen Receptor in Living Cells

Martin E. van Royen

The work described in this thesis was performed at the Department of Pathology of the Josephine Nefkens Institute, Erasmus MC, Rotterdam and was financially supported by the Dutch Cancer Society (KWF).

Printed by: Optima grafische communicatie, Rotterdam

The printing of this thesis was financially supported by:
Erasmus University Rotterdam (EUR)
Department of Pathology, Erasmus MC
Dutch Cancer Society (KWF)
Stichting tot Bevordering van de Electronenmicroscopie in Nederland (SEN)

ISBN-978-90-8559-463-5

Protein-protein Interactions of the Androgen Receptor in Living Cells

Eiwit-eiwit Interacties van de Androgeenreceptor in Levende Cellen

Proefschrift

ter verkrijging van de graad van doctor aan de

Erasmus Universiteit Rotterdam

op gezag van de

rector magnificus

Prof. dr. S.W.J. Lamberts

en volgens besluit van het College voor Promoties.

De openbare verdediging zal plaatsvinden op

woensdag 10 december 2008 om 9.45 uur

door

Martin Eduard van Royen
geboren te Utrecht

PROMOTIECOMMISSIE

Promotor:	Prof. dr. ir. J. Trapman
Overige leden:	Dr. G.W. Jenster Prof. dr. J.N.J. Philipsen Prof. dr. F. Claessens
Copromotor:	Dr. A.B. Houtsmuller

CONTENTS

Chapter 1

General Introduction

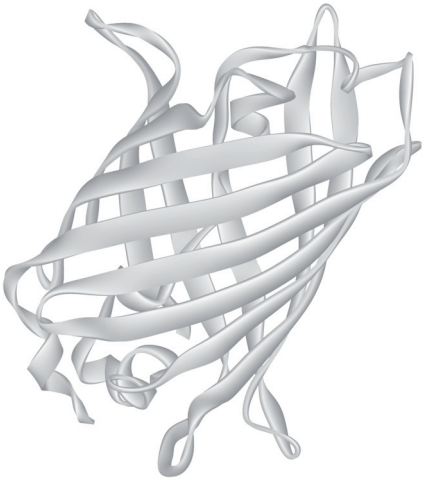

Natural androgens, testosterone (T) and its derivative dihydrotestosterone (DHT) play a crucial role in the development and maintenance of the male phenotype. Androgens are steroids that exert their function via the androgen receptor (AR), a ligand dependent transcription factor. The human *AR* gene, is located on the X chromosome, and contains 8 exons, coding for a 110 kDa, 919 amino acids protein (Brinkmann et al., 1989; Hughes and Deeb, 2006). In the classical model of AR action, the unliganded AR is located in the cytoplasm in complex with chaperone proteins (Pratt and Toft, 1997; Prescott and Coetzee, 2006). Upon androgen binding the chaperone complex is modified and the AR translocates to the nucleus (Georget et al., 1997; Tyagi et al., 2000; Black and Paschal, 2004). In the nucleus, the AR binds to specific sequences in promoters and enhancers of target genes, interacts with specific coregulators and enhances the recruitment of the general transcription machinery, leading to transcription initiation (Fig. 1) (Glass and Rosenfeld, 2000; Claessens et al., 2001; Cosma, 2002; Orphanides and Reinberg, 2002; Heemers and Tindall, 2007). Recently, many reviews on AR function have been published (*e.g.* Dehm and Tindall, 2007; Heemers and Tindall, 2007; Trapman and Dubbink, 2007; Centenera et al., 2008; Claessens et al., 2008). The focus of this thesis is on molecular mechanisms underlying AR function in living cells.

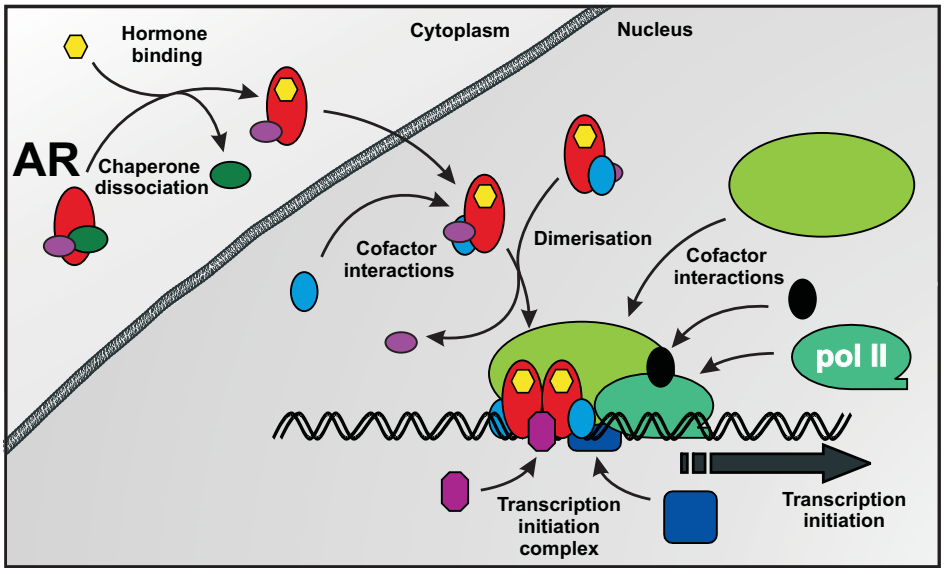

Figure 1. Schematical overview of AR regulated gene expression, (AR = androgen receptor, pol II = RNA polymerase II).

1.1 NUCLEAR RECEPTOR SUPERFAMILY

The AR is a member of the nuclear receptor (NR) superfamily of ligand-regulated transcription factors (reviewed in Gronemeyer and Laudet, 1995; Germain et al., 2006). All NRs have

a modular structure consisting of three functional domains; the N-terminal domain (NTD), the centrally located DNA binding domain (DBD), and the C-terminal ligand binding domain (LBD) (Brinkmann et al., 1989; and reviewed in Kumar and Thompson, 1999; and Claessens et al., 2008). NRs mediate a variety of cellular processes like cell growth, cell differentiation and homeostasis. The modes of action of the 48 known NRs are not only very diverse regarding their ligand and DNA binding properties, but also regarding their protein interactions including homo- and heterodimerization (reviewed in Committee, 1999). A subclassification of the NR superfamily has been defined, on the basis of their sequence alignment and their phylogenic tree (Mangelsdorf et al., 1995; Committee, 1999; Owen and Zelent, 2000; and reviewed in Germain et al., 2006). This classification consists of six evolutionary groups. The AR is classified in the same group as the other steroid receptors (SRs): the estrogen receptor-α and -β (ER-α and -β), the glucocorticoid receptor (GR), the mineralocorticoid receptor (MR), the progesterone receptor (PR) and the estrogen receptor related receptor (ERR) (Germain et al., 2006). Structurally two of the three functional domains, the DBD and the LBD are highly conserved (Gronemeyer and Laudet, 1995).

1.2 MODULAR STRUCTURE OF THE AR

The modular structure of the AR is reflected in the genomic organization of the AR gene. The AR NTD is encoded by the first and largest exon, the AR DBD by two small exons, and the sequence for the AR LBD is distributed over five exons (Fig. 2) (Brinkmann et al., 1989; Kuiper et al., 1989). The DBD and LBD are connected via the highly flexible hinge region and their sequence is highly conserved in the subgroup of SRs (ER, PR, GR, MR and AR) (reviewed in Gronemeyer and Laudet, 1995; Thornton and Kelley, 1998). Despite the sequence similarity in the SR LBD and DBD, the SRs have taken on considerable functional specificity in ligand binding and DNA sequence recognition. In both size and sequence the NTD is barely conserved between the different SRs (Lavery and McEwan, 2005; McEwan et al., 2007). In contrast to most NRs the AR LBD has a weak transactivation function. The stronger transactivation function of the AR is harbored by the AR NTD.

1.2.1 Structure and function of the AR N-terminal domain

The AR NTD is highly flexible, which has hampered elucidation of its three-dimensional structure (Lavery and McEwan, 2005; Lavery and McEwan, 2008b). Biophysical studies indicate that a native AR NTD has a structure that is between a fully folded state and a structured folded conformation: a molten-globule conformation (Lavery and McEwan, 2006; Lavery and McEwan, 2008b). This results in a flexible AR NTD, which may have several advantages over a more rigid folded conformation, including maintaining interaction specificity without the need for high affinity binding, increased contact surface for individual interactions and

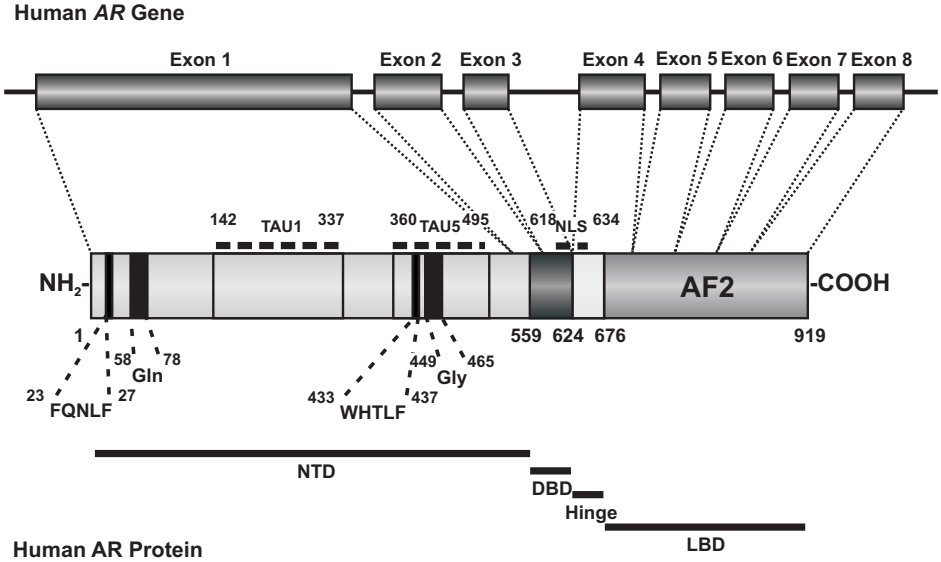

Figure 2. Structural organization of the AR gene and protein. NTD = N-terminal domain, DBD = DNA binding domain, LBD = ligand binding domain, AF = activation function, NLS = nuclear localization signal, FQNLF and WHTLF indicate the amino acid sequences at these positions and Gln and Gly indicate the glutamine- and glycine stretches. Figure is adapter from Gao et al. (2005).

accessibility for modifying enzymes like kinases and ligases (Dunker et al., 2002; Lavery and McEwan, 2008a). In spite of the lack of detailed structural information, several structural or functional NTD subdomains have been identified, including a conserved FQNLF motif, a polyglutamine stretch, a poly-glycine stretch and two transactivation units, termed TAU1 and TAU5 (Jenster et al., 1995).

1.2.1.1 AR activation function 1

In contrast to other SRs, the AR lacks a strong transcription activation function in the LBD, but the activation function in the AR NTD is strong (Fig. 2) (Jenster et al., 1995). The transactivation function of the AR NTD maps to two large transactivation units (TAUs), TAU1 (aa 100 – 370) and TAU5 (aa 360 – 485). TAU1 is active in full length AR and is induced upon ligand binding. In contrast, TAU5 is constitutively active in a truncated AR lacking the LBD (Jenster et al., 1995). TAU1 has been further subdivided in activation function (AF)-1a (aa 172 – 185) and AF-1b (aa 296 – 360) (Chamberlain et al., 1996). Mutational analysis showed that AR AF-1a was important for activity, but the role of AF-1b is unclear (Chamberlain et al., 1996; Callewaert et al., 2006). Recently, an LxxLL-like motif (WHTLF) at position aa 433 – 437, has been identified as the responsible autonomous transactivation domain in TAU5 (Dehm et al., 2007). However, supportive evidence for this observation is required.

The NTD is a protein interaction domain and several interacting proteins have been described, including: CBP/p300 (Fronsdal et al., 1998), SRC/p160 (Alen et al., 1999; Bevan et al.,

1999; Ma et al., 1999; Lavery and McEwan, 2008a), ARA70 (Zhou et al., 2002), MAGE-11 (Bai et al., 2005) and components of the general transcription machinery, such as TFIIF and TFIIH (Lee et al., 2000; Reid et al., 2002; Choudhry et al., 2006; Lavery and McEwan, 2008a). In more detail, TAU5 binds to the glutamine-rich region of SRC1. This interaction is indirectly inhibited by TAU1 (Callewaert et al., 2006).

There is ample evidence that truncated ARs, lacking the AR LBD can activate transiently transfected reporter constructs (Jenster et al., 1991; Jenster et al., 1995). In contrast to observations of full length AR, fluorescence recovery after photobleaching (FRAP) analysis revealed a much higher mobility of the LBD-deletion mutant compared to wt AR, suggesting that this mutant binds very transiently to promoters of target genes (Farla et al., 2004) (see also Chapter 3). The reduced DNA binding deduced from the FRAP data was confirmed by ChIP analysis of wild type AR and AR mutants lacking AR LBD or AR NTD, on stably integrated reporter constructs in Xenopus oocytes and on the enhancer region of the endogenous AR target gene prostate specific antigen (*PSA*) in mammalian cells (Li et al., 2007b). Furthermore, in this study an AR NTD fused to a Gal4-DBD was not able to activate a reporter assembled into chromatin indicating that the AR NTD is not sufficient for AR transcriptional activity.

1.2.1.2 AR N-terminal FQNLF motif

The N-terminal region of the AR NTD harbors an among species highly conserved helical region (aa 16 – 36) that contains an LxxLL-like motif, FQNLF at position aa 23 – 27 (Fig. 2) (He et al., 2000; Steketee et al., 2002a). This motif is essential in the ligand dependent interaction of the AR NTD with the coactivator groove in the AR LBD, the N/C interaction (He et al., 2000; Steketee et al., 2002a). Mutating the phenylalanine residues at position 23 or 27, or the leucine residue at position 26 strongly inhibits or completely disrupts the N/C interaction, mutations of most flanking amino acid residues have less dramatic effects and modulate N/C interaction (He et al., 2000; Steketee et al., 2002a; Dubbink et al., 2004; Dubbink et al., 2006). The AR N/C interaction is discussed in detail in Section 1.3.2. Melanoma antigen gene protein (MAGE-11) might compete with the cofactor binding groove in the AR LBD for interaction with the region in AR NTD overlapping the FQNLF motif and thereby enhancing the availability of the AR coactivator groove for coactivator binding (Bai et al., 2005).

A second LxxLL-like motif, the WHTLF motif at position aa 433 – 437 in the NTD has been described to interact with a different region of the LBD, but unpublished data showed that a peptide containing the WHTLF motif was not able to interact with the AR LBD (Fig. 2) (Berrevoets et al., 1998; He et al., 2000, Steketee, personal communication). Recently, this WHTLF motif was identified as the major transactivation motif in TAU5 that does not rely on interaction with the LBD to mediate its ligand-independent AR activity (Dehm et al., 2007). However, further research will be necessary to substantiate a role of the WHTLF motif in AR function.

1.2.1.3 AR NTD Gln and Gly stretches

The AR NTD contains two stretches, a poly-glutamine tract with variable length ranging from 9 to 36 residues, and a poly-glycine stretch with a length ranging from 10 to 30 residues. There is a weak inverse correlation between the length of the glutamine stretch and the risk of developing prostate cancer (Casella et al., 2001; Ferro et al., 2002). More importantly a strong correlation has been found between an extended glutamine stretch (over 40 residues) and Kennedy's disease, a severe neurodegenerative syndrome (Spada et al., 1991; Casella et al., 2001; Palazzolo et al., 2008). A shortened glycine stretch might enhance AR activity as a risk factor for the development of prostate cancer (Ding et al., 2005).

1.2.2 Structure and function of the AR DNA binding domain

The highly conserved AR DBD is positioned centrally in the AR (Brinkmann et al., 1989). Crystallographic studies revealed overall very similar structures of the different SR DBDs, both in solution (Härd et al., 1990; Baumann et al., 1993; Schwabe et al., 1993b) and bound to DNA (Luisi et al., 1991; Schwabe et al., 1993a; Shaffer et al., 2004; Roemer et al., 2006). They consist of three α-helices that are organized in two zinc finger motifs and a more loosely structured carboxy-terminal extension (CTE) (Luisi et al., 1991; Roemer et al., 2006; Jakób et al., 2007). The first helix in the first zinc finger contains the P-box sequence that enters the major groove of the DNA and makes base specific contacts (Nelson et al., 1993). Additional contacts with DNA are made via the CTE (Roemer et al., 2006; Jakób et al., 2007). The second and third helix form the second zinc finger with the D-box involved in dimerization (Freedman, 1992; Zilliacus et al., 1995; Claessens et al., 2001; Shaffer et al., 2004).

1.2.2.1 Selective DNA recognition

In general, steroid response elements (SREs) are organized as inverted repeats of hexameric SR binding sequences, separated by 3 nucleotides. These SREs are bound by SRs via their DBD as dimers in a head to head conformation (Fig. 3) (Luisi et al., 1991; Zilliacus et al., 1995; Verrijdt et al., 2003). The consensus high affinity androgen response element (ARE) consists of an inverted repeat of the sequence 5'TGTTCT-3' (5'-AGAACAnnnTGTTCT-3') (Cato et al., 1987). This sequence is not only recognized by the AR, but also by the GR, PR and MR (Funder, 1993; Beato et al., 1995; Horie-Inoue et al., 2006).

The contacts of the DBD with DNA consist of a number of hydrogen bonds between amino acid residues in the first and second zinc finger with the phosphate deoxyribose backbone and nucleotide side chains. The key DNA interacting amino acid residues are located the first α-helix of the DBD, which form the P-box. These amino acid residues make base specific contracts and are therefore involved in the SRE sequence recognition (Luisi et al., 1991; Gewirth and Sigler, 1995). The AR DBD interaction with the ARE half-site is nearly identical to that of GR (Shaffer et al., 2004). An additional contact is being made by AR R585 flanking the P-box, with the C5 methyl group of T6 of the ARE (Shaffer et al., 2004).

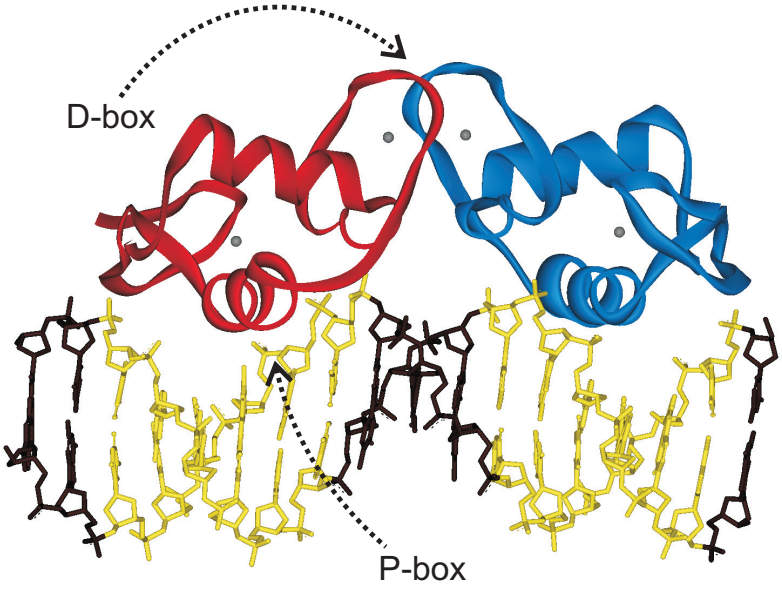

Figure 3. The AR DBD in complex with an ARE with two half sites. The two AR DBDs are in red and blue, the ARE half-sites in yellow, and the spacer and flanking base pairs in black.

More selective AREs have been identified that deviate from inverse repeats of the consensus sequence and preferentially bind AR but not other SRs. Initially, it has been postulated that these AREs are composed of a sequence more related to a direct repeat of the half side 5′-TGTTCT-3′ and that these sequences are bound by the AR in a head to tail conformation (Claessens et al., 2001; Haelens et al., 2003; Verrijdt et al., 2003). Later crystallographic analysis revealed a AR DBD dimer on such a repeat in a similar head to head conformation as was found on other SREs (Fig. 3) (Shaffer et al., 2004). This head to head AR conformation on a direct ARE repeat could be explained by the relative strong dimerization interface in the AR D-box, enabling binding of AR dimers to the second low affinity ARE half-site, where the weaker dimerization in other SRs does not compensate for the lower affinity of the SR for these specific AREs.

The major residues responsible for SR DBD dimerization are organized in a 5 amino acid region called the D-box in the second zinc finger (Dahlman-Wright et al., 1991). The dimerization interface consists of a network of hydrogen bonds and an extensive complementary surface. Importantly, the AR DBD dimer contains three supplementary hydrogen bonds (A596 – T602, S597 – S597 and T602 – A596) and an extended Van der Waals surface (Shaffer et al., 2004). The molecular background of the D-box dimerization is discussed in Section 1.3.1. The spatio-temporal organization of D-box interactions is discussed in detail in Chapter 6, where we propose a crucial role for D-box dimerization in AR dimerization and the transition from intramolecular to intermolecular N/C interaction.

The hypothesis of strong AR DBD dimerization was not confirmed by the lack of effect by introduction of the AR D-box in the GR DBD (Verrijdt et al., 2006). An alternative explanation lies in a role for an α-helical structure in the C-terminal extension (CTE) of the DBD, which is involved in stabilization of binding of some SRs, including the AR, to SREs with one high and one low affinity half site, but is poorly conserved in other SRs (Rastinejad et al., 1995; Schoenmakers et al., 1999; Haelens et al., 2003). The AR-DBD requires a CTE of minimally four residues (AR 625-TLGA-628) for proper binding to an ARE with an inverted repeat of high affinity ARE-half sites and a CTE of at least twelve residues (AR 625-TLGARKLKKLGN-636) for binding to an ARE with one high and one low affinity half site (Haelens et al., 2007).

1.2.2.2 Hinge region

A poorly conserved flexible linker, the hinge region, separates the NR DBD and LBD (Fig. 2). The hinge region can be defined as the fragment between the third α-helix of the DBD and the first α-helix of the LBD (in AR: aa 623 - 671). Only in the last decade a functional role for the hinge region was recognized. This region contains sequences involved in nuclear import and export, DNA binding selectivity and affinity via the CTE, and transcriptional activity of the AR. Furthermore, interaction with cofactors involved in sumoylation of the AR-NTD (Poukka et al., 2000), protein components of the SWI/SNF and p300/PCAF complexes have been described (Link et al., 2005; Link et al., 2008), and members of the heat shock protein complex (Buchanan et al., 2007; Yong et al., 2007; reviewed in Claessens et al., 2008).

The hinge region is flanked by a bipartite nucleoplasmin-like nuclear localization signal (NLS) at position 605–624, which is essential for nuclear import of the receptor (Zhou et al., 1994; Cutress et al., 2008). In unliganded AR the NLS is shielded, keeping the AR in the cytoplasm (Prescott and Coetzee, 2006). The truncated AR, lacking the LBD, is translocated to the nucleus without requirement of hormone binding (Jenster et al., 1993; Zhou et al., 1994; Kaku et al., 2008).

1.2.3 Structure and function of the AR ligand binding domain

The AR LBD shares its overall three-dimensional structure with other SRs (Matias et al., 2000). Unlike the other SR LBDs, which consist of 12 α-helices, the AR LBD has 11 α-helices due to the absence of helix 2 (H2). Nevertheless, the AR LBD helices are numbered 1 – 12 (H1 – H12), with H2 omitted to reflect the similarity in the overall structure. Together with two short β-turns, the α helices are arranged in three layers that form an anti-parallel "α-helical sandwich" with a central hydrophobic ligand binding cavity. Upon agonist binding, helix H12 is repositioned over the ligand binding pocket and acts as a flexible lid to stabilize the ligand binding (Matias et al., 2000; Sack et al., 2001; and reviewed in Gao et al., 2005; and Dehm and Tindall, 2007). Repositioning of helix 12 induced also the formation of a hydrophobic groove at the surface, allowing binding of cofactors and the AR N-terminal domain.

1.2.3.1 Ligand binding

Known AR ligands can be classified as steroidal or non-steroidal based on their structure or as agonist or antagonist based on their ability to activate or inhibit AR transcriptional activity. The natural AR ligands are the steroids testosterone (T) and its more active metabolite dihydrotestosterone (DHT). Approximately 20 amino acid residues in the ligand binding pocket in the AR LBD, mostly in helices H3, H5, and H11 directly interact with potent agonistic steroidal ligands (Poujol et al., 2000; Bohl et al., 2005b; Gao et al., 2005). These interactions along the body of the ligand are mostly hydrophobic, but also hydrogen bonds with the ligand extremities play a critical role in steroidal ligand binding. Crystal structures of agonist (T, DHT or the synthetic androgen R1881) bound AR LBD revealed that the most important interactions are the polar interactions (hydrogen bonds) between AR amino acids Q711, and R752 and the O-3 in the A-ring of steroidal ligands, and between N705 and T877 and the 17β-OH in the steroid D-ring (Matias et al., 2000; Poujol et al., 2000; Sack et al., 2001; Pereira de Jesus-Tran et al., 2006). Differences between steroidal ligands determine the precise interaction scheme with the ligand binding pocket, and explain the specificity and variation in binding affinity. The ligand binding pocket is somewhat flexible and can accomodate ligands with different structures (Matias et al., 2000; Poujol et al., 2000; Sack et al., 2001; Bohl et al., 2005a; Bohl et al., 2005b; Gao et al., 2005; Pereira de Jesus-Tran et al., 2006; Bohl et al., 2007). The structural data are being used in design of optimized selective androgen receptor modulators (SARMs) (Bohl et al., 2004).

In general, antagonist activity of mainly non-steroidal ligands seems to be related to sterical hindrance of the ligand in the ligand binding pocket (Bohl et al., 2005b; Gao et al., 2005). This might result in the disruption of the overall structure of the LBD and incorrect positioning of helix 12 abolishing the formation of the coactivator binding groove, as was found for the ER (Brzozowski et al., 1997). A number of mutations in the AR LBD have been described in prostate cancer that broaden the ligand responsiveness by providing a different set of pocket-ligand interactions and by avoiding sterical hindrance for ligand binding (Bohl et al., 2005a; Bohl et al., 2005b; Gao et al., 2005; Bohl et al., 2007). For example, crystallographic studies showed that the common AR T877A mutation leaves additional space for more bulky ligands (like CPA) or accommodates a water molecule that mediates hydrogen bonding interactions of helix 11 with non-steroidal ligands like OH-flutamide (Bohl et al., 2005b; Bohl et al., 2007). This and other mutations in AR LBD bound by their cognate antagonists (*e.g.* T877A, W741C/L and M895T) and possibly non-androgenic ligands (*e.g.* L701H and L701H/T877A) restore the overall LBD structure and allow activation by these ligands (Zhao et al., 2000; Bohl et al., 2005a; Bohl et al., 2005b; Gao et al., 2005; Bohl et al., 2007; van de Wijngaart et al., 2008). Unlike for the ER, no wild type AR LBD bound with antagonists has been crystallized, thus further studies are required to determine the structural background for AR antagonism.

In Chapter 7, we describe a FRET based sensor of induced activity in wild type and mutant AR and show the strong correlation between the ligand induced N/C interaction and AR transcriptional activity.

1.2.3.2 Cofactor binding groove in the AR LBD

In all NRs, ligand initiated repositioning of helix H12 in the LBD not only seals the ligand binding pocket but also forms together with H3, H4 and the loop in between these helices, the coactivator binding surface (Danielian et al., 1992; Feng et al., 1998; Moras and Gronemeyer, 1998). The function of this hydrophobic cleft was later confirmed in co-crystal structures of several NR LBDs including AR in complex with peptides (Darimont et al., 1998; Nolte et al., 1998; Shiau et al., 1998; Bledsoe et al., 2002; Hur et al., 2004). The cofactor groove is a hydrophobic cleft flanked by concentrated regions of positive and negative charged amino acid residues enabling cofactor binding mediated by short α-helical structures containing LxxLL-like motifs (Heery DM, 1997). Several cofactors, including the p160 cofactor family members TIF2/GRIP1 (Leers et al., 1998), SRC1/NCoA1 (Ding et al., 1998; Dubbink et al., 2004; He et al., 2004) and p/CIP/AIB1/ACTR (McInerney et al., 1998; Dubbink et al., 2004) have been described to interact with NR LDBs via LxxLL or LxxLL-like motifs. LxxLL motifs have also been found in CBP, RIP140, TRAP220/DRIP205, PGC1, RAP250/TRBP, TIP60 (McInerney et al., 1998; Dubbink et al., 2004). In addition, the corepressors NCoR and SMRT interact with the coactivator groove via extended LxxLL motifs (with consensus sequence Lxx I/H Ixxx I/L) (Perissi et al., 1999).

In contrast to the other NRs, the AR coactivator groove preferentially binds FxxLF-like motifs instead of LxxLL-like motifs (Dubbink et al., 2006). This prevalence for FxxLF motifs is probably due to the deeper AR cofactor groove compared to other NRs, by which it can accommodate bulkier side chains like the phenylalanines in the FxxLF motif (Dubbink et al., 2004; He et al., 2004; Hur et al., 2004). These bulky side chains are necessary to form optimal hydrophobic interactions in the AR coactivator groove (Dubbink et al., 2004; He et al., 2004; Hur et al., 2004). Computer modeling and random mutagenesis of the FxxLF motifs and specific mutagenesis of residues in the cofactor groove showed that the two phenylalanine residues are bound deeply in the cofactor groove and that the motif is positioned between K720 in helix 3 and E897 in helix 12 (Fig. 4). These residues form a charge clamp enabling electrostatic interactions with the main chain atoms at the ends of the FxxLF helix, similar to residues present in LBDs of other NRs in complex with LxxLL motifs.

Nevertheless, the mode of AR LBD interaction with LxxLL/FxxLF motifs seems to differ from classical charge clamp models and include not only E897 and K720, but also K717, R726 and possibly E709 and E893 (He and Wilson, 2003; Dubbink et al., 2004; He et al., 2004; Hur et al., 2004). In general, interactions with LxxLL motifs lack a hydrogen bond with E897 and mainly depend on a hydrogen bond between an LxxLL backbone with K720 and R726 (He et al., 2004; Hur et al., 2004). Compared to LxxLL peptide motifs, FxxLF peptide motifs is slightly shifted towards E897, contacting both amino acid residues of the classical charge clamp E897

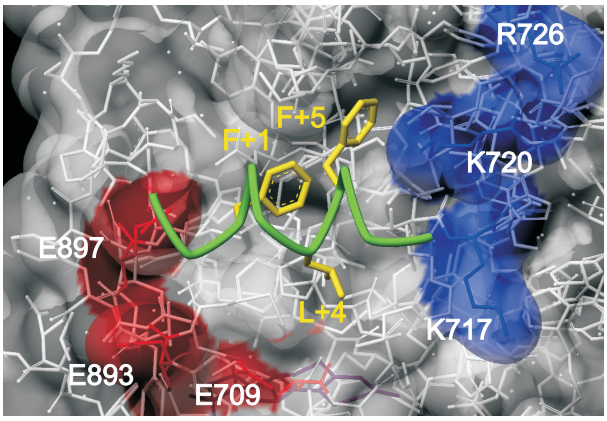

Figure 4. Crystal structure of AR coactivator groove with a bound AR FQNLF fragment (aa 20-30). FQNLF is charge clamped by E897 and K720. AR E897, E893, and E709 with K720, K717, and R726 create charge clusters (positive in blue, negative in red) that flank and make contact with the FQNLF motif.

and K720 via electrostatic interactions, but not the repositioned R726 (He et al., 2004; Hur et al., 2004; Estébanez-Perpiñá et al., 2005). In addition, interaction studies suggested that E897 is the major determinant for interaction with FxxLF-like motifs (Dubbink et al., 2004). Detailed crystallographic studies show that the phenylalanine residue at position 1 (F+1) makes hydrophobic contacts with L712, V716, M734, Q738, M894 and I898. The F+5 residue in the motif binds in a pocket formed by V716, K720, F725, I737, V730, Q733 and M734. The leucine at position 4 in an FxxLF motif is more solvent exposed and binds in a shallow hydrophobic patch consisting of L712 and V716 flanked by V713 and M894 (Hur et al., 2004). Precise interaction schemes with different LxxLL and FxxLF motifs are influenced by the flanking amino acid residues in the peptide motif and by the motif induced repositioning of involved amino acid residues in the groove (He et al., 2004).

Recently, a functional and structural screen for compounds that bind the AR surface and block binding of coactivators to AR AF-2 identified an allosterical second regulatory surface cleft, binding function (BF)-3, close to the coactivator groove (Estébanez-Perpiñá et al., 2007). Binding of three selected compounds to the allosterical surface inhibit AR activity and weaken binding of cofactor motifs reorganizing residues involved in the AF-2 function. Although the natural role of BF-3 *in vivo* is unknown, structural and functional studies, in combination with the observation that naturally occurring mutations in BF-3 are involved in prostate cancer and androgen insensitivity syndrome (AIS) suggest that this site is important (Estébanez-Perpiñá et al., 2007).

1.2.3.3 Motifs interacting with the AR coactivator groove

One of the most studied interactions of the coactivator groove with FxxLF-like motifs is not, as one may expect, with cofactors containing these motifs, but with the FQNLF motif in the NTD

of the AR itself at positions 23 to 27. For obvious reasons, this interaction is usually referred to as the AR N/C interaction (Fig. 4) (Langley et al., 1995; Doesburg et al., 1997; Ikonen et al., 1997; Berrevoets et al., 1998; He et al., 2000; Steketee et al., 2002a; He et al., 2004). Mutational analysis of the phenylalanine residues at positions F+1 and F+5 in AR FQNLF showed that some structural freedom is allowed at position F+5 but not at F+1 for interaction with the coactivator groove, but F to L or A substitutions disrupt the interaction completely (Dubbink et al., 2004). Random mutagenesis and alanine scanning of the AR FQNLF motif showed that Q+2 and N+3 and the flanking sequences have modulating effects (He et al., 2000; Steketee et al., 2002a; Dubbink et al., 2004; Dubbink et al., 2006). The function of the AR N/C interaction will be discussed in more detail in Section 1.3.2.

FxxLF motifs are essential for interaction of some cofactors with the coactivator groove. The AR cofactors ARA54, ARA55, ARA70 and RAD9 harbor FxxLF motifs (He et al., 2002b; Zhou et al., 2002; Hu et al., 2004; Wang et al., 2004b). Mutating this motif in either one of the ARA-cofactors abolished their interaction with the coactivator groove, but did not inhibit or modestly inhibited AR transcriptional activity. The lack of effect on AR activity is possibly due to alternative interactions with the AR NTD as were found for ARA70 (He et al., 2002b; Zhou et al., 2002). More significant was the effect of mutating the FxxLF motif in RAD9, which abolished its inhibiting function on AR transcription activity (Wang et al., 2004b).

The structural freedom of amino acid residues at some positions in the FxxLF motif in cofactors feeded the search for coactivator groove interacting FxxLF related motifs. FxxLF-like motifs with variable binding affinities were identified by phage display screens of randomized peptide libraries (Hsu et al., 2003; Hur et al., 2004; Chang et al., 2005). These studies showed that at position +1 instead of an F, a W allowed a weak interaction. Next to F at position +5 also a W and a Y generated motifs that interact with the AR coactivator groove. Even more variability was found at +4 where the leucine could be replaced with F, Y, M or V. The peptide approach was used to identify potent and selective inhibiting peptides of AR activity by blocking the coactivator groove (Chang et al., 2005; Fletterick, 2005). In Chapter 4 of this thesis we applied amino acid substitution at position +4 in AR FQNLF, ARA54 FNRLF and ARA70 FKLLF and identified two novel AR AF-2 interacting FxxLF, like motifs that enables specific and direct interactions with AR AF-2. Using these motifs, we identified the FxxLF and FxxMF motifs as the mode of interaction of two AR cofactors, gelsolin and PAK6 (Van de Wijngaart et al., 2006).

Selective recruitment of cofactors carrying functional FxxLF-like motifs by AR AF-2 and less efficient binding of cofactors with LxxLL-like motifs might contribute to selective activation of AR over other NRs (Dubbink et al., 2004; Dubbink et al., 2006). Although the AR AF-2 prefers interactions with FxxLF-like motifs over LxxLL-like motifs, some LxxLL motifs have been reported to interact with AR AF-2 (Chang and McDonnell, 2002; Dubbink et al., 2004; Dubbink et al., 2006). Moreover, the proteins carrying these LxxLL-like motifs, like the p160 cofactors SRC1 and TIF2/GRIP1 have been shown to be functionally relevant in AR function,

although this might not be via their LxxLL-like motifs (reviewed in Heinlein and Chang, 2002). Evidence is available that the Tau-5 region in the AR NTD interacts with a glutamine-rich domain in these cofactors (Bevan et al., 1999; Christiaens et al., 2002; Callewaert et al., 2006; reviewed in Claessens et al., 2008).

1.3 AR DOMAIN INTERACTIONS

In SRs multiple interactions between functional domains have been described (reviewed in Centenera et al., 2008). The best characterized interaction motif is the D-box involved in DBD-DBD dimerization (Dahlman-Wright et al., 1991; Luisi et al., 1991; Schwabe et al., 1993c). A dimerization interface between LBDs has been reported for several SRs including the ER, RXR, PR and GR (Brzozowski et al., 1997; Tanenbaum et al., 1998; Williams and Sigler, 1998; Bledsoe et al., 2002). Previously, such an interaction was also suggested for the AR (Nemoto et al., 1994), but, in contrast to other NR LBDs, the AR LBD crystallized as a monomer (Matias et al., 2000; Sack et al., 2001; reviewed in Centenera et al., 2008). A third functional domain interaction is the interaction between the AR NTD and the AR LBD, usually referred to as the N/C interaction (Doesburg et al., 1997). A similar interaction has been indicated for other SRs, but only for the AR the direct interaction between the domains has clearly been established (Kraus et al., 1995; He et al., 2000; Rogerson and Fuller, 2003; Dong et al., 2004).

1.3.1 AR D-box interaction

The major amino acid residues responsible for AR DBD dimerization in a head to head orientation are organized in a 5 amino acid region called the D-box in the second zinc finger (Dahlman-Wright et al., 1991; Shaffer et al., 2004). SR D-box interactions consist of a network of hydrogen bonds between residues in both D-boxes and by an extensive complementary surface (Luisi et al., 1991). The GR dimer interface contains a void in the middle of the two DBDs, the "glycine hole". In the AR dimer this hole is filled by a serine (S597) in the D-box of both AR DBDs. These serine residues form an extra hydrogen bond between the DBDs. Two additional hydrogen bonds are formed, by an alanine (A596) and a threonine (T602) with their counterpart in the other subunit (Shaffer et al., 2004). These additional interactions between two AR DBDs compared to other DBDs strengthen the dimerization. The relatively stronger dimerization interface increases the affinity for AREs and possibly contribute to AR binding to a low affinity half-site present in specific AREs (Shaffer et al., 2004; Centenera et al., 2008).

Mutations of the amino acid residues involved in AR DBD dimerisation have been linked to the partial form of the androgen insensitivity syndrome (PAIS) (Zoppi et al., 1992; Kaspar F, 1993; Gast et al., 1995; Holterhus PM, 1999; Nordenskjold A, 1999; Lundberg Giwercman et al., 2000; Melo et al., 2003; Giwercman et al., 2004; Deeb et al., 2005). Surprisingly, in transient

transfection assays the A596T mutation resulted in an increased AR transcription activity on reporters driven by high affinity AREs, whereas the transcription activity of AR A596T was lower on reporters driven by AREs composed of one high affinity and one low affinity half-site (Geserick et al., 2003). In Chapter 6 we show that the D-box interaction is a key event in AR dimerization in the AR, prior to DNA binding. In Chapter 6 we introduce also a model describing the effect of dimerization on AR regulated gene expression.

1.3.2 AR N/C interaction

The shift from the TAU1 transactivion function, active in full length AR where a LBD is present, to TAU5 as a constitutively active transactivator in a truncated AR without LBD suggested an interaction between the AR NTD and AR LBD, later specified as the N/C interaction (Fig. 4) (Berrevoets et al., 1998; He et al., 2000; Steketee et al., 2002a).

The AR N/C interaction is ligand dependent. Agonists, like T, DHT and R1881, but not antagonists, like OH-flutamide or bicalutamide induce the N/C interaction in full length AR. Partial antagonists and low affinity agonists are also able to induce N/C interaction in wild type AR, but to a lesser degree and not found in all studies on this subject (Wong et al., 1993; Langley et al., 1995; Doesburg et al., 1997; Kemppainen et al., 1999; Song et al., 2004; Schaufele et al., 2005; Hodgson et al., 2007). In Chapter 7 of this thesis a fluorescence resonance energy transfer (FRET) assay based on the AR N/C interaction is validated using different ligands on wild type and mutant ARs.

For many years it was unclear whether the AR N/C interaction in AR homodimers is intramolecular or intermolecular (Wong et al., 1993; Langley et al., 1995; Doesburg et al., 1997; Langley et al., 1998). Recently a FRET study clearly showed that the AR N/C interaction is rapidly initiated in the cytoplasm after hormone binding as an intramolecular interaction and is followed by an intermolecular N/C interaction in the nucleus, contributing to AR dimerisation (Schaufele et al., 2005). In Chapter 6 we included the role of the AR D-box dimerization domain in AR dimerization and the intermolecular N/C interaction.

The AR N/C interaction stabilizes the AR by slowing the rate of ligand dissociation and decreasing receptor degradation (Zhou et al., 1995; He et al., 2000; He et al., 2001; Dubbink et al., 2004; Centenera et al., 2008). It has been suggested that a conformational change in the AR, as a result of the N/C interaction plays a role in ligand dependent AR AF-1 phosphorylation (Yang et al., 2007). The AR N/C interaction on its turn could promote changes in the AR AF-1 structure that might increase AF-1 solvent exposure, release proteins that otherwise repress phosphorylation of the AF-1, or directly promote AF-1 kinase recruitment to the AR (Yang et al., 2007). Although the biological relevance is not yet understood, reported correlations with prostate cancer growth suggest that AR phosphorylation is of importance for its function (McCall et al., 2008; Ponguta et al., 2008). In Chapter 5 we show that the N/C interaction occurs preferentially in the mobile AR, where it protects the coactivator binding groove for

untimely and unfavorable protein-protein interactions. On the DNA, the N/C interaction is lost allowing cofactor binding (Van Royen et al., 2007).

In transient transfections, loss of the AR N/C interaction by mutations of the FQNLF motif in the NTD results in a significant decrease of transcriptional activity on an MMTV- and probasin-promoter driven reporter construct (He et al., 2000). This is contradicted by the finding that the AR N/C interaction is essential for transcriptional activity on promoters embedded in chromatin and endogenous promoters, but not on plasmid based promoters (Li et al., 2006). Possibly, this discrepancy is due to promoter specificity of these N/C interaction deficient mutants (He et al., 2002a). The need for the N/C interaction in chromatin embedded promoters is lost if the promoter is composed of multiple AREs, suggesting synergistic binding of the AR N/C mutants to these promoters (Li et al., 2006).

Cofactors with a functional LxxLL-like motif, like the p160 family members SRC1/NcoA1, SRC2/TIF2/GRIP1 and p/CIP/AIB1/ACTR bind to the cofactor groove in the NR LBD (McInerney et al., 1998; Dubbink et al., 2004). In the AR, the N/C interaction competes with the recruitment of cofactors with LxxLL-like interaction motifs but also with the FxxLF motif of ARA54 and ARA70, for the cofactor binding groove in the AR LBD (McInerney et al., 1998; He et al., 2001; Dubbink et al., 2004; Toumazou et al., 2007). However, both p160 family members and ARA-type cofactors exert their coactivator function via additional interactions with AR NTD (Alen et al., 1999; Bevan et al., 1999; He et al., 2002b; Zhou et al., 2002).

Several studies have shown that cofactors in their turn differentially influence the N/C interaction. Where ARA24, c-Jun, SRC1, TIF2/GRIP1 and ARA67 enhance the N/C interaction, caspase 8, MAGE11, cyclin D1, the N-terminal domain of ARA70, SMRT, and Rad9 inhibit the N/C interaction (Bubulya et al., 2001; Liao et al., 2003; Bai et al., 2005; Burd et al., 2005; Hsu et al., 2005; Shen et al., 2005; Qi et al., 2007; Harada et al., 2008).

Mutations in the AR LBD with diminished N/C interaction (like D695N, R774H, L907F, I737T, F725L, Y763C, R885H, V889M, R752Q, G743V, F754L), but also in the AR hinge region (R629W) (Deeb et al., 2008), correlate with partial or complete androgen insensitivity syndrome (PAIS / CAIS) (Langley et al., 1998; Thompson et al., 2001; Quigley et al., 2004; Jaaskelainen et al., 2006). It must be noted that there is no direct evidence that altered AR N/C interaction can be the cause of AIS because in all mutants also other functions might be affected, including binding of cofactors.

1.4 AR REGULATED TRANSCRIPTION

In order to initiate transcription, the chromatin structure in the vicinity of (the promoter/enhancer regions of) AR target genes requires reorganization. Binding of the AR to an ARE is considered as an initiating event in transcription of the target genes. It is likely that AR binding leads to subsequent recruitment of different classes of cofactors that affect chro-

matin structure and facilitate access of the basal transcription machinery to the promoter. Important steps in transcription initiation include histone modifications and recruitment of ATP-dependent chromatin remodeling complexes (reviewed in Hermanson et al., 2002; Smith and O'Malley, 2004; Roeder, 2005; Heemers and Tindall, 2007; Trapman and Dubbink, 2007).

1.4.1 Chromatin modifications

Many histone modifications including acetylation, methylation, phosphorylation, ubiquiniation, ADT-ribosylation, and glycosylation have been described. These histone modifications in general result in either loosening or tightening of DNA-histone interactions (and reviewed in Mellor, 2006; Heemers and Tindall, 2007; Li et al., 2007a).

1.4.1.1 Histone acetyltransferases (HATs) and histone deacetylases (HDACs)

Recruitment of histone acetylase (HAT) activity to chromatin, mediating the acetylation status of core-histone 3 and 4 amino acid residues, is associated with transcriptional activity. Examples of AR cofactors with (weak) HAT activity are two members of the p160 SRC family SRC1 and SRC3 (p/CIP/RAC3/ACTR/AIB1/TRAM1) (reviewed in Heinlein and Chang, 2002; Heemers and Tindall, 2007). The p160 family members, including SRC2 (GRIP1/TIF2), which does not have intrinsic HAT activity, harbor LxxLL-motifs enabling direct interaction with the AR cofactor groove, but they also interact with the AR NTD (Alen et al., 1999; Bevan et al., 1999; Xu and Li, 2003). More importantly, the p160 proteins recruit cofactors with stronger HAT activity, like p300, the p300 homologue CBP, and p300/CBP-associated factor (P/CAF) (Xu and Li, 2003). These proteins and other HATs like Tip60 might also directly interact with the AR. HATs are not only involved in transcription by modifying histones but also by acetylating coregulators and transcription factors including the AR, thereby facilitating the recruitment of SWI/SNF and Mediator coactivator complexes (Aarnisalo et al., 1998; Brady et al., 1999; Fu et al., 2000; Gaughan et al., 2001; Gaughan et al., 2002; Fu et al., 2003; Huang et al., 2003). Furthermore, p300 and CBP function as a direct bridge between DNA bound AR and the basal transcription machinery and possibly a number of other transcriptional regulators (Fu et al., 2000; reviewed in Heemers and Tindall, 2007).

HATs are counteracted by histone deacetylases (HDACs) resulting in transcriptional repression. Examples of HDACs that can directly interact with the AR are the nicotinamide adenine dinucleotide-dependent HDAC Sirtuin1 (SIRT1) and HDAC7 (Fu et al., 2006; Karvonen et al., 2006). Moreover, several other HDACs interact with the AR via multisubunit corepressor complexes such as NCoR and SMRT (reviewed in Wang et al., 2004a).

1.4.1.2 Methyltransferases and demethylases

Methylation has long been considered as an irreversible epigenetic mark, but recently it has been shown that AR-dependent transcription relies on both methyltransferase and demethylase activities. Histone methylation can be indicative of both active and repressed transcrip-

tional states of chromatin, dependent of the position of the modified residue and extend of methylation (reviewed in Mellor, 2006; Heemers and Tindall, 2007; Li et al., 2007a). Examples of methyltransferases involved in AR regulated transcription are coactivator-associated arginine methyltransferase 1 (CARM1) and protein arginine methyltransferarase (PRMT)-5, acting on proteins in the transcriptional complex including CBP/p300, and histones, respectively. Both interact indirectly with the AR via p160 coactivators and possibly p44 (Chen et al., 1999; Wang et al., 2001; Hosohata et al., 2003; Majumder et al., 2006).

In contrast, demethylation of methylated lysines of histone H3 (H3K9) by JHDM2A, lysine-specific demethylase 1 (LSD1) and JHDM2C stimulates AR dependent transcription. All three factors directly interact with the AR but only the latter two are constitutively present at promoter regions of AR target genes, whereas JHDM2A is hormone dependently recruited (Metzger et al., 2005; Yamane et al., 2006; Wissmann et al., 2007).

1.4.1.3 Factors involved in ubiquitination and sumoylation

A third and fourth functional group of cofactors are components of the ubiquitination and sumoylation pathways (reviewed in Heemers and Tindall, 2007). Target proteins, including histones and transcription factors, can be either poly- or mono-ubiquitinated, functioning in protein degradation or protein stability and recognition, activity, and intracellular localization (Kodadek et al., 2006; Mukhopadhyay and Riezman, 2007; Weake and Workman, 2008). These processes allow proper progression though rounds of transcription and appropriate assembly of protein complexes, and they modulate the activation status of transcription factors and coregulators. Coregulators in the ubiquitin-proteasome pathway, like E3 ligase E6-associated protein (E6-AP), Mdm2, ARA54 and many others mostly exhibit E3 ligase activity and directly tag the target protein with ubiquitin (reviewed in Heemers and Tindall, 2007). These cofactors interact directly with different domains of the AR, sometimes dependent on the acetylation status of the AR and enhance its transactivation function (Gaughan et al., 2005). Although ARA54 harbors direct interacts with the AR AF-2 cofactor groove, its involvement in AR or AR-cofactor ubiquitination has not been assessed (Kang et al., 1999). Ubiquitinilation of the AR and AR-cofactors enhances or inhibits the AR transactivation function and also influences its stability (Khan et al., 2006; reviewed in Heemers and Tindall, 2007).

By very similar mechanism the small ubiquitin-related modifier SUMO posttranscriptionally modifies several proteins involved in regulation of transcription and chromatin structure and regulates their localization and activity (reviewed in Heemers and Tindall, 2007). Multiple proteins, like the SUMO homologues SUMO1, 2 and 3, SUMO E2 conjugating enzyme Ubc9 and the protein inhibitors of activated STAT (PAIS) family, involved in several aspects of the sumoylation pathway can modulate the AR transcription machinery by sumoylating the AR and AR-associated cofactors such as TIF2 (Poukka et al., 2000; Kotaja et al., 2002; Zheng et al., 2006).

Taken together, numerous proteins with functions in ubiquitination and sumoylation pathways act on components of the AR transcriptional machinery by regulating their turnover, stability, degradation, and intracellular localization.

1.4.1.4 ATP-dependent chromatin-remodeling complexes

Cofactors also include components of chromatin-remodeling complexes. Chromatin remodeling complexes can dislocate or displace nucleosomes in an ATP dependent manner, leading to a chromatin status that is more permissive to transcription. Generally, the ATP-dependent remodeling machines are divided into four major classes according to the identity of their ATPase subunit: SWI/SNF, ISWI, Mi-2/NuRD, and INO80 (Eberharter and Becker, 2004). Of these the SWI/SNF complexes are the best characterized with regard to structure, function, and enzymatic activity. These multi-protein complexes consist of BRG1 or hBrm as the central catalytic ATPases and a heterogeneous mixture of 7-12 subunits, mostly BRG1-associated factors (BAFs) (Wang et al., 1996; Mohrmann and Verrijzer, 2005; Trotter and Archer, 2007; Wang et al., 2007a). Targeting of SWI/SNF complexes to specific promoters is thought to take place through interactions with transcription factors and coactivators, but also components of the basal transcription machinery. BAF subunits with bromodomains target acetylated histone tails whereas several other components including BRG1, hBRM, BAF250, BAF60a and BAF57 mediate in interactions between NRs, and chromatin remodeling complexes (Inoue et al., 2002; Belandia and Parker, 2003; Garcia-Pedrero et al., 2006; Trapman and Dubbink, 2007). More specific, one member of the BAF family, BAF57 and possibly the BRG-like ATPase ARIP4 directly bind to the AR (Link et al., 2005; Domanskyi et al., 2006; Link et al., 2008). Moreover, hBRM-containing SWI/SNF complexes potently regulate AR activity on promoters of target genes (Marshall et al., 2003).

1.4.1.5 Mediators

A next class of cofactors, the Mediator (MED) or TRAP/DRIP/ARC complexes, function as bridging complex between SRs and factors of the basal transcription machinery and RNA polymerase II (reveiwed in Kornberg, 2005; Malik and Roeder, 2005; Belakavadi and Fondell, 2006). Furthermore, transient overexpression of subunits of the TRAP/DRIP/ARC complex (TRAP220, TRAP170, and TRAP100) enhances AR mediated transcription (Wang et al., 2002). One of these subunits, MED1/TRAP220 directly interacts with the AR via an extended LxxLL motif (Wang et al., 2002; Coulthard et al., 2003).

1.4.1.6 Basal transcription machinery

Transcriptional activation ultimately needs the recruitment of RNA polymerase II (RNA pol II) to the promoter region of target genes. RNA pol II recruitment is mediated through the assembly of a complex of general transcription factors, starting with the recruitment of TATA binding protein (TBP) in the multi-protein complex TFIID, to the TATA box near the transcrip-

tional start site. On the TATA box, TBP induces DNA bending, bringing sequences upstream of the TATA-box in closer proximity, and presumably enabling interaction between general transcription factors, specific transcription factors like AR and coregulator complexes. This leads to the subsequent recruitment of a large series of multi-subunit transcription factor complexes. TFIIA and TFIIB stabilize TBP on the TATA box. TFIIB also recruits RNA pol II, which is in complex with TFIIF to prevent nonspecific RNA pol II DNA interactions. In addition, TFIIF regulates transcriptional elongation. Subsequently, TFIIE binds directly to RNA pol II and potentially TFIIF and TBP, and has been reported to recruit TFIIH, to modulate its helicase activity and may participate in DNA unwinding around the transcriptional initiation site (reviewed in Heinlein and Chang, 2002; Lee and Chang, 2003; Roeder, 2005). Various general transcription factors have been shown to interact with NRs. For example, the AR NTD is able to directly recruit TFIIE, TFIIF and TFIIH (McEwan and Gustafsson, 1997; Lee and Chang, 2003).

1.4.2 AR Corepressors

In contrast to coactivators, AR corepressors repress its transcriptional activity, keeping the balance between activation and repression in transcription regulation. Corepressors can be functionally classified in factors that inhibit nuclear translocation or DNA binding, factors that recruit HDACs, and factors that interrupt AR coactivator interaction (reviewed in Wang et al., 2004a; Burd et al., 2006). The best-characterized AR corepressors are SMRT and NCoR. Both these factors have been described to directly interact with the AR and act by competing with coactivators and recruiting HDACs (Cheng et al., 2002; Dotzlaw et al., 2003; Liao et al., 2003; Song et al., 2004; Hodgson et al., 2005; Burd et al., 2006; Yoon and Wong, 2006).

1.4.3 Cooperative transcription factors

The transcriptional outcome of AR target genes is further determined by specific transcription factors that bind to specific DNA sequences. These transcription factors cooperate with AR by different mechanisms and might interact directly or indirectly with the AR, in this way forming a more stable or more specific transcription initiation complex or they might compete with the AR for DNA binding sites or coregulators, in this way inhibiting AR activity. Multiple specific transcription factors seem to cooperate with AR by binding to DNA sequences close to AREs in promoters/enhancers of target genes or seem to facilitate AR binding on an ARE half site or even in the absence of ARE-like motifs, allowing coregulation of transcription of these genes (reviewed in Heemers and Tindall, 2007). AR binding sites seem selectively enriched in binding sequences for multiple specific transcription factors, including Foxa1, Oct1, GATA2, ETS1, and AP-1 (Bolton et al., 2007; Massie et al., 2007; Wang et al., 2007b). These transcription factors are critical for the collaboration with the AR in a finely tuned spatio-temporal regulation of target gene expression in a cell specific manner (Wang et al., 2007b).

1.5 AR IN DISEASE

Androgens play key roles in the development and maintenance of the male reproductive tissues including the prostate. In the prostate, androgens mediate key physiological processes such as differentiation, secretory function, metabolism, morphology, proliferation, and survival (Dehm and Tindall, 2006). Aberrant AR action has been linked to completely different types of disease, ranging from poor AR action in androgen insensitivity syndrome (AIS) to aberrant activation of the AR in hormone refractory prostate cancer (reviewed in Heinlein and Chang, 2004; Hughes and Deeb, 2006; Richter et al., 2007; Trapman and Dubbink, 2007).

1.5.1 Androgen insensitivity

AIS is characterized by the failure of a normal masculinization in genetically male individuals. In AIS individuals, cells that would normally be sensitive to androgens, are now unable to respond to androgens because of qualitative or quantitative defects in AR function or other defects in the androgen signaling axis (reviewed in Poletti et al., 2005; Hughes and Deeb, 2006). AIS is scaled according the severity of the degree of AR dysfunction in complete (CAIS), partial (PAIS) and mild (MAIS) androgen insensitivity syndrome. The phenotype (external) of CAIS patient is that of a normal female, despite the XY karyotype and the presence of a testis that produces sufficient testostererone (T) that can be metabolized to dihydrotestosterone (DHT). In PAIS the biological response to androgens is partial male genital development. The severity of PAIS ranges from hypospadias to clitoromegaly, in severe PAIS that is only marginally different from CAIS. The third category, MAIS, can occur without clear symptoms or with normal male development with mild female features (Hughes and Deeb, 2006).

The majority of *AR* mutations listed in the Androgen Receptor Gene Mutations Database at McGill University (http://www.androgendb.mcgill.ca) give rise to AIS. There is no specific 'hot spot' of mutations, although certain locations, such as exon 5, are affected more frequently (Hughes and Deeb, 2006). About two thirds of reported mutations are located in the LBD, approximately 20% in the DBD, and a small minority in the NTD, despite this region of the AR is encoded by the largest of the eight exons (Hughes and Deeb, 2006). Different types of mutations account for AIS. About half the mutations, including frame shift mutations, and all complete and partial deletions of the *AR* gene result in CAIS. Fifty-five % of missense mutations result in CAIS, 40% in PAIS and 5% in MAIS (Poletti et al., 2005).

Mutations in the *AR* that cause AIS generally interfere with DNA binding (CAIS) or androgen binding, but also can affect coregulator interaction and disable transcription complex formation (reviewed in Brinkmann et al., 1996; Adachi et al., 2000; Nitsche and Hiort, 2000; McPhaul, 2002; Poletti et al., 2005; Trapman and Dubbink, 2007; Werner R, 2008). In addition, specific mutations in the D-box that disrupt AR homodimerisation can also cause PAIS (Trapman and Dubbink, 2007). In Chapter 6 we utilized AR DBD mutations that are found in CAIS

patients (AR R585K) and D-box mutations found in PAIS patients (A596T and S597T) in the AR to study AR homodimerisation.

1.5.2 AR in prostate cancer

Not only normal prostate development, but also the growth of primary prostate cancer is dependent on androgens. Blockade of the AR pathway, by androgen depletion by chemical or surgical castration or by blockade of the AR function by anti-androgens is a frequently used therapy for metastasized prostate cancer. Despite initial success, in late stages all endocrine manipulated tumors escape to a therapy resistant stage (reviewed in Feldman and Feldman, 2001; Grossmann et al., 2001; Trapman, 2001; Navarro et al., 2002; Nieto et al., 2007). Importantly, in many of these resistant tumors the AR is still expressed and functionally active.

Mechanisms of transition to androgen-refractory prostate cancer involve amplification of the *AR* gene or mutations in the *AR* gene that allows the AR to respond to low doses of androgens, or inappropriate activation of the AR by other steroids or anti-androgens. The relative prevalence of *AR* mutations described in endocrine therapy resistant prostate cancer varies between different studies, but most reliable data estimate that it is approximately 10% (Taplin et al., 2003). The first reported and frequently found *AR* mutation in endocrine therapy resistant prostate cancer was a substitution of alanine for threonine at aa 877 in the AR LBD (AR T877A) (Veldscholte et al., 1990). This mutation results in an AR that cannot only be activated by T and DHT but also by estrogens, progestagens and adrenal androgens. More importantly, this mutation enables activation of the AR by the anti-androgen OH-flutamide (Veldscholte et al., 1990; Veldscholte et al., 1992). Several AR mutations found in prostate tumors have been evaluated functionally, including T877S, T877A, H874T, V715M, W741C, and L701H, as a single mutation or in combination with T877A. Similarly to T877A, these AR mutants have a broadened ligand specificity and are activated by different low affinity ligands like estradiol, progestagens, glucocordicoids and different partial and full antagonists (Veldscholte et al., 1992; Taplin et al., 1995; Taplin et al., 1999; Zhao et al., 1999; Zhao et al., 2000; Krishnan et al., 2002; Shi et al., 2002; Steketee et al., 2002b; Hara et al., 2003; Taplin et al., 2003; and reviewed in Taplin and Balk, 2004). In Chapter 7 we used some of these mutants to validate a FRET based ligand dependent AR activity assay. We show that the N/C interaction correlates very well with the transcriptional activity of wild type AR and AR mutants incubated with a variety of ligands.

A different mechanism of the progression to androgen refractory prostate cancer involves AR coactivators. Overexpression of cofactors, or mutations in coactivators could enable non-androgenic steroids or anti-androgens to activate the wild type AR or AR mutants (Grossmann et al., 2001). Examples are overexpression of SRC1 and SRC2/TIF2 in androgen-independent prostate cancer, resulting in increased AR activity and broadened ligand specificity of the AR (Gregory et al., 2001). Additionally, *AR* mutations may result in conformational changes of the AR that, in combination with certain coactivators, result in activation of the AR (Grossmann

et al., 2001; Renée Chmelar, 2007). Yet another mechanism of androgen independency are alterations in the expression or function of genes in regulatory pathways involving peptide growth factors or cytokines that could cause inappropriate AR activation (reviewed in Jenster et al., 1999; Grossmann et al., 2001). Finally, androgen-stimulated growth of a prostate tumor can be bypassed by a mechanism that is regulated by a signal transduction pathway, which is independent of the AR. Here the AR is no longer involved in the prostate cancer progression (reviewed in Grossmann et al., 2001).

Despite accumulating data on inappropriate activation of the AR in prostate cancer, the question remains what makes the AR important for prostate cancer development and growth. In other words, which are the target genes that are responsible for AR regulated tumor growth? In this regard, recent findings concerning specific genomic rearrangements that occur with variable frequency in prostate cancer seem very significant. These rearrangements result in fusions between the 5' part the of *TMPRSS2* gene or another prostate specific, androgen regulated gene and the 3' part of genes encoding ETS transcription factor family members of (proto)oncogenes (Tomlins et al., 2005; Hermans et al., 2006; Hermans et al., 2008; and reviewed in Kumar-Sinha et al., 2008). As can be predicted, these translocations result in inappropriate AR responsive (over-)expression of oncogenic transcription factors. The exact role of these gene fusions in the development of prostate cancer is still under investigation.

1.6 OUTLINE OF THIS THESIS

SR activity, including that of the AR, is not only regulated by ligand binding and DNA binding but also by interactions between functional domains and by interaction with cofactors. The best-described site for cofactor interactions is the cofactor groove in the LBD that binds LxxLL-like motifs. The AR cofactor groove preferentially binds FxxLF-like motifs. These motifs are found in cofactors, but also in the AR NTD giving rise to the N/C interaction. In this thesis molecular mechanisms responsible for AR function in living cells intensively using tagging with fluorescent proteins, high resolution confocal microscopy and quantitative imaging techniques like fluorescence resonance energy transfer (FRET) and fluorescence recovery after photobleaching (FRAP) are described. In **Chapter 2** and **3** these quantitative imaging techniques are discussed in detail.

In **Chapter 4**, amino acid substitution at position +4 in the FQNLF motif identified residues that are allowed in this motif without losing the interaction capacity with the AR LBD. The compatibility of the identified residues was tested in two other FxxLF motifs and the motifs with the identified residues were used to screen for novel potential AR cofactors. Fragments of these candidate cofactors containing the FxxLF-like motifs were tested in living cells on their ability to interact with the AR LBD.

In Chapter 5, a novel combination of FRET and FRAP was developed and used YFP / CFP ratio imaging to study the spatio-temporal distribution of protein-protein interactions of the AR in living cells. YFP / CFP ratio imaging showed the spatial distribution of the ARs with N/C interaction. FRET-FRAP was applied on cells expressing YFP- and CFP-double tagged ARs, to separately detect the mobility of ARs with N/C interaction and that of ARs without N/C interaction to find that the N/C interactions occur in the freely mobile AR and are lost when ARs bind to promoters. Furthermore, it was investigated what the results implied for the time and place of cofactor interactions with the AR cofactor groove. This study was extended in **Chapter 6**, with the establishment of the critical role of the D-box dimerization domain in AR dimerization and the inter-molecular N/C interaction studied by FRET analysis on YFP- and CFP- single tagged ARs. The data reveal D-box driven transition from intramolecular to inter-molecular domain interaction and show the spatio-temporal organization of these interactions in AR function.

YFP- and CFP- double tagged ARs were also used in a FRET based assay to screen for effects of agonistic and antagonistic ligands on the AR. In **Chapter 7** this FRET based assay was validated by studying the effects of known agonists and antagonists on the AR N/C interaction of wild type and mutant ARs. A strong correlation between transcriptional activity of the AR and its N/C interactions status was shown.

In **Chapter 8** the findings of these studies are brought together in an extensive model describing the spatio-temporal organization of essential AR interactions and put into a future perspective.

1.7 REFERENCES

Aarnisalo, P., J.J. Palvimo, and O.A. Jänne. 1998. CREB-binding protein in androgen receptor-mediated signaling. *Proc Natl Acad Sci U S A.* 95:2122-2127.

Adachi, M., R. Takayanagi, A. Tomura, K. Imasaki, S. Kato, K. Goto, T. Yanase, S. Ikuyama, and H. Nawata. 2000. Androgen-Insensitivity Syndrome as a Possible Coactivator Disease. *N Engl J Med.* 343:856-862.

Alen, P., F. Claessens, G. Verhoeven, W. Rombauts, and B. Peeters. 1999. The Androgen Receptor Amino-Terminal Domain Plays a Key Role in p160 Coactivator-Stimulated Gene Transcription. *Mol Cell Biol.* 19:6085-6097.

Bai, S., B. He, and E.M. Wilson. 2005. Melanoma Antigen Gene Protein MAGE-11 Regulates Androgen Receptor Function by Modulating the Interdomain Interaction. *Mol Cell Biol.* 25:1238-1257.

Baumann, H., K. Paulsen, H. Kovacs, H. Berglund, A.P. Wright, J.A. Gustafsson, and T. Hard. 1993. Refined solution structure of the glucocorticoid receptor DNA-binding domain. *Biochemistry.* 32:13463-13471.

Beato, M., P. Herrlich, and G. Schutz. 1995. Steroid hormone receptors: Many Actors in search of a plot. *Cell.* 83:851-857.

Belakavadi, M., and J. Fondell. 2006. Role of the mediator complex in nuclear hormone receptor signaling. *Rev Physiol Biochem Pharmacol.* 156:23-43.

Belandia, B., and M.G. Parker. 2003. Nuclear Receptors: A Rendezvous for Chromatin Remodeling Factors. *Cell.* 114:277-280.

Berrevoets, C.A., P. Doesburg, K. Steketee, J. Trapman, and A.O. Brinkmann. 1998. Functional Interactions of the AF-2 Activation Domain Core Region of the Human Androgen Receptor with the Amino-Terminal Domain and with the Transcriptional Coactivator TIF2 (Transcriptional Intermediary Factor 2). *Mol Endocrinol.* 12:1172-1183.

Bevan, C.L., S. Hoare, F. Claessens, D.M. Heery, and M.G. Parker. 1999. The AF1 and AF2 Domains of the Androgen Receptor Interact with Distinct Regions of SRC1. *Mol Cell Biol.* 19:8383-8392.

Black, B.E., and B.M. Paschal. 2004. Intranuclear organization and function of the androgen receptor. *Trends Endocrinol Metab.* 15:411-417.

Bledsoe, R.K., V.G. Montana, T.B. Stanley, C.J. Delves, C.J. Apolito, D.D. McKee, T.G. Consler, D.J. Parks, E.L. Stewart, and T.M. Willson. 2002. Crystal Structure of the Glucocorticoid Receptor Ligand Binding Domain Reveals a Novel Mode of Receptor Dimerization and Coactivator Recognition. *Cell.* 110:93-105.

Bohl, C.E., C. Chang, M.L. Mohler, J. Chen, D.D. Miller, P.W. Swaan, and J.T. Dalton. 2004. A Ligand-Based Approach To Identify Quantitative Structure-Activity Relationships for the Androgen Receptor. *J. Med. Chem.* 47:3765-3776.

Bohl, C.E., W. Gao, D.D. Miller, C.E. Bell, and J.T. Dalton. 2005a. Structural basis for antagonism and resistance of bicalutamide in prostate cancer. *Proc Natl Acad Sci U S A.* 102:6201-6206.

Bohl, C.E., D.D. Miller, J. Chen, C.E. Bell, and J.T. Dalton. 2005b. Structural Basis for Accommodation of Nonsteroidal Ligands in the Androgen Receptor. *J Biol Chem.* 280:37747-37754.

Bohl, C.E., Z. Wu, D.D. Miller, C.E. Bell, and J.T. Dalton. 2007. Crystal Structure of the T877A Human Androgen Receptor Ligand-binding Domain Complexed to Cyproterone Acetate Provides Insight for Ligand-induced Conformational Changes and Structure-based Drug Design. *J Biol Chem.* 282:13648-13655.

Bolton, E.C., A.Y. So, C. Chaivorapol, C.M. Haqq, H. Li, and K.R. Yamamoto. 2007. Cell- and gene-specific regulation of primary target genes by the androgen receptor. *Genes Dev.* 21:2005-2017.

Brady, M.E., D.M. Ozanne, L. Gaughan, I. Waite, S. Cook, D.E. Neal, and C.N. Robson. 1999. Tip60 is a nuclear hormone receptor coactivator. *J Biol Chem.* 274:17599-17604.

Brinkmann, A., G. Jenster, C. Ris-Stalpers, H. van der Korput, H. Brüggenwirth, A. Boehmer, and J. Trapman. 1996. Molecular basis of androgen insensitivity. *Steroids.* 61:172-175.

Brinkmann, A.O., P.W. Faber, H.C.J. van Rooij, G.G.J.M. Kuiper, C. Ris, P. Klaassen, J.A.G.M. van der Korput, M.M. Voorhorst, J.H. van Laar, E. Mulder, and J. Trapman. 1989. The human androgen receptor: domain structure, genomic organization and regulation of expression. *J Steroid Biochem.* 34:307-310.

Brzozowski, A.M., A.C.W. Pike, Z. Dauter, R.E. Hubbard, T. Bonn, O. Engstrom, L. Ohman, G.L. Greene, J.-A. Gustafsson, and M. Carlquist. 1997. Molecular basis of agonism and antagonism in the oestrogen receptor. *Nature.* 389:753-758.

Bubulya, A., S.-Y. Chen, C.J. Fisher, Z. Zheng, X.-Q. Shen, and L. Shemshedini. 2001. c-Jun Potentiates the Functional Interaction between the Amino and Carboxyl Termini of the Androgen Receptor. *J Biol Chem.* 276:44704-44711.

Buchanan, G., C. Ricciardelli, J.M. Harris, J. Prescott, Z.C.-L. Yu, L. Jia, L.M. Butler, V.R. Marshall, H.I. Scher, W.L. Gerald, G.A. Coetzee, and W.D. Tilley. 2007. Control of Androgen Receptor Signaling in Prostate Cancer by the Cochaperone Small Glutamine Rich Tetratricopeptide Repeat Containing Protein α. *Cancer Res.* 67:10087-10096.

Burd, C.J., L.M. Morey, and K.E. Knudsen. 2006. Androgen receptor corepressors and prostate cancer. *Endocr Relat Cancer.* 13:979-994.

Burd, C.J., C.E. Petre, H. Moghadam, E.M. Wilson, and K.E. Knudsen. 2005. Cyclin D1 Binding to the Androgen Receptor (AR) NH2-Terminal Domain Inhibits Activation Function 2 Association and Reveals Dual Roles for AR Corepression. *Mol Endocrinol.* 19:607-620.

Callewaert, L., N. Van Tilborgh, and F. Claessens. 2006. Interplay between Two Hormone-Independent Activation Domains in the Androgen Receptor. *Cancer Res.* 66:543-553.

Casella, R., M.R. Maduro, L.I. Lipshultz, and D.J. Lamb. 2001. Significance of the polyglutamine tract polymorphism in the androgen receptor. *Urology.* 58:651-656.

Cato, A., D. Henderson, and H. Ponta. 1987. The hormone response element of the mouse mammary tumour virus DNA mediates the progestin and androgen induction of transcription in the proviral long terminal repeat region. *EMBO J.* 6:363-368.

Centenera, M.M., J.M. Harris, W.D. Tilley, and L.M. Butler. 2008. The Contribution of Different Androgen Receptor Domains to Receptor Dimerization and Signaling. *Mol Endocrinol.* (in press)

Chamberlain, N.L., D.C. Whitacre, and R.L. Miesfeld. 1996. Delineation of Two Distinct Type 1 Activation Functions in the Androgen Receptor Amino-terminal Domain. *J Biol Chem.* 271:26772-26778.

Chang, C., J. Abdo, T. Hartney, and D.P. McDonnell. 2005. Development of peptide antagonists for the androgen receptor using combinatorial peptide phage display. *Mol Endocrinol.*19:2478-2490.

Chang, C., and D.P. McDonnell. 2002. Evaluation of Ligand-Dependent Changes in AR Structure Using Peptide Probes. *Mol Endocrinol.* 16:647-660.

Chen, D., H. Ma, H. Hong, S.S. Koh, S.-M. Huang, B.T. Schurter, D.W. Aswad, and M.R. Stallcup. 1999. Regulation of Transcription by a Protein Methyltransferase. *Science.* 284:2174-2177.

Cheng, S., S. Brzostek, S. Lee, A. Hollenberg, and B. SP. 2002. Inhibition of the dihydrotestosterone-activated androgen receptor by nuclear receptor corepressor. *Mol Endocrinol.* 16:1492-1501.

Choudhry, M.A., A. Ball, and I.J. McEwan. 2006. The Role of the General Transcription Factor IIF in Androgen Receptor-Dependent Transcription. *Mol Endocrinol.* 20:2052-2061.

Christiaens, V., C.L. Bevan, L. Callewaert, A. Haelens, G. Verrijdt, W. Rombauts, and F. Claessens. 2002. Characterization of the Two Coactivator-interacting Surfaces of the Androgen Receptor and Their Relative Role in Transcriptional Control. *J Biol Chem.* 277:49230-49237.

Claessens, F., S. Denayer, N. Van Tilborgh, S. Kerkhofs, C. Helsen, and A. Haelens. 2008. Diverse roles of androgen receptor (AR) domains in AR-mediated signaling. *Nucl Recept Signal.* 6:e008.

Claessens, F., G. Verrijdt, E. Schoenmakers, A. Haelens, B. Peeters, G. Verhoeven, and W. Rombauts. 2001. Selective DNA binding by the androgen receptor as a mechanism for hormone-specific gene regulation. *J Steroid Biochem Mol Biol.* 76:23-30.

Committee, N.R.N. 1999. A Unified Nomenclature System for the Nuclear Receptor Superfamily. Cell. 97:161-163.

Cosma, M.P. 2002. Ordered Recruitment: Gene-Specific Mechanism of Transcription Activation. *Mol Cell.* 10:227-236.

Coulthard, V.H., S. Matsuda, and D.M. Heery. 2003. An Extended LXXLL Motif Sequence Determines the Nuclear Receptor Binding Specificity of TRAP220. *J Biol Chem.* 278:10942-10951.

Cutress, M.L., H.C. Whitaker, I.G. Mills, M. Stewart, and D.E. Neal. 2008. Structural basis for the nuclear import of the human androgen receptor. *J Cell Sci.* 121:957-968.

Dahlman-Wright, K., A. Wright, J. Gustafsson, and J. Carlstedt-Duke. 1991. Interaction of the glucocorticoid receptor DNA-binding domain with DNA as a dimer is mediated by a short segment of five amino acids. *J Biol Chem.* 266:3107-3112.

Danielian, P., R. White, J. Lees, and M. Parker. 1992. Identification of a conserved region required for hormone dependent transcriptional activation by steroid hormone receptors. *EMBO J.* 11:1025-1033.

Darimont, B.D., R.L. Wagner, J.W. Apriletti, M.R. Stallcup, P.J. Kushner, J.D. Baxter, R.J. Fletterick, and K.R. Yamamoto. 1998. Structure and specificity of nuclear receptor-coactivator interactions. *Genes Dev.* 12:3343-3356.

Deeb, A., J. Jaaskelainen, M. Dattani, H.C. Whitaker, C. Costigan, and I.A. Hughes. 2008. A novel mutation in the human androgen receptor suggests a regulatory role for the hinge region in amino-terminal and carboxy-terminal interactions. *J Clin Endocrinol Metab.* (in press).

Deeb, A., C. Mason, Y. Lee, and I. Hughes. 2005. Correlation between genotype, phenotype and sex of rearing in 111 patients with partial androgen insensitivity syndrome. *Clin Endocrinol (Oxf).* 63:56-62.

Dehm, S., and D. Tindall. 2006. Molecular regulation of androgen action in prostate cancer. *J Cell Biochem.* 99:333-344.

Dehm, S.M., K.M. Regan, L.J. Schmidt, and D.J. Tindall. 2007. Selective Role of an NH2-Terminal WxxLF Motif for Aberrant Androgen Receptor Activation in Androgen Depletion Independent Prostate Cancer Cells. *Cancer Res.* 67:10067-10077.

Dehm, S.M., and D.J. Tindall. 2007. Androgen Receptor Structural and Functional Elements: Role and Regulation in Prostate Cancer. *Mol Endocrinol.* 21:2855-2863.

Ding, D., L. Xu, M. Menon, G.P. Veer Reddy, and E.R. Barrack. 2005. Effect of GGC (glycine) repeat length polymorphism in the human androgen receptor on androgen action. *Prostate.* 62:133-139.

Ding, X.F., C.M. Anderson, H. Ma, H. Hong, R.M. Uht, P.J. Kushner, and M.R. Stallcup. 1998. Nuclear Receptor-Binding Sites of Coactivators Glucocorticoid Receptor Interacting Protein 1 (GRIP1) and Steroid

Receptor Coactivator 1 (SRC-1): Multiple Motifs with Different Binding Specificities. *Mol Endocrinol.* 12:302-313.

Doesburg, P., C.W. Kuil, C.A. Berrevoets, K. Steketee, P.W. Faber, E. Mulder, A.O. Brinkmann, and J. Trapman. 1997. Functional in vivo interaction between the amino-terminal, transactivation domain and the ligand binding domain of the androgen receptor. *Biochemistry.* 36:1052-1064.

Domanskyi, A., K.T. Virtanen, J.J. Palvimo, and O.A. Jänne. 2006. Biochemical characterization of androgen receptor-interacting protein 4. *Biochem J.* 393:789-795.

Dong, X., Challis, JR, and S. Lye. 2004. Intramolecular interactions between the AF3 domain and the C-terminus of the human progesterone receptor are mediated through two LXXLL motifs. *J Mol Endocrinol.* 32:843-857.

Dotzlaw, H., M. Papaioannou, U. Moehren, F. Claessens, and A. Baniahmad. 2003. Agonist-antagonist induced coactivator and corepressor interplay on the human androgen receptor. *Mol Cell Endocrinol.* 213:79-85.

Dubbink, H.J., R. Hersmus, A.C.W. Pike, M. Molier, A.O. Brinkmann, G. Jenster, and J. Trapman. 2006. Androgen Receptor Ligand-Binding Domain Interaction and Nuclear Receptor Specificity of FXXLF and LXXLL Motifs as Determined by L/F Swapping. *Mol Endocrinol.* 20:1742-1755.

Dubbink, H.J., R. Hersmus, C.S. Verma, J.A.G.M. van der Korput, C.A. Berrevoets, J. van Tol, A.C.J. Ziel-van der Made, A.O. Brinkmann, A.C.W. Pike, and J. Trapman. 2004. Distinct recognition modes of FXXLF and LXXLL motifs by the androgen receptor. *Mol Endocrinol.* 18:2132-2150.

Dunker, A.K., C.J. Brown, J.D. Lawson, L.M. Iakoucheva, and Z. Obradovic. 2002. Intrinsic Disorder and Protein Function. Biochemistry. 41:6573-6582.

Eberharter, A., and P.B. Becker. 2004. ATP-dependent nucleosome remodelling: factors and functions. *J Cell Sci.* 117:3707-3711.

Estébanez-Perpiñá, E., L.A. Arnold, P. Nguyen, E.D. Rodrigues, E. Mar, R. Bateman, P. Pallai, K.M. Shokat, J.D. Baxter, R.K. Guy, P. Webb, and R.J. Fletterick. 2007. A surface on the androgen receptor that allosterically regulates coactivator binding. *Proc Natl Acad Sci U S A.* 104:16074-16079.

Estébanez-Perpiñá, E., J.M.R. Moore, E. Mar, E. Delgado-Rodrigues, P. Nguyen, J.D. Baxter, B.M. Buehrer, P. Webb, R.J. Fletterick, and R.K. Guy. 2005. The Molecular Mechanisms of Coactivator Utilization in Ligand-dependent Transactivation by the Androgen Receptor. *J. Biol. Chem.* 280:8060-8068.

Farla, P., R. Hersmus, B. Geverts, P.O. Mari, A.L. Nigg, H.J. Dubbink, J. Trapman, and A.B. Houtsmuller. 2004. The androgen receptor ligand-binding domain stabilizes DNA binding in living cells. *J Struct Biol.* 147:50-61.

Feldman, B.J., and D. Feldman. 2001. The development of androgen-independent prostate cancer. *Nat Rev Cancer.* 1:34-45.

Feng, W., R.C.n.J. Ribeiro, R.L. Wagner, H. Nguyen, J.W. Apriletti, R.J. Fletterick, J.D. Baxter, P.J. Kushner, and B.L. West. 1998. Hormone-Dependent Coactivator Binding to a Hydrophobic Cleft on Nuclear Receptors. *Science.* 280:1747-1749.

Ferro, P., M.G. Catalano, R. Dell'Eva, N. Fortunati, and U. Pfeffer. 2002. The androgen receptor CAG repeat: a modifier of carcinogenesis? *Mol Cell Endocrinol.* 193:109-120.

Fletterick, R.J. 2005. Molecular modelling of the androgen receptor axis: rational basis for androgen receptor intervention in androgen-independent prostate cancer. *BJU Int.* 96:2-9.

Freedman, L. 1992. Anatomy of the steroid receptor zinc finger region. *Endocr Rev.* 13:129-145.

Fronsdal, K., N. Engedal, T. Slagsvold, and F. Saatcioglu. 1998. CREB Binding Protein Is a Coactivator for the Androgen Receptor and Mediates Cross-talk with AP-1. *J Biol Chem.* 273:31853-31859.

Fu, M., M. Liu, A.A. Sauve, X. Jiao, X. Zhang, X. Wu, M.J. Powell, T. Yang, W. Gu, M.L. Avantaggiati, N. Pattabiraman, T.G. Pestell, F. Wang, A.A. Quong, C. Wang, and R.G. Pestell. 2006. Hormonal Control of Androgen Receptor Function through SIRT1. *Mol Cell Biol.* 26:8122-8135.

Fu, M., M. Rao, C. Wang, T. Sakamaki, J. Wang, D. Di Vizio, X. Zhang, C. Albanese, S. Balk, C. Chang, S. Fan, E. Rosen, J.J. Palvimo, O.A. Janne, S. Muratoglu, M.L. Avantaggiati, and R.G. Pestell. 2003. Acetylation of Androgen Receptor Enhances Coactivator Binding and Promotes Prostate Cancer Cell Growth. *Mol Cell Biol.* 23:8563-8575.

Fu, M., C. Wang, A.T. Reutens, J. Wang, R.H. Angeletti, L. Siconolfi-Baez, V. Ogryzko, M.-L. Avantaggiati, and R.G. Pestell. 2000. p300 and p300/cAMP-response Element-binding Protein-associated Factor Acetylate the Androgen Receptor at Sites Governing Hormone-dependent Transactivation. *J Biol Chem.* 275:20853-20860.

Funder, J.W. 1993. Mineralocorticoids, Glucocorticoids, Receptors and Response Elements. *Science.* 259: 1132-1133.

Gao, W., C.E. Bohl, and J.T. Dalton. 2005. Chemistry and structural biology of androgen receptor. *Chem Rev.* 105:3352-3370.

Garcia-Pedrero, J.M., E. Kiskinis, M.G. Parker, and B. Belandia. 2006. The SWI/SNF Chromatin Remodeling Subunit BAF57 Is a Critical Regulator of Estrogen Receptor Function in Breast Cancer Cells. *J Biol Chem.* 281:22656-22664.

Gast, A., F. Neuschmid-Kaspar, H. Klocker, and A.C.B. Cato. 1995. A single amino acid exchange abolishes dimerization of the androgen receptor and causes Reifenstein syndrome. *Mol Cell Endocrinol.* 111:93-98.

Gaughan, L., M.E. Brady, S. Cook, D.E. Neal, and C.N. Robson. 2001. Tip60 is a co-activator specific for class I nuclear hormone receptors. *J Biol Chem.* 276:46841-46848.

Gaughan, L., I.R. Logan, S. Cook, D.E. Neal, and C.N. Robson. 2002. Tip60 and histone deacetylase 1 regulate androgen receptor activity through changes to the acetylation status of the receptor. *J Biol Chem.* 277:25904-25913.

Gaughan, L., I.R. Logan, D.E. Neal, and C.N. Robson. 2005. Regulation of androgen receptor and histone deacetylase 1 by Mdm2-mediated ubiquitylation. *Nucl. Acids Res.* 33:13-26.

Georget, V., J.M. Lobaccaro, B. Terouanne, P. Mangeat, J.-C. Nicolas, and C. Sultan. 1997. Trafficking of the androgen receptor in living cells with fused green fluorescent protein-androgen receptor. *Mol Cell Endocrinol.* 129:17-26.

Germain, P., B. Staels, C. Dacquet, M. Spedding, and V. Laudet. 2006. Overview of Nomenclature of Nuclear Receptors. *Pharmacol Rev.* 58:685-704.

Geserick, C., H.A. Meyer, K. Barbulescu, and B. Haendler. 2003. Differential modulation of androgen receptor action by deoxyribonucleic acid response elements. *Mol Endocrinol.* 17:1738-1750.

Gewirth, D.T., and P.B. Sigler. 1995. The basis for half-site specificity explored through a non-cognate steroid receptor-DNA complex. *Nat Struct Biol.* 2:386-394.

Giwercman, Y.L., S.A. Ivarsson, J. Richthoff, K. Lundin, and A. Giwercman. 2004. A Novel Mutation in the D-Box of the Androgen Receptor Gene (S597R) in Two Unrelated Individuals Is Associated with both Normal Phenotype and Severe PAIS. *Horm Res.* 61:58-62.

Glass, C.K., and M.G. Rosenfeld. 2000. The coregulator exchange in transcriptional functions of nuclear receptors. Genes Dev. 14:121-141.

Gregory, C.W., B. He, R.T. Johnson, O.H. Ford, J.L. Mohler, F.S. French, and E.M. Wilson. 2001. A Mechanism for Androgen Receptor-mediated Prostate Cancer Recurrence after Androgen Deprivation Therapy. *Cancer Res.* 61:4315-4319.

Gronemeyer, H., and V. Laudet. 1995. Transcription factors 3: nuclear receptors. *Protein Profile.* 2:1173-1308.

Grossmann, M.E., H. Huang, and D.J. Tindall. 2001. Androgen Receptor Signaling in Androgen-Refractory Prostate Cancer. *J. Natl. Cancer Inst.* 93:1687-1697.

Haelens, A., T. Tanner, S. Denayer, L. Callewaert, and F. Claessens. 2007. The Hinge Region Regulates DNA Binding, Nuclear Translocation, and Transactivation of the Androgen Receptor. *Cancer Res.* 67:4514-4523.

Haelens, A., G. Verrijdt, L. Callewaert, V. Christiaens, K. Schauwaers, B. Peeters, W. Rombauts, and F. Claessens. 2003. DNA recognition by the androgen receptor: evidence for an alternative DNA-dependent dimerization, and an active role of sequences flanking the response element on transactivation. *Biochem J.* 369:141-151.

Hara, T., J. Miyazaki, H. Araki, M. Yamaoka, N. Kanzaki, M. Kusaka, and M. Miyamoto. 2003. Novel mutations of androgen receptor: a possible mechanism of bicalutamide withdrawal syndrome. *Cancer Res.* 63:149-153.

Harada, N., Y. Ohmori, R. Yamaji, Y. Higashimura, K. Okamoto, F. Isohashi, Y. Nakano, and H. Inui. 2008. ARA24/Ran enhances the androgen-dependent NH2- and COOH-terminal interaction of the androgen receptor. *Biochem Biophys Res Commun.* 373:373-377.

Härd, T., E. Kellenbach, R. Boelens, B. Maler, K. Dahlman, L. Freedman, J. Carlstedt-Duke, K. Yamamoto, J. Gustafsson, and R. Kaptein. 1990. Solution structure of the glucocorticoid receptor DNA-binding domain. *Science.* 249:157-60.

He, B., N.T. Bowen, J.T. Minges, and E.M. Wilson. 2001. Androgen-induced NH2- and COOH-terminal interaction inhibits p160 coactivator recruitment by activation function 2. *J Biol Chem.* 276:42293-42301.

He, B., J. Gampe, Robert T., A.J. Kole, A.T. Hnat, T.B. Stanley, G. An, E.L. Stewart, R.I. Kalman, J.T. Minges, and E.M. Wilson. 2004. Structural Basis for Androgen Receptor Interdomain and Coactivator Interactions Suggests a Transition in Nuclear Receptor Activation Function Dominance. *Mol Cell.* 16:425-438.

He, B., J.A. Kemppainen, and E.M. Wilson. 2000. FXXLF and WXXLF sequences mediate the NH2-terminal interaction with the ligand binding domain of the androgen receptor. *J Biol Chem.* 275:22986-22994.

He, B., L.W. Lee, J.T. Minges, and E.M. Wilson. 2002a. Dependence of Selective Gene Activation on the Androgen Receptor NH2- and COOH-terminal Interaction. *J Biol Chem.* 277:25631-25639.

He, B., J.T. Minges, L.W. Lee, and E.M. Wilson. 2002b. The FXXLF motif mediates androgen receptor-specific interactions with coregulators. *J Biol Chem.* 277:10226-10235.

He, B., and E.M. Wilson. 2003. Electrostatic Modulation in Steroid Receptor Recruitment of LXXLL and FXXLF Motifs. *Mol Cell Biol.* 23:2135-2150.

Heemers, H.V., and D.J. Tindall. 2007. Androgen Receptor (AR) Coregulators: A Diversity of Functions Converging on and Regulating the AR Transcriptional Complex. *Endocr Rev.* 28:778-808.

Heery DM, K.E., Hoare S, Parker MG. 1997. A signature motif in transcriptional co-activators mediates binding to nuclear receptors. *Nature.* 387:733-736.

Heinlein, C.A., and C. Chang. 2002. Androgen Receptor (AR) Coregulators: An Overview. *Endocr Rev.* 23:175-200.

Heinlein, C.A., and C. Chang. 2004. Androgen Receptor in Prostate Cancer. *Endocr Rev.* 25:276-308.

Hermans, K.G., A.A. Bressers, H.A. van der Korput, N.F. Dits, G. Jenster, and J. Trapman. 2008. Two Unique Novel Prostate-Specific and Androgen-Regulated Fusion Partners of ETV4 in Prostate Cancer. *Cancer Res.* 68:3094-3098.

Hermans, K.G., R. van Marion, H. van Dekken, G. Jenster, W.M. van Weerden, and J. Trapman. 2006. TMPRSS2:ERG Fusion by Translocation or Interstitial Deletion Is Highly Relevant in Androgen-Dependent Prostate Cancer, But Is Bypassed in Late-Stage Androgen Receptor-Negative Prostate Cancer. *Cancer Res.* 66:10658-10663.

Hermanson, O., C.K. Glass, and M.G. Rosenfeld. 2002. Nuclear receptor coregulators: multiple modes of modification. *Trends Endocrinol Metab.* 13:55-60.

Hodgson, M.C., I. Astapova, S. Cheng, L.J. Lee, M.C. Verhoeven, E. Choi, S.P. Balk, and A.N. Hollenberg. 2005. The Androgen Receptor Recruits Nuclear Receptor CoRepressor (N-CoR) in the Presence of Mifepristone via Its N and C Termini Revealing a Novel Molecular Mechanism for Androgen Receptor Antagonists. *J Biol Chem.* 280:6511-6519.

Hodgson, M.C., I. Astapova, A.N. Hollenberg, and S.P. Balk. 2007. Activity of Androgen Receptor Antagonist Bicalutamide in Prostate Cancer Cells Is Independent of NCoR and SMRT Corepressors. *Cancer Res.* 67:8388-8395.

Holterhus, P.M., J. Wiebel, G.H. Sinnecker, H.T. Bruggenwirth, W.G. Sippell, A.O. Brinkmann, K. Kruse, O. Hiort. 1999. Clinical and molecular spectrum of somatic mosaicism in androgen insensitivity syndrome. *Pediatr Res.* 46:648-690.

Horie-Inoue, K., K. Takayama, H.U. Bono, Y. Ouchi, Y. Okazaki, and S. Inoue. 2006. Identification of novel steroid target genes through the combination of bioinformatics and functional analysis of hormone response elements. *Biochem Biophys Res Commun.* 339:99-106.

Hosohata, K., P. Li, Y. Hosohata, J. Qin, R.G. Roeder, and Z. Wang. 2003. Purification and Identification of a Novel Complex Which Is Involved in Androgen Receptor-Dependent Transcription. *Mol Cell Biol.* 23:7019-7029.

Hsu, C.-L., Y.-L. Chen, H.-J. Ting, W.-J. Lin, Z. Yang, Y. Zhang, L. Wang, C.-T. Wu, H.-C. Chang, S. Yeh, S.W. Pimplikar, and C. Chang. 2005. Androgen Receptor (AR) NH2- and COOH-Terminal Interactions Result in the Differential Influences on the AR-Mediated Transactivation and Cell Growth. *Mol Endocrinol.* 19:350-361.

Hsu, C.-L., Y.-L. Chen, S. Yeh, H.-J. Ting, Y.-C. Hu, H. Lin, X. Wang, and C. Chang. 2003. The Use of Phage Display Technique for the Isolation of Androgen Receptor Interacting Peptides with (F/W)XXL(F/W) and FXXLY New Signature Motifs. *J Biol Chem.* 278:23691-23698.

Hu, Y.-C., S. Yeh, S.-D. Yeh, E.R. Sampson, J. Huang, P. Li, C.-L. Hsu, H.-J. Ting, H.-K. Lin, L. Wang, E. Kim, J. Ni, and C. Chang. 2004. Functional Domain and Motif Analyses of Androgen Receptor Coregulator ARA70 and Its Differential Expression in Prostate Cancer. *J Biol Chem.* 279:33438-33446.

Huang, Z., J. Li, L. Sachs, P. Cole, and J. Wong. 2003. A role for cofactor-cofactor and cofactor-histone interactions in targeting p300, SWI/SNF and Mediator for transcription. *EMBO J.* 22:2146-55.

Hughes, I.A., and A. Deeb. 2006. Androgen resistance. *Best Pract Res Clin Endocrinol Metab.* 20:577-598.

Hur, E., S.J. Pfaff, E.S. Payne, H. Gron, B.M. Buehrer, and R.J. Fletterick. 2004. Recognition and accommodation at the androgen receptor coactivator binding interface. *PLoS Biol.* 2:E274.

Ikonen, T., J.J. Palvimo, and O.A. Jänne. 1997. Interaction between the Amino- and Carboxyl-terminal Regions of the Rat Androgen Receptor Modulates Transcriptional Activity and Is Influenced by Nuclear Receptor Coactivators. *J Biol Chem.* 272:29821-29828.

Inoue, H., T. Furukawa, S. Giannakopoulos, S. Zhou, D.S. King, and N. Tanese. 2002. Largest Subunits of the Human SWI/SNF Chromatin-remodeling Complex Promote Transcriptional Activation by Steroid Hormone Receptors. *J Biol Chem.* 277:41674-41685.

Jaaskelainen, J., A. Deeb, J.W. Schwabe, N.P. Mongan, H. Martin, and I.A. Hughes. 2006. Human androgen receptor gene ligand-binding-domain mutations leading to disrupted interaction between the N- and C-terminal domains. *J Mol Endocrinol.* 36:361-368.

Jakób, M., R. Kolodziejczyk, M. Orlowski, S. Krzywda, A. Kowalska, J. Dutko-Gwózdz, T. Gwózdz, M. Kochman, M. Jaskólski, and A. Ozyhar. 2007. Novel DNA-binding element within the C-terminal extension of the nuclear receptor DNA-binding domain. *Nucl. Acids Res.* 35:2705-2718.

Jenster, G., J. Trapman, and A.O. Brinkmann. 1993. Nuclear import of the human androgen receptor. *Biochem J.* 293:761-768.

Jenster, G., H.A. van der Korput, C. van Vroonhoven, T.H. van der Kwast, J. Trapman, and A.O. Brinkmann. 1991. Domains of the human androgen receptor involved in steroid binding, transcriptional activation, and subcellular localization. *Mol Endocrinol.* 5:1396-404.

Jenster, G., H.A.G.M. van der Korput, and J. Trapman. 1995. Identification of Two Transcription Activation Units in the N-terminal Domain of the Human Androgen Receptor. *J Biol Chem.* 270:7341-7346.

Jenster, G.. 1999. The role of the androgen receptor in the development and progression of prostate cancer. *Semin Oncol*. 26:407-421.

Kaku, N., K.-i. Matsuda, A. Tsujimura, and M. Kawata. 2008. Characterization of Nuclear Import of the Domain-Specific Androgen Receptor in Association with the Importin α/β and Ran-Guanosine 5′-Triphosphate Systems. *Endocrinology.* 149:3960-3969.

Kang, H.-Y., S. Yeh, N. Fujimoto, and C. Chang. 1999. Cloning and characterization of human prostate coactivator ARA54, a novel protein that associates with the androgen receptor. *J Biol Chem.* 274:8570-8576.

Karvonen, U., O.A. Jänne, and J.J. Palvimo. 2006. Androgen receptor regulates nuclear trafficking and nuclear domain residency of corepressor HDAC7 in a ligand-dependent fashion. *Exp Cell Res.* 312:3165-3183.

Kaspar F, K.H., Denninger A, Cato AC. 1993. A mutant androgen receptor from patients with Reifenstein syndrome: identification of the function of a conserved alanine residue in the D box of steroid receptors. *Mol Cell Biol.* 13:7850-7858.

Kemppainen, J.A., E. Langley, C.-i. Wong, K. Bobseine, W.R. Kelce, and E.M. Wilson. 1999. Distinguishing Androgen Receptor Agonists and Antagonists: Distinct Mechanisms of Activation by Medroxyprogesterone Acetate and Dihydrotestosterone. *Mol Endocrinol.* 13:440-454.

Khan, O.Y., G. Fu, A. Ismail, S. Srinivasan, X. Cao, Y. Tu, S. Lu, and Z. Nawaz. 2006. Multifunction Steroid Receptor Coactivator, E6-Associated Protein, Is Involved in Development of the Prostate Gland. *Mol Endocrinol.* 20:544-559.

Kodadek, T., D. Sikder, and K. Nalley. 2006. Keeping Transcriptional Activators under Control. *Cell.* 127:261-264.

Kornberg, R.D. 2005. Mediator and the mechanism of transcriptional activation. *Trends Biochem Sci.* 30:235-239.

Kotaja, N., U. Karvonen, O.A. Jänne, and J.J. Palvimo. 2002. PIAS Proteins Modulate Transcription Factors by Functioning as SUMO-1 Ligases. *Mol Cell Biol.* 22:5222-5234.

Kraus, W.L., E.M. McInerney, and B.S. Katzenellenbogen. 1995. Ligand-dependent, transcriptionally productive association of the amino- and carboxyl-terminal regions of a steroid hormone nuclear receptor. *Proc Natl Acad Sci U S A.* 92:12314-12318.

Krishnan, A.V., X.-Y. Zhao, S. Swami, L. Brive, D.M. Peehl, K.R. Ely, and D. Feldman. 2002. A Glucocorticoid-Responsive Mutant Androgen Receptor Exhibits Unique Ligand Specificity: Therapeutic Implications for Androgen-Independent Prostate Cancer. *Endocrinology.* 143:1889-1900.

Kuiper, G.G., P.W. Faber, H.C. van Rooij, J.A. van der Korput, C. Ris-Stalpers, P. Klaassen, J. Trapman, and A.O. Brinkmann. 1989. Structural organization of the human androgen receptor gene. *J Mol Endocrinol.* 2:R1-4.

Kumar, R., and E.B. Thompson. 1999. The structure of the nuclear hormone receptors. *Steroids.* 64:310-319.

Kumar-Sinha, C., S.A. Tomlins, and A.M. Chinnaiyan. 2008. Recurrent gene fusions in prostate cancer. *Nat Rev Cancer.* 8:497-511.

Langley, E., J.A. Kemppainen, and E.M. Wilson. 1998. Intermolecular NH2-/Carboxyl-terminal Interactions in Androgen Receptor Dimerization Revealed by Mutations That Cause Androgen Insensitivity. *J Biol Chem.* 273:92-101.

Langley, E., Z.-x. Zhou, and E.M. Wilson. 1995. Evidence for an Anti-parallel Orientation of the Ligand-activated Human Androgen Receptor Dimer. *J Biol Chem.* 270:29983-29990.

Lavery, D., and I. McEwan. 2005. Structure and function of steroid receptor AF1 transactivation domains: induction of active conformations. *Biochem J.* 391:449-464.

Lavery, D., and I. McEwan. 2006. The human androgen receptor AF1 transactivation domain: interactions with transcription factor IIF and molten-globule-like structural characteristics. *Biochem Soc Trans.* 34:1054-1057.

Lavery, D.N., and I.J. McEwan. 2008a. Functional Characterization of the Native NH2-Terminal Transactivation Domain of the Human Androgen Receptor: Binding Kinetics for Interactions with TFIIF and SRC-1a. *Biochemistry.* 47:3352-3359.

Lavery, D.N., and I.J. McEwan. 2008b. Structural Characterization of the Native NH2-Terminal Transactivation Domain of the Human Androgen Receptor: A Collapsed Disordered Conformation Underlies Structural Plasticity and Protein-Induced Folding. *Biochemistry.* 47:3360-3369.

Lee, D.K., and C. Chang. 2003. Molecular communication between androgen receptor and general transcription machinery. *J Steroid Biochem Mol Biol.* 84:41-49.

Lee, D.K., H.O. Duan, and C. Chang. 2000. From Androgen Receptor to the General Transcription Factor TFIIH. Identification of cdk avtivating kinase (CAK) as an androgen receptor NH2-terminal associated coactivator. *J Biol Chem.* 275:9308-9313.

Leers, J., E. Treuter, and J.-Å. Gustafsson. 1998. Mechanistic Principles in NR Box-Dependent Interaction between Nuclear Hormone Receptors and the Coactivator TIF2. *Mol Cell Biol.* 18:6001-6013.

Li, B., M. Carey, and J.L. Workman. 2007a. The Role of Chromatin during Transcription. *Cell.* 128:707-719.

Li, J., J. Fu, C. Toumazou, H.-G. Yoon, and J. Wong. 2006. A Role of the Amino-Terminal (N) and Carboxyl-Terminal (C) Interaction in Binding of Androgen Receptor to Chromatin. *Mol Endocrinol.* 20:776-785.

Li, J., D. Zhang, J. Fu, Z. Huang, and J. Wong. 2007b. Structural and Functional Analysis of Androgen Receptor in Chromatin. *Mol Endocrinol.* (in press).

Liao, G., L.-Y. Chen, A. Zhang, A. Godavarthy, F. Xia, J.C. Ghosh, H. Li, and J.D. Chen. 2003. Regulation of Androgen Receptor Activity by the Nuclear Receptor Corepressor SMRT. *J Biol Chem.* 278:5052-5061.

Link, K.A., S. Balasubramaniam, A. Sharma, C.E.S. Comstock, S. Godoy-Tundidor, N. Powers, K.H. Cao, A. Haelens, F. Claessens, M.P. Revelo, and K.E. Knudsen. 2008. Targeting the BAF57 SWI/SNF Subunit in Prostate Cancer: A Novel Platform to Control Androgen Receptor Activity. *Cancer Res.* 68:4551-4558.

Link, K.A., C.J. Burd, E. Williams, T. Marshall, G. Rosson, E. Henry, B. Weissman, and K.E. Knudsen. 2005. BAF57 governs androgen receptor action and androgen-dependent proliferation through SWI/SNF. *Mol Cell Biol.* 25:2200-2215.

Luisi, B.F., W.X. Xu, Z. Otwinowski, L.P. Freedman, K.R. Yamamoto, and P.B. Sigler. 1991. Crystallographic analysis of the interaction of the glucocorticoid receptor with DNA. *Nature.* 352:497-505.

Lundberg Giwercman, Y., A. Nikoshkov, K. Lindsten, B. Byström, Å. Pousette, J. Knudtzon, J. Alm, and A. Wedell. 2000. Response to Treatment in Patients with Partial Androgen Insensitivity due to Mutations in the DNA-Binding Domain of the Androgen Receptor. *Horm Res.* 53:83-88.

Ma, H., H. Hong, S.-M. Huang, R.A. Irvine, P. Webb, P.J. Kushner, G.A. Coetzee, and M.R. Stallcup. 1999. Multiple Signal Input and Output Domains of the 160-Kilodalton Nuclear Receptor Coactivator Proteins. *Mol Cell Biol.* 19:6164-6173.

Majumder, S., Y. Liu, O.H. Ford III, J.L. Mohler, and Y.E. Whang. 2006. Involvement of arginine methyltransferase CARM1 in androgen receptor function and prostate cancer cell viability. *Prostate.* 66:1292-1301.

Malik, S., and R.G. Roeder. 2005. Dynamic regulation of pol II transcription by the mammalian Mediator complex. *Trends Biochem. Sci.* 30:256-263.

Mangelsdorf, D.J., C. Thummel, M. Beato, P. Herrlich, G. Schutz, K. Umesono, B. Blumberg, P. Kastner, M. Mark, P. Chambon, and R.M. Evans. 1995. The nuclear receptor superfamily: The second decade. *Cell.* 83:835-839.

Marshall, T.W., K.A. Link, C.E. Petre-Draviam, and K.E. Knudsen. 2003. Differential Requirement of SWI/SNF for Androgen Receptor Activity. *J Biol Chem.* 278:30605-30613.

Massie, C.E., B. Adryan, N.L. Barbosa-Morais, A.G. Lynch, M.G. Tran, D.E. Neal, and I.G. Mills. 2007. New androgen receptor genomic targets show an interaction with the ETS1 transcription factor. *EMBO Rep.* 8:871-878.

Matias, P.M., P. Donner, R. Coelho, M. Thomaz, C. Peixoto, S. Macedo, N. Otto, S. Joschko, P. Scholz, A. Wegg, S. Basler, M. Schafer, U. Egner, and M.A. Carrondo. 2000. Structural Evidence for Ligand Specificity in the Binding Domain of the Human Androgen Receptor. Implications for pathogenic gene mutations. *J Biol Chem.* 275:26164-26171.

McCall, P., L.K. Gemmell, R. Mukherjee, J.M.S. Bartlett, and J. Edwards. 2008. Phosphorylation of the androgen receptor is associated with reduced survival in hormone-refractory prostate cancer patients. *Br J Cancer.* 98:1094-1101.

McEwan, I., D. Lavery, K. Fischer, and K. Watt. 2007. Natural disordered sequences in the amino terminal domain of nuclear receptors: lessons from the androgen and glucocorticoid receptors. *Nucl Recept Signal.* 5:e001.

McEwan, I.J., and J.-Ã. Gustafsson. 1997. Interaction of the human androgen receptor transactivation function with the general transcription factor TFIIF. *Proc Natl Acad Sci U S A.* 94:8485-8490.

McInerney, E.M., D.W. Rose, S.E. Flynn, S. Westin, T.-M. Mullen, A. Krones, J. Inostroza, J. Torchia, R.T. Nolte, N. Assa-Munt, M.V. Milburn, C.K. Glass, and M.G. Rosenfeld. 1998. Determinants of coactivator LXXLL motif specificity in nuclear receptor transcriptional activation. *Genes Dev.* 12:3357-3368.

McPhaul, M.J. 2002. Androgen receptor mutations and androgen insensitivity. *Mol Cell Endocrinol.* 198:61-67.

Mellor, J. 2006. Dynamic nucleosomes and gene transcription. *Trends Genet.* 22:320-329.

Melo, K.F.S., B.B. Mendonca, A.E.C. Billerbeck, E.M.F. Costa, M. Inacio, F.A.Q. Silva, A.M.O. Leal, A.C. Latronico, and I.J.P. Arnhold. 2003. Clinical, Hormonal, Behavioral, and Genetic Characteristics of Androgen Insensitivity Syndrome in a Brazilian Cohort: Five Novel Mutations in the Androgen Receptor Gene. *J Clin Endocrinol Metab.* 88:3241-3250.

Metzger, E., M. Wissmann, N. Yin, J.M. Muller, R. Schneider, A.H.F.M. Peters, T. Gunther, R. Buettner, and R. Schule. 2005. LSD1 demethylates repressive histone marks to promote androgen-receptor-dependent transcription. *Nature.* 437:436-439.

Mohrmann, L., and C.P. Verrijzer. 2005. Composition and functional specificity of SWI2/SNF2 class chromatin remodeling complexes. *Biochimica Biophysica Acta.* 1681:59-73.

Moras, D., and H. Gronemeyer. 1998. The nuclear receptor ligand-binding domain: structure and function. *Curr. Opin. Cell Biol.* 10:384-391.

Mukhopadhyay, D., and H. Riezman. 2007. Proteasome-Independent Functions of Ubiquitin in Endocytosis and Signaling. *Science.* 315:201-205.

Navarro, D., O.P. Luzardo, L. Fernandez, N. Chesa, and B.N. Diaz-Chico. 2002. Transition to androgen-independence in prostate cancer. *J Steroid Biochem Mol Biol.* 81:191-201.

Nelson, C., J. Faris, S. Hendy, and P. Romaniuk. 1993. Functional analysis of the amino acids in the DNA recognition alpha- helix of the human thyroid hormone receptor. *Mol Endocrinol.* 7:1185-1195.

Nemoto, T., Y. Ohara-Nemoto, S. Shimazaki, M. Ota. 1994. Dimerization characteristics of the DNA- and steroid-binding domains of the androgen receptor. *J Steroid Biochem Mol Biol.* 50:225-33.

Nieto, M., S. Finn, M. Loda, and W.C. Hahn. 2007. Prostate cancer: Re-focusing on androgen receptor signaling. *Int J Biochem Cell Biol.* 39:1562-1568.

Nitsche, E.M., and O. Hiort. 2000. The Molecular Basis of Androgen Insensitivity. *Horm Res.* 54:327-333.

Nolte, R.T., G.B. Wisely, S. Westin, J.E. Cobb, M.H. Lambert, R. Kurokawa, M.G. Rosenfeld, T.M. Willson, C.K. Glass, and M.V. Milburn. 1998. Ligand binding and co-activator assembly of the peroxisome proliferator-activated receptor-γ. *Nature.* 395:137-143.

Nordenskjold A, F.E., Tapper-Persson M, Soderhall C, Leviav A, Svensson J, Anvret M. 1999. Screening for mutations in candidate genes for hypospadias. *Urol Res.* 27:49-55.

Orphanides, G., and D. Reinberg. 2002. A Unified Theory of Gene Expression. *Cell.* 108:439-451.

Owen, G., and A. Zelent. 2000. Origins and evolutionary diversification of the nuclear receptor superfamily. *Cell Mol Life Sci.* 57:809-827.

Palazzolo, I., A. Gliozzi, P. Rusmini, D. Sau, V. Crippa, F. Simonini, E. Onesto, E. Bolzoni, and A. Poletti. 2008. The role of the polyglutamine tract in androgen receptor. *J Steroid Biochem Mol Biol.* 108:245-253.

Pereira de Jesus-Tran, K., P.-L. Cote, L. Cantin, J. Blanchet, F. Labrie, and R. Breton. 2006. Comparison of crystal structures of human androgen receptor ligand-binding domain complexed with various agonists reveals molecular determinants responsible for binding affinity. *Protein Sci.* 15:987-999.

Perissi, V., L.M. Staszewski, E.M. McInerney, R. Kurokawa, A. Krones, D.W. Rose, M.H. Lambert, M.V. Milburn, C.K. Glass, and M.G. Rosenfeld. 1999. Molecular determinants of nuclear receptor-corepressor interaction. *Genes Dev.* 13:3198-3208.

Poletti, A., P. Negri-Cesi, and L. Martini. 2005. Reflections on the diseases linked to mutations of the androgen receptor. *Endocrine.* 28:243-262.

Ponguta, L.A., C.W. Gregory, F.S. French, and E.M. Wilson. 2008. Site-specific Androgen Receptor Serine Phosphorylation Linked to Epidermal Growth Factor-dependent Growth of Castration-recurrent Prostate Cancer. *J Biol Chem.* 283:20989-21001.

Poujol, N., J.-M. Wurtz, B. Tahiri, S. Lumbroso, J.-C. Nicolas, D. Moras, and C. Sultan. 2000. Specific Recognition of Androgens by Their Nuclear Receptor. A structure-function study. *J Biol Chem.* 275:24022-24031.

Poukka, H., U. Karvonen, O.A. Jänne, and J.J. Palvimo. 2000. Covalent modification of the androgen receptor by small ubiquitin-like modifier 1 (SUMO-1). *Proc Natl Acad Sci U S A.* 97:14145-14150.

Pratt, W.B., and D.O. Toft. 1997. Steroid Receptor Interactions with Heat Shock Protein and Immunophilin Chaperones. *Endocr Rev.* 18:306-360.

Prescott, J., and G.A. Coetzee. 2006. Molecular chaperones throughout the life cycle of the androgen receptor. *Cancer Lett.* 231:12-19.

Qi, W., H. Wu, L. Yang, D.D. Boyd, and Z. Wang. 2007. A novel function of caspase-8 in the regulation of androgen-receptor-driven gene expression. *EMBO J.* 26:65-75.

Quigley, C.A., J. Tan, B. He, Z. Zhou, F. Mebarki, Y. Morel, M.G. Forest, P. Chatelain, E.M. Ritzen, F.S. French, and E.M. Wilson. 2004. Partial androgen insensitivity with phenotypic variation caused by androgen receptor mutations that disrupt activation function 2 and the NH2- and carboxyl-terminal interaction. *Mech Ageing Dev.* 125:683-695.

Rastinejad, F., T. Perlmann, R.M. Evans, and P.B. Sigler. 1995. Structural determinants of nuclear receptor assembly on DNA direct repeats. *Nature.* 375:203-211.

Reid, J., I. Murray, K. Watt, R. Betney, and I.J. McEwan. 2002. The Androgen Receptor Interacts with Multiple Regions of the Large Subunit of General Transcription Factor TFIIF. *J Biol Chem.* 277:41247-41253.

Renée Chmelar, G.B., Eleanor F. Need, Wayne Tilley, Norman M. Greenberg,. 2007. Androgen receptor coregulators and their involvement in the development and progression of prostate cancer. *Int J Cancer.* 120:719-733.

Richter, E., S. Srivastava, and A. Dobi. 2007. Androgen receptor and prostate cancer. *Prostate Cancer Prostatic Dis.* 12:114-118.

Roeder, R.G. 2005. Transcriptional regulation and the role of diverse coactivators in animal cells. *FEBS Lett.* 579:909-915.

Roemer, S.C., D.C. Donham, L. Sherman, V.H. Pon, D.P. Edwards, and M.E.A. Churchill. 2006. Structure of the Progesterone Receptor-Deoxyribonucleic Acid Complex: Novel Interactions Required for Binding to Half-Site Response Elements. *Mol Endocrinol.* 20:3042-3052.

Rogerson, F.M., and P.J. Fuller. 2003. Interdomain interactions in the mineralocorticoid receptor. *Mol Cell Endocrinol.* 200:45-55.

Sack, J.S., K.F. Kish, C. Wang, R.M. Attar, S.E. Kiefer, Y. An, G.Y. Wu, J.E. Scheffler, M.E. Salvati, S.R. Krystek, R. Weinmann, and H.M. Einspahr. 2001. Crystallographic structures of the ligand-binding domains of the androgen receptor and its T877A mutant complexed with the natural agonist dihydrotestosterone. *Proc Natl Acad Sci U S A.* 98:4904-4909.

Schaufele, F., X. Carbonell, M. Guerbadot, S. Borngraeber, M.S. Chapman, A.A.K. Ma, J.N. Miner, and M.I. Diamond. 2005. The structural basis of androgen receptor activation: Intramolecular and intermolecular amino-carboxy interactions. *Proc Natl Acad Sci U S A.* 102:9802-9807.

Schoenmakers, E., P. Alen, G. Verrijdt, B. Peeters, G. Verhoeven, W. Rombauts, and F. Claessens. 1999. Differential DNA binding by the androgen and glucocorticoid receptors involves the second Zn-finger and a C-terminal extension of the DNA-binding domains. *Biochem J.* 341:515-521.

Schwabe, J.W., L. Chapman, J.T. Finch, and D. Rhodes. 1993a. The crystal structure of the estrogen receptor DNA-binding domain bound to DNA: how receptors discriminate between their response elements. *Cell.* 75:567-578.

Schwabe, J.W., L. Chapman, J.T. Finch, D. Rhodes, and D. Neuhaus. 1993b. DNA recognition by the oestrogen receptor: from solution to the crystal. *Structure.* 1:187-204.

Schwabe, J.W.R., L. Chapman, J.T. Finch, and D. Rhodes. 1993c. The crystal structure of the estrogen receptor DNA-binding domain bound to DNA: How receptors discriminate between their response elements. *Cell.* 75:567-578.

Shaffer, P.L., A. Jivan, D.E. Dollins, F. Claessens, and D.T. Gewirth. 2004. Structural basis of androgen receptor binding to selective androgen response elements. *Proc Natl Acad Sci U S A.* 101:4758-4763.

Shen, H., G. Buchanan, L. Butler, J. Prescott, M. Henderson, W. Tilley, and G. Coetzee. 2005. GRIP1 mediates the interaction between the amino- and carboxyl-termini of the androgen receptor. *Biol Chem.* 386:69-74.

Shi, X.-B., A.-H. Ma, L. Xia, H.-J. Kung, and R.W. de Vere White. 2002. Functional Analysis of 44 Mutant Androgen Receptors from Human Prostate Cancer. *Cancer Res.* 62:1496-1502.

Shiau, A.K., D. Barstad, P.M. Loria, L. Cheng, P.J. Kushner, D.A. Agard, and G.L. Greene. 1998. The Structural Basis of Estrogen Receptor/Coactivator Recognition and the Antagonism of This Interaction by Tamoxifen. *Cell.* 95:927-937.

Smith, C.L., and B.W. O'Malley. 2004. Coregulator Function: A Key to Understanding Tissue Specificity of Selective Receptor Modulators. *Endocr Rev.* 25:45-71.

Song, L.-N., M. Coghlan, and E.P. Gelmann. 2004. Antiandrogen Effects of Mifepristone on Coactivator and Corepressor Interactions with the Androgen Receptor. *Mol Endocrinol.* 18:70-85.

Spada, A.R.L., E.M. Wilson, D.B. Lubahn, A.E. Harding, and K.H. Fischbeck. 1991. Androgen receptor gene mutations in X-linked spinal and bulbar muscular atrophy. *Nature.* 352:77-79.

Steketee, K., C.A. Berrevoets, H.J. Dubbink, P. Doesburg, R. Hersmus, A.O. Brinkmann, and J. Trapman. 2002a. Amino acids 3-13 and amino acids in and flanking the 23 FxxLF 27 motif modulate the interaction between the N-terminal and ligand-binding domain of the androgen receptor. *Eur J Biochem.* 269:5780-5791.

Steketee, K., L. Timmerman, A. Ziel-van der Made, P. Doesburg, A. Brinkmann, and J. Trapman. 2002b. Broadened ligand responsiveness of androgen receptor mutants obtained by random amino acid substitution of H874 and mutation hot spot T877 in prostate cancer. *Int J Cancer.* 100:309-317.

Tanenbaum, D.M., Y. Wang, S.P. Williams, and P.B. Sigler. 1998. Crystallographic comparison of the estrogen and progesterone receptor's ligand binding domains. *Proc Natl Acad Sci U S A.* 95:5998-6003.

Taplin, M.-E., and S. Balk. 2004. Androgen receptor: A key molecule in the progression of prostate cancer to hormone independence. *J Cell Biochem.* 91:483-490.

Taplin, M.-E., G.J. Bubley, Y.-J. Ko, E.J. Small, M. Upton, B. Rajeshkumar, and S.P. Balk. 1999. Selection for Androgen Receptor Mutations in Prostate Cancers Treated with Androgen Antagonist. *Cancer Res.* 59:2511-2515.

Taplin, M.-E., G.J. Bubley, T.D. Shuster, M.E. Frantz, A.E. Spooner, G.K. Ogata, H.N. Keer, and S.P. Balk. 1995. Mutation of the Androgen-Receptor Gene in Metastatic Androgen-Independent Prostate Cancer. *N Engl J Med.* 332:1393-1398.

Taplin, M.-E., B. Rajeshkumar, S. Halabi, C.P. Werner, B.A. Woda, J. Picus, W. Stadler, D.F. Hayes, P.W. Kantoff, N.J. Vogelzang, and E.J. Small. 2003. Androgen Receptor Mutations in Androgen-Independent Prostate Cancer: Cancer and Leukemia Group B Study 9663. *J Clin Oncol.* 21:2673-2678.

Thompson, J., F. Saatcioglu, O.A. Jänne, and J.J. Palvimo. 2001. Disrupted Amino- and Carboxyl-Terminal Interactions of the Androgen Receptor Are Linked to Androgen Insensitivity. *Mol Endocrinol.* 15:923-935.

Thornton, J., and D. Kelley. 1998. Evolution of the androgen receptor: structure-function implications. *Bioessays.* 20:860-869.

Tomlins, S.A., D.R. Rhodes, S. Perner, S.M. Dhanasekaran, R. Mehra, X.-W. Sun, S. Varambally, X. Cao, J. Tchinda, R. Kuefer, C. Lee, J.E. Montie, R.B. Shah, K.J. Pienta, M.A. Rubin, and A.M. Chinnaiyan. 2005. Recurrent Fusion of TMPRSS2 and ETS Transcription Factor Genes in Prostate Cancer. *Science.* 310:644-648.

Toumazou, C., J. Li, and J. Wong. 2007. Cofactor Restriction by Androgen Receptor N-terminal and C-terminal Interaction. *Mol Endocrinol.* (in press).

Trapman, J. 2001. Molecular mechanisms of prostate cancer. *Eur J Cancer.* 37:S119-125.

Trapman, J., and H.J. Dubbink. 2007. The role of cofactors in sex steroid action. *Best Pract Res Clin Endocrinol Metab.* 21:403-414.

Trotter, K.W., and T.K. Archer. 2007. Nuclear receptors and chromatin remodeling machinery. *Mol Cell Endocrinol.* 265-266:162-167.

Tyagi, R.K., Y. Lavrovsky, S.C. Ahn, C.S. Song, B. Chatterjee, and A.K. Roy. 2000. Dynamics of Intracellular Movement and Nucleocytoplasmic Recycling of the Ligand-Activated Androgen Receptor in Living Cells. *Mol Endocrinol.* 14:1162-1174.

Van de Wijngaart, D.J., M. Molier, S.J. Lusher, R. Hersmus, G. Jenster, J. Trapman, and H.J. Dubbink. 2008. Differential ligand-responsiveness of androgen receptor L701 mutants. (in press).

Van de Wijngaart, D.J., M.E. van Royen, R. Hersmus, A.C.W. Pike, A.B. Houtsmuller, G. Jenster, J. Trapman, and H.J. Dubbink. 2006. Novel FXXFF and FXXMF Motifs in Androgen Receptor Cofactors Mediate High Affinity and Specific Interactions with the Ligand-binding Domain. *J Biol Chem.* 281:19407-19416.

Van Royen, M.E., S.M. Cunha, M.C. Brink, K.A. Mattern, A.L. Nigg, H.J. Dubbink, P.J. Verschure, J. Trapman, and A.B. Houtsmuller. 2007. Compartmentalization of androgen receptor protein-protein interactions in living cells. *J Cell Biol.* 177:63-72.

Veldscholte, J., C.A. Berrevoets, C. Ris-Stalpers, G.G.J.M. Kuiper, G. Jenster, J. Trapman, A.O. Brinkmann, and E. Mulder. 1992. The androgen receptor in LNCaP cells contains a mutation in the ligand binding domain which affects steroid binding characteristics and response to antiandrogens. *J Steroid Biochem Mol Biol.* 41:665-669.

Veldscholte, J., C. Ris-Stalpers, G.G.J.M. Kuiper, G. Jenster, C. Berrevoets, E. Claassen, H.C. van Rooij, J. Trapman, A.O. Brinkmann, and E. Mulder. 1990. A mutation in the ligand binding domain of the androgen receptor of human LNCaP cells affects steroid binding characteristics and response to anti-androgens. *Biochem Biophys Res Commun.* 173:534-540.

Verrijdt, G., A. Haelens, and F. Claessens. 2003. Selective DNA recognition by the androgen receptor as a mechanism for hormone-specific regulation of gene expression. *Mol Genet Metab.* 78:175-185.

Verrijdt, G., T. Tanner, U. Moehren, L. Callewaert, A. Haelens, and F. Claessens. 2006. The androgen receptor DNA-binding domain determines androgen selectivity of transcriptional response. *Biochem Soc Trans.* 34:1089-1094.

Wang, G.G., C.D. Allis, and P. Chi. 2007a. Chromatin remodeling and cancer, part II: ATP-dependent chromatin remodeling. *Trends Mol Med.* 13:373-380.

Wang, H., Z.-Q. Huang, L. Xia, Q. Feng, H. Erdjument-Bromage, B.D. Strahl, S.D. Briggs, C.D. Allis, J. Wong, P. Tempst, and Y. Zhang. 2001. Methylation of Histone H4 at Arginine 3 Facilitating Transcriptional Activation by Nuclear Hormone Receptor. *Science.* 293:853-857.

Wang, L., C. Hsu, and C. Chang. 2004a. Androgen receptor corepressors: An overview. *Prostate.* 63:117-130.

Wang, L., C.-L. Hsu, J. Ni, P.-H. Wang, S. Yeh, P. Keng, and C. Chang. 2004b. Human Checkpoint Protein hRad9 Functions as a Negative Coregulator To Repress Androgen Receptor Transactivation in Prostate Cancer Cells. *Mol Cell Biol.* 24:2202-2213.

Wang, Q., W. Li, X.S. Liu, J.S. Carroll, O.A. Jänne, E.K. Keeton, A.M. Chinnaiyan, K.J. Pienta, and M. Brown. 2007b. A hierarchical network of transcription factors governs androgen receptor-dependent prostate cancer growth. *Mol Cell.* 27:380-392.

Wang, Q., D. Sharma, Y. Ren, and J.D. Fondell. 2002. A coregulatory role for the TRAP-mediator complex in androgen receptor-mediated gene expression. *J Biol Chem.* 277:42852-42858.

Wang, W., Y. Xue, S. Zhou, A. Kuo, B.R. Cairns, and G.R. Crabtree. 1996. Diversity and specialization of mammalian SWI/SNF complexes. *Genes Dev.* 10:2117-2130.

Weake, V.M., and J.L. Workman. 2008. Histone Ubiquitination: Triggering Gene Activity. *Mol Cell.* 29:653-663.

Werner R, Z.J., Gesing J, Struve D, Hiort O. 2008. In-vitro characterization of androgen receptor mutations associated with complete androgen insensitivity syndrome reveals distinct functional deficits. *Sex Dev.* 2:73-83.

Williams, S.P., and P.B. Sigler. 1998. Atomic structure of progesterone complexed with its receptor. *Nature.* 393:392-396.

Wissmann, M., N. Yin, J.M. Muller, H. Greschik, B.D. Fodor, T. Jenuwein, C. Vogler, R. Schneider, T. Gunther, R. Buettner, E. Metzger, and R. Schule. 2007. Cooperative demethylation by JMJD2C and LSD1 promotes androgen receptor-dependent gene expression. *Nat Cell Biol.* 9:347-353.

Wong, C., Z. Zhou, M. Sar, and E. Wilson. 1993. Steroid requirement for androgen receptor dimerization and DNA binding. Modulation by intramolecular interactions between the NH2-terminal and steroid-binding domains. *J Biol Chem.* 268:19004-19012.

Xu, J., and Q. Li. 2003. Review of the in Vivo Functions of the p160 Steroid Receptor Coactivator Family. *Mol Endocrinol.* 17:1681-1692.

Yamane, K., C. Toumazou, Y.-i. Tsukada, H. Erdjument-Bromage, P. Tempst, J. Wong, and Y. Zhang. 2006. JHDM2A, a JmjC-Containing H3K9 Demethylase, Facilitates Transcription Activation by Androgen Receptor. *Cell.* 125:483-495.

Yang, C.-S., H.-W. Xin, J.B. Kelley, A. Spencer, D.L. Brautigan, and B.M. Paschal. 2007. Ligand Binding to the Androgen Receptor Induces Conformational Changes That Regulate Phosphatase Interactions. *Mol Cell Biol.* 27:3390-3404.

Yong, W., Z. Yang, S. Periyasamy, H. Chen, S. Yucel, W. Li, L.Y. Lin, I.M. Wolf, M.J. Cohn, L.S. Baskin, E.R. Sanchez, and W. Shou. 2007. Essential Role for Co-chaperone Fkbp52 but Not Fkbp51 in Androgen Receptor-mediated Signaling and Physiology. *J Biol Chem.* 282:5026-5036.

Yoon, H.-G., and J. Wong. 2006. The Corepressors Silencing Mediator of Retinoid and Thyroid Hormone Receptor and Nuclear Receptor Corepressor Are Involved in Agonist- and Antagonist-Regulated Transcription by Androgen Receptor. *Mol Endocrinol.* 20:1048-1060.

Zhao, X., B. Boyle, A. Krishnan, N. Navone, D. Peehl, and D. Feldman. 1999. Two mutations identified in the androgen receptor of the new human prostate cancer cell line MDA PCa 2a. *J Urol.* 162:2192-2199.

Zhao, X., P. Malloy, A. Krishnan, S. Swami, N. Navone, D. Peehl, and D. Feldman. 2000. Glucocorticoids can promote androgen-independent growth of prostate cancer cells through a mutated androgen receptor. *Nat Med.* 6:703-706.

Zheng, Z., C. Cai, J. Omwancha, S.-Y. Chen, T. Baslan, and L. Shemshedini. 2006. SUMO-3 Enhances Androgen Receptor Transcriptional Activity through a Sumoylation-independent Mechanism in Prostate Cancer Cells. *J Biol Chem.* 281:4002-4012.

Zhou, Z., M. Lane, J. Kemppainen, F. French, and E. Wilson. 1995. Specificity of ligand-dependent androgen receptor stabilization: receptor domain interactions influence ligand dissociation and receptor stability. *Mol Endocrinol.* 9:208-218.

Zhou, Z., M. Sar, J. Simental, M. Lane, and E. Wilson. 1994. A ligand-dependent bipartite nuclear targeting signal in the human androgen receptor. Requirement for the DNA-binding domain and modulation by NH2-terminal and carboxyl-terminal sequences. *J Biol Chem.* 269:13115-13123.

Zhou, Z.-x., B. He, S.H. Hall, E.M. Wilson, and F.S. French. 2002. Domain Interactions between Coregulator ARA70 and the Androgen Receptor (AR). *Mol Endocrinol.* 16:287-300.

Zilliacus, J., A. Wright, J. Carlstedt-Duke, and J. Gustafsson. 1995. Structural determinants of DNA-binding specificity by steroid receptors. *Mol Endocrinol.* 9:389-400.

Zoppi, S., M. Marcelli, J. Deslypere, J. Griffin, J. Wilson, and M. McPhaul. 1992. Amino acid substitutions in the DNA-binding domain of the human androgen receptor are a frequent cause of receptor-binding positive androgen resistance. *Mol Endocrinol.* 6:409-415.

Chapter 2

FRAP to Study Nuclear Protein Dynamics in Living Cells

Van Royen, M.E., P. Farla, K.A. Mattern, B. Geverts, J. Trapman, and A.B. Houtsmuller.

In The Nucleus. (2009) Vol. 464. R. Hancock, editor.

Humana Press / Springer, Totowa. 363-385.

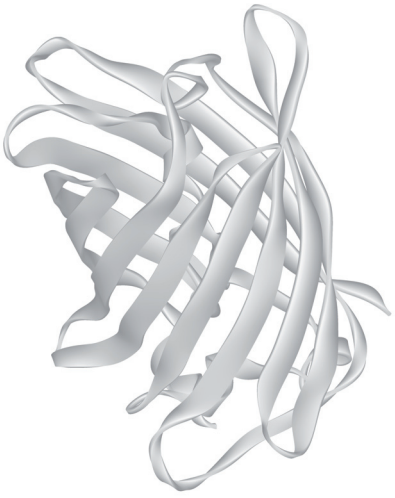

ABSTRACT

Proteins involved in chromatin-interacting processes, like gene transcription, DNA replication and DNA repair, bind directly or indirectly to DNA, leading to their immobilization. However, to reach their target sites in the DNA the proteins have to somehow move through the nucleus. Fluorescence recovery after photobleaching (FRAP) has been shown to be a strong approach to study exactly these properties, i.e. mobility and (transient) immobilization of the proteins under investigation. Here, we provide and discuss detailed protocols for some of the FRAP procedures that we used to study protein behavior in living cell nuclei. In addition, we provide examples of their application in the investigation of the androgen receptor (AR), a hormone inducible transcription factor, and of two DNA-maintenance factors, the telomere binding proteins TRF1 and TRF2. We also provide protocols for qualitative FRAP-analysis and a general scheme for computer modelling of the presented FRAP procedures that can be used to quantitatively analyse experimental FRAP curves.

Key words: FRAP, Protein Mobility, Confocal Microscopy, Androgen Receptor and Fluorescent Proteins

1 INTRODUCTION

1.1 Green Fluorescent Protein

In the past decade genetic labeling with fluorescent proteins has caused a revolution in molecular cell biological research. Ever since they became available, GFP and its color variants have been used at a tremendous scale to study the dynamic behavior of proteins in their most natural environment, the living cell. GFP was derived from the jellyfish *Aequorea Victoria* (Tsien, 1998). By mutagenesis of wild type GFP, enhanced versions such as EGFP with improved brightness and expression properties (reviewed in Lippincott-Schwartz and Patterson, 2003). In addition, currently a large array of color variants has been generated (reviewed in Heim and Tsien, 1996; Shaner et al., 2005). GFP and its color variants provide minimally invasive tools, not only to determine the dynamic intracellular localization using *e.g.* confocal time-lapse imaging, but also to study of the dynamic behavior of proteins in living cells (reviewed in Giepmans et al., 2006).

1.2 Fluorescence Recovery After Photobleaching (FRAP)

Proteins involved in DNA-interacting processes, like DNA repair, DNA replication and transcription, bind directly or indirectly to DNA to exert their function. To reach their target sites in the DNA, either DNA damage, replication origins or transcription sites, nuclear proteins have to move through the nucleus. Fluorescence recovery after photobleaching (FRAP) has proven to be a strong approach to qualitatively or quantitatively study exactly these properties, *i.e.* the mobility and (transient) immobilization of molecules in living cells (McNally et al., 2000; Stenoien et al., 2001; Schaaf and Cidlowski, 2003; Farla et al., 2004; Agresti et al., 2005; Farla et al., 2005; and reviewed in Houtsmuller, 2005; Rayasam et al., 2005). FRAP was developed in the 1970s, by Axelrod and coworkers. Early FRAP investigations were focused on the mobility of fluorescently labelled constituents of the cell membrane (Axelrod D, 1976). The development in the 1980s and 1990s of confocal microscopy and GFP-technology enormously enhanced the applicability of FRAP. Currently, by far the most FRAP studies use confocal microscopes, although also wide-field systems are becoming increasingly available (*e.g.* Fukano et al., 2004).

In a typical FRAP experiment, a small defined region within a larger volume (for instance the cell nucleus) is shortly illuminated at high laser intensity (Fig. 1A) (Houtsmuller, 2005). Immediately after the bleach-pulse the majority of the GFP-tagged proteins within the region irreversibly have lost their fluorescent properties, a process referred to as photobleaching. In a situation where all GFP-tagged proteins are mobile, proteins from outside will diffuse into the bleached region resulting in an increase of the fluorescent signal in the region until the signal inside the bleached region is equal to the signal outside the bleached region. In contrast, if permanently immobile proteins are present, these will not diffuse into the strip, resulting in an incomplete recovery of the fluorescent signal inside the bleached region relative to the

remainder of the nucleus (Fig. 1B) (*see* **Note 1**). Transient immobilization, as was observed for many active nuclear proteins, including the AR, results in a delayed, secondary fluorescence recovery in the bleached region because the fraction of immobilized proteins will release and become mobile during the FRAP experiment, and then contribute to fluorescence recovery but later than the mobile fraction (Fig. 1) (Houtsmuller, 2005). Summarizing, FRAP experiments yield information on essentially three mobility parameters: diffusion coefficient, immobile fraction and the time spent in the immobile state. Assuming elementary binding kinetics, the size of the immobile fraction and the duration of immobilization are determined by the on- and off-rates of the investigated protein to and from immobile complexes (*see* **Note 2**).

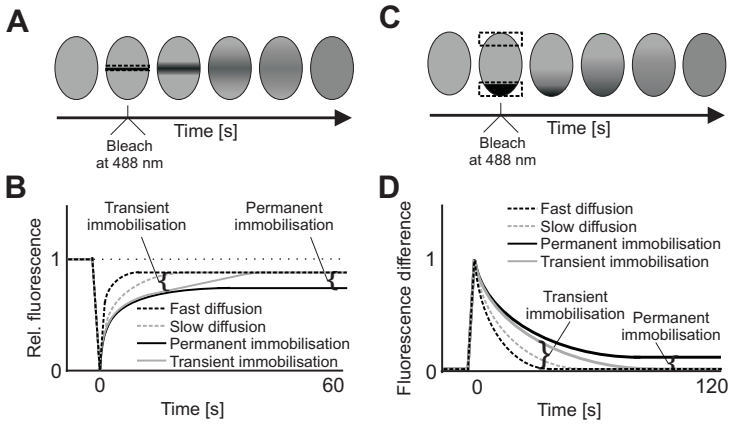

Figure 1. Schematic representation of the principles of strip-FRAP and combined FLIP-FRAP. (A) In strip FRAP, the recovery of GFP fluorescence is recorded in time after shortly bleaching a small strip spanning the nucleus. (B) Strip-FRAP curves representing different scenarios are expressed relative to prebleach values and the intensity directly after bleaching. Permanent immobilization of GFP tagged proteins (*solid black curve*) can be identified by an incomplete recovery compared to FRAP curves of molecules that are freely mobile (*dotted black curve* with fast diffusion and *dotted grey curve* with slow diffusion). Transient immobilization leads to a secondary recovery of fluorescence (*solid grey curve*). (C) In FLIP-FRAP experiments the fluorescence in the bleached region and in the region at the opposite nuclear pole are recorded in time after photobleaching until a new steady state is reached. (D) The differences in fluorescence between the two opposite poles identify the different scenarios. Similar to strip FRAP a permanent immobilization results is an incomplete redistribution and thus a constant difference between both signals in the two measured regions.

Several variants of FRAP have been developed, including spot-FRAP, strip-FRAP, FLIP (fluorescence loss in photobleaching) (Houtsmuller and Vermeulen, 2001), combined FLIP-FRAP (Hoogstraten et al., 2002; Farla et al., 2004; Mattern et al., 2004; Farla et al., 2005) and iFRAP (inverted FRAP) (Dundr et al., 2002). Spot-FRAP is based on photobleaching of a small spot whereas in strip-FRAP, a larger region, for instance a narrow strip spanning the nucleus is bleached. The latter method is favorable when signals are very low, *e.g.* due to low expression of the GFP-tagged protein. In a very common variant of FRAP, FLIP the loss of fluorescence in a region or structure distant from the bleached region is monitored. FRAP and FLIP can also

be combined (FLIP-FRAP): two regions at two poles of an ellipsoid nucleus are monitored simultaneously after bleaching only one of them. FLIP and combined FLIP/FRAP are specifically useful to determine the residence time of proteins inside subnuclear structures, such as telomeres, repair foci or speckles. In iFRAP the entire nucleus is bleached with exception of a structure of interest. Immediately after bleaching, loss of fluorescence in the structure fully represents the off-rate of the associated protein (*see* **Note 3**).

1.3 Application of FRAP to proteins in the living cell nucleus

Application of FRAP to investigate the dynamic behavior of nuclear proteins have provided new insights in nuclear protein function. The first FRAP studies revealed an unexpected high mobility of many nuclear factors, including components of the nucleotide excision repair (NER) machinery, which removes certain types of single strand DNA damage (Houtsmuller et al., 1999; Sporbert et al., 2002; Rademakers et al., 2003; Essers et al., 2005; Zotter et al., 2006), transcription factors (McNally et al., 2000) and RNA-splicing factors (Phair and Misteli, 2000). It was shown that in the absence of DNA damage the NER-factors ERCC1/XPF (Houtsmuller et al., 1999), XPA (Rademakers et al., 2003), PCNA (Sporbert et al., 2002; Essers et al., 2005) and recently XPG (Zotter et al., 2006) were highly mobile in living cells and bind transiently to DNA damage. Similarly, high mobility and transient immobilization due to DNA-binding were found for steroid receptors (McNally et al., 2000; Farla et al., 2004) and for many more nuclear proteins with roles in a diversity of other processes (Phair et al., 2004), including double strand break repair (Essers J, 2002; Lukas et al., 2003; Lukas et al., 2004; Bekker-Jensen et al., 2005), DNA replication (Leonhardt et al., 2000; Sporbert et al., 2002; Essers et al., 2005), chromatin structure (Kimura and Cook, 2001; Mattern et al., 2004; Chen et al., 2005; Kimura, 2005) and RNA processing and transcription (Kruhlak et al., 2000; Phair and Misteli, 2000; Dundr et al., 2002; Kimura et al., 2002; Chen et al., 2005).

1.4 Examples of FRAP applications: Androgen receptors and telomere binding proteins

In this chapter we provide detailed procedures for two types of FRAP, strip-FRAP and combined FLIP-FRAP to study the dynamic behavior of the androgen receptor (AR) and give an example of a investigation of the telomere binding proteins TRF1 TRF2. We will also provide methods to qualitatively analyze FRAP-curves (Fig. 2) as well as an elementary modeling algorithm to generate FRAP curves with varying mobility parameters to fit and quantify the experimental data (Fig. 3).

The AR is a hormone-induced transcription factor and a member of the nuclear receptor (NR) superfamily. The AR is involved in the development and maintenance of the male phenotype and also plays a crucial role in the development and progression of prostate cancer (Feldman and Feldman, 2001; Trapman, 2001). Like all NRs the AR consists of three domains: a conserved DNA binding domain (DBD), a C-terminal ligand-binding domain (LBD) and a

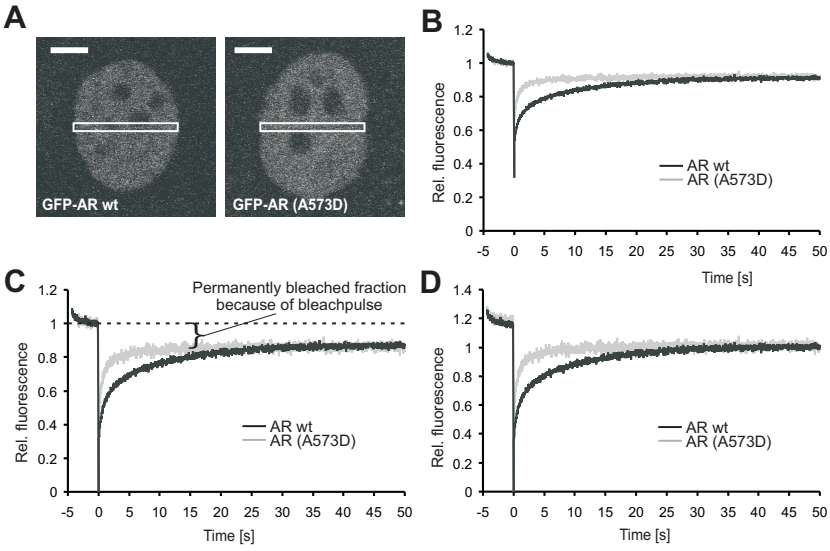

Figure 2. Strip FRAP applied to wild type and mutant ARs. (A and B) Confocal images of Hep3B cells stably expressing GFP-AR (wild type) or the DNA binding deficient mutant (GFP-AR (A573D)) (A) and their strip FRAP curves normalized by the three different normalization procedures given in 3.4.3 (B-D) (Bar corresponds to 5 μm). The recovery of fluorescence in a small strip spanning the nucleus (white box in A) is recorded in time after shortly photobleaching the fluorescence. (B) The most straightforward normalization procedure is to normalize the data relative to prebleach fluorescence intensities. Comparing normalized data of active versus inactive proteins like wild type AR and AR (A573D) used here enables identification of transient and permanent immobilization. The wild type AR shows a slower total recovery of fluorescence compared to the non-DNA binding mutant (AR (A573D)) due to transient immobilization of wild type AR. The difference in intensity of the DNA binding deficient AR (A573D) before and after complete recovery does not reflect a permanent immobilization but is caused by the permanent bleaching of a fraction of protein by the bleach pulse. Curves represent data of at least 10 cells. (C) Applying a second normalization procedure, correcting possible variations in bleach-depths, data is expressed relative to prebleach intensities and the intensity directly after bleaching. The difference between prebleach intensity and the intensity after complete redistribution of AR (A573D) reflects the permanently bleached fraction due to the bleach pulse. (D) A third way of normalization yields a curve running from 0 directly after bleaching, to 1 after complete recovery, allowing also quantitative analysis by fitting the data to any equation that represents the diffusion process (and transient immobilization) (Houtsmuller, 2005). After this normalization it is no longer possible to extract information on permanent immobilization (3.4.3).

more variable N-terminal domain (NTD) (Brinkmann et al., 1989). Ligand activated ARs translocate to the nucleus where they exert their activity by binding to specific androgen response elements (AREs) in promoter and enhancer sequences of AR regulated genes (Cleutjens et al., 1997; Claessens et al., 2001). Several FRAP studies show a high mobility and transient immobilization not only of the AR but also of other nuclear receptors (NRs) (Fig. 4) (McNally et al., 2000; Stenoien et al., 2001; Farla et al., 2004; Farla et al., 2005; Rayasam et al., 2005; Schaaf et al., 2005; Van Royen et al., 2007). This immobilization is lost in a non-DNA-binding AR mutant (AR A573D) (Bruggenwirth et al., 1998; Farla et al., 2004) and in wild type AR in the presence of antagonists (Farla et al., 2005). In FRAP experiments direct comparison of active versus inactive states, like DNA repair proteins in the presence or absence of DNA damage or non-DNA binding transcription factor mutants in transcription greatly simplifies the interpre-

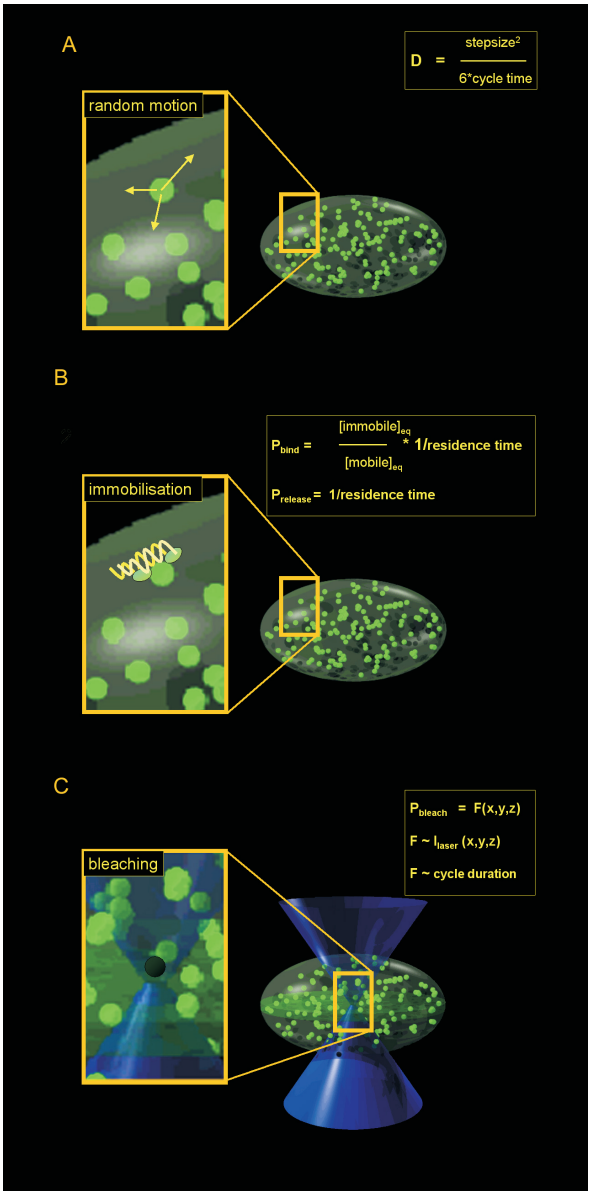

Figure 3. General scheme for Monte Carlo simulation of FRAP on nuclear proteins.

(A) Schematic drawing of a cell nucleus (green ellipsoid) containing randomly distributed GFP-tagged proteins (green spheres). Random Brownian motion (inset) is simulated on the basis of the Einstein-Smoluchowsky equation D = stepsize² / 6 * cycle time (see 3.4.4). (B) Simulation of binding to randomly distributed immobile target sites in the DNA (inset) is simulated by evaluating a chance to bind or to release based on simple binding kinetics, where the ratio between on- and off-rates (defined by k_{on} and k_{off}, see 3.4.4) equals the ratio between the number of immobile and mobile molecules. (C) Photobleaching is simulated by evaluating a chance to get bleached based on the intensity profile of the laser beam. This profile can be obtained experimentally by illuminating a paraformaldehyde-fixed nucleus with a stationary laser beam at different intensities and collecting 3-D image stacks afterwards. Also GFP-blinking can be simulated (*see* **Note 25**).

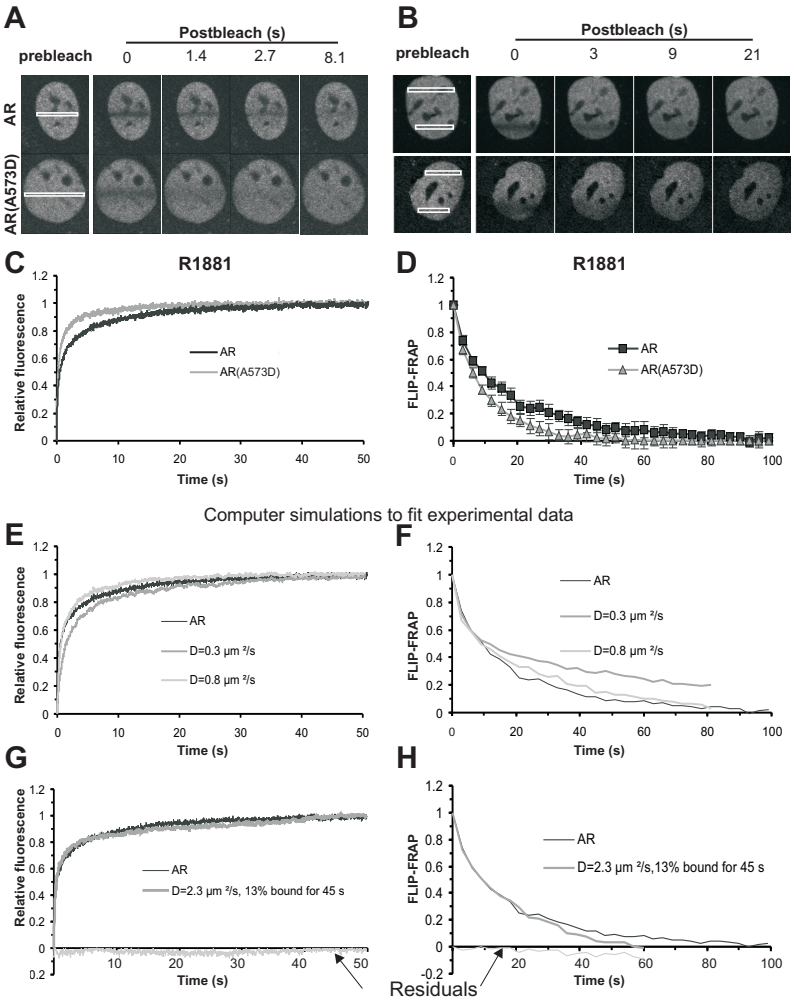

Figure 4. Combined strip-FRAP and FLIP-FRAP reveal that a fraction of agonist-liganded GFP-ARs is transiently immobilized. (A) In the strip-FRAP procedure a strip in the center of a nucleus is bleached (rectangle) at high laser power. Subsequently, fluorescence in the strip is measured at regular time intervals. (B) In the FLIP-FRAP procedure a strip at one pole of the nucleus was bleached for a relatively long period. The difference between fluorescence signals in the bleached region (FRAP, lower rectangle) and a distal region at 10 µm from the bleached region of the nucleus (FLIP, upper rectangle) was determined at regular time intervals. (C, D) Strip-FRAP and FLIP-FRAP experiments of GFP-AR or the non-DNA-binding mutant GFP-AR(A573D) in the presence of an agonistic ligand (10^{-9} M R1881). (C) Graph showing fluorescence intensities relative to complete redistribution of the non-DNA-binding mutant GFP-AR(A573D) in the presence of R1881 plotted as a function of time. Mean values of at least 10 cells are plotted. All experiments were performed at least three times. (D) Graph showing the difference between fluorescence intensity in the FLIP and FRAP regions (rectangles in B) relative to the difference directly after bleaching, plotted against time. Mean values +/- two times the S.E.M. of two independent experiments on at least ten cells are plotted. (E, F) Computer simulations of strip-FRAP and FLIP-FRAP of freely diffusing molecules do not explain the experimental FRAP data obtained with both methods. Experimental strip-FRAP data on wild-type GFP-AR lies in between curves representing indicated scenarios of free diffusion (E), whereas experimental FLIP-FRAP data on wild-type GFP-AR lies outside these boundaries (F). (G, H) Computer simulations representing a model where, next to freely diffusing molecules, a fraction is transiently immobilized, fitted to both strip-FRAP and FLIP-FRAP experimental curves on wild-type GFP-AR. Computer simulations correspond to the average

of best fits of FRAP and FLIP-FRAP experiments respectively, so are not necessarily the best fits of the individual experiments. Absolute value of residuals of the computer simulation fit and the experimental data on each time point are plotted below the x-axis. (Figure adapted from Farla et al., 2005).

tation of the generated data. Computer simulation aided analysis of combined experimental strip-FRAP and FLIP-FRAP data (Fig. 4A-D) showed that the wild type AR kinetics could not be described by a model of freely diffusing molecules only (Fig. 4E and F). A model of freely diffusing molecules together with a transiently immobilized fraction fitted to both strip-FRAP and FLIP-FRAP curves (Fig. 4G and H) (Farla et al., 2005).

A second example of FRAP application concerns the investigation of telomere binding proteins. Telomeres are nucleoprotein structures at chromosome ends. Telomere binding proteins play a key role in the regulation of the length of the telomeric DNA tract. In addition these proteins prevent end-to-end fusion of chromosomes. Application of FRAP to two telomeric proteins (TRF1 and 2) revealed that telomere binding occurs in a complex dynamic fashion (Fig. 5).

2 MATERIALS

2.1 Constructs

1. Standard EGFP, EYFP and ECFP vectors are used for cloning (Clontech, Palo Alto, CA)(*see* **Note 4**).
2. pAR0, expressing human full-length wild-type AR (Brinkmann et al., 1989) is used to fuse the AR with the fluorescent proteins.

2.2 Cell Culture and transfection

1. Hep3B Human Hepatocellular Carcinoma Cell line (ATCC #HB-8064)(*see* **Note 5**).
2. Alfa Minimal Essential Medium (αMEM) (Bio-Whittaker/Cambrex, Verviers, Belgium) supplemented with 2 mM L-glutamine (Bio-Whittaker/Cambrex), 100 U/mL Penicillin / 100 µg/mL Streptomycin (Bio-Whittaker/Cambrex) and 5% triple 0.1µM sterile filtered fetal bovine serum (FBS)(HyClone, South Logan, UT). Store at 2-8˚C.
3. HyQ G418 sulfate (HyClone), working solution is 100 mg/mL active concentration in PBS. Final concentration in culture medium is 0.6 mg/mL G418 (*see* **Note 6**).
4. Methyltrienolone (R1881) (NEN DuPont, Boston, USA). R1881 is dissolved in EtOH to 1 mM stock solution. The stock is stepwise diluted (1:10) in EtOH up to 1 nM R1881 to generate an array of working solutions. For our experiments we used the 1 µM R1881 working solution to obtain a final concentration of 1 nM of hormone in our culture medium. R1881 is light sensitive and store at –18˚C.

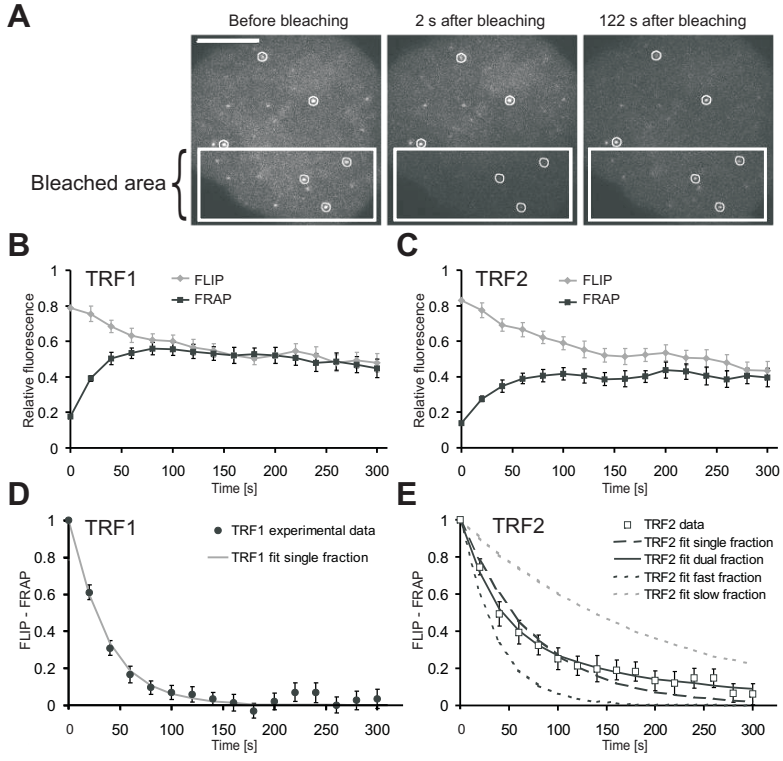

Figure 5. Simultaneous FLIP-FRAP of telomere-bound proteins TRF1 and TRF2. (A) FLIP-FRAP on living HeLa cells expressing GFP-TRF1. Cells are photobleached over a region covering about one-half of the nucleus (indicated by a white box). The images were acquired before bleaching and at 20 s intervals after bleaching, starting at 2 s. The circles in the bleached area and unbleached area indicate the regions that are used to calculate fluorescence redistribution. Scale bar, 5 μm. (B, C) Quantitative analysis of redistribution of GFP-TRF1 (B) and GFP-TRF2 (C) at telomeres separately in bleached (*in white box*) and unbleached (*upper*) half of the nucleus. Values are means +/- the SEM from at least 40 cells. (D) Difference (Δ) in telomere intensity in bleached and unbleached part of cell, calculated from the data shown in panels B (TRF1) and C (TRF2). (E) A fitting analysis of the experimental data in panel D to the equation $\Delta I_{rel}(t) = f_1 e{-}k_1 t + f_2 e{-}k_2 t$ indicated a good fit with the single binding kinetics of GFP-TRF1 (*solid grey line*). In contrast, GFP-TRF2 redistribution does not fit with single binding kinetics (*dotted black line*) but does fit with dual binding kinetics (*solid black line*). Note the similarity between the fitted curves of the fast fraction of TRF2 and of TRF1. (Figure adapted from Mattern et al., 2004).

5. Trypsin EDTA (Bio-Whittaker/Cambrex), 200 mg/L Versene (EDTA), 500 mg/L Trypsin 1:250. Sterile filtered. Store stock at –10˚C and working solution at 2-8˚C.
6. Ø 24 mm cover slips (thickness: 0,13 - 0,16 mm) (Menzer-Gläser/Menzel Gerhard GmbH, Braunschweig, Germany)(*see* **Note 7**).
7. Polystyrene 6 Wells Cell Culture Cluster (Corning B.V. Life Sciences, Schiphol-Rijk, Netherlands).
8. FuGENE6 transfection medium (Roche Molecular Biochemicals, Indianapolis, IN). Store at 2 - 8˚C.

2.3 Generation of stable cell lines

1. Falcon 100 x 20 mm polystyrene Tissue Culture Dishes (Falcon; BD Biosciences, Alphen an den Rijn, Netherlands).
2. Polystyrene 6 Wells Cell Culture Cluster (Corning B.V. Life Sciences).
3. HyQ G418 sulfate (HyClone), working solution is 100 mg/mL active concentration in PBS. Final concentration in culture medium is 0.6 mg/mL (*see* **Note 6**).

2.4 Fluorescence Recovery After Photobleaching (FRAP)

1. All the quantitative FRAP procedures are performed on a Zeiss Confocal Laser Scanning Microscope LSM510 META equipped with a 40x/1.3A NA oil immersion objective, a Lasos LGK 7812 ML-4 Laser Class 3 B Argon laser (30 mW) with the excitation laser lines 458, 488 and a acousto-optical tunable filter (AOTF) (Carl Zeiss MicroImaging GmbH, Jena, Germany) (*see* **Note 8**).
2. The filter set to specifically image GFP is shown in Table 1 (*see* **Note 4**).
3. Temperature is controlled by a heatable stage and a lens-heating device both developed in our laboratory (*see* **Note 9**). The LSM 5 software, Version 3.2 controls the microscope, the scanning and laser modules, and the image acquisition process. This software is also used to analyze the images.

Table 1: Filter sets used in FRAP experiments.

Fluorophore	Excitation	Main beam splitter	Secondary beam splitter	Emission filter
EGFP	488 nm	HFT 488	Mirror	BP 505-530
ECFP	458 nm	HFT 458/514	NFT 515	BP 470-500
EYFP	514 nm	HFT 458/514	NFT 515	LP 560

3 METHODS

3.1 Constructs

1. The GFP-AR coding construct is generated by performing PCR on pAR0 (Brinkmann et al., 1989) using a sense primer (5′-GCAGAAGATCT**GCAGGTGCTGGAGCAGGTGCTGGAGCAGGTGCTGGA**GAAGTGCAGTTAG-3′) to introduce a *Bgl*II restriction site and a flexible $(GlyAla)_6$ spacer sequence and an anti-sense primer in the AR cDNA overlapping a *Sma*I site (5′-TTGCTGTTCCTCATCCAGGA-3′) (*see* **Note 10**). The PCR product is cloned in pGEM-T-Easy (Promega, Madison, WI) and the sequence is verified. The *Bgl*II-*Sma*I fragment is inserted in the corresponding sites of pEGFP-C1. Next the SmaI fragment from pAR0 is inserted into the *Sma*I site to generate pGFP-$(GlyAla)_6$-AR (further referred to as GFP-AR).

2. The non-DNA-binding mutant is obtained by exchanging the *Asp*718I-ScaI fragment from pAR(A573D) in GFP-AR.

3.2 Cell Culture and Cell Transfection (*see* Note 11)

1. Hep3B cells are grown in αMEM supplemented with L-Glutamine, Penicillin, Streptomycin and 5% FCS at 37˚C and 5% CO_2 and passaged when approaching confluence (every 3-4 days) with Trypsin/EDTA to provide experimental cultures.
2. Two days before confocal microscopy Hep3B cells are seeded on a coverslip in a 6-wells plate at a concentration of approx. 3.10^5 cells per well in 2 mL αMEM with 5% FCS (*see* **Note 12**). This concentration will provide near confluent cultures at the time of the experiment and a sufficient amount of cells at the time of transfection. The cells are grown overnight at 37˚C with 5% CO_2.
3. Between 24 and 32 hours before confocal microscopy the medium is replaced by 1 mL αMEM supplemented with 5% charcoal striped serum (DCC), L-gutamine and antibiotics, without washing the cells.
4. After 2 hours the transfection mix is prepared for the transfection of 1 μg of GFP-AR coding vector. Three μL FuGENE6 per μg DNA to be transfected is added to 100 μL serum free αMEM. After five minutes incubation DNA is added. The transfection mix is then gently mixed by pipeting up and down, and left at room temperature for at least 30 minutes (*see* **Note 13**).
5. Four hours after medium replacement the transfection mix is gently added to the cells under gentle mixing. The cells are then incubated for 4 hours at 37˚C and 5% CO_2.
6. Four hours after transfection the medium is replaced again by 2 mL αMEM supplemented with charcoal striped serum (DCC) with or without 1 nM R1881. The cells are further incubated overnight at 37˚C and 5% CO_2.

3.3 Generation of stable cell lines

To avoid transfections before each experiment and to simplify the selection of cells with physiologically relevant expression level of the tagged protein, a cell line stably expressing a receptor with fluorescent label(s) can be generated. It is often stated that the use of cells stably expressing fusion proteins is essential to avoid overexpression, but microscopic approaches enables preselection of cells with a physiological expression level also in transient transfected cells. With this in mind, also transiently transfected cells can be studied when a sufficient number of cells in the required expression range can be found (*see* **Note 11**).

1. Hep3B cells are seeded in 6 wells of a 6 wells plate in αMEM with 5 % FCS as described before and incubated overnight at 37˚C and 5 % CO_2.
2. After overnight incubation cells in all 6 wells are transfected with the same expression vector (1 μg DNA for each well) as described before.

3. Four hours after transfection the medium is replaced by 2 mL αMEM / 5 % FCS and the cells are incubated overnight at 37˚C and 5 % CO_2.
4. After overnight incubation the cells are trypsinated and an array of dilutions ranging from (9:10 to 1:1000) are seeded in 10 cm dishes. The Hep3B cells are incubated again overnight at 37˚C and 5 % CO_2.
5. After another overnight incubation the medium is replaced by αMEM with 5% FCS supplemented with 0.6 mg/mL G418 (active concentration). The cells are further incubated at 37˚C / 5 % CO_2. Twice a week the medium is replaced by fresh medium with G418.
6. When clones grown from single cells consist of 100 to 200 cells, the locations of the colonies are indicated with a fine marker underneath the bottom of the dish. Using a 200 μL pipette each clone is carefully scrapped while slowly collecting the cells by pipetting.
7. The collected cells are seeded in a glass bottomed 24 wells dish in 1 mL αMEM with G418 and incubated for 1 or 2 weeks.
8. When the clones have grown the expression of GFP-AR is judged by confocal microscopy. The clones with sufficient expression are passaged and used for experiments (*see* **Note 14**).

3.4 Fluorescence Recovery After Photobleaching (FRAP)

3.4.1 Strip-FRAP

In the most elementary FRAP experiment the small circular area that is illuminated by a stationary laser beam (the diffraction limited spot) is bleached and the recovery of fluorescence inside the spot is monitored in time (Axelrod D, 1976). The use of a confocal scanning microscope makes it possible to bleach larger areas by scanning at high intensity. In addition, not only the recovery of fluorescence in the bleached area, but also the fluorescence in the entire nucleus can be monitored.

There may be several potential drawbacks of bleaching a small area. First, the recovery of fluorescence is very fast, possibly too fast for the imaging system, especially when the entire nucleus is imaged. Second, the amount of fluorescence emitted by the limited number of molecules in a single spot is relatively low, leading to low signal-to-noise levels. Third, the relative location of the bleached spot inside the nucleus may influence the recovery curve. Therefore, we provide a FRAP protocol, designated strip-FRAP, in which a narrow is strip is bleached with a width of ~700nm (corresponding to 10 pixels at zoom 6 on a Zeiss LSM 510 microscope) and spanning the entire nucleus. To assure a sufficient time resolution to also follow fast diffusion processes (like diffusion of free GFP), only the fluorescence in the bleached strip is monitored after photobleaching (Fig. 1A and Fig. 4A and C).

1. These instructions assume use of a Zeiss CLSM 510 confocal laser-scanning microscope. For GFP-imaging in general an Argon laser is used. The Argon laser is adjusted to 6.1 A tube current and allowed to prewarm for at least 15 min.
2. For live cell imaging an inverted microscope is used. Cells are grown on a coverslip that forms the bottom of a container enabling the addition of medium on top of the cells. In the examples given here we investigated Hep3B cells expressing GFP-tagged androgen receptor (GFP-AR). The glass bottom container containing the cells and medium is transferred into a heatable stage holder at 37°C (*see* **Note 9**), which is mounted on a motorized scan stage
3. GFP-fluorescence is detected using 488 nm excitation, usually by an argon laser, using a 488 nm beam splitter, a band pass emission filter passing GFP emission at 505-530 nm (Table 1) (*see* **Note 4**). Cells were imaged using a 40x/1.3 NA oil objective. The confocal pinhole is adjusted such that the estimated optical slice thickness is ~2 μm (corresponding to 2.48 Aery Units). Scanning is performed unidirectional with scan speed 9 to enable fast recording of the fluorescent signal in the strip. Laser intensity is attenuated to approximately 1% of the maximum output using an AOTF for scanning (~0.5-0.8 μW). Detector gain is set on 900, the amplifier offset of 0 and an amplifier gain of 1. Fluorescent signals are recorded with an 8-bit data depth (*see* **Note 15-17**).
4. A nucleus expressing GFP-AR at physiologically relevant expression level (*see* **Note 18**) is selected at zoom 1 (*see* **Note 19**). To limit potential effects of nuclear shape, all nuclei are oriented in the same way relative to the bleaching strip (in our experiments we make sure that the longer axis of the more or less ellipsoid shaped nucleus is perpendicular to the strip. When the nucleus is oriented correctly zoom is adjusted to 6 corresponding to a lateral pixel distance of 70 nm. A 10 pixel wide (700 nm) strip spanning the nucleus is selected in the Edit ROI panel, for recording the recovery of the signal. (Fig. 1A) (*see* **Note 20**).
5. The fluorescent signal is monitored at 21 msec intervals by scanning the ROI for 4000 iterations (~80 sec) (Time Series Control) at low excitation (*see* **Note 21**). After 200 scans GFP is bleached locally inside the ROI using a scan (1 or 2 iterations) of at maximum intensity (Fig. 1A). The time-series are initiated using the Mean ROI option in the time-series control (*see* **Note 22** and **23**). After the scan the data can be copied directly to Excel or the file can be saved as data-file for later analysis.

3.4.2 FLIP-FRAP

Next to the comparison of FRAP curves obtained from proteins under different experimental conditions it may be useful to apply two different FRAP variants to a protein under the same conditions. For instance, the combination of strip-FRAP (Fig. 1A and B) and combined FLIP-FRAP (Fig. 1C and D) can be used to investigate transient immobilization (Houtsmuller and Vermeulen, 2001; Farla et al., 2004; Houtsmuller, 2005). This approach is based on the fact that

often more than one scenario (with different diffusion coefficient, immobile fraction and time of immobilization) fits the experimental data. To differentiate between different scenarios that fit well to the results of a strip-FRAP experiment, it is possible to perform a complementary combined FLIP-FRAP experiment (Fig. 1C and D), since two different scenarios which result in similar curves in a strip FRAP experiment give clearly different curves in a complementary FLIP-FRAP experiment (Houtsmuller, 2005). In FLIP-FRAP, the recovery of the fluorescence in a region at one end of the nucleus after bleaching for a relative long period (FRAP) is measured in parallel with the decrease of the signal in a similar region at the other pole of the nucleus (FLIP) (Fig. 1C and D). As stated above, the combination of strip-FRAP and FLIP-FRAP is especially applicable for studying transient immobilization as found for proteins (Fig. 4) (Farla et al., 2004; Farla et al., 2005).

1. Confocal settings are similar to those used in the strip-FRAP procedure (steps 1-3) except for the Detector Gain, which is set on 1000.
2. A 20 pixel wide region of interest (ROI) spanning the nucleus at one pole is selected in the Edit ROI panel, for recording the recovery of the signal after bleaching. Using the Define Region option the Bleach Control panel the same ROI is selected to locally bleach GFP. A second ROI of similar width is selected spanning the nucleus at the other pole where the decrease of fluorescence due to redistribution of the proteins from the bleached area is measured (Fig. 1C). The distance between the two regions should be kept constant in the different cells.
3. The fluorescent signal is monitored by scanning the two regions of interest for 35 iterations (approx. 100 seconds) at a low excitation level with a 3 sec time interval (Time Series Control) (*see* **Note 21**). After the first scan the GFP is bleached locally inside the lowest region of interest using 10 iterations of 488 nm laser light at maximum voltage (Fig. 1C). The time-series are initiated using the mean region of interest option in the time-series control (*see* **Note 22** and **23**). After the scan the data can be copied directly to Excel or the file can be saved as data-file for later analysis.

3.4.3 Qualitative FRAP analysis

FRAP data can initially be qualitatively analyzed by comparing data from experiments applied when the protein under investigation is active or inactive. In the case of the study of steroid receptors like the androgen receptor comparison of non-DNA-binding mutant versions and wild type is possible, where the differences observed between those can be ascribed to DNA-binding. In our studies, direct comparison of a wild type or mutant androgen receptor to a non-DNA binding mutant (*e.g.* AR (A573D)) greatly simplifies the interpretation of the data, because this mutant is not immobilized (Fig. 2) (Bruggenwirth et al., 1998; Farla et al., 2004; Farla et al., 2005).

In strip FRAP the recovery of fluorescence in a narrow strip spanning the nucleus is scanned at low laser intensity after shortly bleaching the fluorescence inside this region (Fig. 1A and B). The qualitative comparison between FRAP curves from different experimental conditions requires some kind of normalization of the data. There are several ways to normalize FRAP data, each of which enables the extraction of different parameters (Fig. 2B-D) (Houtsmuller, 2005).

1. The most straightforward normalization of FRAP data is to express intensities relative to the average of a sufficient number of measurements before bleaching ($I_{prebleach}$): $I_{norm,\,t} = (I_t - I_{background})/(I_{prebleach} - I_{background})$, where $I_{background}$ is the background signal (Fig. 2B) (*see* **Note 24**).
2. Straightforward normalization can be extended with the normalization to the fluorescence intensity directly after bleaching (I_0), by expressing intensity values relative to the intensity directly after bleaching as well as to the average prebleach intensity: $I_{norm,\,t} = (I_t - I_0)/(I_{pre} - I_0)$. This way of normalization enables the quickly visually estimate the size of a potentially present immobilized fraction (Fig. 2C) (*see* **Note 1**)
3. A third way of normalization is to express intensity values relative to the fluorescence after complete recovery (I_∞), and the intensity directly after bleaching (I_0): $I_{norm,\,t} = (I_t - I_0)/(I_\infty - I_0)$. This yields a curve running from 0 directly after bleaching, to 1 after final recovery, allowing to directly compare apparent diffusion rate irrespective of a potentially present immobile fraction, since different final recoveries due to different immobile fraction are not visible. In addition, this normalization is also often used for quantitative analysis by fitting the data to any equation that represents the diffusion process (and transient immobilization) (Fig. 2D) (Houtsmuller, 2005).
4. Combined FLIP-FRAP data can be analyzed by first calculating the fluorescence intensity difference between the FLIP-region and the FRAP-region: $I_{FLIP\text{-}FRAP} = (I_{FLIP\text{-}ROI} - I_{FRAP\text{-}ROI})$. Subsequently the intensity differencees can be expressed relative to the highest difference, *i.e.* immediately after bleaching (Fig. 1D and Fig. 4D).

3.4.4 Quantitative FRAP analysis

Quantitative analysis of FRAP is mostly performed by fitting experimental data to mathematical models. Many different models have been brought forward ranging from simplified models based on 1-dimensional diffusion (Ellenberg et al., 1997; Houtsmuller et al., 1999) to very sophisticated 3-D models incorporating as many aspects of the FRAP experiment as possible (Blonk, 1993; Braeckmans et al., 2003; Carrero et al., 2003; Braga et al., 2004; Sprague et al., 2004; Sprague and McNally, 2005; Braga et al., 2007). These approaches have shown to be very useful for quantitative FRAP analysis, a slight drawback being for instance diffusion in ellipsoid volumes or conically shaped laser beams are relatively difficult to solve analytically. Another possible approach to quantitatively analyse FRAP results is to generate FRAP

curves by Monte Carlo simulation of diffusion of individual molecules and their binding to immobile elements (representing chromatin binding) in an ellipsoidal volume (representing the nucleus) as well as the shape and intensity distribution of the applied laser beam (Fig. 3) (Houtsmuller et al., 1999; Hoogstraten et al., 2002; Farla et al., 2004). The strength of Monte Carlo simulation is that it generates the highly complicated outcome of a set of relatively simple mathematically definable rules, such as diffusion of single particles in an ellipsoid volume, the presence of nucleoli, or the typical shape and intensity distribution of a focused laser beam, which are hard to solve analytically. The drawback of Monte Carlo simulations is that they are very time consuming.

1. In our simulations, the size of the ellipsoid representing the nuclear volume is based on the experimentally determined average size of the investigated nuclei.
2. At the start of a Monte Carlo simulation, all tagged proteins start at a random position inside an ellipsoid volume representing the nucleus (Fig. 3A). Subsequently, the simulation goes through cycles representing a minimum time span. Typically in our simulations the time step was 21 msec, corresponding to the time it takes to scan a 10-pixels wide strip spanning the width of the nucleus one time.
3. Diffusion of single particles (representing GFP-tagged proteins) is simulated using the strikingly simple Einstein-Smoluchowski relationship for 3-D Brownian motion: $D = s^2/6T$, where D is the diffusion coefficient, s is the average distance moved by the particles and T is the time span in which the particles move, in our strip-FRAP simulations 20 msec (Fig. 3A). Simulation of Brownian motion of individual particles only involves the additional consideration that the equation predicts the average movement of all particles, whereas single particles will travel over slightly different distances. Therefore, diffusion of each particle is simulated by displacing it over a certain distance (corresponding to a certain diffusion coefficient) plus or minus a small variation defined by a Gaussian with standard deviation σ, which represents the stepsize per unit time and is related to the diffusion coefficient according to the above equation: $\sigma = \sqrt{6D\Delta t}$. In practice the step to be made by the molecule is split in three steps, in x-, y- and z- direction respectively: at each new time $t + \Delta t$ a new position $(x_{t+\Delta t}, y_{t+\Delta t}, z_{t+\Delta t})$ is derived for all mobile molecules from their current position (x_t, y_t, z_t) by $x_{t+\Delta t} = x_t + G(r_1)$, $y_{t+\Delta t} = y_t + G(r_2)$, and $z_{t+\Delta t} = z_t + G(r_3)$, where r_i is a random number ($0 \le r_i \le 1$) chosen from a uniform distribution, and $G(r_i)$ is an inversed cumulative Gaussian distribution with $\mu = 0$ and $\sigma^2 = 6D\Delta t$, where D is the diffusion coefficient. Note that the latter follows directly from the Einstein-Smulochowski equation, the average stepsize being equal to the standard deviation of the Gaussian distribution.
4. Binding to and releasing from immobile elements in the nucleus (like chromatin) can also be simulated by simple mathematical expressions (Fig. 3B). The probability for an immobile molecule to release is the most easy to explain since, in simple binding kinetics, this only depends on the affinity of the protein, yielding an equation defining the

chance of a molecule to release: $P_{mobilise} = k_{off} = 1 / T_{imm}$, where T_{imm} is the time spent in the immobile state expressed in number of time steps. If for instance the average immobilisation time is 3 time steps (60 milliseconds in our typical strip FRAP simulation), each step an immobile molecule will have a chance of 1/3 to release leading to an expected residence time of 3 steps. From this simple equation, the chance for a free molecule to become immobile can be calculated when one takes into account the fact that the ratio of immobile and mobile molecules is equal to the ratio between k_{on} and k_{off} (law of mass action): $k_{on}/k_{off} = F_{imm}/F_{mob}$, where F_{mob} is the number of mobile molecules and F_{imm} is the number of immobile molecules. The probability for each particle to become immobilized (representing chromatin-binding) then is $P_{immobilise} = k_{on} = k_{off} \cdot F_{imm} / F_{mob}$. Since above we saw that $k_{off} = 1 / T_{imm}$ the chance to immobilise can be expressed fully in terms of immobile fraction and immobilisation time, the two typical mobility parameters obtained from FRAP experiments: $P_{immobilise} = k_{on} = (F_{imm}) / (T_{imm} \cdot F_{mob})$

5. For bleaching simulation we use experimentally derived three-dimensional laser intensity profiles, determining the probability for each molecule to get bleached considering their 3-D position relative to the laser beam (Fig. 3C). The 3-D laser intensity profile is derived from the bleach pattern in confocal image stacks of chemically fixed nuclei containing GFP that were exposed to a stationary laser beam at various intensities and varying exposure times.
6. For quantitative analysis of the FRAP data, raw FRAP curves are normalized to pre-bleach values and the best fitting curve (by ordinary least squares) is selected from a large set of FRAP curves generated as described above in which three parameters representing mobility properties were varied: diffusion rate (ranging from *e.g.* 0.04 to 25 $\mu m^2/s$), k_{on} and k_{off} (corresponding to immobile fractions of *e.g.* 0, 10, 20, …, 90%) and time spent in immobile state (*e.g.* 2, 4, 8, 16, 32, 64, 128, 256, 512, 1024, ∞ sec).

4 NOTES

1. In FRAP, a considerable fraction of the fluorescent proteins inside a nucleus will be irreversibly bleached during the bleach pulse, resulting in incomplete recovery of the fluorescent signal independent of any immobile fraction.
2. Next to a diffusion coefficient, an immobile fraction and residence time in the immobile state can be derived from FRAP curves. It is also possible to describe the dynamic binding and release from immobile components of the nucleus in terms of immobilisation (k_{on}) and release rate (k_{off}). The ratio between k_{on} and k_{off} then is equal to the ratio between mobile and immobile fraction. The residence time is equal to the inverse of the release rate k_{off} (*see also* 3.4.4).

3. Analysis of FRAP or FLIP curves is more complicated, since the recovery or loss of fluorescence is a result of dissociation and association of tagged proteins (Houtsmuller, 2005).
4. The examples given here are all based on EGFP-tagged proteins. If ECFP, EYFP or other fluorescent dyes are used, imaging protocols should be modified according to the fluorescent properties of the chosen dye (*see* Table 1).
5. Hep3B cells do not express endogenous androgen receptors, are easy to transfect and are relatively large, enhancing microscopic analysis. When using other cell types the expression of endogenous nuclear receptors needs to be taken into account. Although many GFP-tagged proteins are functional, their functionality will usually be less than the wild-type. Endogenously expressed proteins compete with the tagged version, thereby limiting its activity compared to when no endogenous protein is present. A potential threat to the use of cell lines lacking endogenous expression is the potential absence of specific cofactors that modulate or enhance the activity of the studied protein.
6. Antibiotics are potential harmful and should always be treated with proper personal protection.
7. Coverslips should not be thicker than 0.16 mm, because of the high numeric aperture of some of the lenses of the confocal microscope.
8. The LSM 510 is a laser hazard class 3 B instrument and is marked as such. This moderate-risk class includes medium-power lasers. You must take care not to expose yourself to the radiation of such lasers.
9. We used temperature control equipment developed in our laboratory. Alternatively, commercially available equipment can be used varying from heatable plates up to complete incubators mounted on the microscope.
10. The insertion of a flexible stretch, for instance a short glycine-alanine repeat, between the protein of interest and the fluorescent label may decrease the potential (negative) effect of the label on the functionality of the protein of interest. For tagged ARs most often reporter assays using androgen regulated luciferase reporter genes are used to verify the functionality. (Farla et al., 2004).
11. Although the use of cell lines stably expressing the tagged protein has a number of advantages, it may under circumstances be more convenient to investigate transiently transfected cells. In these cases it is important to only select cells that do not overexpress the protein. This can be achieved for example by selecting cells at the same settings as used for stably expressing cells. Using these settings, fluorescence levels should be similar to cells stably expressing the protein at physiological levels. Fluorescence of overexpressing cells will be at the maximum in the entire nucleus (each pixel will have maximum intensity, in 8-bit imaging corresponding to a value of 255).
12. Coverslips in 6-wells plate are sterilized by a 45 minutes to UV treatment. Alternatively, the coverslips are submerged in ethanol and flame before placed in the 6-wells plate.

13. Do not vortex the transfection mix (refer to the FuGENE6 Transfection Reagent Instruction Manual). Contact between the undiluted FuGENE6 and any plastic surface (except for the pipette-tip) should be avoided.
14. Alternatively, modern FACS-sorters could be used to select single cells on the basis of their fluorescent level, representing the expression level of the tagged protein. Each cell can be deposited in a separate well of for instance a 96-wells plate. After incubation, the clones can be selected that have the appropriate expression level (step 7-8 above).
15. Although a higher detector gain (DG) is favorable to obtain higher signals, it increases noise. Therefore, a trade-off of settings to reduce both noise (*e.g.* lower DG, averaging) and monitor bleaching (*e.g.* lower excitation level, rapid scanning) still giving high enough signal in low expressing cells is necessary to optimize the experimental setup (*e.g.* wider pin-hole, higher DG, higher excitation level). These settings may also depend on the level or pattern of expression of the protein of interest. In general, for FRAP excitation laser intensity should be as low as possible, to avoid monitor bleaching, which is hard to correct for (Houtsmuller, 2005) (*see* **Note 16**).
16. The rate at which monitor bleaching occurs can be determined in a non-bleached area of the nucleus or by performing a FRAP experiment without applying the bleach pulse. Subsequently, experimental FRAP curves can be corrected according to the observed monitor bleach rate. However, when a significant immobile fraction is present, this fraction will contribute more to the monitor bleaching in the control measurements, than the mobile fraction, since immobile molecules stay constantly in the illuminated area, whereas mobile ones move in and out. In a FRAP-experiment this immobile fraction is largely bleached, leading to less monitor bleaching after photobleaching than estimated on the basis of the control curves. Thus, the presence of a (transiently) immobile fraction will lead to overcorrection of the experimental curve and subsequent underestimation or failure to detect this fraction. Therefore, it is important to avoid monitor bleaching or to limit it as much as possible.
17. Settings for imaging in the LSM510 software must be selected in several panels; Scan Control, Edit ROI, Time Series Control and Bleach Control. Settings for imaging are selected using the Scan- and Time Series control- menus.
18. For all the discussed approaches it is essential to select cells with physiologically relevant expression levels. Overexpression can lead to aggregation and artificial immobilization of the receptors (Marcelli et al., 2006). For quantitative measurements like FRAP described here, high-resolution imaging is not essential.
19. To speed up the procedure it is advisable to use software to put the center of the nucleus in the middle of the scanning area ('center' macro in the macro-directory).
20. It is not essential to use the exact values given here, but the values chosen should be kept constant (similar) over sets of experiments to allow comparison between curves of different proteins/conditions.

21. It is important to limit monitor bleaching by applying excitation at a low laser power. Although monitor bleaching correction procedures are designed for FRAP experiments, it is favorable to limit the monitor bleaching during data collection.
22. By selecting the Mean ROI option in the time series control panel only the mean intensity inside the ROI is plotted. In contrast, by selecting StartB (or StartT) all scans of the ROI are saved for later analysis.
23. In the configuration the monitor diode (ChM) can be selected also to monitor potential fluctuations of laser intensity during scanning, and used afterwards for correction. Note that lasers become less stable towards the end of their life.
24. In data normalisation where the intensity after bleaching is set to 0, some information is lost, since the depth of the bleach pulse is not only determined by laser intensity but also by protein mobility and size of the immobile fraction: the slower the protein and the larger the immobile fraction the deeper the bleach pulse will be. If experimental curves are fit to models that take into account bleach depth, the estimates of D, k_{on} and k_{off}, (or immobile fraction and residence time in immobile state) may be more accurate than when bleach depth is not taken into account.
25. Although in many FRAP analyses it is assumed that proteins are irreversibly photobleached, it has been shown that a fraction of proteins will regain their fluorescence, a process often referred to as blinking. Blinking not only occurs when GFP is illuminated at high intensity for photobleaching, but also at lower monitor intensities, although the time spent in the fluorescent state (on-time) of blinking GFPs is shorter at higher intensities. In contrast, the off-times are independent of excitation intensity (Garcia-Parajo et al., 2000). Therefore, in a FRAP-experiment the fraction of GFPs in the reversible off-state will increase during the high intensity bleach pulse, and decrease again during subsequent monitoring at low intensity, leading to a recovery of fluorescence that is not related to protein mobility. Although the contribution of this will be limited if molecules are relatively mobile, in cases where the majority or all of the investigated proteins are immobile (for instance core histones) the effect will be substantial, leading to underestimation of the immobile fraction.

5 REFERENCES

Agresti, A., P. Scaffidi, A. Riva, V.R. Caiolfa, and M.E. Bianchi. 2005. GR and HMGB1 interact only within chromatin and influence each other's residence time. *Mol Cell.* 18:109-121.

Axelrod D, K.D., Schlessinger J, Elson E, Webb WW. 1976. Mobility measurement by analysis of fluorescence photobleaching recovery kinetics. *Biophys J.* 16:1055-1069.

Bekker-Jensen, S., C. Lukas, F. Melander, J. Bartek, and J. Lukas. 2005. Dynamic assembly and sustained retention of 53BP1 at the sites of DNA damage are controlled by Mdc1/NFBD1. *J Cell Biol.* 170:201-211.

Blonk, J.C.G., A. Don, H. Van Aalst, and J. J. Birmingham. 1993. Fluorescence photobleaching recovery in the confocal scanning light microscope. *J Micros.* 169:363-374.

Braeckmans, K., L. Peeters, N.N. Sanders, S.C. De Smedt, and J. Demeester. 2003. Three-dimensional fluorescence recovery after photobleaching with the confocal scanning laser microscope. *Biophys J.* 85:2240-2252.

Braga, J., J. Desterro, and M. Carmo-Fonseca. 2004. Intracellular macromolecular mobility measured by fluorescence recovery after photobleaching with confocal laser scanning microscopes. *Mol Biol Cell.* 15:4749-4760.

Braga, J., J.G. McNally, and M. Carmo-Fonseca. 2007. A Reaction-Diffusion Model to Study RNA Motion by Quantitative Fluorescence Recovery after Photobleaching. *Biophys J.* 92:2694-2703.

Brinkmann, A.O., P.W. Faber, H.C.J. van Rooij, G.G.J.M. Kuiper, C. Ris, P. Klaassen, J.A.G.M. van der Korput, M.M. Voorhorst, J.H. van Laar, E. Mulder, and J. Trapman. 1989. The human androgen receptor: domain structure, genomic organization and regulation of expression. *J Steroid Biochem.* 34:307-310.

Bruggenwirth, H.T., A.L.M. Boehmer, J.M. Lobaccaro, L. Chiche, C. Sultan, J. Trapman, and A.O. Brinkmann. 1998. Substitution of Ala564 in the First Zinc Cluster of the Deoxyribonucleic Acid (DNA)-Binding Domain of the Androgen Receptor by Asp, Asn, or Leu Exerts Differential Effects on DNA Binding. *Endocrinology.* 139:103-110.

Carrero, G., D. McDonald, E. Crawford, G. de Vries, and M.J. Hendzel. 2003. Using FRAP and mathematical modeling to determine the in vivo kinetics of nuclear proteins. *Methods.* 29:14-28.

Chen, D., M. Dundr, C. Wang, A. Leung, A. Lamond, T. Misteli, and S. Huang. 2005. Condensed mitotic chromatin is accessible to transcription factors and chromatin structural proteins. *J Cell Biol.* 168:41-54.

Claessens, F., G. Verrijdt, E. Schoenmakers, A. Haelens, B. Peeters, G. Verhoeven, and W. Rombauts. 2001. Selective DNA binding by the androgen receptor as a mechanism for hormone-specific gene regulation. *J Steroid Biochem Mol Biol.* 76:23-30.

Cleutjens, K.B.J.M., J.A.G.M. van der Korput, C.C.E.M. van Eekelen, H.C.J. van Rooij, P.W. Faber, and J. Trapman. 1997. An androgen response element in a far upstream enhancer region is essential for high, androgen-regulated activity of the prostate-specific antigen promoter. *Mol Endocrinol.* 11:148-161.

Dundr, M., U. Hoffmann-Rohrer, Q. Hu, I. Grummt, L.I. Rothblum, R.D. Phair, and T. Misteli. 2002. A Kinetic Framework for a Mammalian RNA Polymerase in Vivo. *Science.* 298:1623-1626.

Ellenberg, J., E.D. Siggia, J.E. Moreira, C.L. Smith, J.F. Presley, H.J. Worman, and J. Lippincott-Schwartz. 1997. Nuclear Membrane Dynamics and Reassembly in Living Cells: Targeting of an Inner Nuclear Membrane Protein in Interphase and Mitosis. *J Cell Biol.* 138:1193-1206.

Essers J, H.A., van Veelen L, Paulusma C, Nigg AL, Pastink A, Vermeulen W, Hoeijmakers JH, Kanaar R. 2002. Nuclear dynamics of RAD52 group homologous recombination proteins in response to DNA damage. *EMBO J.* 21:2030-2037.

Essers, J., A.F. Theil, C. Baldeyron, W.A. van Cappellen, A.B. Houtsmuller, R. Kanaar, and W. Vermeulen. 2005. Nuclear Dynamics of PCNA in DNA Replication and Repair. *Mol Cell Biol.* 25:9350-9359.

Farla, P., R. Hersmus, B. Geverts, P.O. Mari, A.L. Nigg, H.J. Dubbink, J. Trapman, and A.B. Houtsmuller. 2004. The androgen receptor ligand-binding domain stabilizes DNA binding in living cells. *J Struct Biol.* 147:50-61.

Farla, P., R. Hersmus, J. Trapman, and A.B. Houtsmuller. 2005. Antiandrogens prevent stable DNA-binding of the androgen receptor. *J Cell Sci.* 118:4187-4198.

Feldman, B.J., and D. Feldman. 2001. The development of androgen-independent prostate cancer. *Nat Rev Cancer.* 1:34-45.

Fukano, T., H. Hama, and A. Miyawaki. 2004. Similar diffusibility of membrane proteins across the axon-soma and dendrite-soma boundaries revealed by a novel FRAP technique. *J Struct Biol.* 147:12-18.

Garcia-Parajo, M.F., G.M.J. Segers-Nolten, J.-A. Veerman, J. Greve, and N.F. van Hulst. 2000. Real-time light-driven dynamics of the fluorescence emission in single green fluorescent protein molecules. *Proc Natl Acad Sci U S A.* 97:7237-7242.

Giepmans, B.N.G., S.R. Adams, M.H. Ellisman, and R.Y. Tsien. 2006. The Fluorescent Toolbox for Assessing Protein Location and Function. *Science.* 312:217-224.

Heim, R., and R.Y. Tsien. 1996. Engineering green fluorescent protein for improved brightness, longer wavelengths and fluorescence resonance energy transfer. *Curr Biol.* 6:178-182.

Hoogstraten, D., A.L. Nigg, H. Heath, L.H.F. Mullenders, R. van Driel, J.H.J. Hoeijmakers, W. Vermeulen, and A.B. Houtsmuller. 2002. Rapid Switching of TFIIH between RNA Polymerase I and II Transcription and DNA Repair In Vivo. *Mol Cell.* 10:1163-1174.

Houtsmuller, A.B. 2005. Fluorescence recovery after photobleaching: application to nuclear proteins. In *Adv Biochem Eng Biotechnol.* Vol. 95. J. Rietdorf, editor. Springer-Verlag GmbH, Berlin. 177-199.

Houtsmuller, A.B., S. Rademakers, A.L. Nigg, D. Hoogstraten, J.H.J. Hoeijmakers, and W. Vermeulen. 1999. Action of DNA repair endonuclease ERCC1/XPF in living cells. *Science.* 284:958-961.

Houtsmuller, A.B., and W. Vermeulen. 2001. Macromolecular dynamics in living cell nuclei revealed by fluorescence redistribution after photobleaching. *Histochem Cell Biol*. 115:13-21.

Kimura, H. 2005. Histone dynamics in living cells revealed by photobleaching. *DNA Rep (Amst)*. 4:939-950.

Kimura, H., and P.R. Cook. 2001. Kinetics of Core Histones in Living Human Cells: Little Exchange of H3 and H4 and Some Rapid Exchange of H2B. *J Cell Biol.* 153:1341-1354.

Kimura, H., K. Sugaya, and P.R. Cook. 2002. The transcription cycle of RNA polymerase II in living cells. *J Cell Biol.* 159:777-782.

Kruhlak, M.J., M.A. Lever, W. Fischle, E. Verdin, D.P. Bazett-Jones, and M.J. Hendzel. 2000. Reduced Mobility of the Alternate Splicing Factor (ASF) through the Nucleoplasm and Steady State Speckle Compartments. *J Cell Biol.* 150:41-52.

Leonhardt, H., H.-P. Rahn, P. Weinzierl, A. Sporbert, T. Cremer, D. Zink, and M.C. Cardoso. 2000. Dynamics of DNA Replication Factories in Living Cells. *J Cell Biol.* 149:271-280.

Lippincott-Schwartz, J., and G.H. Patterson. 2003. Development and Use of Fluorescent Protein Markers in Living Cells. *Science.* 300:87-91.

Lukas, C., J. Falck, J. Bartkova, J. Bartek, and J. Lukas. 2003. Distinct spatiotemporal dynamics of mammalian checkpoint regulators induced by DNA damage. *Nat Cell Biol.* 5:255-260.

Lukas, C., F. Melander, M. Stucki, J. Falck, S. Bekker-Jensen, M. Goldberg, Y. Lerenthal, S. Jackson, J. Bartek, and J. Lukas. 2004. Mdc1 couples DNA double-strand break recognition by Nbs1 with its H2AX-dependent chromatin retention. *EMBO J.* 23:2674-2683.

Marcelli, M., D.L. Stenoien, A.T. Szafran, S. Simeoni, I.U. Agoulnik, N.L. Weigel, T. Moran, I. Mikic, J.H. Price, and M.A. Mancini. 2006. Quantifying effects of ligands on androgen receptor nuclear translocation, intranuclear dynamics, and solubility. *J Cell Biochem.* 98:770-788.

Mattern, K.A., S.J.J. Swiggers, A.L. Nigg, B. Lowenberg, A.B. Houtsmuller, and J.M.J.M. Zijlmans. 2004. Dynamics of Protein Binding to Telomeres in Living Cells: Implications for Telomere Structure and Function. *Mol Cell Biol.* 24:5587-5594.

McNally, J.G., W.G. Müller, D. Walker, R. Wolford, and G.L. Hager. 2000. The glucocorticoid receptor: rapid exchange with regulatory sites in living cells. *Science.* 287:1262-1265.

Phair, R.D., and T. Misteli. 2000. High mobility of proteins in the mammalian cell nucleus. *Nature.* 404:604-609.

Phair, R.D., P. Scaffidi, C. Elbi, J. Vecerova, A. Dey, K. Ozato, D.T. Brown, G. Hager, M. Bustin, and T. Misteli. 2004. Global Nature of Dynamic Protein-Chromatin Interactions In Vivo: Three-Dimensional Genome Scanning and Dynamic Interaction Networks of Chromatin Proteins. *Mol Cell Biol.* 24:6393-6402.

Rademakers, S., M. Volker, D. Hoogstraten, A.L. Nigg, M.J. Mone, A.A. van Zeeland, J.H.J. Hoeijmakers, A.B. Houtsmuller, and W. Vermeulen. 2003. Xeroderma Pigmentosum Group A Protein Loads as a Separate Factor onto DNA Lesions. *Mol Cell Biol.* 23:5755-5767.

Rayasam, G.V., C. Elbi, D.A. Walker, R. Wolford, T.M. Fletcher, D.P. Edwards, and G.L. Hager. 2005. Ligand-specific dynamics of the progesterone receptor in living cells and during chromatin remodeling in vitro. *Mol Cell Biol.* 25:2406-2418.

Schaaf, M.J., and J.A. Cidlowski. 2003. Molecular determinants of glucocorticoid receptor mobility in living cells: the importance of ligand affinity. *Mol Cell Biol.* 23:1922-1934.

Schaaf, M.J.M., L.J. Lewis-Tuffin, and J.A. Cidlowski. 2005. Ligand-selective targeting of the glucocorticoid receptor to nuclear subdomains is associated with decreased receptor mobility. *Mol Endocrinol.* 19:1501-1515.

Shaner, N.C., P.A. Steinbach, and R.Y. Tsien. 2005. A guide to choosing fluorescent proteins. *Nat Meth.* 2:905-909.

Sporbert, A., A. Gahl, R. Ankerhold, H. Leonhardt, and M.C. Cardoso. 2002. DNA Polymerase Clamp Shows Little Turnover at Established Replication Sites but Sequential De Novo Assembly at Adjacent Origin Clusters. *Mol Cell.* 10:1355-1365.

Sprague, B.L., and J.G. McNally. 2005. FRAP analysis of binding: proper and fitting. *Trends Cell Biol.* 15:84-91.

Sprague, B.L., R.L. Pego, D.A. Stavreva, and J.G. McNally. 2004. Analysis of binding reactions by fluorescence recovery after photobleaching. *Biophys J.* 86:3473-3495.

Stenoien, D.L., K. Patel, M.G. Mancini, M. Dutertre, C.L. Smith, B.W. O'Malley, and M.A. Mancini. 2001. FRAP reveals that mobility of oestrogen receptor-alpha is ligand- and proteasome-dependent. *Nat Cell Biol.* 3:15-23.

Trapman, J. 2001. Molecular mechanisms of prostate cancer. *Eur J Cancer.* 37:S119-125.

Tsien, R.Y. 1998. The green fluorescent protein. Ann Rev Biochem. 67:509-544.

Van Royen, M.E., S.M. Cunha, M.C. Brink, K.A. Mattern, A.L. Nigg, H.J. Dubbink, P.J. Verschure, J. Trapman, and A.B. Houtsmuller. 2007. Compartmentalization of androgen receptor protein-protein interactions in living cells. *J Cell Biol.* 177:63-72.

Zotter, A., M.S. Luijsterburg, D.O. Warmerdam, S. Ibrahim, A. Nigg, W.A. van Cappellen, J.H.J. Hoeijmakers, R. van Driel, W. Vermeulen, and A.B. Houtsmuller. 2006. Recruitment of the Nucleotide Excision Repair Endonuclease XPG to Sites of UV-Induced DNA Damage Depends on Functional TFIIH. *Mol Cell Biol.* 26:8868-8879.

Chapter 3

FRAP and FRET Methods to Study Nuclear Receptors in Living Cells

Van Royen, M.E., C. Dinant, P. Farla,
J. Trapman, and A.B. Houtsmuller.

In The Nuclear Receptor superfamily.
(2009) Vol. 505. I.J. McEwan, editor.

Humana Press / Springer, in press.

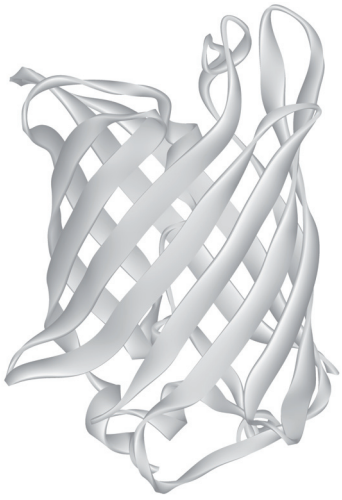

ABSTRACT

Quantitative imaging techniques of fluorescently tagged proteins have been instrumental in the study of the behavior of nuclear receptors (NRs) and coregulators in living cells. Ligand activated NRs exert their function in transcription regulation by binding to specific response elements in promotor and enhancer sequences of genes. Fluorescence recovery after photobleaching (FRAP) has proven to be a powerful tool to study the mobility of fluorescently labeled molecules in living cells. Since binding to DNA leads to the immobilization of DNA-interacting proteins like NRs, FRAP is especially useful for determining DNA-binding kinetics of these proteins. The coordinated interaction of NRs with promoters/enhancers and subsequent transcription activation is not only regulated by ligand but also by interactions with sets of cofactors and, at least in the case of the androgen receptor (AR), by dimerization and inter-domain interactions. In living cells these interactions can be studied by fluorescence resonance energy transfer (FRET).

Here we provide and discuss detailed protocols for FRAP and FRET procedures to study the behavior of nuclear receptors in living cells. On the basis of our studies of the androgen receptor (AR), we provide protocols for two different FRAP methods (strip-FRAP and FLIP-FRAP) to quantitatively investigate DNA-interactions and for two different FRET approaches, ratio imaging, and acceptor photobleaching FRET to study AR domain interactions and interactions with cofactor motifs. Finally, we provide a protocol of a technique where FRAP and acceptor photobleaching FRET are combined to study the dynamics of interacting ARs.

Key words: Androgen Receptor, N/C interaction, Confocal Microscopy, FRET, FRAP

1 INTRODUCTION

1.1 Nuclear Receptors

Nuclear receptors (NRs) are ligand activated transcription factors amongst which are the steroid receptors including the estrogen- (ER), mineralocorticoid (MR), glucocorticoid- (GR), progesterone- (PR) and androgen- (AR) receptors (1). The members of the steroid receptor subfamily have roles in regulating cell growth, development, differentiation and homeostasis.

As our research focus is on AR function in living cells, we use this steroid receptor for the examples presented throughout this chapter. The AR is important in the development and maintenance of the male phenotype and also plays a role in the development and progression of prostate cancer (2). Like all nuclear receptors the AR consists of three functional domains; a highly conserved DNA binding domain (DBD) flanked by a C-terminal ligand-binding domain (LBD) and a more variable N-terminal domain (NTD) (3). In the absence of ligand, the AR is predominantly, but not exclusively, localized in the cytoplasm in most cell types. Upon binding to ligand ARs translocate from the cytoplasm to the nucleus where they exert their function through interaction with coregulators and binding to specific androgen response elements (AREs) in promoter and enhancer sequences of AR regulated genes (4-7).

1.2 FRAP to study protein mobility

For the AR and for other nuclear receptors the live cell dynamics and interactions with chromatin have been investigated extensively. A powerful approach to study proteins mobility in living cells is fluorescence recovery after photobleaching (FRAP)(*see* **Note 1**) (8-14). In FRAP, fluorescence is recorded in a small volume within a larger volume before and after shortly illuminating the small volume at high laser intensity (Fig. 1 A-D) (15, 16, and reviewed in 17). During the high intensity laser-pulse the majority of the fluorescent molecules within the illuminated region irreversibly lose their fluorescent properties, a process termed photobleaching. After (and during) the pulse mobile fluorescent and bleached molecules will diffuse in and out of the bleached region eventually leading to their complete redistribution. In contrast, immobilized bleached molecules inside the bleached region will not be exchanged by non-bleached molecules from outside the region, and vice versa. Therefore, the presence of an immobile fraction results in incomplete recovery of the fluorescent signal inside the bleached region relative to the remainder of the nucleus. When molecules are immobilized only transiently (and shorter or not much longer than the period of measurement), as was found for NRs (see below), this will result in a secondary, slower recovery of fluorescence in the bleached region by diffusion of initially immobilized molecules that release from their immobile binding sites (for instance promoters/enhancers of genes) during the measurement period after bleaching (Fig. 1 B) (9, 11).

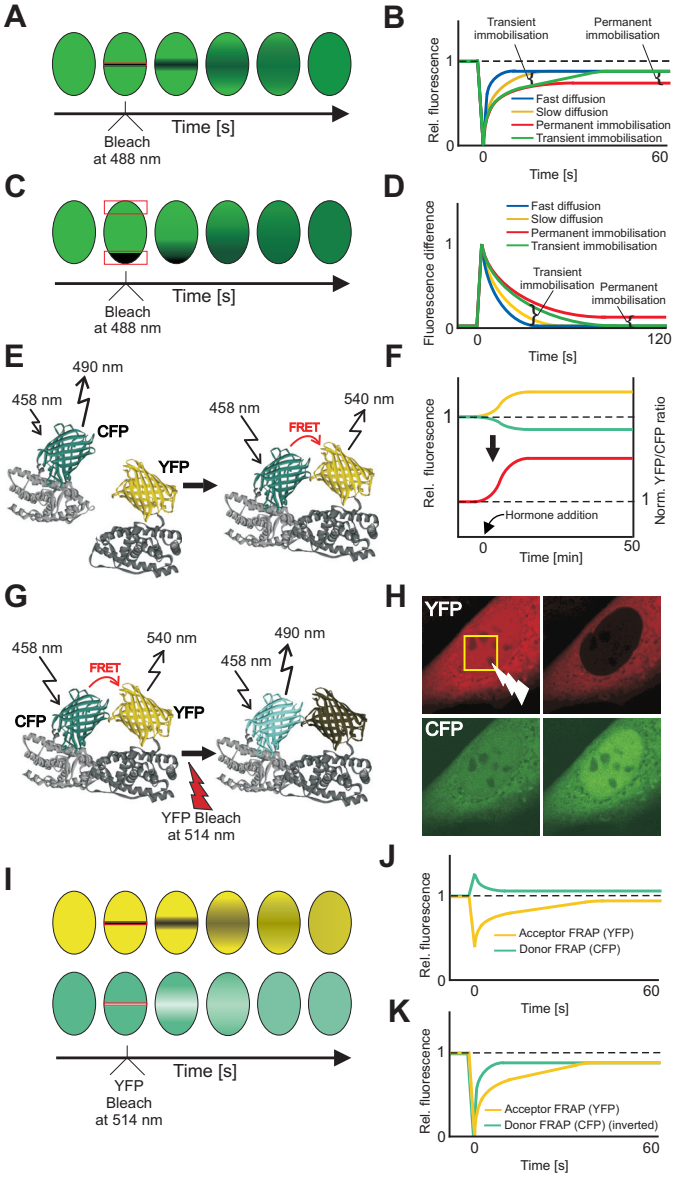

In order to compare FRAP curves form different experiments, and to visually analyze them it is necessary to normalize the raw fluorescence data. There are several ways to do this, each revealing specific kinetic parameters (see also step 7 in the strip-FRAP protocol) (17, 18). The most straightforward normalization is to express measured intensities relative to the average prebleach intensity ($I_{prebleach}$) after background subtraction, revealing the fraction of molecules bleached during the bleach pulse, which can be read from the first measurement

Figure 1. Schematic representations of strip-FRAP, FLIP-FRAP, abFRET and simultaneous FRAP and FRET experiments. (A) In strip-FRAP, the recovery of fluorescence is recorded in time after shortly bleaching a small strip spanning the nucleus. (B) FRAP curves of different scenarios normalized to prebleached values and to zero directly after bleaching. Permanent immobilization of GFP tagged proteins (red curve) can be identified by an incomplete recovery compared to FRAP curves of freely molecules (blue curve with fast diffusion and yellow curve with slow diffusion). A transient immobilization results in a delayed fluorescence recovery (green curve). (C) In FLIP-FRAP experiments the fluorescence in a bleached region at one pole of the nucleus and in a region at the opposite nuclear pole are recorded in time after photobleaching until steady state is regained. (D) The normalized difference in fluorescence between the two opposite poles is plotted in time. Similar to strip-FRAP a permanent immobilization results is an incomplete redistribution and thus a permanent difference between both signals in the two measured regions (red curve) and a transient immobilization results in a delayed fluorescence redistribution (green curve). (E) Principle of FRET measurement by YFP/CFP ratio imaging. In an inducible system FRET can readily be measured using YFP/CFP ratio imaging. In absence of interaction, before induction, no FRET occurs. After induction, when YFP and CFP are in each other's vicinity, energy is transferred from CFP to YFP resulting in a decrease in CFP emission and an increase in YFP emission. (F) When both CFP and YFP intensities and the YFP/CFP ratio are plotted, FRET is indicated by the decrease of CFP emission (cyan curve) and a subsequent increase of YFP emission (yellow curve), resulting in a clear YFP/CFP ratio increase (red curve). The curve indicates the kinetics of the interaction. (G) Principle of imaging FRET by acceptor photobleaching. When cyan fluorescent protein (CFP) and yellow fluorescent protein (YFP) are close to each other (< 10 nm), that is, if interaction occurs, excitation energy absorbed by CFP is non-irradiatively transferred to YFP resulting in YFP emission (sensitized emission). FRET was evaluated by the increase of donor (CFP) emission intensity after specifically photobleaching of the acceptor (YFP) in the nucleus thereby eliminating its quenching effect on the donor. (H) Images of YFP and CFP in living cells before and after YFP photobleaching in cells transfected with a construct expressing a CFP-YFP fusion protein. The square indicates the region of bleaching. Bleaching of YFP results in a clear increase of CFP emission. (I) Schematic representation of simultaneous FRAP and FRET measurements. YFP in a small strip spanning the width of the nucleus is bleached shortly and the recovery of YFP (acceptor) fluorescence is monitored at 100 msec intervals. In the presence of FRET, YFP bleaching results in an accompanying increase of CFP (donor) fluorescence. The redistribution of CFP fluorescence therefore represents the mobility of interacting molecules only (donor-FRAP). Acceptor emission represents the total pool of YFP-tagged molecules irrespective of interaction (acceptor-FRAP). (J) After background subtraction, normalization to prebleach values and inversion of the donor-FRAP signal, shows directly the kinetics of both donor and acceptor signals. (K) Normalization to values directly after bleaching inverts the donor FRAP curve and the kinetics of both signals can now be compared.

after bleaching. In addition, if molecules are largely immobile, the recovery of fluorescence in the bleached area will be limited, so a first impression on overall mobility can be obtained from these curves. (Note that in principle the volume containing the molecules (in our case the nucleus) can also be seen from these curves if freely mobile molecules (for instance GFP) are used and the volume of the bleached region is known). To readily extract more precise information, a second way to normalize the data can be used where the measured fluorescence is expressed relative to both intensities before as well as directly after bleaching (I_0). This way of normalization yields a curve that starts at 1 before bleaching and 0 immediately after bleaching, thereby removing potential differences in the percentage of molecules bleached, and thus allowing comparison between experiments using different laser settings. The final recovery of these curves, when corrected for the fraction of bleached molecules (*see* **Note 2**), reveals the immobilized fraction, if present. A third way of normalization is achieved by expressing fluorescence relative to both the fluorescence directly after bleaching (I_0) and after complete recovery ($I_{postbleach}$). This yields a curve running from 0 immediately after bleaching to 1 at complete recovery, allowing fitting the data to any analytically derived equation that represents the diffusion process (and transient immobilization) (17). In addition, since this

normalization removes the immobile fraction, the apparent diffusion coefficient of the freely mobile fraction can be compared directly between different curves, irrespective of the size of the immobile fraction, if present.

In our investigation of the nuclear dynamics of the AR, we have previously used a combination of FRAP and FLIP (fluorescence loss in photobleaching) assays (see below and Fig. 1 C, D, and Fig. 2) (11, 15, 17). The reason for this dual approach was that in straightforward FRAP experiments often more than one scenario may fit the data, where a scenario of slow diffusion versus a scenario of fast diffusion and transient immobilization are difficult to distinguish. In the case of the AR, we observed a strongly reduced mobility of liganded ARs compared to non-liganded ARs or liganded mutants that cannot bind DNA. However, although strip-FRAP (see Methods section) analysis favored a model of unaltered diffusion and ligand-induced transient immobilization, the difference with a model of ligand-induced slower mobility (for instance by formation of large transcription holocomplexes) was small. We then verified by computer modeling that two different scenarios (slow mobility versus high mobility and transient immobilization) often result in two similar curves in a strip-FRAP experiment but very different curves in a complementary FLIP-FRAP experiment or vice versa (17, 18). Therefore, to corroborate the strip-FRAP experiments we performed another FRAP variant, where we analyzed the recovery of fluorescence in a bleached area (FRAP) at one pole of the nucleus together with the loss of fluorescence at the other pole, distant from the bleached area (fluorescence loss in photobleaching, FLIP) (9, 11). Both procedures are described in detail in the Methods section.

1.3 Steroid receptors are transiently immobilized due to DNA-binding

The transient immobilization in the nucleus of NRs (and many other DNA-interacting proteins) identified in FRAP measurements, most likely reflects the binding of NRs to chromatin. This is corroborated by the absence of an immobile fraction in several AR mutants with mutations in the first zinc finger of the AR DBD (*e.g.* A573D) that were shown to abolish DNA binding (Fig. 2 A-D) (11, 19). Surprisingly, FRAP experiments on ARs lacking the AR LBD showed that not only the AR DBD but also the AR LBD is important for stable binding of the AR to DNA but that this stabilization is not essential for transcriptional activity (11). Other studies applying FRAP on NRs also identified a role for chaperones as Hsp90 and proteosome function in the regulation of NR immobilization at a target sequence (20, 21). In addition, the ligand specificity of several NRs has been studied. For the AR very similar transient immobilizations are found in the presence of the natural agonists testosterone, dehydrotestosterone or the synthetic variant R1881. Antagonist bound ARs (bicalutamide or hydroxyflutamide) are much more mobile, only showing very transient immobilizations in the order of hundreds of milliseconds to seconds (9, 22, 23). However, ChIP data suggested that antagonist bound ARs still bind to their recognition sites (24, 25). Taken together ChIP and FRAP results suggest that anti-androgens prevent stable DNA-binding of the AR (9). These antagonists act as agonists

in specific AR mutants like T877A and W741C, which were found in patients that developed therapy resistant metastases (26, 27). Interestingly the agonist effect was accompanied by a reduced mobility comparable to R1881, strongly suggesting that we are observing DNA binding in the FRAP experiments shown (9). The effect of partial antagonists on wild type ARs is less clear, ranging from fast recoveries of ARs in the presence of cyproterone acetate (CPA) to transient immobilizations comparable with agonist of RU486 bound ARs (22). Similar results have been found for other pure and partial antagonist bound NRs (8, 12, 13, 28-31).

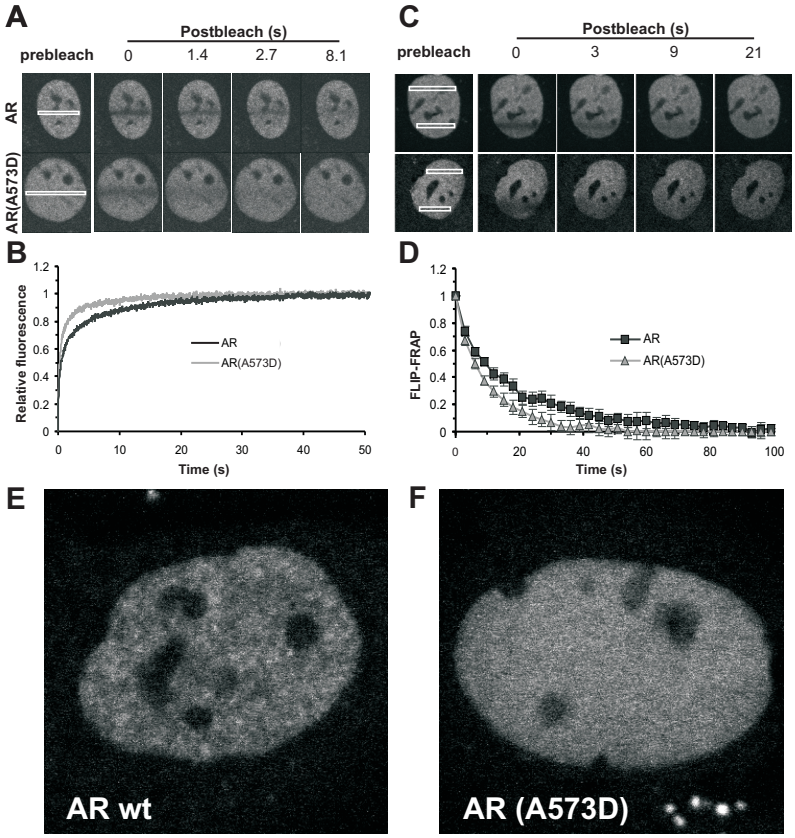

Figure 2. FRAP on wild type and mutant ARs. (A and B) Confocal images (A) and the strip-FRAP curve of Hep3B cells stably expressing GFP-AR (wild type) or the non DNA binding mutant (GFP-AR (A573D). The recovery of fluorescence in a small strip spanning the nucleus (white box in A) is recorded in time after shortly photobleaching the fluorescence. The wild type AR shows a slower total recovery of the fluorescence compared to the non-DNA binding mutant (AR (A573D)) because of transient immobilization of the wild type AR (B). (C and D) Confocal images of Hep3B cells stably expressing the GFP tagged wild type AR and the non-DNA-binding mutant and their FLIP-FRAP curves (D). The normalized differences in fluorescence intensity in both regions of interests (ROIs) (white boxes at both poles of the cells) (C) is plotted in time (D). In agreement with the strip-FRAP results a reduced mobility is found for the wild type AR compared with the non-DNA binding mutant (A573D). (E and F) Confocal images of wild type AR and the non-DNA binding mutant. Immobilization of wild type AR found with FRAP is accompanied with a typical nuclear speckled distribution (E), whereas the non-DNA binding mutant (AR (A573D)) lacks this pattern (F). Figure adapted from ref. 9 with permission from The Company of Biologists Limited Ltd.

An interesting approach to study interaction of NRs with promoters of NR-regulated genes was introduced by Gordon Hager and others. In this approach, cell lines are generated containing a long tandem array of promoters controlling the expression of a reporter gene. The local high concentration of response elements (like the MMTV LTR for GR, PR and AR studies (8, 14, 21, 22, 31) and prolactin-regulatory element array to study the ER (30)) enables visualization of binding of fluorescently tagged NRs to these specific sequences. FRAP data obtained with the cell line containing the MMTV LTR array cell line is in line with FRAP data obtained using cells which lack these arrays and show residence times in the range from seconds to a minute (8, 12, 21, 28, 31).

Immobilization of NRs is accompanied with a typical nuclear speckled distribution (Fig. 2 E), whereas non-DNA binding mutants and antagonist bound wild type NRs lack this pattern (Fig. 2 F) (9, 28). The correlation between (transient) immobilization and this speckled pattern suggests that these speckles are NRs bound to specific regulatory sequences in gene promoters. This is corroborated by the partial overlap observed in an in vivo transcription assay visualizing sites of active transcription using BrUTP incorporation with NR speckles (32). Recently others and we provided evidence that the speckled pattern observed for many SRs represent transcriptionally active sites, and may be considered the endogenous variant to the MMTV LTR array. Taken together, immobilization of activated NRs most likely reflects DNA binding and leads to a speckled NR distribution in the nucleus.

1.4 FRET to study protein-protein interactions

Nuclear receptor activity is not only regulated by hormone binding but also by interactions between their domains (DBD, LBD and NTD) and interactions with cofactors (33). A powerful method to study protein-protein interactions in living cells is fluorescence resonance energy transfer (FRET) (Fig. 1 E-H) (34-38). FRET is the nonradiative transfer of energy from a donor fluorophore in excited state to a nearby acceptor fluorophore, with an excitation spectrum significantly overlapping the emission spectrum of the donor. The critical distance between donor and acceptor fluorophores to allow energy transfer is within only 10 nm, since FRET efficiency falls off with the sixth power of the distance between the two fluorophores (38, 39). Because these distances are in the range of protein sizes FRET can be used not only to detect protein-protein interactions but also to study conformational changes proteins tagged with a FRET donor as well as a FRET acceptor (*see* **Note 3**). The most frequently used fluorophore couples in FRET assays to determine protein-protein interactions currently are GFP variants from the bioluminescent jellyfish *Aequorea Victoria* such as cyan fluorescent protein (CFP) and yellow fluorescent protein (YFP). Site directed mutagenesis of GFP-like proteins has generated a range of variants with better spectral properties, improved brightness and solubility (40-43). In particular, optimized CFPs like mCerulean (44), mTFP1 (45) and SCFP3A (46) and optimized YFPs like mCitrine (47, 48), mVenus (49) and SYFP2 (46) are promising candidates for sensitive FRET studies. Furthermore in recent years a series of improved red shifted fluoro-

phores have been developed, opening up a new range of potential FRET couples (42, 50-52). Spectral unmixing procedures also enable the utilization of spectrally close fluorophores (*e.g.* a GFP2 or GFP in combination with YFP) (53, 54) (*see* **Note 4**).

Like in FRAP, in FRET several different approaches have been developed, the most frequently used being sensitized emission, ratio imaging, acceptor photobleaching FRET (abFRET) and fluorescence lifetime imaging (FLIM) (reviewed in 55). The classical approach in FRET experiments is sensitized emission, where the emission of the acceptor fluorophore is detected while the donor fluorophore is excited (acceptors are sensitized to shorter wavelength excitation by adding donors, hence the term 'sensitized emission'). Although sensitized emission is still widely used, cross talk of the donor signal in the acceptor channel and vice versa as well as the direct excitation of the acceptor by the donor excitation wavelength makes the analysis highly dependent on (and sensitive to noise in) control measurements of cells in which only one of the two fluorophore is present (56-58).

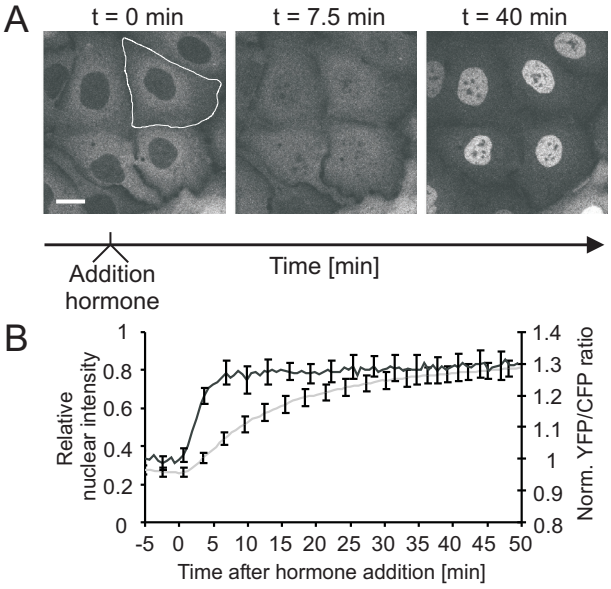

Figure 3. FRET measurement by YFP/CFP ratio imaging. (A) Cells expressing the YFP-AR-CFP double-tagged AR are grown in the absence of hormone, when the AR is predominantly localized in the cytoplasm. Upon induction by hormone the AR rapidly translocates to the nucleus. To determine FRET, as an indication of the AR N/C interaction, both YFP and CFP signals in the whole cell are detected simultaneously when CFP is excited (458 nm). In addition the translocation of the AR can be determined by separately measuring the YFP signal (with YFP specific excitation (514 nm)) in the nucleus relatively to the signal in the whole cell. (B) Simultaneous detection of YFP and CFP signals (at 458 nm excitation) shows a prompt increase of YFP/CFP ratio after hormone addition at t = 0 minutes (black curve; n = 10). Translocation of the AR to the nucleus (gray curve) is much slower, indicating the N/C interaction (black curve) depends on hormone binding rather than cytoplasmatic or nuclear localization (83). Error bars represent 2x SEM. Figure 3 B adapted from ref. 32 with permission from The Rockefeller University Press.

An alternative approach to determine FRET is acceptor/donor (*e.g.* YFP/CFP) ratio imaging where both donor and acceptor emission are detected simultaneously when excited at the excitation wavelength of the donor (Fig. 1 E). However, the application of ratio imaging is limited to systems where CFP and YFP-tagged proteins are expressed in a constant ratio (*e.g.* double tagged ER / AR) or in inducible systems where changes in YFP/CFP ratio can be observed in the same cells after initiating or abolishing the interactions of interest (Fig. 1 E, F and Fig. 3). A procedure more applicable for determining protein-protein interaction in steady state, also when CFP and YFP-tagged proteins are not stoichiometrically expressed, is abFRET where photobleaching of the acceptor results in unquenching of the donor and consequently in an increased donor signal (Fig. 1 G, H and Fig. 4 A) (38, 59-61). It is required to include the proper positive and negative control samples in the experiments, also to be able to correct for inter-experimental variation (61). Moreover, a proper negative control should be used to correct for monitor bleaching effects (*see* **Note 5**). A fourth method to detect FRET is based on the reduced lifetime of excited donor molecules when they are in the proximity of acceptors (reviewed in 62, 63). The fluorescent lifetime, or the average time that a molecule will stay in an excited state before returning to the ground state is a property of the fluorophore. In the occurrence of FRET, donors have an extra way to relax from the excited state by transfer of the energy to the nearby acceptor fluorophore, which will result in a shortened average fluorescent lifetime of the donor fluorophores (64).

1.5 Protein interactions in steroid receptor function

One of the most intensively studied cofactor binding sites on the NR surface is the hydrophobic cleft in the LBD formed by ligand induced repositioning of helix 12. Several cofactors, including the p160-coregulators SRC1, TIF2 (SRC2) and RAC1 (SRC3) are able to bind to this cleft via LxxLL-like motifs. FRET has been used extensively to study interactions of NRs or NR LBDs with peptides containing cofactor interaction motifs (32, 65-70). To investigate these interactions, several FRET based ligand activity reporters have been designed in which NR LBDs are fused to cofactor fragments through a flexible linker and tagged with YFP and CFP at either terminus. Interaction of the ligand activated NR LBD and the cofactor peptide brings the two FRET fluorophores in close proximity resulting in an increased FRET signal (71-75). Furthermore, several others have applied FRET in studies on interactions of NRs with full length or fractions of cofactors and other transcription factors (76-78).

Intramolecular domain interactions lead to conformational changes of NRs. For the AR such a conformational change is explained by the prevalence of the hydrophobic cleft in the AR LBD for FxxLF motifs, one of which is present in the AR NTD initiating the N/C interaction (79-82). To be able to study the AR N/C interaction in living cells by applying FRET technologies others and we tagged both the N-terminal domain and de C-terminal LBD of the AR with YFP and CFP (22, 32, 83). FRET based experiments confirmed the results of previous two hybrid interaction assays indicating that the ligand induced N/C interaction is dependent

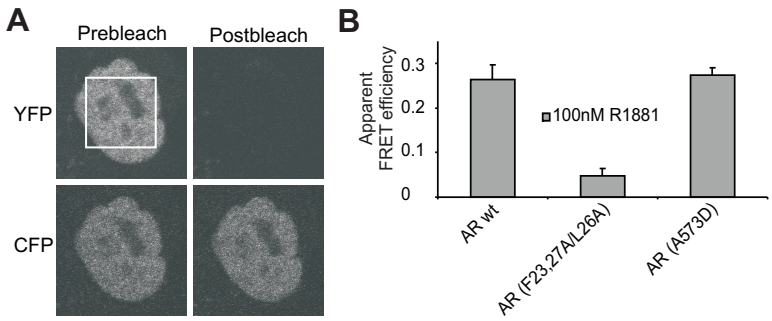

Figure 4. Acceptor bleaching FRET on cells expressing double tagged (YFP and CFP) ARs. (A) Confocal images of YFP and CFP fluorescence in Hep3B cells expressing YFP-AR-CFP before and after photobleaching YFP in the indicated region. (B) The apparent FRET efficiency of wild type YFP-AR-CFP and two mutants deficient in the N/C interaction (AR (F23,27A/L26A)) or DNA binding (AR(A573D)). The apparent FRET efficiency is calculated as the fraction CFP increase after bleaching of all the YFP fluorescence and presented normalized to the CFP-YFP chimera (= 1) and cotransfected CFP and YFP (= 0). The N/C interaction is disabled when the FQNLF motif is mutated (AR F23,27A/L26A) but not in the non DNA binding mutant (AR(A573D)). Figure 4 B adapted from ref. 32 with permission from The Rockefeller University Press.

on the N-terminal FQNLF motif (Fig. 4 B). In contrast to intramolecular domain interactions, intermolecular domain interactions (*e.g.* intermolecular N/C interaction) lead to homo- or hetero-dimerization. Several studies used FRET to detect dimerization of NRs including the AR (83-85). Interestingly, intramolecular N/C interactions are already initiated in the cytoplasm before translocation of the AR to the nucleus (Fig. 3 B), whereas intermolecular N/C interactions in a dimer configuration are observed only after translocation to the nucleus (32, 83). Similar YFP/CFP ratio imaging experiments were used where it was observed that anti-estrogens alter the configurations of ERs (86, 87).

The prevalence of the hydrophobic cleft in the AR LBD for FxxLF motifs initiating the N/C interactions suggest a competition with cofactor binding to this cleft and raises questions on the role of the N/C interaction in orchestrating these cofactor interactions. To extend our data with information on the mobility of specifically the subpopulation of N/C interacting ARs we developed a new technology where we combined FRAP and abFRET (Fig. 1 I-K) (32). As explained above YFP bleaching results in a CFP increase, but only when FRET occurs. By applying FRAP on cells expressing FRETing proteins and simultaneously recording YFP recovery in the strip after photobleaching and the redistribution of the increased (because of YFP photobleaching) CFP signal it is possible to compare the mobility of the interacting proteins (the CFP redistribution) relative to the mobility of the total pool of proteins (the YFP recovery as in conventional strip FRAP) (Fig. 1 I-K and Fig. 5). By recording both the recovery of the YFP signal in time and the redistribution in time of the increased CFP signal after YFP photobleaching and comparing the two we were able to conclude that ARs with N/C interaction are not immobilized and therefore not bound to DNA (32).

The procedures of YFP/CFP ratio imaging, abFRET and simultaneous FRAP and FRET measurements are described here in detail.

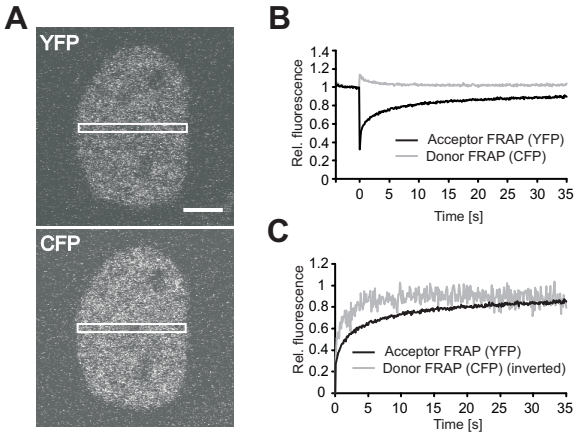

Figure 5. Simultaneous FRAP and FRET measurements on cells expressing double tagged ARs (see also Figure 1 I-K). (A) Confocal images of Hep3B cells expressing YFP-AR-CFP imaged with the simultaneous FRAP and FRET configuration. The recovery of both YFP and CFP fluorescence in a small strip spanning the nucleus (white box in A) is recorded in time after shortly photobleaching YFP fluorescence. Bar represents 5 µm. (B) In the presence of FRET YFP bleaching results in a local increase of CFP fluorescence. Similar to conventional strip-FRAP the YFP fluorescence recovery represents the redistribution of the complete pool of ARs whereas the redistribution of the CFP fluorescence only represents the mobility of the interacting molecules. (C) When the CFP curve is inverted, and both curves are normalized to prebleach values at 1 and the intensity directly after YFP photobleaching at 0, the mobility of the interacting molecules can be compared with the total pool of ARs. Simultaneous FRAP and FRET on cells expressing YFP-AR-CFP indicates that the N/C interacting ARs have a higher mobility compared to the total pool of ARs. Figure 5 C adapted from ref. 32 with permission from The Rockefeller University Press.

2 MATERIALS

2.1 Constructs

1. Standard EGFP, EYFP and ECFP vectors are used for cloning (Clontech, Palo Alto, CA).
2. pAR0, expressing human full-length wild-type AR (3) and pcDNA-AR0mcs (lacking the AR stop codon) (88) are used to fuse the AR with the fluorescent proteins.

2.2 Cell Culture and transfection

1. Hep3B Human Hepatocellular Carcinoma Cell line (ATCC)(*see* **Note 6**).
2. Alfa Minimal Essential Medium (αMEM) (Bio-Whittaker/Cambrex, Verviers, Belgium) supplemented with 2 mM L-glutamine (Bio-Whittaker/Cambrex), 100 U/mL Penicillin / 100 µg/mL Streptomycin (Bio-Whittaker/Cambrex) and 5% triple 0.1 µm sterile filtered fetal bovine serum (FBS)(HyClone, South Logan, UT). Store at 2-8˚C.
3. HyQ G418 sulfate (HyClone, South Logan, UT), working solution is 100 mg/mL active concentration in PBS. Final concentration in culture medium is 0.6 mg/mL G418.
4. Methyltrienolone (R1881) (NEN DuPont, Boston, USA). R1881 is dissolved in EtOH to 1 mM stock solution. The stock is stepwise diluted (1:10) in EtOH up to 1 nM R1881 to generate an array of working solutions. For our experiments we used the 1 µM R1881

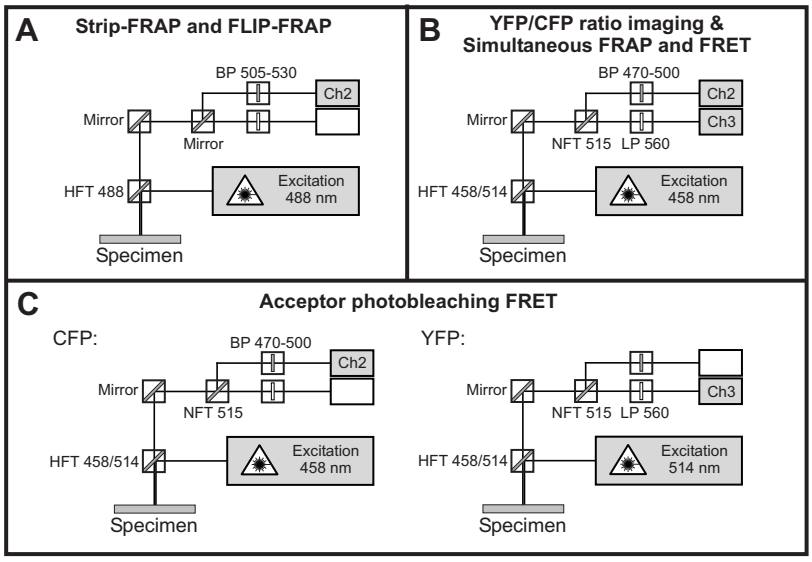

Figure 6. (A-C) Schematic representation of the configurations to monitor the fluorophores in Strip-FRAP, FLIP-FRAP, abFRET and simultaneous FRAP and FRET experiments. (A) GFP tagged proteins in strip-FRAP and FLIP-FRAP experiments are monitored using a 488 nm excitation and a specific beam splitter (HFT 488). GFP emission is collected specifically using a 505-530 band-pass filter (BP 505-530). (B) In abFRET both YFP and CFP are monitored independently by collecting both emissions sequentially, each using their specific beam path. CFP and YFP fluorescence is imaged by applying respectively 458 nm and 514 nm excitations. Both emissions are collected using a HFT 458/514, NFT 515 and a 470-500 nm band pass filter (BP470-500) for CFP and a 560nm longpass filter (LP560) for YFP. (C) In simultaneous FRAP and FRET experiments YFP and CFP are monitored simultaneously using the same filters as for abFRET. Both, CFP and YFP are excited at 458 nm.

working solution to obtain a final concentration of 1 nM of hormone in our culture medium. R1881 is light sensitive and store at –18˚C.

5. Trypsin EDTA: 200 mg/L Versene (EDTA), 500 mg/L Trypsin 1:250. Sterile filtered. Store stock at –10˚C and working solution at 2-8˚C.
6. Ø 24 mm cover slips (thickness: 0,13 - 0,16 mm) (Menzer-Gläser/Menzel Gerhard GmbH, Braunschweig, Germany)(*see* **Note 7**).
7. Polystyrene 6 Wells Cell Culture Cluster (Corning B.V. Life Sciences, Schiphol-Rijk, Netherlands)
8. FuGENE6 transfection medium (Roche Molecular Biochemicals, Indianapolis, IN). Store at 2 - 8˚C.

2.3 Confocal Microscopy (FRAP and FRET)

1. All the described techniques are performed on a Zeiss Laser Scanning Microscope LSM-510META equipped with a 30 mW Lasos LGK 7812 ML-4 Laser Class 3 B Argon laser using the 458, 488 and 514 nm lines, a acousto-optical tunable filter (AOTF) (Carl Zeiss MicroImaging GmbH, Jena, Germany) and appropriate filters for GFP, YFP and CFP imaging (Fig. 6).

2. The filter sets we used to specifically image the different fluorophores are shown in Table 1.
3. The LSM 5 software, Version 3.2 controls the microscope, the scanning and laser modules, and the image acquisition process. This software is also used to analyze the images.

Table 1: Filter sets used in FRAP and FRET experiments.

Fluorophore	Excitation	Main beam splitter	Secondary beam splitter	Emission filter
EGFP	488 nm	HFT 488	Mirror	BP 505-530
ECFP	458 nm	HFT 458/514	NFT 515	BP 470-500
EYFP	514 nm	HFT 458/514	NFT 515	LP 560

3 METHODS

3.1 Constructs

1. The GFP-AR coding construct was generated by performing PCR on pAR0 (3) using a sense primer (5′-GCAGAAGATCT**GCAGGTGCTGGAGCAGGTGCTGGAGCAGGTGCTGGA**-GAAGTGCAGTTAG-3′) to introduce a *Bgl*II restriction site and a $(GlyAla)_6$ spacer sequence and an anti-sense primer in the AR cDNA overlapping a *Sma*I site (5′-TTGCTGTTCCTCATC-CAGGA-3′). The PCR product was cloned in pGEM-T-Easy (Promega, Madison, WI) and the sequence was verified. The *Bgl*II-*Sma*I fragment was inserted in the corresponding sites of pEGFP-C1 (Clontech, Palo Alto, CA). Next the *Sma*I fragment from pAR0 was inserted into the *Sma*I site to generate pGFP-$(GlyAla)_6$-AR (further referred to as GFP-AR) (see Note 8). The non DNA binding mutant was obtained by exchanging the *Asp*718I-*Sca*I fragment from pAR(A573D) in GFP-AR.
2. The construct coding for AR double tagged with YFP and CFP (pEYFP-$(GA)_6$-AR-$(GA)_6$-ECFP) used for the FRET assays were generated by combining an N-terminally YFP-tagged AR with a C-terminally CFP-tagged AR (pAR-$(GA)_6$-ECFP). The N-terminally YFP-tagged AR was generated by replacing EGFP in the EGFP-tagged AR described earlier by an *Nhe*I/*Bgl*II EYFP-C1 (Clontech, Palo Alto, CA) fragment. The C-terminally CFP-tagged AR was generated from AR-$(GA)_6$-EGFP in which two AR fragments, a *Hin*dIII/*Kpn*I C-terminal AR fragment from pcDNA-AR0mcs (88) lacking the AR stop codon and a N-terminal *Hin*dIII AR fragment from pAR0 where sequentially inserted in EGFP-N3 (Clontech, Palo Alto, CA) followed by a introduction of a $(GlyAla)_6$ spacer sequence in the *Sac*II site between the AR and ECFP using primers (5′-G**GGTGCTGGAGCAGGTGCTGGAGCAGGTGCTGGAGC-C**GC-3′ and 5′-**GGCTCCAGCACCTGCTCCAGCACCTGCTCCAGCACC**CGC-3′) (*see* **Note 8**). After sequence verification EGFP is replaced by an ECFP-N3 (Clontech, Palo Alto, CA) *Bam*HI/*Not*I fragment for pAR-$(GA)_6$-ECFP. By insertion of the *Nhe*I/*Asp*718I EYFP-$(GA)_6$-AR fragment containing the EYFP, the spacer sequence and a part of the AR, in the *Nhe*I/

*Asp*718I sites of pAR-$(GA)_6$-ECFP a cDNA constructs coding for a EYFP and ECFP tagged AR's were generated (further referred to as YFP-AR-CFP).

3. pCYFP encoding the ECFP-EYFP chimera was generated by introducing an EYFP PCR fragment in the *Asp*718I site of pECFP-C1. Primers used for PCR: 5'-GCGAAAGGTACCGATATCACCATGGTGAGCAAGGGC-3' (sense primer) to introduce an *Asp*718I site N-terminal of EYFP and 5'-GCGAAACGTACGGTTAACGGACTTGATCAGCTCGTCCATGC-3' (anti-sense primer) to introduce a *Bsi*WI site at the C-terminus of EYFP which forms is compatible with an *Asp*718I overhang. pCYFP was kindly provided by Dr. Claude Gazin.

3.2 Cell Culture and Cell Transfection

1. Hep3B cells are grown in αMEM supplemented with L-Glutamide, Penicillin, Streptomycin and 5% FCS at 37˚C and 5% CO_2 and passaged when approaching confluence (every 3-4 days) with Trypsin/EDTA to provide experimental cultures.
2. Two days before confocal microscopy Hep3B cells are seeded on a coverslip in a 6-wells plate at a concentration of approx. $3x10^5$ cells per well in 2 mL αMEM with 5% FCS. This concentration will provide near confluent cultures at the time of the experiment and enough cells at the time of transfection. The cells are grown overnight at 37˚C with 5% CO_2.
3. Between 24 and 32 hours before confocal microscopy the medium is replaced by 1 mL αMEM supplemented with 5% charcoal striped serum (DCC), L-Glutamide and antibiotics, without washing the cells.
4. After 2 hours the transfection mix is prepared for the transfection of 1 mg of GFP-AR coding vector. Three μL FuGENE6 per μg DNA to be transfected is added to 100 μL serum free αMEM. Five minutes later DNA is added. The transfection mix is gently mixed by pipeting up and down and left at room temperature for at least 30 minutes.
5. Four hours after medium replacement the transfection mix is gently added to the cells under gentle mixing. The cells further incubated for 4 hours at 37˚C and 5 % CO_2.
6. Four hours after transfection the medium is replaced again by 2 mL αMEM supplemented with charcoal striped serum (DCC) with or without 100 nM R1881. The cells are further incubated overnight at 37 ˚C and 5 % CO_2 until the experiment.

3.3 Confocal Microscopy

3.3.1 Fluorescence Recovery After Photobleaching (FRAP)

3.3.1.1 Strip-FRAP

1. These instructions assume the use of a Zeiss CLSM 510 confocal laser-scanning microscope equipped with an Argon laser (Fig. 6 A). The Argon laser is adjusted to 6.1 A tube current and allowed to stabilize for at least 15 min.

2. A cover slip with Hep3B cells expressing GFP tagged AR (EGFP-AR) is placed in a metal holder in which 1.5 mL culture medium is added on top of the coverslip. The holder including the coverslip is placed on a temperature-controlled plate at 37°C. In addition, the objective lens is also kept at 37°C by a temperature controlled ring, in order to prevent cooling of cells near the lens, which are exactly the ones being investigated.
3. GFP fluorescence is monitored using 488 nm excitation at the low intensity of 0.5-0.8 μW (measured in the focal plane of the 40X objective lens used) (*see* **Note 9**), a main beamsplitter reflecting only light at a wavelength of 488 nm, and a band pass filter BP505-530 (Fig. 6 A) (*see* Table 1). The pinhole is adjusted to a diameter corresponding to an 'optical slice' of approximately 2 μm and a high detector gain (900) (*see* **Notes 10** and **11**). Scanning is performed unidirectional with scan speed of 1.9 msec per line of 512 pixels spaced 70 nm to enable fast recording of the fluorescent signal in the strip. Fluorescent signals are recorded with an 8-bit data depth.
4. A nucleus with a physiologically relevant expression level of GFP-AR is selected at low zoom (*see* **Note 12**). The scanning area is adjusted using the 'center' macro in the macro-directory to put the center of the nucleus in the middle of the scanning area after which the nucleus is aligned vertically using the crop function (*see* **Note 13**). When the nucleus is oriented correctly sample distance (pixel size) is adjusted to 70 nm.
5. A 10 pixel (= 700 nm) wide region of interest (ROI) spanning the nucleus is selected in the Edit ROI panel, for recording the recovery of the signal. Using the Define Region option the Bleach Control panel the same ROI is selected to locally bleach GFP (Fig. 2 A).
6. The fluorescent signal is monitored by scanning the ROI for 4000 scans (approx. 80 seconds) with a 21 msec time interval (Time Series Control) at low excitation (*see* **Note 9**) (Fig. 2A). After 200 scans the GFP is bleached locally inside the ROI using a scan (1 iteration) of 488nm laser light at maximum laser intensity. The time-series are initiated using the Mean ROI option in the time-series control (*see* **Note 14**). After the scan the data can be copied to for instance a spreadsheet file or can be directly saved as MDB-file for later analysis.
7. Before averaging a sufficient amount of curves the data have to be normalized (*see* **Note 15**). The most straightforward normalization is to express the data relative to prebleach intensities ($I_{prebleach}$) after background subtraction: $I_{norm,t} = (I_{t,raw} - I_{background}) / (I_{prebleach} - I_{background})$. Alternatively, it is also possible to express the raw data relative to both fluorescence before, as well as immediately after bleaching: $I_{norm,t} = (I_{t,raw} - I_0) / (I_{prebleach} - I_0)$. This normalization not only removes variations in expression levels but also of the laser intensity used for bleaching, which can lead to differences in bleach depth (see Note 16). To allow fitting of the data to simple analytical equations representing the diffusion process, the data can also be expressed relative to the fluorescence intensities immediately after the bleach and after complete recovery, resulting in curves starting at 0 after the bleach and 1 at complete recovery: $I_{norm,t} = (I_{t,raw} - I_0) / (I_{postbleach} - I_0)$ (Fig. 2 B) (*see* **Note 17**) (18).

3.3.1.2 FLIP-FRAP

1. Cells are placed in the Zeiss CLSM 510 confocal laser-scanning microscope and positioned in the focal plane as described in the strip-FRAP section. For FLIP-FRAP similar settings are used for GFP imaging. A correctly oriented nucleus is imaged using a zoom corresponding to a pixel interval of 70 nm. The pinhole is adjusted to a diameter corresponding to an 'optical slice' of approximately 2 μm. Scanning is performed unidirectional with scan speed of 1.9 msec per line of 512 pixels to enable fast recording of the fluorescent signal in the strip. Fluorescent signals are recorded with an 8-bit data depth using a high detector gain (1000) (*see* **Notes 10** and **11**).
2. A region of interest (ROI) with a width between approximately 1 and 2 μm (but constant in all experiments to be compared) and spanning the nucleus at one pole is selected in the Edit ROI panel, for recording the recovery of the signal after bleaching. Using the Define Region option the Bleach Control panel the same ROI is selected to locally bleach GFP. A second ROI of similar width spanning the nucleus at the opposite pole is selected, to measure the decrease of fluorescence due to redistribution of the proteins from the bleached area (FLIP) (Fig. 2 C).
3. The fluorescent signal is monitored by scanning the two ROIs at a low excitation level with a 3 sec time interval for approximately 100 seconds, dependent on the mobility of the protein under surveillance (Time Series Control) (*see* **Note 9**). After the first scan GFP is bleached locally inside one of the two ROIs (but always the same in experiments to be compared) using 10 iterations of 488nm laser light at maximum laser intensity. After the experiment the data can be copied directly to a spreadsheet file or can be saved as MDB-file for later analysis.
4. The most straight forward analysis is to calculate the fluorescence intensity difference between the FLIP-ROI and the FRAP-ROI and normalize the data ($I_{FLIP\text{-}FRAP} = (I_{FLIP\text{-}ROI} - I_{FRAP\text{-}ROI}$) and normalize to the intensity directly after bleaching (Fig. 2 D).

3.3.2 Fluorescence Resonance Energy Transfer (FRET)

3.3.2.1 Ratio imaging

1. A coverslip with Hep3B cells expressing double, EYFP and ECFP, tagged AR (EYFP-AR-ECFP) in the absence of hormone is placed in the Zeiss CLSM 510 confocal laser-scanning microscope and cells are positioned in the focal plane as described in the strip-FRAP section.
2. EYFP and ECFP images were collected sequentially using the single-track configuration. Both CFP and YFP are detected using 458 nm excitation at low laser power to avoid monitorbleaching (*see* **Note 9**), a 458/514 nm dichroic beam splitter (HFT 458/514) and a 515 nm beam splitter (NFT 515). ECFP and EYFP signals were further separated a 470-500 nm band pass emission filter (BP470-500) and a 560 nm long pass emission filter (LP560),

respectively (Fig. 6 B). A group of cells with an EYFP-AR-ECFP expression at physiological relevant expression level (*see* **Note 12**) is selected at a zoom corresponding to a pixel interval of 220 nm. Scanning is performed unidirectional at a scan speed corresponding to 3.84 msec per line of 512 pixels and an average of 2, with the pinhole diameter such that the "optical slice" has an approximate thickness of 3 μm. Detector gain in both the YFP and CFP track is set on 900 (*see* **Notes 10** and **11**). Sequential images of 512x512 pixels are collected with an 8-bit data depth using the timeseries macro or the multitime macro with an interval of 30 seconds (*see* **Note 18**) (Fig. 3 A). At a user specified moment during the collection of images the AR is induced by adding 100 nM R1881 (synthetic derivate of testosterone).

3. EYFP and ECFP image sequences were analyzed using the Zeiss Laser Scanning Microscope LSM510 software selecting regions of interest (ROIs) covering each cell (*see* **Note 19**). After background subtraction FRET is simply calculated as: I_{YFP} / I_{CFP} and plotted in time (Fig. 3 B) (*see* **Note 20**).

3.3.2.2 Acceptor photobleaching FRET (abFRET)

1. A coverslip with Hep3B cells expressing double, YFP and CFP, tagged AR (YFP-AR-CFP) is placed in the Zeiss CLSM 510 confocal laser-scanning microscope and cells are positioned in the focal plane as described in the strip-FRAP section.
2. YFP and CFP images of cells with a low EYFP-AR-ECFP expression were collected sequentially using the multitrack option (*see* **Notes 12** and **21**). For both fluorophores two specific beam paths are used. Both tracks include a 458/514 nm dichroic beam splitter (HFT 458/514) and a 515 nm beam splitter (NFT 515). ECFP was excited with 10 μW (measured at the focus of the 40X objective lens with aperture 1.35) 458 nm laser light of an Argon laser and imaged with a 470-500 nm band pass emission filter (BP470-500). EYFP was excited with 5 μW 514 nm laser light and imaged with a 560 nm long pass emission filter (LP560) (Fig. 6 C).
3. In both tracks the pinhole diameter is adjusted such that the 'optical slice' is 1.2 μm. Scanning is preformed unidirectional with scan speed corresponding with 3.07 msec per line of 512 pixels at a pixel interval of 100 nm. Detector gain in the YFP track is set on 800 in the CFP track on 900, the amplifier offset and amplifier gain in both tracks are 0.1 and 1 respectively (*see* **Notes 10** and **11**). Images of 512x512 pixels are generated with an 8-bit data depth.
4. After sequential collection of YFP and CFP images, YFP is bleached by scanning 25 times a nuclear region of ~100 μm^2, covering a large part of the nucleus using the 514 nm argon laser line at high (~80 μW) laser power. After acceptor photobleaching a second YFP and CFP image pair was collected (*see* **Note 22**) (Fig. 4 A).
5. YFP and CFP images were analyzed using the Zeiss Laser Scanning Microscope LSM510 software. After background subtraction the apparent FRET efficiency was calculated as;

Apparent FRET efficiency = $((CFP_{after} - CFP_{before}) \times YFP_{before}) \times ((CFP_{after} \times YFP_{before}) - (CFP_{before} \times YFP_{after}))^{-1}$, in which the relative CFP increase due to YFP bleaching is corrected for the fraction of YFP bleached (54). The apparent FRET efficiency was finally expressed relative to control measurements in cells expressing either free CFP and YFP ($abFRET_0$) or the CFP-YFP fusion protein ($abFRET_{CFP\text{-}YFP\ fusion}$): apparent FRET efficiency = $(abFRET - abFRET_0) / (abFRET_{CFP\text{-}YFP\ fusion} - abFRET_0)$ (Fig. 4 B).

3.3.2.3 Simultaneous FRAP and FRET

1. A coverslip with Hep3B cells expressing YFP and CFP double-tagged AR (EYFP-AR-ECFP) is placed in the Zeiss CLSM 510 confocal laser-scanning microscope and are positioned in the focal plane as described in the strip-FRAP section.
2. In contrast to acceptor bleaching FRET, YFP and CFP signals, are collected simultaneously using two parallel channels but only one 458nm excitation at low laser intensity and a 458/514 nm dichroic beam splitter (HFT 458/514) (*see* **Note 23**). The two specific emission beam paths for both fluorophores are similar to those used for acceptor bleaching FRET. The emission signal is separated using a 515 nm beam splitter (NFT 515). ECFP emission is collected via a 470-500 nm band pass emission filter (BP470-500). EYFP emission is simultaneously collected via a 560 nm long pass emission filter (LP560) (Fig. 6 B). Scanning is performed unidirectional with scan speed of 1.9 msec per line of 512 pixels spaced 70 nm to enable fast recording of the fluorescent signal in the strip. The pinhole is adjusted to a diameter corresponding to an 'optical slice' of approximately 3 μm. Similar as in strip-FRAP experiments a high detector gain (1000) is used (*see* **Notes 10** and **11**). Fluorescent signals at are recorded with an 8-bit data depth.
3. A nucleus with a low expression of YFP-AR-CFP is selected at low zoom (*see* **Note 12**). The scanning area is adjusted using the 'center' macro in the macro-directory to put the center of the nucleus in the middle of the scanning area. The nucleus is rotated using the crop function to align the nucleus vertically.
4. A 700 nm wide region of interest (ROI) (corresponding to 10 pixels at zoom 6 on a Zeiss LSM 510 meta) spanning the nucleus is selected in the Edit ROI panel, for recording the recovery of the signal. Using the Define Region option the Bleach Control panel the same ROI is selected to locally bleach YFP (Fig. 5 A).
5. The fluorescent signal is monitored at low laser intensity (*see* **Note 9**), by scanning the ROI with interval of 100 msec (Time Series Control) for approximately 80 seconds, dependent on the mobility of the protein under surveillance. After 400 scans the YFP is specifically bleached locally inside the ROI using a scan (5 iterations) of 514 nm laser light at maximum laser intensity (*see* **Note 23**). The time-series are initiated using the Mean ROI option in the time-series control. After the scan the data can be copied directly to a spreadsheet or can be saved as MDB-file for later analysis.

6. Like in strip-FRAP it is possible to normalize the donor fluorescence data in different ways. By expressing the raw data relative to prebleach values one can visualize directly the increase of CFP signal when YFP is bleached ($I_{norm,t} = (I_{t,raw} - I_{background}) / (I_{prebleach} - I_{background})$) (Fig. 5 B), but comparison between the interacting proteins vs. the total pool (*i.e.* the donor and acceptor fluorescence signals respectively) requires expressing raw data relative to intensity values immediately after bleaching and to prebleach intensities ($I_{norm,t} = (I_{t,raw} - I_0) / (I_{prebleach} - I_0)$) or after complete redistribution ($I_{norm,t} = (I_{t,raw} - I_0) / (I_{postbleach} - I_0)$) where $I_{prebleach}$, I_0 and $I_{postbleach}$ are the fluorescent intensities before, immediately after the bleach and after complete recovery, respectively (Fig. 5 C) (*see* **Note 24**).

4 NOTES

1. Fluorescence *redistribution* after photobleaching may be better description rather than fluorescence *recovery* after photobleaching: in the absence of a permanently immobilised fraction the fluorescence intensity in the measured region will level of to the average intensity in the nucleus, which will be lower than the initial intensity because of the permanently bleached fraction. The term "recovery" suggests that fluorescence intensity in general returns to the initial levels.
2. In FRAP, a fraction of the fluorescent proteins inside a nucleus will be irreversibly bleached during the bleach pulse, resulting in an incomplete recovery of the fluorescent signal independent of the presence of an immobile fraction. In the case of the AR this can be corrected by comparing wild type AR with the non-DNA binding mutant (*e.g.* AR(A573D)), which does not get immobilized due to DNA-binding. Therefore the incomplete recovery of fluorescence of for instance a tagged non-DNA binding AR mutant is only due to irreversibly bleaching of a significant fraction of the molecules during the bleach pulse. In the experimental settings of the strip-FRAP procedure described here, approximately 10% of a nucleus of average size is photobleached.
3. The efficiency of energy transfer does not only depend on the distance between the two fluorophores but also their relative orientation plays a role in FRET efficiency (39). However, in fusion proteins using a flexible linker between the fluorescent protein and the protein of interest, this may be limited because of the rotational freedom of the fluorophores.
4. FRET only occurs when the excitation spectrum of the acceptor fluorophore overlaps significantly with the emission spectrum of the donor fluorophore. On the other hand, the excitation and emission spectra of the FRET couple need sufficient separation to be able to sufficiently separate the two signals. The most widely used FRET couple is the combination between CFP and YFP, but improved fluorophore variants will certainly

contribute to the applicability of FRET in protein-protein interaction studies (Discussed in 42).

5. In our experience monitorbleaching does not fluctuate very much when settings are kept constant and is mostly dependent on excitation power. Therefore, normalisation to FRET values measured for cotransfected free YFP and CFP as negative control can be used to correct the apparent FRET efficiency for monitor bleaching when the excitation power is kept constant.
6. Hep3B-cells lack endogenous nuclear receptors, are easy to transfect and they are relatively large, simplifying microscopy. Other type of cells can be used but the presence of endogenous nuclear receptors needs to be taken into account. Endogenous expression of nuclear receptors will dilute FRET values.
7. Coverslips should not be thicker than 0.16 mm, because of the high numerical aperture and short working distance of most lenses used for high-resolution confocal microscopy.
8. It is essential to check the fusion proteins for functionality. For tagged ARs most often ARE driven luciferase gene reporter assays are used. By using such a luciferase gene reporter assay we showed that a flexible stretch between the AR and the fluorophores limits the degree to which the activity of the AR is affected by the presence of the large GFP-tag(s). Our data indicated that GFP-AR with a $(GlyAla)_6$ stretch functions better than with a $(Gly)_6$ spacer (11). In addition, the flexible stretch most likely also gives the fluorophores more rotational freedom limiting the influence of fluorophore orientations on FRET efficiencies (*see also* **Note 3**).
9. At this intensity no significant bleaching of GFP, YFP or CFP should occur during the experiment, which takes between 10-80 seconds. In FRAP experiments it is important to avoid monitor bleaching by applying excitation at lowest possible laser power. In simultaneous FRAP and FRET experiments monitor bleaching hampers the analysis because of the opposite effect of monitor bleaching on the redistributions of the YFP and CFP signals. In the acceptor bleaching FRET experiments monitor bleaching is less problematic because the apparent FRET efficiency can be corrected by normalization to the FRET efficiency of cotransfected CFP and YFP (*see also* **Note 5**).
10. Although a higher detector gain (DG) can be used to obtain higher signals, it does not improve the signal-to-noise ratio. Therefore, a trade-off between settings is necessary to optimize the experimental setup to reduce both noise (*e.g.* averaging) and monitor bleaching (*e.g.* lower excitation level, rapid scanning) but still producing a high enough signal in low expressing cells (*e.g.* wider pinhole; although this is at the cost of resolution, in many interaction studies the interaction as such is more important than its precise location; however, if it is important, higher laser excitation intensity may be required). These settings might also depend on the level or pattern of expression of the protein of interest.

11. It is important to choose settings that allow selecting low expressing cells in your experiments. This can be achieved by *e.g.* higher detector gain, wider pinhole or higher laser excitation intensity, but might be at the cost of signal to noise ratio and resolution (*see also* **Notes 10** and **12**).
12. For all the discussed approaches it is essential to select cells that express the investigated protein at a physiologically relevant level, since overexpression may lead to aggregation and artificial immobilization of the receptors (23) and false positive FRET signals due to high concentration.
13. Not only the size of a nucleus, but also the shape and the relative position of the bleached region will influence the fluorescence recovery curve. Therefore it is highly important to keep these parameters similar. We chose to select ellipsoid nuclei and bleach a strip spanning the nucleus at its shortest ellipsoidal axis (see for instance Fig. 2 A).
14. In the configuration the monitordiode (ChM) can be selected to monitor the fluctuations in the laser intensity during scanning.
15. Normalization of FRAP data before averaging is important in order to remove variation due to differences in absolute amounts of protein. This is justified since fluorescent changes after bleaching are proportional to initial values, and do not depend on fluorophore concentration. Obviously, the investigated cells should have expression levels within physiologically relevant limits. In an average experiment approximately 10-15 cells are measured.
16. In theory this is only true if the bleach pulse is infinitely short and the first measurement is really immediately after bleaching.
17. Any permanently immobile fraction is removed in this case allowing determination of the (apparent) diffusion coefficient of the mobile fraction.
18. Using the multitime-macro in the LSM510 software enables to image more than one position in parallel. Selecting multiple locations limits the time resolution of the time series.
19. Due to movement of cells it might be necessary to adapt location and/or shape of the regions of interest (ROIs) in the analysis of time series.
20. Ratio imaging is only possible in three cases: 1) when signals are compared in the same single cell before and after a specific treatment, 2) when the FRET pair is tagged to the same molecule, and, 3) when the donor and acceptor are expressed at a constant concentration ratio.
21. To specifically image both fluorescence signals and avoid cross talk in the different channels YFP and CFP are imaged sequentially, exciting YFP and CFP each at their specific wavelength (514 nm and 458 nm, respectively) and separating their emission signals through specific filtersets (see table 1).
22. Previously we have shown that in the absence of FRET no CFP signal increase is observed in cells with the low expression level used (32).

23. In principle the experiment is a standard FRAP experiment on the acceptor, in this case YFP, in which in an additional channel the fluorescence of the donor is being recorded.
24. Subtractions in the donor signal normalization lead to negative numbers, yielding a positive result after division, where the curve starts at 0 and increases until it reaches 1. So the donor loss of fluorescence characteristics are represented by an increasing curve allowing direct comparison with the FRAP-data from the acceptor.

5 REFERENCES

1. Germain, P., Staels, B., Dacquet, C., Spedding, M., and Laudet, V. (2006) Overview of nomenclature of nuclear receptors. *Pharmacol. Rev.* 58, 685-704.
2. Trapman, J., and Cleutjens, K. B. (1997) Androgen-regulated gene expression in prostate cancer. Semin. *Cancer Biol.* 8, 29-36.
3. Brinkmann, A. O., Faber, P. W., van Rooij, H. C. J., Kuiper, G. G. J. M., Ris, C., Klaassen, P., van der Korput, J. A. G. M., Voorhorst, M. M., van Laar, J. H., Mulder, E., and Trapman, J. (1989) The human androgen receptor: domain structure, genomic organization and regulation of expression. *J. Steroid Biochem.* 34, 307-310.
4. Claessens, F., Verrijdt, G., Schoenmakers, E., Haelens, A., Peeters, B., Verhoeven, G., and Rombauts, W. (2001) Selective DNA binding by the androgen receptor as a mechanism for hormone-specific gene regulation. *J. Steroid Biochem. Mol. Biol.* 76, 23-30.
5. Cleutjens, K. B. J. M., van der Korput, J. A. G. M., van Eekelen, C. C. E. M., van Rooij, H. C. J., Faber, P. W., and Trapman, J. (1997) An androgen response element in a far upstream enhancer region is essential for high, androgen-regulated activity of the prostate-specific antigen promoter. Mol. Endocrinol. 11, 148-161.
6. Tyagi, R. K., Lavrovsky, Y., Ahn, S. C., Song, C. S., Chatterjee, B., and Roy, A. K. (2000) Dynamics of intracellular movement and nucleocytoplasmic recycling of the ligand-activated androgen receptor in living cells. *Mol. Endocrinol.* 14, 1162-1174.
7. Georget, V., Lobaccaro, J. M., Terouanne, B., Mangeat, P., Nicolas, J.C., and Sultan, C. (1997) Trafficking of the androgen receptor in living cells with fused green fluorescent protein-androgen receptor. *Mol. Cell. Endocrinol.* 129, 17-26.
8. Rayasam, G. V., Elbi, C., Walker, D. A., Wolford, R., Fletcher, T. M., Edwards, D. P., and Hager, G. L. (2005) Ligand-specific dynamics of the progesterone receptor in living cells and during chromatin remodeling in vitro. *Mol. Cell. Biol.* 25, 2406-2418.
9. Farla, P., Hersmus, R., Trapman, J., and Houtsmuller, A. B. (2005) Antiandrogens prevent stable DNA-binding of the androgen receptor. *J. Cell Sci.* 118, 4187-4198.
10. Agresti, A., Scaffidi, P., Riva, A., Caiolfa, V. R., and Bianchi, M. E. (2005) GR and HMGB1 interact only within chromatin and influence each other's residence time. *Mol. Cell* 18, 109-121.
11. Farla, P., Hersmus, R., Geverts, B., Mari, P. O., Nigg, A. L., Dubbink, H. J., Trapman, J., and Houtsmuller, A. B. (2004) The androgen receptor ligand-binding domain stabilizes DNA binding in living cells. *J. Struct. Biol.* 147, 50-61.
12. Schaaf, M. J., and Cidlowski, J. A. (2003) Molecular determinants of glucocorticoid receptor mobility in living cells: the importance of ligand affinity. *Mol. Cell. Biol.* 23, 1922-1934.
13. Stenoien, D. L., Patel, K., Mancini, M. G., Dutertre, M., Smith, C. L., O'Malley, B. W., and Mancini, M. A. (2001) FRAP reveals that mobility of oestrogen receptor-alpha is ligand- and proteasome-dependent. *Nat. Cell Biol.* 3, 15-23.
14. McNally, J. G., Müller, W. G., Walker, D., Wolford, R., and Hager, G. L. (2000) The glucocorticoid receptor: rapid exchange with regulatory sites in living cells. *Science* 287, 1262-1265.
15. Houtsmuller, A. B., and Vermeulen, W. (2001) Macromolecular dynamics in living cell nuclei revealed by fluorescence redistribution after photobleaching. *Histochem. Cell Biol.* 115, 13-21.

16. Houtsmuller, A. B., Rademakers, S., Nigg, A. L., Hoogstraten, D., Hoeijmakers, J. H. J., and Vermeulen, W. (1999) Action of DNA repair endonuclease ERCC1/XPF in living cells. *Science* 284, 958-961.

17. Houtsmuller, A. B. (2005) Fluorescence recovery after photobleaching: application to nuclear proteins. *in* "Adv. Biochem. Eng. Biotechnol." (Rietdorf, J., ed.), Vol. 95, Springer-Verlag GmbH, Berlin, pp. 177-199.

18. Van Royen, M. E., Farla, P., Mattern, K. A., Geverts, B., Trapman, J., and Houtsmuller, A. B. (2009) FRAP to study nuclear protein dynamics in living cells. *in* "The Nucleus, Volume 2: Chromatin, Transcription, Envelope, Proteins, Dynamics, and Imaging" (Hancock, R., ed.), Vol. 464, Humana Press / Springer, Totowa. pp. 363-385.

19. Bruggenwirth, H. T., Boehmer, A. L. M., Lobaccaro, J. M., Chiche, L., Sultan, C., Trapman, J., and Brinkmann, A. O. (1998) Substitution of Ala564 in the first zinc cluster of the deoxyribonucleic acid (DNA)-binding domain of the androgen receptor by Asp, Asn, or Leu exerts differential effects on DNA binding. *Endocrinology* 139, 103-110.

20. Elbi, C., Walker, D. A., Romero, G., Sullivan, W. P., Toft, D. O., Hager, G. L., and DeFranco, D. B. (2004) Molecular chaperones function as steroid receptor nuclear mobility factors. *Proc. Natl. Acad. Sci. U.S.A.* 101, 2876-2881.

21. Stavreva, D. A., Muller, W. G., Hager, G. L., Smith, C. L., and McNally, J. G. (2004) Rapid glucocorticoid receptor exchange at a promoter is coupled to transcription and regulated by chaperones and proteasomes. *Mol. Cell. Biol.* 24, 2682-2697.

22. Klokk, T. I., Kurys, P., Elbi, C., Nagaich, A. K., Hendarwanto, A., Slagsvold, T., Chang, C.Y., Hager, G. L., and Saatcioglu, F. (2007) Ligand-specific dynamics of the androgen receptor at its response element in living cells. *Mol. Cell. Biol.* 27, 1823-1843.

23. Marcelli, M., Stenoien, D. L., Szafran, A. T., Simeoni, S., Agoulnik, I. U., Weigel, N. L., Moran, T., Mikic, I., Price, J. H., and Mancini, M. A. (2006) Quantifying effects of ligands on androgen receptor nuclear translocation, intranuclear dynamics, and solubility. *J. Cell. Biochem.* 98, 770-788.

24. Masiello, D., Cheng, S., Bubley, G. J., Lu, M. L., and Balk, S. P. (2002) Bicalutamide functions as an androgen receptor antagonist by assembly of a transcriptionally inactive receptor. *J. Biol. Chem.* 277, 26321-26326.

25. Kang, Z., Pirskanen, A., Janne, O. A., and Palvimo, J. J. (2002) Involvement of proteasome in the dynamic assembly of the androgen receptor transcription complex. *J. Biol. Chem.* 277, 48366-48371.

26. Veldscholte, J., Ris-Stalpers, C., Kuiper, G. G., Jenster, G., Berrevoets, C., Claassen, E., van Rooij, H. C., Trapman, J., Brinkmann, A. O., and Mulder, E. (1990) A mutation in the ligand binding domain of the androgen receptor of human LNCaP cells affects steroid binding characteristics and response to anti-androgens. *Biochem. Biophys. Res. Commun.* 173, 534-540.

27. Hara, T., Miyazaki, J., Araki, H., Yamaoka, M., Kanzaki, N., Kusaka, M., and Miyamoto, M. (2003) Novel mutations of androgen receptor: a possible mechanism of bicalutamide withdrawal syndrome. *Cancer Res.* 63, 149-53.

28. Schaaf, M. J. M., Lewis-Tuffin, L. J., and Cidlowski, J. A. (2005) Ligand-selective targeting of the glucocorticoid receptor to nuclear subdomains is associated with decreased receptor mobility. *Mol. Endocrinol.* 19, 1501-1515.

29. Martinez, E. D., Rayasam, G. V., Dull, A. B., Walker, D. A., and Hager, G. L. (2005) An estrogen receptor chimera senses ligands by nuclear translocation. *J. Steroid Biochem. Mol. Biol.* 97, 307-321.

30. Sharp, Z. D., Mancini, M. G., Hinojos, C. A., Dai, F., Berno, V., Szafran, A. T., Smith, K. P., Lele, T. T., Ingber, D. E., and Mancini, M. A. (2006) Estrogen-receptor-α exchange and chromatin dynamics are ligand- and domain-dependent. *J. Cell Sci.* 119, 4101-4116.

31. Meijsing, S. H., Elbi, C., Luecke, H. F., Hager, G. L., and Yamamoto, K. R. (2007) The ligand binding domain controls glucocorticoid receptor dynamics independent of ligand release. *Mol. Cell. Biol.* 27, 2442-2451.

32. Van Royen, M. E., Cunha, S. M., Brink, M. C., Mattern, K. A., Nigg, A. L., Dubbink, H. J., Verschure, P. J., Trapman, J., and Houtsmuller, A. B. (2007) Compartmentalization of androgen receptor protein-protein interactions in living cells. *J. Cell Biol.* 177, 63-72.

33. Rosenfeld, M. G., Lunyak, V. V., and Glass, C. K. (2006) Sensors and signals: a coactivator/corepressor/epigenetic code for integrating signal-dependent programs of transcriptional response. *Genes Dev.* 20, 1405-1428.

34. Griekspoor, A., Zwart, W., Neefjes, J., Michalides, R. (2007) Visualizing the action of steroid hormone receptors in living cells. *Nucl. Recept. Signal.* 5, e003.

35. Sato, M. (2006) Imaging molecular events in single living cells. *Anal. Bioanal. Chem.* 386, 435-443.

36. Day, R. N., Periasamy, A., and Schaufele, F. (2001) Fluorescence resonance energy transfer microscopy of localized protein interactions in the living cell nucleus. *Methods* 25, 4-18.

37. Day, R. N., Nordeen, S. K., and Wan, Y. (1999) Visualizing protein-protein interactions in the nucleus of the living cell. *Mol. Endocrinol.* 13, 517-526.

38. Kenworthy, A. K. (2001) Imaging protein-protein interactions using fluorescence resonance energy transfer microscopy. *Methods* 24, 289-296.

39. Clegg, R. M. (1995) Fluorescence resonance energy transfer. *Curr. Opin. Biotechnol.* 6, 103-110.

40. Labas, Y. A., Gurskaya, N. G., Yanushevich, Y. G., Fradkov, A. F., Lukyanov, K. A., Lukyanov, S. A., and Matz, M. V. (2002) Diversity and evolution of the green fluorescent protein family. *Proc. Natl. Acad. Sci. U.S.A.* 99, 4256-4261.

41. Zhang, J., Campbell, R. E., Ting, A. Y., and Tsien, R. Y. (2002) Creating new fluorescent probes for cell biology. *Nat. Rev. Mol. Cell Biol.* 3, 906-918.

42. Shaner, N. C., Steinbach, P. A., and Tsien, R. Y. (2005) A guide to choosing fluorescent proteins. *Nat. Methods* 2, 905-909.

43. Piston, D. W., and Kremers, G. J. (2007) Fluorescent protein FRET: the good, the bad and the ugly. *Trends Biochem. Sci.* 32, 407-414.

44. Rizzo M. A., Springer G. H., Granada B, Piston D. W. (2004) An improved cyan fluorescent protein variant useful for FRET. *Nat. Biotechnol.* 22, 445-449.

45. Ai, H. W., Henderson, J. N., Remington, S. J., and Campbell, R. E. (2006) Directed evolution of a monomeric, bright and photostable version of Clavularia cyan fluorescent protein: structural characterization and applications in fluorescence imaging. *Biochem. J.* 400, 531-540.

46. Kremers, G. J., Goedhart, J., van Munster, E. B., and Gadella, Jr, T. W. J. (2006) Cyan and yellow super fluorescent proteins with improved brightness, protein folding, and FRET Forster radius. *Biochemistry* 45, 6570-6580.

47. Zacharias, D. A., Violin, J. D., Newton, A. C., and Tsien, R. Y. (2002) Partitioning of lipid-modified monomeric GFPs into membrane microdomains of live cells. *Science* 296, 913-916.

48. Griesbeck, O., Baird, G. S., Campbell, R. E., Zacharias, D. A., and Tsien, R. Y. (2001) Reducing the environmental sensitivity of yellow fluorescent protein. Mechanism and applications. *J. Biol. Chem.* 276, 29188-29194.

49. Nagai, T., Ibata, K., Park, E. S., Kubota, M., Mikoshiba, K., and Miyawaki, A. (2002) A variant of yellow fluorescent protein with fast and efficient maturation for cell-biological applications. *Nat. Biotechnol.* 20, 87-90.

50. Shaner, N. C., Campbell, R. E., Steinbach, P. A., Giepmans, B. N., Palmer, A. E., and Tsien, R. Y. (2004) Improved monomeric red, orange and yellow fluorescent proteins derived from Discosoma sp. red fluorescent protein. *Nat. Biotechnol.* 22, 1567-1572.

51. Karasawa, S., Araki, T., Nagai, T., Mizuno, H., and Miyawaki, A. (2004) Cyan-emitting and orange-emitting fluorescent proteins as a donor/acceptor pair for fluorescence resonance energy transfer. *Biochem J.* 381, 307-312.

52. Merzlyak, E. M., Goedhart, J., Shcherbo, D., Bulina, M. E., Shcheglov, A. S., Fradkov, A. F., Gaintzeva, A., Lukyanov, K. A., Lukyanov, S., Gadella, Jr, T. W. J., and Chudakov, D. M. (2007) Bright monomeric red fluorescent protein with an extended fluorescence lifetime. *Nat. Methods* 4, 555-557.

53. Zimmermann, T., Rietdorf, J., Girod, A., Georget, V., and Pepperkok, R. (2002) Spectral imaging and linear un-mixing enables improved FRET efficiency with a novel GFP2-YFP FRET pair. *FEBS Lett.* 531, 245-249.

54. Dinant, C., Van Royen, M. E., Vermeulen, W., and Houtsmuller, A. B. (2008) Fluorescence resonance energy transfer of GFP and YFP by spectral imaging and quantitative acceptor photobleaching. *J. Microsc.* 231:97-104.

55. Jares-Erijman EA, J. T. (2003) FRET imaging. *Nat. Biotechnol.* 21, 1387-95.

56. Xia, Z., and Liu, Y. (2001) Reliable and global measurement of fluorescence resonance energy transfer using fluorescence microscopes. *Biophys. J.* 81, 2395-2402.

57. Gordon, G. W., Berry, G., Liang, X. H., Levine, B., and Herman, B. (1998) Quantitative fluorescence resonance energy transfer measurements using fluorescence microscopy. *Biophys. J.* 74, 2702-2713.

58. Van Rheenen, J., Langeslag, M., and Jalink, K. (2004) Correcting confocal acquisition to optimize imaging of fluorescence resonance energy transfer by sensitized emission. *Biophys. J.* 86, 2517-2529.

59. Bastiaens, P. I. H., Majoul, I. V., Verveer, P. J., Söling, H.D., and Jovin, T. M. (1996) Imaging the intracellular trafficking and state of the AB5 quaternary structure of cholera toxin. *EMBO J.* 15, 4246-4253.

60. Bastiaens, P. I. H., and Jovin, T. M. (1996) Microspectroscopic imaging tracks the intracellular processing of a signal transduction protein: Fluorescent-labeled protein kinase C βI. *Proc. Natl. Acad. Sci. U.S.A.* 93, 8407-8412.

61. Karpova, T. S., Baumann, C. T., He, L., Wu, X., Grammer, A., Lipsky, P., Hager, G. L., and McNally, J. G. (2003) Fluorescence resonance energy transfer from cyan to yellow fluorescent protein detected by acceptor photobleaching using confocal microscopy and a single laser. *J. Microsc.* 209, 56-70.

62. Bastiaens, P. I. H., and Squire, A. (1999) Fluorescence lifetime imaging microscopy: spatial resolution of biochemical processes in the cell. *Trends Cell Biol.* 9, 48-52.

63. Wallrabe, H., and Periasamy, A. (2005) Imaging protein molecules using FRET and FLIM microscopy. *Curr. Opin. Biotechnol.* 16, 19-27.

64. Van Munster, E. B., and Gadella, Jr, T. W. J. (2005) Fluorescence Lifetime Imaging Microscopy (FLIM) *in* "Adv. Biochem. Eng. Biotechnol." (Rietdorf, J., ed.), Vol. 95, Springer-Verlag GmbH, Berlin, pp. 143-175.

65. Van de Wijngaart, D. J., van Royen, M. E., Hersmus, R., Pike, A. C. W., Houtsmuller, A. B., Jenster, G., Trapman, J., and Dubbink, H. J. (2006) Novel FXXFF and FXXMF motifs in androgen receptor cofactors mediate high affinity and specific interactions with the ligand-binding domain. *J. Biol. Chem.* 281, 19407-19416.

66. Bai, Y., and Giguere, V. (2003) Isoform-selective interactions between estrogen receptors and steroid receptor coactivators promoted by estradiol and ErbB-2 signaling in living cells. *Mol. Endocrinol.* 17, 589-599.

67. Weatherman, R. V., Chang, C.Y., Clegg, N. J., Carroll, D. C., Day, R. N., Baxter, J. D., McDonnell, D. P., Scanlan, T. S., and Schaufele, F. (2002) Ligand-selective interactions of ER detected in living cells by fluorescence resonance energy transfer. *Mol. Endocrinol.* 16, 487-496.

68. Llopis, J., Westin, S., Ricote, M., Wang, J., Cho, C. Y., Kurokawa, R., Mullen, T. M., Rose, D. W., Rosenfeld, M. G., Tsien, R. Y., and Glass, C. K. (2000) Ligand-dependent interactions of coactivators steroid receptor coactivator-1 and peroxisome proliferator-activated receptor binding protein with nuclear hormone receptors can be imaged in live cells and are required for transcription. *Proc. Natl. Acad. Sci. U.S.A.* 97, 4363-4368.

69. Mukherjee, R., Sun, S., Santomenna, L., Miao, B., Walton, H., Liao, B., Locke, K., Zhang, J.H., Nguyen, S. H., and Zhang, L. T. (2002) Ligand and coactivator recruitment preferences of peroxisome proliferator activated receptor-α. *J. Steroid Biochem. Mol. Biol.* 81, 217-225.

70. Schaufele, F., Chang, C.Y., Liu, W., Baxter, J. D., Nordeen, S. K., Wan, Y., Day, R. N., and McDonnell, D. P. (2000) Temporally distinct and ligand-specific recruitment of nuclear receptor-interacting peptides and cofactors to subnuclear domains containing the estrogen receptor. *Mol. Endocrinol.* 14, 2024-2039.

71. Awais, M., Sato, M., Umezawa, Y. (2007) Imaging of selective nuclear receptor modulator-induced conformational changes in the nuclear receptor to allow interaction with coactivator and corepressor proteins in living cells. *ChemBioChem.* 8, 737-743.

72. Awais, M., Sato, M., Sasaki, K., and Umezawa, Y. (2004) A genetically encoded fluorescent indicator capable of discriminating estrogen agonists from antagonists in living cells. *Anal. Chem.* 76, 2181-2186.

73. Awais, M., Sato, M., and Umezawa, Y. (2007) Optical probes to identify the glucocorticoid receptor ligands in living cells. *Steroids* 72, 949-954.

74. Awais, M., Sato, M., and Umezawa, Y. (2007) A fluorescent indicator to visualize ligand-induced receptor/coactivator interactions for screening of peroxisome proliferator-activated receptor-γ ligands in living cells. *Biosens. and Bioelectron.* 22, 2564-2569.

75. Awais, M., Sato, M., Lee X., Umezawa Y. (2006) A fluorescent indicator to visualize activities of the androgen receptor ligands in single living cells. *Angew. Chem. Int. Ed. Engl.* 45, 2707-2712.

76. Zhou, G., Cummings, R., Li, Y., Mitra, S., Wilkinson, H. A., Elbrecht, A., Hermes, J. D., Schaeffer, J. M., Smith, R. G., and Moller, D. E. (1998) Nuclear receptors have distinct affinities for coactivators: characterization by fluorescence resonance energy transfer. *Mol. Endocrinol.* 12, 1594-1604.

77. Day, R. N. (1998) Visualization of Pit-1 transcription factor interactions in the living cell nucleus by fluorescence resonance energy transfer microscopy. *Mol. Endocrinol.* 12, 1410-1419.

78. Zwart, W., Griekspoor, A., Berno, V., Lakeman, K., Jalink, K., Mancini, M., Neefjes, J., Michalides, R. (2007) PKA-induced resistance to tamoxifen is associated with an altered orientation of ERalpha towards co-activator SRC-1. *EMBO J.* 26, 3534-3544.

79. Dubbink, H. J., Hersmus, R., Verma, C. S., van der Korput, J. A. G. M., Berrevoets, C. A., van Tol, J., Ziel-van der Made, A. C. J., Brinkmann, A. O., Pike, A. C. W., and Trapman, J. (2004) Distinct recognition modes of FXXLF and LXXLL motifs by the androgen receptor. *Mol. Endocrinol.* 18, 2132-2150.

80. Hur, E., Pfaff, S. J., Payne, E. S., Gron, H., Buehrer, B. M., and Fletterick, R. J. (2004) Recognition and accommodation at the androgen receptor coactivator binding interface. *PLoS Biol.* 2, E274.

81. Doesburg, P., Kuil, C. W., Berrevoets, C. A., Steketee, K., Faber, P. W., Mulder, E., Brinkmann, A. O., and Trapman, J. (1997) Functional in vivo interaction between the amino-terminal, transactivation domain and the ligand binding domain of the androgen receptor. *Biochemistry* 36, 1052-1064.

82. He, B., Kemppainen, J. A., and Wilson, E. M. (2000) FXXLF and WXXLF sequences mediate the NH2-terminal interaction with the ligand binding domain of the androgen receptor. *J. Biol. Chem.* 275, 22986-22994.

83. Schaufele, F., Carbonell, X., Guerbadot, M., Borngraeber, S., Chapman, M. S., Ma, A. A. K., Miner, J. N., and Diamond, M. I. (2005) The structural basis of androgen receptor activation: Intramolecular and intermolecular amino-carboxy interactions. *Proc. Natl. Acad. Sci. U.S.A.* 102, 9802-9807.

84. Nishi, M., Tanaka, M., Matsuda, K., Sunaguchi, M., and Kawata, M. (2004) Visualization of glucocorticoid receptor and mineralocorticoid receptor interactions in living cells with GFP-based fluorescence resonance energy transfer. *J. Neurosci.* 24, 4918-4927.

85. Padron, A., Li, L., Kofoed, E. M., and Schaufele, F. (2007) Ligand-selective interdomain conformations of estrogen receptor-α. *Mol. Endocrinol.* 21, 49-61.

86. Michalides, R., Griekspoor, A., Balkenende, A., Verwoerd, D., Janssen, L., Jalink, K., Floore, A., Velds, A., van 't Veer, L., and Neefjes, J. (2004) Tamoxifen resistance by a conformational arrest of the estrogen receptor-α PKA activation in breast cancer. *Cancer Cell* 5, 597-605.

87. Zwart, W., Griekspoor, A., Rondaij, M., Verwoerd, D., Neefjes, J., and Michalides, R. (2007) Classification of anti-estrogens according to intramolecular FRET effects on phospho-mutants of estrogen receptor-α. *Mol. Cancer Ther.* 6, 1526-1533.

88. Sui, X., Bramlett, K. S., Jorge, M. C., Swanson, D. A., von Eschenbach, A. C., and Jenster, G. (1999) Specific androgen receptor activation by an artificial coactivator. *J. Biol. Chem.* 274, 9449-9454.

Chapter 4

Novel FxxFF and FxxMF Motifs in Androgen Receptor Cofactors Mediate High Affinity and Specific Interactions with the Ligand-Binding Domain

Van de Wijngaart, D.J., M.E. van Royen, R. Hersmus, A.C.W. Pike, A.B. Houtsmuller, G. Jenster, J. Trapman, and H.J. Dubbink.

J Biol Chem. (2006) 281:19407-19416.

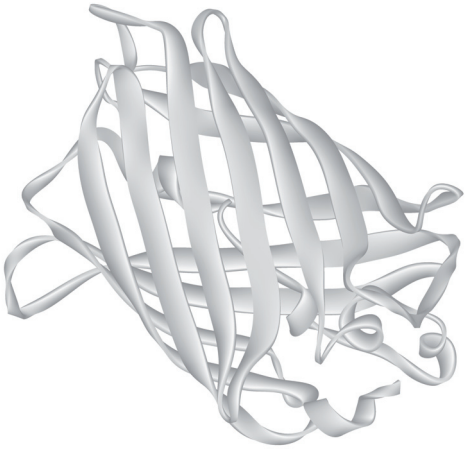

ABSTRACT

Upon hormone binding, a hydrophobic coactivator-binding groove is induced in the androgen receptor (AR) ligand-binding domain (LBD). This groove serves as high affinity docking site for a-helical FxxLF motifs present in the AR N-terminal domain and in AR cofactors. Study of the amino acid requirements at position +4 of the AR FxxLF motif revealed that most amino acid substitutions strongly reduced or completely abrogated AR LBD interaction. Strong interactions were still observed following substitution of L+4 by F or M residues. L+4 to M or F substitutions in the FxxLF motifs of AR cofactors ARA54 and ARA70 were also compatible with strong AR LBD binding. Like the corresponding FxxLF motifs, interactions of FxxFF and FxxMF variants of AR and ARA54 motifs were AR specific, whereas variants of the less AR-selective ARA70 motif displayed increased AR specificity. A survey of currently known AR-binding proteins revealed the presence of an FxxFF motif in gelsolin and an FxxMF motif in PAK6. In vivo fluorescence resonance energy transfer (FRET) and functional protein-protein interaction assays showed direct, efficient and specific interactions of both motifs with AR LBD. Mutation of these motifs abrogated interaction of gelsolin and PAK6 proteins with AR. In conclusion, we demonstrate strong interaction of FxxFF and FxxMF motifs to the AR coactivator-binding groove thereby mediating specific binding of a subgroup of cofactors to the AR LBD.

INTRODUCTION

The androgen receptor (AR) is a key player in development and maintenance of male reproductive tissues (1,2). AR is a ligand-inducible transcription factor of the nuclear receptor (NR) superfamily. Members of this family share a common structural and functional organization, including an N-terminal domain (NTD) harboring activation function 1 (AF-1), a central DNA-binding domain (DBD), and a C-terminal ligand-binding domain (LBD) containing activation function 2 (AF-2) (3-5). Upon binding of its ligand, testosterone or 5a-dihydrotestosterone (DHT), AR LBD undergoes conformational changes leading to dissociation from heat-shock proteins and translocation to the nucleus (6). At the DNA, AR binds to specific androgen response elements to initiate target gene expression. Cofactors facilitate AR transcription function by histone modifications, chromatin remodeling, and bridging of the receptor to other components of the transcription initiation process, including general transcription factors and RNA polymerase II (7-9).

Although cofactors may functionally interact with all three NR domains, most extensive knowledge is available of LBD interaction. Crystal structures of NR LBDs have shown that ligand binding triggers repositioning of helix 12 (10-13). As a result a hydrophobic groove is formed, which serves as a docking site for amphipathic a-helical LxxLL motifs present in many cofactors. The specific affinity of LxxLL motifs for distinct NR LBDs depends on amino acid residues flanking the core L residues (10,14-16). Until now, only a limited number of LxxLL motifs have been reported to interact with the AR LBD (17-20). Instead, AR LBD prefers binding of FxxLF motifs, one of which is located in the AR NTD (17,21,22). Although the function of the FxxLF motif-mediated interaction of AR NTD with AR LBD (N/C interaction) is not fully understood, it contributes to slowing of the androgen dissociation rate and selectively affects transcription of AR target genes (17,22-25). Functional FxxLF motifs are also essential for interaction between AR LBD and cofactors ARA54, ARA70, and RAD9 (17,26-28). However, for the majority of AR binding proteins the mode of interaction remains to be elucidated (29).

Alanine-scan mutagenesis of the AR FxxLF motif demonstrated that amino acid residues at positions +1, +4, and +5 are essential for interaction with the coactivator groove (21). Modeling and crystal structures of AR LBD in complex with FxxLF-like peptides, including AR and ARA70 FxxLF motifs, showed that amino acid residues at positions +1 and +5 are buried in the coactivator groove, rendering these residues entirely solvent inaccessible (17,30-32). In contrast, the amino acid residue at position +4 rests in a shallow pocket on the periphery of the coactivator groove and is largely solvent exposed. Phage display screens for AR LBD interacting peptides and directed mutagenesis studies of the AR FxxLF motif demonstrated that not only F, but also M, Y, and W residues at positions +1 and +5 could be compatible with binding to the AR coactivator-binding groove, although F residues seem to be preferred (17,18,30).

Although it is presumed that the requirements for the amino acid residue at +4 in the FxxLF motif are less stringent than those at +1 and +5, our actual knowledge in this respect is limited. Here we performed a systematic functional analysis of the AR FxxLF motif mutated at +4. Yeast two-hybrid and mammalian one-hybrid experiments demonstrated that L to F and L to M substitutions in the AR FxxLF motif are compatible with high affinity and specific AR LBD interaction. Strong and specific interaction was also obtained if the same substitutions were introduced in the ARA54 and ARA70 FxxLF motifs. As assessed by *in vivo* fluorescence resonance energy transfer (FRET) analysis, functional protein-protein interaction assays and mutagenesis, the AR partners gelsolin and PAK6 were found to contain an FxxFF and FxxMF motif, respectively, necessary and sufficient for AR LBD interaction.

EXPERIMENTAL PROCEDURES

Plasmids

Yeast and mammalian expression plasmids encoding Gal4AD-, Gal4DBD-, and YFP-peptide fusion proteins were generated by in-frame insertion of double-stranded synthetic oligonucleotides with 5′-*Bam*HI and 3′-*Eco*RI cohesive ends into the corresponding sites of pACT2 (Takara Bio, Otsu, Shiga, Japan), pM-B/E (17), or in the *Bgl*II and *Eco*RI sites of pEYFP-C2 (Takara Bio), as described previously (17). Mutagenesis of position +4 in the AR FxxLF motif was performed in oligonucleotides encoding AR_{18-30}. Mutant oligonucleotides were inserted into pACT2 as described above. All peptide expression constructs were verified by sequence analysis.

Yeast expression construct pGalDBD-AR LBD ($AR_{661-919}$) has been described previously (33). Constructs encoding Gal4DBD-fusions with LBDs of ERa, PR, and RXRa were generously provided by Michael Stallcup (34). Mammalian constructs expressing wild-type AR ($pCMVAR_0$) and F23L/F27L-AR (pCMVF23L/F27L-AR) have been described previously (17). $pM\text{-}PAK_{612-681}$ was generated by subcloning a *Bgl*II-*Xba*I fragment from pSPORT6-PAK6 (IRAKp961I1968Q; RZPD, Berlin, Germany) into the *Bam*HI and *Xba*I sites of pM (Takara Bio). pM-Gelsolin was obtained by subcloning an *Eco*RI-digested PCR fragment encoding amino acid residues 281-731 of gelsolin into pM. PCR was performed using primers 5′-GATC**GAATTC**TTCATCCTGGACCACG-3′ and 5′-GATC**GAATTC**CTCAGGCAGCCAGCTC-3′ (*Eco*RI sites in bold) on pOTB7-Gelsolin (IMAGp958I211459Q; RZPD). FxxAA variants of pM-PAK6 and pM-gelsolin were generated by QuikChange (Stratagene, La Jolla, USA) using primer pair 5′-CTATTCCGAAGC**GC**G**GC**-CCTGTCCACTG-3′ and 5′-CAGTGGACAGG**GC**C**GC**GCTTCGGAATAG-3′ for PAK6 and 5′-CTGTTCAAGCAG**GC**C**GC**CAAGAACTGGCGG-3′ and 5′-CCGCCAGTTCTTG**GC**G**GC**CTGCTTGAACAG-3′ for gelsolin, respectively (substitutions in bold), according to the manufacturer's instructions. For generation of pCFP-ARLBD ($AR_{612-919}$) a BamHI-digested PCR fragment from pAR0 (35) was cloned into the corresponding site of pECFP-C2 (Takara Bio). Primers used were 5′-AATTG-

G**GGATCC**GACCATCTTCTCGTCTTCGGAAATG-3′ and 5′-AATTGG**GGATCC**GATCACTGGGTGTG-GAAATAGATG-3′ (*Bam*HI sites in bold). pCYFP encoding the ECFP-EYFP chimera was kindly provided by Dr. Claude Gazin. The (ARE)2TATA-LUC reporter construct has been previously described as (PRE)2-E1b-LUC (36). The (UAS)4TATA-LUC reporter construct was kindly provided by Magda Meester. All constructs generated with PCR fragments and QuikChange mutagenesis were verified by sequence analysis.

Yeast culture, transformation, and β-galactosidase assay

Y190 yeast culture, transformation, and liquid culture β-galactosidase assays to quantify NR LBD-peptide interactions were performed as described previously (33,37). Liquid culture β-galactosidase assays were performed in the presence of 1 μM DHT (for AR, Steraloids, Wilton, USA), 1 μM progesterone (PR, Steraloids), 100 nM estradiol (ERa) (Steraloids), 10 nM retinoic acid (RXRa) (Sigma, St. Louis, USA), or vehicle.

Mammalian cell culture, transient transfections, and luciferase activity

Hep3B cells were cultured and transfected as described previously (37). For one-hybrid assays, cells were transfected with 50 ng Gal4DBD-peptide or Gal4DBD-protein expression construct, 50 ng AR expression construct, and 150 ng (UAS)4TATA-LUC construct, in the presence of 100 nM DHT or vehicle. Luciferase activity was determined as described previously (17,37).

For FRET experiments, Hep3B cells were cultured overnight on glass cover slips in 9.5 cm^2 wells in α-minimal essential medium (α-MEM) supplemented with 5% FCS, L-glutamine and antibiotics. Four h prior to transfection the medium was substituted by 1 mL α-MEM containing 5% charcoal-stripped FCS. Cells were transfected with 1 μg pCYFP, or 1 μg pCFP-ARLBD and 0.5 μg YFP-peptide expression construct, together with 3 μL Fugene 6 (Roche Diagnostics, Mannheim, Germany) per mg DNA in 100 mL α-MEM. Four h after transfection the medium was substituted by 2 mL α-MEM containing 100 nM DHT. FRET assays were done the next day.

Western blot analysis

Yeast protein extraction and Western blot analysis for detection of Gal4AD fusion proteins were performed as described previously (21,33). Proteins were visualized using a monoclonal antibody against Gal4AD (Takara Bio).

FRET measurement by acceptor photobleaching

Live cell imaging was performed using a Zeiss LSM510 confocal laser scanning microscope equipped with a Plan-Neofluar 40x/1.3 NA oil objective (Carl Zeiss, Jena, Germany) at a lateral resolution of 100 nm. CFP and YFP images were collected sequentially at 458 nm and 514 nm excitation, respectively, using a 458/514 nm dichroic beam splitter, a 515 nm beam splitter, and specific emission filters. CFP was excited with the 458 nm laser line of an Argon laser at

moderate laser power and detected using a 470-500 nm band pass emission filter. YFP excitation was at 514 nm at moderate laser power and detected using a 560 nm emission filter. After sequential collection of YFP and CFP images, YFP was bleached by scanning 25 times a nuclear region of ~100 μm^2, covering a large part of the nucleus, using the 514 nm argon laser line at high laser power. After acceptor photobleaching a second YFP and CFP image pair was collected. The apparent FRET efficiency was calculated after background subtraction as: $FRET = ((CFP_{after} - CFP_{before}) \cdot YFP_{before}) / ((YFP_{before} - YFP_{after}) \cdot CFP_{after})$ where CFP_{before} and YFP_{before} are the average fluorescence intensities measured in the nuclei before bleaching and CFP_{after} and YFP_{after} the average fluoresence intensities after bleaching.

RESULTS

L to F and L to M substituted AR FxxLF motifs strongly interact with AR LBD

Although the importance of the core hydrophobic amino acid residues at positions +1 and +5 in FxxLF motifs has been described (17,21,26), little is known about the amino acid requirements at +4 for AR LBD binding. To study this, we tested every amino acid at this position in the context of the AR FxxLF motif using a yeast two-hybrid read-out system (Fig. 1A). In this assay, peptides were expressed as fusions to Gal4AD and AR LBD was fused to Gal4DBD. All assays were done in the presence of DHT (17). Western blot analysis of transformed yeast cells demonstrated that all Gal4AD-peptide fusion proteins were appropriately expressed (Fig. 1B). The yeast two-hybrid screening showed that most L+4 substitutions completely abolished AR LBD interaction (Fig. 1B). Reduced interaction was observed with peptides containing a W, T, I, V, C, or Y residue at position +4 instead of an L. In contrast, AR LBD interactions were identical or even stronger than wild-type motif if L+4 were substituted by F or M.

FxxFF and FxxMF variants of AR, ARA54, and ARA70 FxxLF motifs interact with AR LBD in mammalian cells

Next, we evaluated interaction capacities of FxxFF and FxxMF variants of AR FxxLF with full-length wild-type AR in a mammalian one-hybrid assay (Fig. 2A and (17)). Interaction was assayed in Hep3B cells co-transfected with Gal4DBD-peptide and full-length wild-type AR expression constructs and a (UAS)4TATA-LUC reporter. The results of this assay closely resembled the results obtained in yeast, as both FxxFF and FxxMF variants displayed hormone-dependent binding capacities comparable to the wild-type motif (Fig. 2B). We also investigated the interaction of the peptides with full-length F23L/F27L-mutated AR (F23L/F27L-AR), which abrogates AR N/C interaction (17). This resulted in increased interactions of the FxxFF and FxxMF variants (Fig. 2C), indicating that both compete with the FxxLF motif in the AR NTD for AR LBD binding.

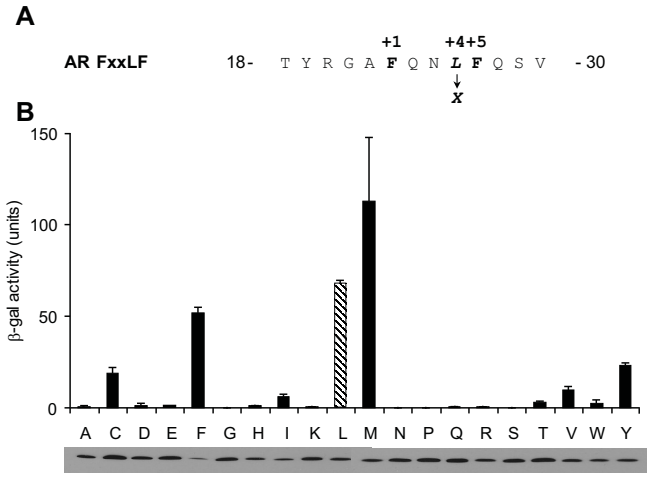

Figure 1. The effect of substitution of L+4 in the AR FxxLF motif on AR LBD interaction. (A) Amino acid sequence of the AR 18-30 peptide motif applied for mutagenesis of L+4. (B) Yeast two-hybrid analysis of L+4 substitution of the AR FxxLF motif for interaction with AR LBD. Y190 yeast cells were transformed with expression constructs encoding Gal4DBD-AR LBD and Gal4AD-peptide fusion proteins as described in Experimental Procedures. The amino acid single letter code of L+4 substitutions is indicated on the x-axis. Bars represent mean β-galactosidase activity of three independent experiments (+/- SD) in the presence of 1 μM DHT. No interactions were observed in the absence of hormone (data not shown). AR LBD interaction with wild-type AR FxxLF motif is indicated with a hatched bar. The lower panel represents a Western blot visualizing the expression of Gal4AD-peptide fusion proteins by Gal4AD-antibody staining.

Subsequently, interaction of F+4 and M+4 variants of ARA54 and ARA70 FxxLF motifs with AR LBD were assessed (Fig. 2A). The variants of both ARA54 (Fig. 2D) and ARA70 (Fig. 2F) interacted strongly with wild- type AR. All variants showed increased interactions with F23L/F27L-AR, indicative of interaction with the coactivator-binding groove (Figs 2E and G). Summarizing, L+4 can be substituted by F or M residues in distinct FxxLF peptide motifs, thereby retaining AR LBD interaction.

Effects of F and M residues at position +4 on AR specificity

Previously, we and others have demonstrated that FxxLF motifs, including those of AR and ARA54, display high specificity for AR (17,26,38,39). However, some FxxLF motifs, including the ARA70 motif, also interacted with PR (39). We studied in yeast two-hybrid experiments the effect of L to F and L to M substitutions at position +4 in the AR, ARA54, and ARA70 FxxLF motifs on AR specificity. Peptides were fused to Gal4AD and LBDs of ERα, PR, and RXRα were fused to Gal4DBD. Upon ligand binding all NR LBDs adopted a functional conformation since strong interaction with a control LxxLL peptide D11 was observed ((40) and data not shown). Contrary to a potent interaction with AR LBD (Fig. 3A), none of the FxxFF and FxxMF variant motifs interacted with LBDs of ERα, PR, or RXRα (Fig. 3B and data not shown). The specificity of the ARA70 FxxLF motif even increased upon L to F and L to M substitutions as no PR LBD interaction was observed with the variant ARA70 motifs (Fig. 3B). The weak β-galactosidase

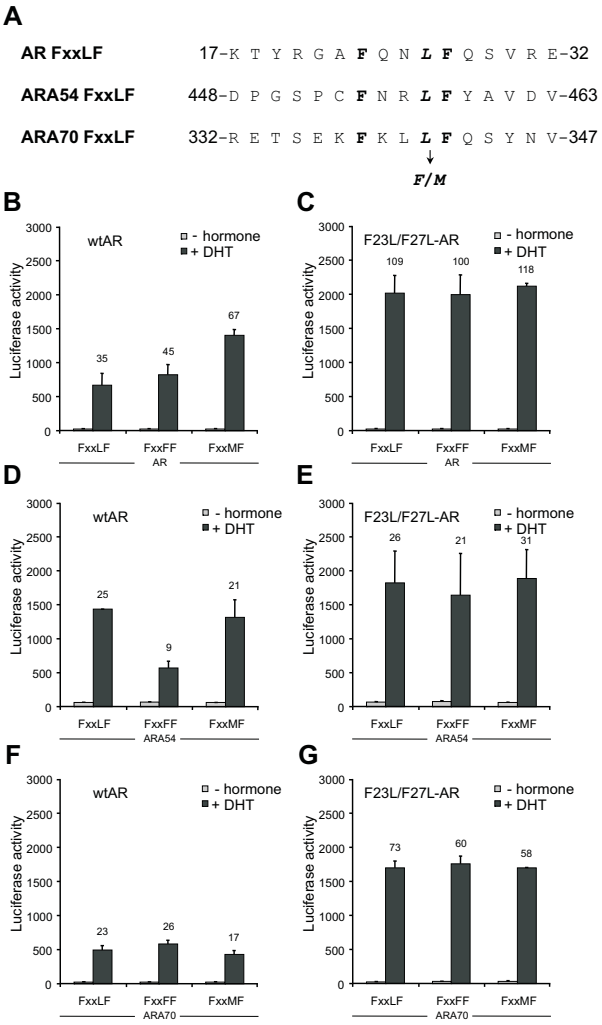

Figure 2. FxxFF and FxxMF variants of AR, ARA54, and ARA70 FxxLF motifs interact with AR LBD in mammalian cells. (A) Amino acid sequences of AR, ARA54, and ARA70 FxxLF peptides. (B to G) Mammalian one-hybrid analysis of L to F and L to M substituted FxxLF motifs of AR (B, C), ARA54 (D, E), and ARA70 (F, G) with full-length wild-type AR (B, D, F) or F23L/F27L-AR (C, E, G). Hep3B cells were cotransfected with expression constructs encoding the indicated Gal4DBD-peptide fusion protein and AR in the presence of the (UAS)4TATA-LUC reporter. Interactions were determined in the absence and presence of 100 nM DHT. Each bar represents mean luciferase activity of two independent experiments (+/- SD). Mean fold inductions are shown above bars.

activities detected with PR LBD were due to the intrinsic activity of Gal4DBD-PR LBD since similar values were obtained when this construct was expressed in the absence of a peptide expression construct (data not shown). These results demonstrate that L to F and L to M substitution variants of FxxLF motifs remain AR specific or become even more specific.

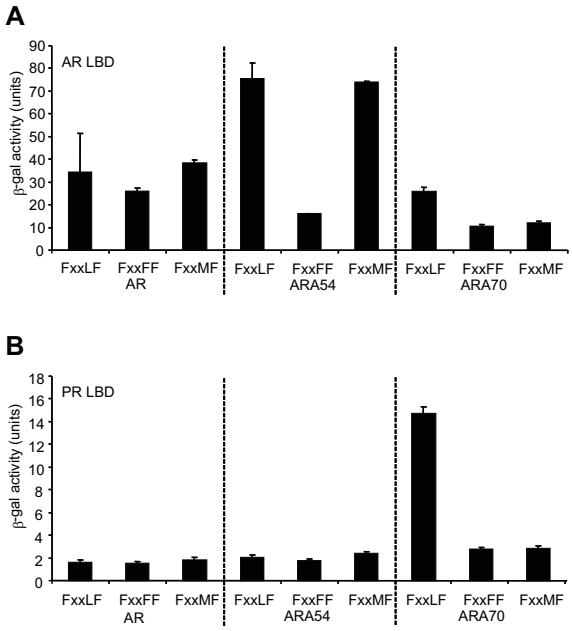

Figure 3. L to F and L to M substituted FxxLF motifs specifically interact with AR LBD. Yeast two-hybrid experiments were carried out to assess hormone-dependent interactions of L to F and L to M substituted FxxLF motifs of AR, ARA54, and ARA70 fused to Gal4AD with the indicated NR LBDs fused to Gal4DBD. Interaction was determined in the presence of 1 μM DHT for AR (A) and 1 μM progesterone for PR (B). Bars represent mean β-galactosidase activity of two independent experiments (+/- SD).

Naturally occurring AR-interacting FxxFF and FxxMF motifs

To assess a role of FxxFF and FxxMF motifs in cofactor-AR LBD interaction, we screened all AR interacting proteins present in the AR gene mutations database (www.mcgill.ca/androgendb; (29)) and in the human protein reference database (www.hprd.org) for the presence of these motifs. This yielded two proteins with an FxxFF (gelsolin and cdc37) and two with an FxxMF motif (PAK6 and supervillin). Mammalian one-hybrid experiments showed that the cdc37 FxxFF and supervillin FxxMF motifs weakly interacted with F23L/F27L-AR, but not with wild-type AR (data not shown). In contrast, the gelsolin FxxFF and PAK6 FxxMF motifs displayed strong hormone-dependent interactions with both F23L/F27L-AR and wild-type AR (Figs 4A and B). AR N/C interaction did not affect gelsolin FxxFF binding to AR LBD, but reduced binding of the AR FxxLF and PAK6 FxxMF motifs, indicating that the gelsolin FxxFF motif had a higher affinity for AR LBD than the AR FxxLF and PAK6 FxxMF motifs. Both motifs are predicted to adopt an amphipathic α-helical structure (Figs 4C and D). FxxFF and FxxMF motifs present in AR cofactors gelsolin and PAK6 may thus be essential for interaction with AR.

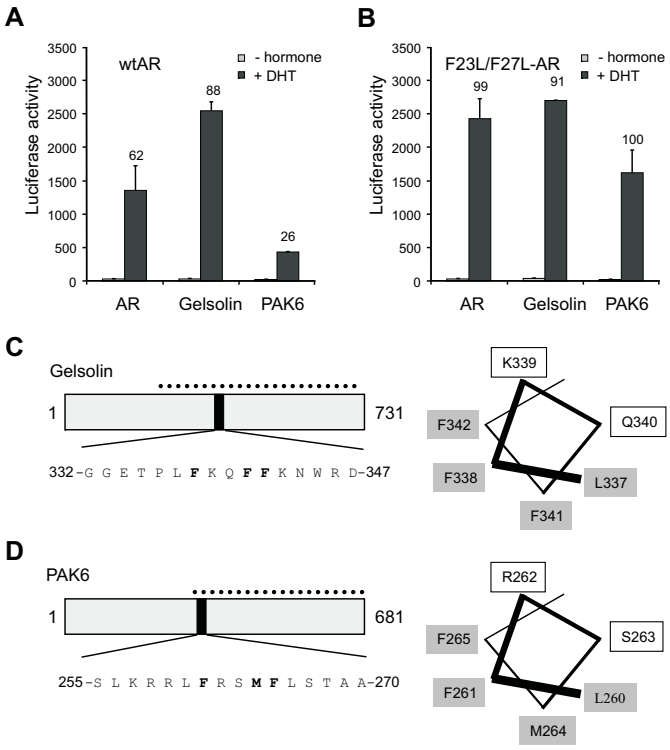

Figure 4. An FxxFF motif in gelsolin and an FxxMF motif in PAK6 interact with AR LBD. (A, B) Hep3B cells were cotransfected with expression constructs encoding Gal4DBD-peptide (see for peptide sequences Figs 4C, D, left) and wild-type (A) or F23L/F27L-substituted (B) full-length AR and a (UAS)4TATA-LUC reporter plasmid. Interaction was determined in the absence and presence of 100 nM DHT. Bars represent mean luciferase activity of two independent experiments (+/- SD). Mean fold inductions are indicated above bars. (C, D, left) Schematic representation of gelsolin (C) and PAK6 (D) proteins. Positions of the FxxFF motif in gelsolin and the FxxMF motif in PAK6 and the corresponding peptide sequences tested for interaction with AR are indicated. The dotted lines represent gelsolin (C) and PAK6 (D) fragments originally identified in yeast two-hybrid screenings (43,48,49). (C, D, right) Helical wheel presentation of gelsolin FxxFF and PAK6 FxxMF motifs. Polar residues are indicated in white boxes and hydrophobic residues in grey boxes.

To extend our knowledge on the interactions between AR LBD and gelsolin FxxFF and PAK6 FxxMF peptide motifs, *in vivo* FRET experiments were carried out (Fig. 5A). Hep3B cells were transiently cotransfected with constructs expressing CFP-tagged AR LBD and YFP-tagged peptide motifs. Close association of ligand-bound CFP-tagged AR LBD and YFP-tagged peptide results in energy transfer (FRET) by excitated CFP donor to YFP acceptor (Fig. 5A; left) (41). FRET efficiency was estimated by acceptor photobleaching (Figs 5A middle and right) (42,43). FRET intensity was calculated based on the difference in CFP emission intensities before and after YFP photo destruction as described in Experimental Procedures.

FRET signals between AR LBD and FxxLF motifs of AR, ARA54, and ARA70 were readily detected in the presence of ligand (Fig. 5B). FRET signals between AR LBD and either gelsolin

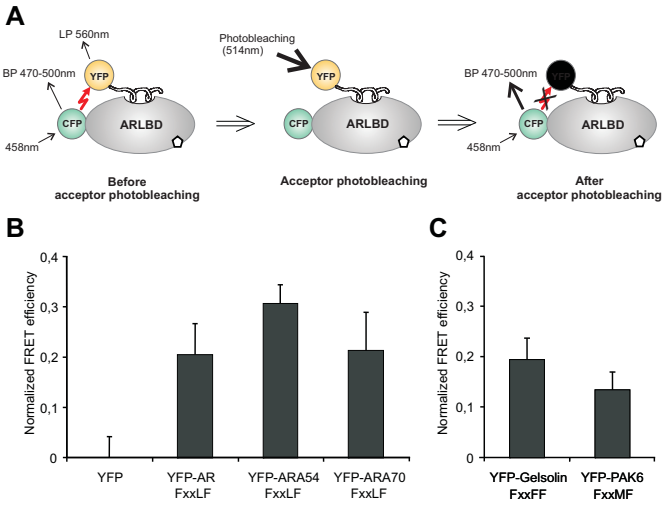

Figure 5. Direct *in vivo* interaction of AR LBD with FxxLF, FxxFF, and FxxMF motifs of AR NTD and AR cofactors. (A) Schematic representation of acceptor photobleaching FRET. Photo destruction of YFP of an interacting pair of CFP-tagged AR LBD and YFP-tagged peptide will result in enhanced CFP emission. (B, C) Direct interaction of AR LBD with the FxxLF motifs of AR, ARA54, and ARA70 (B) and with gelsolin FxxFF and PAK6 FxxMF motifs (C) as determined by *in vivo* FRET. Hep3B cells were transiently cotransfected with constructs expressing CFP-tagged AR LBD and YFP-tagged peptides. Western blot analysis demonstrated that all fusion proteins were expressed at the correct size (not shown). Confocal microscopy showed that both in the absence and presence of DHT CFP-AR LBD was localized in the nucleus, whereas the YFP-tagged peptides distributed over both nucleus and cytoplasm (data not shown). FRET was estimated based on emission intensities of CFP and YFP, before and after YFP photo destruction as described in Experimental Procedures. FRET efficiency is expressed relative to the values of co-expressed CFP-AR LBD and YFP without peptide (B) and normalized to values obtained for the CFP-YFP chimera. FRET efficiencies of peptides were determined in three independent experiments in a total of 30 cells in the presence of 100 nM DHT. Error bars represent 2 x SEM.

FxxFF or PAK6 FxxMF motifs were similar (Fig. 5C). These findings demonstrate direct *in vivo* interactions of AR LBD with gelsolin FxxFF and PAK6 FxxMF peptides.

Alanine scanning and AR LBD specificity of gelsolin FxxFF and PAK6 FxxMF motifs

To further characterize the gelsolin FxxFF and PAK6 FxxMF motifs we performed an alanine-scan by substituting consecutive doublet residues in both motifs into alanine residues (Fig. 6A). Mammalian one-hybrid results show that alanine substitutions encompassing the core hydrophobic residues at positions +1, +4, and +5 of both gelsolin and PAK6 completely abrogated AR interactions (Figs 6B and C). Residues at positions +6 and +7 of the PAK6 motif, but not of the gelsolin FxxFF motif, also appeared important for AR LBD interaction. All other alanine substitutions hardly interfered with AR binding.

As found for AR, ARA54, and ARA70 peptide motifs, gelsolin FxxFF and PAK6 FxxMF strongly bound to AR LBD, but hardly or not to the LBDs of ERα, PR, and RXRα (Fig. 7).

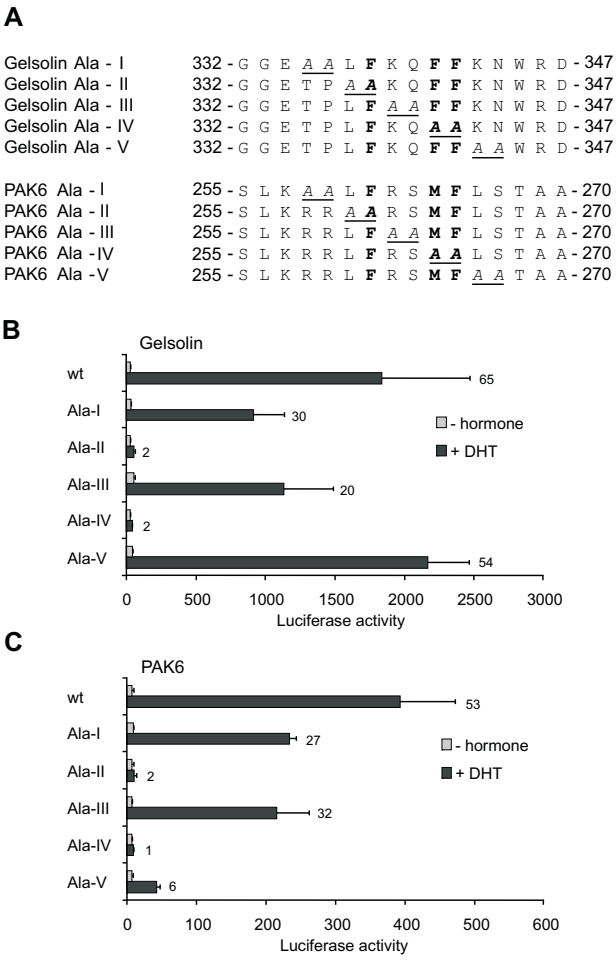

Figure 6. Alanine-scan of gelsolin FxxFF and PAK6 FxxMF motifs interacting with AR LBD. (A) Amino acid sequences of peptides used for the alanine scan of gelsolin FxxFF and PAK6 FxxMF motifs. (B, C) Gal4DBD-fused gelsolin (B) and PAK6 (C) peptides were studied for interaction with F23L/F27L-AR using (UAS)4TATA-LUC as reporter in transiently cotransfected Hep3B cells. Interaction was assayed in the absence and presence of 100 nM DHT. Bars represent mean luciferase activity of two independent experiments (+/- SD). Mean fold inductions are shown above bars.

AR LBD binding of cofactors gelsolin and PAK6 is FxxFF and FxxMF-mediated

Next, we investigated the importance of the FxxFF and FxxMF motifs for interaction of gelsolin and PAK6 with AR. PAK6 (aa 12-681) and gelsolin (aa 281-731) were fused to Gal4DBD and allowed to interact with AR in the mammalian read-out system. As expected, both proteins interacted with wild-type AR (Fig. 8A) and binding was increased if the competing FxxLF motif in AR NTD was inactivated (Fig. 8B). However, if the FxxFF motif in gelsolin and the FxxMF motif in PAK6 were mutated into FxxAA, interactions with both wild-type AR and F23L/F27L-AR were abolished. Gelsolin and PAK6 protein expression levels were not affected by the

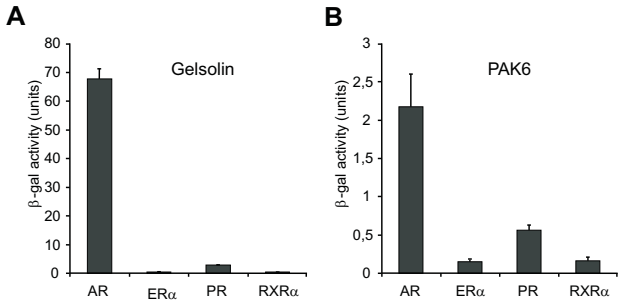

Figure 7. Gelsolin FxxFF and PAK FxxMF motifs specifically interact with AR LBD in a yeast two-hybrid assay. Y190 yeast cells were transformed with gelsolin FxxFF (A) and PAK6 FxxMF (B) motifs fused to Gal4AD and LBDs of AR, ERα, PR, and RXRα fused to Gal4DBD. Interaction was determined in the presence of 1 μM DHT, 100 nM 17β-estradiol, 1 μM progesterone, and 10 μM all-trans-retinoic acid, respectively. Bars represent mean β-galactosidase units of two independent experiments (+/- SD). A positive control, LxxLL peptide D11 (39), interacted with all NR LBDs ensuring proper LBD expression (data not shown).

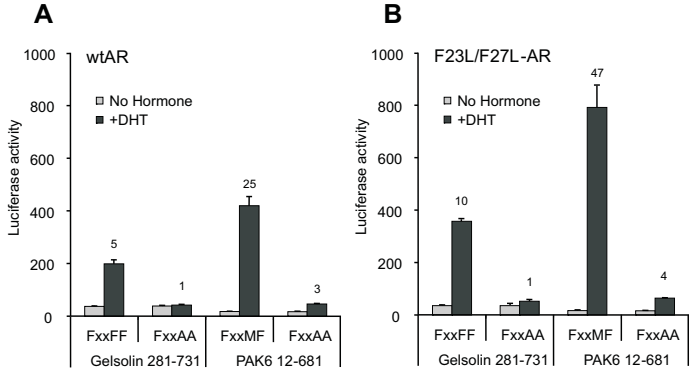

Figure 8. AR LBD binding of cofactors gelsolin and PAK6 is mediated by FxxFF and FxxMF motifs, respectively. (A, B) Hep3B cells were cotransfected with expression constructs for Gal4DBD-PAK6 (aa12-681) or Gal4DBD-gelsolin (aa 281-731) containing either wild-type or FxxAA-mutated motifs and wild-type (A) or F23L/F27L-substituted (B) full length AR and a (UAS)4TATA-LUC reporter plasmid. Interaction was assayed in the absence and presence of 100 nM DHT. Bars represent mean luciferase activity of two independent experiments (+/- SD). Mean fold inductions are indicated above bars.

mutations (data not shown). These data clearly demonstrate that the FxxFF and FxxMF motifs in gelsolin and PAK6, respectively, are necessary and sufficient for AR interaction.

DISCUSSION

Upon agonist binding the architecture of the AR LBD surface is rearranged to allow high affinity binding of FxxLF motifs present in AR NTD and in AR cofactors. Binding of these short amphipathic α-helical structures turned out to depend strongly on optimal docking of the

F residues at +1 and +5 in the coactivator-binding groove of AR LBD (17,21). Although the coactivator groove is sufficiently flexible to accommodate other large hydrophobic amino acid residues, F residues at +1 and +5 are preferred (17,18,30). Based on functional assays we here provide insight in the requirements of the amino acid at position +4 of peptide motifs for optimal AR LBD binding. We demonstrate that L+4 can be substituted by F and M residues in the AR, ARA54, and ARA70 FxxLF motifs, retaining strong and selective AR binding. Novel AR-interacting FxxFF and FxxMF motifs were identified in AR cofactors gelsolin and PAK6, respectively.

Systematic mutation screening of position +4 of the AR FxxLF motif resulted in the identification of three categories of peptides (Fig. 1). (1) The largest group of peptides does not interact with AR LBD. This group includes small hydrophobic, charged, or polar residues at +4; (2) Several peptides showed reduced interaction with AR LBD (C, I, T, V, W, and Y). Most of these variants have a hydrophobic residue at +4; and (3) strongly interacting variants containing bulky hydrophobic side chains (L, F, and M). Strong binding by L, F, and M residues indicates that hydrophobic contacts underlie the ability to interact with AR LBD. The inability or limited potency of most +4 variants to bind AR LBD can be due to destabilization of the peptide by distortion of the helical structure, active interference with LBD interaction caused by the charge or size of the side chains or the incapability to form sufficient hydrophobic contacts with the AR LBD. Our findings underscore the importance of the amino acid residue at +4 for optimal binding of peptide motifs to AR LBD, even though this amino acid residue is not deeply buried in the binding pocket (30,31).

Phage display screens of random peptide libraries with full length AR or AR LBD as bait yielded different AR-interacting motifs containing F residues at positions +1 and +5 (30,38). Besides the classical FxxLF sequences, FxxVF, FxxYF, and FxxFF motifs were identified in these screens. The FxxVF-containing peptide weakly interacted with AR, as is in agreement with our screening results, and strong interactions were observed with FxxYF and FxxFF sequences (38). In our +4 mutation screen of AR FxxLF, the FxxYF variant showed decreased interaction with AR LBD, suggesting that in this specific FxxYF motif the Y residue has a less optimal position for AR LBD binding. Similar data were found for ARA54 and ARA70 FxxLF-based FxxYF variants (data not shown). So, the requirement for the amino acid at +4 might depend on the further context of the motif. Chang and co-workers (38) demonstrated that most FxxYF and FxxFF peptide motifs picked up in phage display screens interacted with AR LBD not only in the presence but also in the absence of ligand. Repetition of these experiments in our interaction assay indicated that ligand was essential for AR LBD interaction (data not shown). This apparent discrepancy might be due to differences in read-out systems.

Recently, crystal structures of AR LBDs in complex with the AR FxxLF and ARA70 FxxLF motifs and FxxLF, FxxFF, and FxxYF peptides selected by phage display have been resolved (30-32). Comparing LBDs with and without bound peptide showed that the side chains of amino acid residues in AR LBD that line the coactivator groove rearrange upon binding of

the peptide motif. Largest conformational changes were observed for K720, M734, M894, and E897, leading to optimal binding sites for residues +1, +4, and +5 of interacting peptide motifs (30-32). The Fs at positions +1 and +5 are buried in a deep solvent inaccessible groove in AR LBD. This mode of interaction is largely conserved suggesting that these residues drive the interaction of the peptide motif (30). In contrast, the binding mode of the residue at position +4 seems less critical. This residue binds to a shallow hydrophobic depression formed by L712, V713, V716, and M894 in AR LBD (Fig. 9) (30-32). Based on the crystal structures, the side chains of the different amino acids at +4 studied so far (L, F, and Y) form hydrophobic contacts with V713, V716, and M894 in the groove with an additional contact formed between the FxxYF peptide and K717 of AR LBD. As shown in Fig. 9, the FxxFF peptide has shifted in the coactivator groove towards the K720 residue as compared to the FxxLF and FxxYF peptide motifs (30). This shift together with a less optimal helical geometry of the peptide backbone makes that the F at +4 has a different orientation than an L or Y at this position (30). We have shown in this study that +4 of the peptide motif can also be an M. Because of the variability of the position of the +4 residue in the complex with AR LBD and because M has a highly flexible side chain, its precise positioning in the coactivator groove cannot be accurately predicted.

In contrast to LxxLL motifs, FxxLF motifs show a strong preference for AR (17,26). Some FxxLF motifs, including the ARA70 FxxLF motif, also interact with PR (38,39). The FxxFF and FxxMF motifs tested in the present study also specifically interacted with AR. L to F and L to M substitutions increased specificity of the ARA70 FxxLF motif. We hypothesize that M and F residues at position +4 select against binding to the coactivator-binding groove of PR. In agreement with this hypothesis, AR-interacting FxxLF and FxxFF peptides selected by phage display show a similar selectivity for AR: only 1 out of 5 FxxFF peptides interacted with PR LBD as compared to 4 out of 6 FxxLF-peptides (38). Of the residues in the AR coactivator-binding groove that contact the +4 side chains in FxxLF and FxxFF peptides (see Fig. 9) only V713 differs from the corresponding L727 residue in PR. As recently shown by He et al., V713L substitution in AR LBD reduced binding of the AR FxxLF motif. Vice versa, L727V substitution in PR LBD increased binding of the AR FxxLF motif (31). We presume that the size and orientation of L727 in PR LBD precludes binding of peptide motifs with bulky F and M residues at position +4.

Although the mode of interaction of the majority of cofactors with AR LBD is unknown, for several, including ARA54, ARA70, and RAD9, an essential FxxLF motif has been established (17,26-28). Here we demonstrated that two other AR interacting proteins, gelsolin and PAK6, interact with AR LBD via an FxxFF and FxxMF motif, respectively. Gelsolin is an actin capping and severing protein, and is presumed to act as an AR cofactor by facilitating nuclear translocation (44). Interestingly, also other members of the gelsolin family, including flightless-1 and supervillin, have been identified as cofactors of AR and other NRs, suggesting an important role in NR function (45,46). The gelsolin FxxFF motif is not only highly conserved among

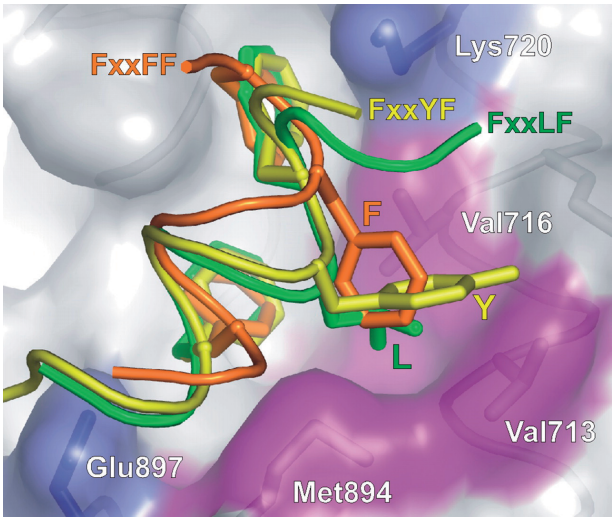

Figure 9. Variable binding modes of the +4 residue in FxxLF, FxxFF, and FxxYF peptide motifs to the coactivator groove. Surface representation of the coactivator groove region of the AR LBD (PDB entry: 1X0W). Residues that form the +4 binding site are in magenta. The binding mode of the FxxLF (*green;* 1X0W), FxxFF (*orange*, 1T73) and FxxYF (*yellow*, 1T7M) peptides are shown after global superposition of the various crystal structures. For clarity, only peptide side chains at positions +1, +4 and +5 are shown. AR side chains that line the +4 binding site are highlighted along with the two charge clamp residues (*blue*).

different species, but also among different members of the gelsolin family. Our preliminary data revealed that the conserved FxxFF motif present in adseverin also strongly binds AR LBD, suggesting that adseverin may act as an AR cofactor as well (data not shown). PAK6 is a member of the PAK family of serine/threonine kinases, which is, based on homology, divided into two subfamilies (Group I: PAK1, PAK2, and PAK3; Group II: PAK4, PAK5, and PAK6) (47). Although the FxxMF motif in PAK6 is conserved in other species, it is not conserved in any of the other members of the PAK family and so far PAK6 is the only member known to modulate NR function. PAK6 might repress AR function by phosphorylation of the DBD (48). Hormone-dependent interactions with AR LBD were observed in yeast two-hybrid and co-immunoprecipitation experiments, whereas GST pull-down experiments indicated that these LBD interactions were hormone-independent and also involved the hinge region (49,50). Our results unambiguously demonstrated that the novel FxxMF motif is sufficient and necessary for hormone-dependent interaction of PAK6 with AR LBD.

The identification of the FxxFF and FxxMF motifs in AR cofactors raises the possibility that other so far unrecognized proteins interact with AR LBD via similar motifs. Based on these findings, it would be of interest to perform a proteome-wide in silico screen for Fxx(L/F/M)F peptide motifs combined with functional protein-protein interaction assays to identify new candidate AR partners.

Prostate cancer growth is dependent on the androgen-AR axis (51,52). Nonetheless, endocrine treatment of metastatic prostate cancer by androgen withdrawal or blocking AR

activity by antagonists is not curative, even though AR is still active in progressive disease in most cases (53). AR N/C interaction and cofactor interactions are important steps in AR activation. Disruption of these interactions might be a complementary or alternative approach to more efficiently inhibit AR function. Increased knowledge of the mode of AR LBD-peptide interaction will be instrumental in the design of small molecules that fit in the AR coactivator-binding groove and block protein interactions.

ACKNOWLEDGEMENTS

The authors would like to thank Michael Stallcup, Magda Meester, and Claude Gazin for providing plasmids. This work was supported by grant DDHK2001-2402 from the Dutch Cancer Society (KWF). ACWP is supported by a Wellcome Trust Career Development Fellowship (Grant number: 064803).

REFERENCES

1. Lee, D. K., and Chang, C. (2003) *J. Clin. Endocrinol. Metab.* 88, 4043-4054
2. Quigley, C. A., De Bellis, A., Marschke, K. B., el-Awady, M. K., Wilson, E. M., and French, F. S. (1995) *Endocr. Rev.* 16, 271-321
3. Tsai, M. J., and O'Malley, B. W. (1994) *Annu. Rev. Biochem.* 63, 451-486
4. Mangelsdorf, D. J., Thummel, C., Beato, M., Herrlich, P., Schutz, G., Umesono, K., Blumberg, B., Kastner, P., Mark, M., Chambon, P., and Evans, R. M. (1995) *Cell* 83, 835-839
5. Warnmark, A., Treuter, E., Wright, A. P., and Gustafsson, J. A. (2003) *Mol. Endocrinol.* 17, 1901-1909
6. Chang, C., Saltzman, A., Yeh, S., Young, W., Keller, E., Lee, H. J., Wang, C., and Mizokami, A. (1995) *Crit. Rev. Eukaryot. Gene Expr.* 5, 97-125
7. Shang, Y., Myers, M., and Brown, M. (2002) Mol. Cell 9, 601-610
8. Heinlein, C. A., and Chang, C. (2002) *Endocr. Rev.* 23, 175-200
9. Kinyamu, H. K., and Archer, T. K. (2004) *Biochim. Biophys. Acta* 1677, 30-45
10. Heery, D. M., Kalkhoven, E., Hoare, S., and Parker, M. G. (1997) *Nature* 387, 733-736
11. Greschik, H., and Moras, D. (2003) *Curr. Top. Med. Chem.* 3, 1573-1599
12. Pike, A. C., Brzozowski, A. M., and Hubbard, R. E. (2000) *J. Steroid Biochem. Mol. Biol.* 74, 261-268
13. Feng, W., Ribeiro, R. C., Wagner, R. L., Nguyen, H., Apriletti, J. W., Fletterick, R. J., Baxter, J. D., Kushner, P. J., and West, B. L. (1998) *Science* 280, 1747-1749
14. Darimont, B. D., Wagner, R. L., Apriletti, J. W., Stallcup, M. R., Kushner, P. J., Baxter, J. D., Fletterick, R. J., and Yamamoto, K. R. (1998) *Genes Dev.* 12, 3343-3356
15. McInerney, E. M., Rose, D. W., Flynn, S. E., Westin, S., Mullen, T. M., Krones, A., Inostroza, J., Torchia, J., Nolte, R. T., Assa-Munt, N., Milburn, M. V., Glass, C. K., and Rosenfeld, M. G. (1998) *Genes Dev.* 12, 3357-3368
16. Needham, M., Raines, S., McPheat, J., Stacey, C., Ellston, J., Hoare, S., and Parker, M. (2000) *J. Steroid Biochem. Mol. Biol.* 72, 35-46
17. Dubbink, H. J., Hersmus, R., Verma, C. S., van der Korput, H. A., Berrevoets, C. A., van Tol, J., Ziel-van der Made, A. C., Brinkmann, A. O., Pike, A. C., and Trapman, J. (2004) *Mol. Endocrinol.*18, 2132-2150
18. Hsu, C. L., Chen, Y. L., Yeh, S., Ting, H. J., Hu, Y. C., Lin, H., Wang, X., and Chang, C. (2003) *J. Biol. Chem.* 278, 23691-23698
19. Chang, C. Y., and McDonnell, D. P. (2002) *Mol. Endocrinol.* 16, 647-660
20. Hall, J. M., Chang, C. Y., and McDonnell, D. P. (2000) *Mol. Endocrinol.* 14, 2010-2023
21. Steketee, K., Berrevoets, C. A., Dubbink, H. J., Doesburg, P., Hersmus, R., Brinkmann, A. O., and Trapman, J. (2002) *Eur. J. Biochem.* 269, 5780-5791
22. He, B., Kemppainen, J. A., and Wilson, E. M. (2000) *J. Biol. Chem.* 275, 22986-22994
23. He, B., Bowen, N. T., Minges, J. T., and Wilson, E. M. (2001) *J. Biol. Chem.* 276, 42293-42301
24. He, B., Lee, L. W., Minges, J. T., and Wilson, E. M. (2002) *J. Biol. Chem.* 277, 25631-25639
25. Callewaert, L., Verrijdt, G., Christiaens, V., Haelens, A., and Claessens, F. (2003) *J. Biol. Chem.* 278, 8212-8218

26. He, B., Minges, J. T., Lee, L. W., and Wilson, E. M. (2002) *J. Biol. Chem.* 277, 10226-10235

27. Hu, Y. C., Yeh, S., Yeh, S. D., Sampson, E. R., Huang, J., Li, P., Hsu, C. L., Ting, H. J., Lin, H. K., Wang, L., Kim, E., Ni, J., and Chang, C. (2004) *J. Biol. Chem.* 279, 33438-33446

28. Wang, L., Hsu, C. L., Ni, J., Wang, P. H., Yeh, S., Keng, P., and Chang, C. (2004) *Mol. Cell. Biol.* 24, 2202-2213

29. Gottlieb, B., Beitel, L. K., Wu, J. H., and Trifiro, M. (2004) *Hum. Mutat.* 23, 527-533

30. Hur, E., Pfaff, S. J., Payne, E. S., Gron, H., Buehrer, B. M., and Fletterick, R. J. (2004) *PLoS Biol.* 2, E274

31. He, B., Gampe, R. T., Jr., Kole, A. J., Hnat, A. T., Stanley, T. B., An, G., Stewart, E. L., Kalman, R. I., Minges, J. T., and Wilson, E. M. (2004) *Mol. Cell* 16, 425-438

32. Estébanez-Perpiñá, E., Moore, J. M., Mar, E., Delgado-Rodrigues, E., Nguyen, P., Baxter, J. D., Buehrer, B. M., Webb, P., Fletterick, R. J., and Guy, R. K. (2005) *J. Biol. Chem.* 280, 8060-8068

33. Doesburg, P., Kuil, C. W., Berrevoets, C. A., Steketee, K., Faber, P. W., Mulder, E., Brinkmann, A. O., and Trapman, J. (1997) *Biochemistry* 36, 1052-1064

34. Ding, X. F., Anderson, C. M., Ma, H., Hong, H., Uht, R. M., Kushner, P. J., and Stallcup, M. R. (1998) *Mol. Endocrinol.* 12, 302-313

35. Brinkmann, A. O., Faber, P. W., van Rooij, H. C., Kuiper, G. G., Ris, C., Klaassen, P., van der Korput, J. A., Voorhorst, M. M., van Laar, J. H., Mulder, E., and Trapman, J. (1989) *J. Steroid Biochem.* 34, 307-310

36. Jenster, G., Spencer, T. E., Burcin, M. M., Tsai, S. Y., Tsai, M. J., and O'Malley, B. W. (1997) *Proc. Natl. Acad. Sci. USA* 94, 7879-7884

37. Steketee, K., Timmerman, L., Ziel-van der Made, A. C., Doesburg, P., Brinkmann, A. O., and Trapman, J. (2002) *Int. J. Cancer* 100, 309-317

38. Chang, C. Y., Abdo, J., Hartney, T., and McDonnell, D. P. (2005) *Mol. Endocrinol.* 19, 2478-2490

39. Dubbink, H. J., Hersmus, R., Pike, A.C., Molier, M., Brinkmann, A.O., Jenster, G., and Trapman, J. (2006) *Mol. Endocinol.* 20, 1742-1755

40. Chang, C., Norris, J. D., Gron, H., Paige, L. A., Hamilton, P. T., Kenan, D. J., Fowlkes, D., and McDonnell, D. P. (1999) *Mol. Cell. Biol.* 19, 8226-8239

41. Patterson, G. H., Piston, D. W., and Barisas, B. G. (2000) *Anal. Biochem.* 284, 438-440

42. Bastiaens, P. I., Majoul, I. V., Verveer, P. J., Soling, H. D., and Jovin, T. M. (1996) *EMBO J.* 15, 4246-4253

43. Bastiaens, P. I., and Jovin, T. M. (1996) *Proc. Natl. Acad. Sci. USA* 93, 8407-8412

44. Nishimura, K., Ting, H. J., Harada, Y., Tokizane, T., Nonomura, N., Kang, H. Y., Chang, H. C., Yeh, S., Miyamoto, H., Shin, M., Aozasa, K., Okuyama, A., and Chang, C. (2003) *Cancer Res.* 63, 4888-4894

45. Lee, Y. H., Campbell, H. D., and Stallcup, M. R. (2004) *Mol. Cell. Biol.* 24, 2103-2117

46. Ting, H. J., Yeh, S., Nishimura, K., and Chang, C. (2002) *Proc. Natl. Acad. Sci. USA* 99, 661-666

47. Jaffer, Z. M., and Chernoff, J. (2002) *Int. J. Biochem. Cell. Biol.* 34, 713-717

48. Schrantz, N., da Silva Correia, J., Fowler, B., Ge, Q., Sun, Z., and Bokoch, G. M. (2004) *J. Biol. Chem.* 279, 1922-1931

49. Lee, S. R., Ramos, S. M., Ko, A., Masiello, D., Swanson, K. D., Lu, M. L., and Balk, S. P. (2002) *Mol. Endocrinol.* 16, 85-99

50. Yang, F., Li, X., Sharma, M., Zarnegar, M., Lim, B., and Sun, Z. (2001) *J. Biol. Chem.* 276, 15345-15353

51. Jenster, G. (1999) *Semin. Oncol.* 26, 407-421

52. Trapman, J. (2001) *Eur. J. Cancer* 37 Suppl 7, S119-125

53. Balk, S. P. (2002) *Urology* 60, 132-138

Chapter 5

Compartmentalization of Androgen Receptor Protein-protein Interactions in Living Cells

Van Royen, M.E., S.M. Cunha, M.C. Brink, K.A. Mattern, A.L. Nigg, H.J. Dubbink, P.J. Verschure, J. Trapman, and A.B. Houtsmuller.

J Cell Biol. (2007) 177:63-72.

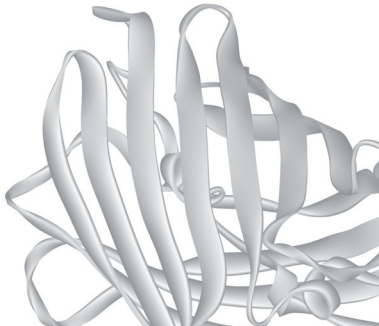

ABSTRACT

Steroid receptors regulate gene expression in a ligand-dependent manner by binding specific DNA sequences. Ligand binding also changes the conformation of the ligand binding domain (LBD), allowing interaction with coregulators via LxxLL-motifs. Androgen receptors (ARs) preferentially interact with coregulators containing LxxLL-related FxxLF-motifs. The AR is regulated at an extra level by interaction of an FQNLF-motif in the N-terminal domain with the C-terminal LBD (N/C interaction). Although it is generally recognized that AR-coregulator and N/C interactions are essential for transcription regulation, their spatiotemporal organization is largely unknown. Here, we performed simultaneous fluorescence resonance energy transfer (FRET) and fluorescence redistribution after photobleaching (FRAP) measurements in living cells expressing ARs double-tagged with yellow (YFP) and cyan (CFP) fluorescent proteins. We provide evidence that AR N/C interactions occur predominantly when ARs are mobile, possibly to prevent unfavorable or untimely cofactor interactions. N/C interactions are largely lost when AR transiently binds to DNA, predominantly in foci partly overlapping transcription sites. AR-coregulator interactions occur preferentially when ARs are bound to DNA.

INTRODUCTION

The androgen receptor (AR) is a ligand-dependent transcription factor of the steroid receptor (SR) subfamily of nuclear receptors. ARs regulate expression of genes involved in development and maintenance of the male phenotype and play a role in growth of prostate cancer. Like all SRs, AR is composed of a central DNA-binding domain (DBD), a C-terminal ligand-binding domain (LBD), and an N-terminal transactivation domain (NTD) (Brinkmann et al., 1989). In the absence of androgens ARs are mainly located in the cytoplasm. Upon ligand-binding ARs rapidly translocate to the nucleus, where they bind to androgen response elements (AREs) in the promoters/enhancers of target genes and recruit transcriptional coregulators (Cleutjens et al., 1997; Claessens et al., 2001; Rosenfeld et al., 2006). Many coregulators, like the p160-family, bind via LxxLL motifs to a hydrophobic cleft in the LBD of SRs formed by ligand-induced repositioning of the C-terminal α-helix. The AR differs from the other SRs in that its LBD preferentially interacts with cofactors containing FxxLF rather than LxxLL-motifs (Dubbink et al., 2004; Hur et al., 2004). In addition, an extra level of regulation of AR function is provided by an FQNLF motif in its NTD, which is able to interact with the liganded C-terminal LBD (N/C interaction) (Doesburg et al., 1997; He et al., 2000). A well recognized function of N/C interaction is stabilization of ligand binding (He et al., 2001; Dubbink et al., 2004). In addition, it has been hypothesized that N/C interactions might block unfavorable protein-protein interactions.

Confocal microscopy of GFP-tagged proteins, as well as quantitative assays such as FRAP and FRET have been instrumental in the investigation of the behavior of SRs in living cells (Georget et al., 1997; McNally et al., 2000; Stenoien et al., 2001; Schaaf and Cidlowski, 2003; Farla et al., 2004; Michalides et al., 2004; Agresti et al., 2005; Farla et al., 2005; Rayasam et al., 2005; Schaufele et al., 2005). Like many other nuclear factors interacting with DNA, SRs, including the AR, were shown to be highly mobile in the living cell nucleus and dynamically interact with specific binding sites (McNally et al., 2000; Stenoien et al., 2001; Farla et al., 2004; Farla et al., 2005; Rayasam et al., 2005). We have previously shown using FRAP-analysis based on computer modeling that agonist-bound ARs are largely mobile in the nucleus and only transiently bind to immobile elements in the nucleus. This transient immobilization was most likely due to DNA-binding, since several non-DNA binding mutants were freely mobile and did not show a detectable immobile fraction (Farla et al., 2004; Farla et al., 2005). In addition, a recent elegant study utilizing ARs double-tagged at the N- and C-terminus with the FRET couple CFP and YFP, respectively, have revealed that N/C interactions are initiated promptly after addition of hormone, prior to transport to the nucleus (Schaufele et al., 2005). However, questions regarding the spatiotemporal organization of AR in the nuclei of live cells remain unanswered: when, where and in what order do interactions with coregulators and N/C interaction take place once an AR has entered the nucleus? Does proper regulation of AR function require compartmentalization of such interactions? In this study we applied

innovative combined FRAP and FRET methodology, and ratio-imaging, utilizing CFP and YFP tagging of wild type ARs and AR mutants, to investigate the spatiotemporal regulation of AR N/C interactions and AR-coregulator interactions in living cells.

RESULTS

ARs double-tagged with CFP and YFP are functional

We tagged the fluorescent proteins YFP and CFP to the N- and C-terminus of wild type AR (YFP-AR-CFP), and to two mutant ARs: an N/C interaction deficient mutant in which the N-terminal FQNLF motif is changed into an AQNAA motif (AR(F23,27A/L26A)), and the non-DNA-binding mutant carrying a point mutation in the DNA-binding domain, leading to the inability of this mutant to bind to androgen regulated promoters (AR(A573D)) (Fig. 1A). Western blot analysis showed that the expressed fusion proteins were all of the expected size (Fig. 1B). In addition, several lines of evidence show that the double tag does not abolish AR function: the wild type YFP-AR-CFP was able to induce expression of a luciferase reporter gene driven by an androgen regulated promoter (at ~35% of the activity of the untagged AR), whereas the DBD mutant YFP-AR(A573D)-CFP was not (Fig. 1C). Importantly, although the transcription activation of double tagged ARs was lower than that of untagged ARs, the presence of the F23,27A/L26A mutations reduced the activity of both double tagged and untagged AR to the same extent (~60% reduction), showing that the transcriptional activity of double tagged ARs is sufficient to investigate its behavior (Fig. 1C). Furthermore, the fusion proteins were mainly cytoplasmic in absence of androgens and after addition of the agonistic ligand R1881 translocated to the nucleus at normal rate (data not shown) (Georget et al., 1997). In the nucleus the typical punctate nuclear distribution patterns were observed for the double-tagged wild type AR and the double-tagged AR(F23,27A/L26A) mutant, whereas the inactive non-DNA binding mutant YFP-AR(A573D)-CFP displayed the typical homogeneous distribution pattern described previously (Fig. 1D) (Farla et al., 2004). Summarizing, the above data show that double-tagging the AR and AR mutants did not interfere with their native behavior.

FRET in double tagged YFP-AR-CFP represents AR N/C interaction

We then investigated if the double-tagged YFP-AR-CFP provided a bonafide tool to study N/C interaction by FRET. The FRET read-out system applied was based on photobleaching of the acceptor and measuring the subsequential increase of the donor (abFRET, Fig. S2A) (Bastiaens and Jovin, 1996; Bastiaens et al., 1996; Kenworthy, 2001). In the presence of R1881, cells with a low expression (Fig. S1) of either the wild type YFP-AR-CFP or the non-DNA binding mutant YFP-AR(A573D)-CFP showed a significant increase in CFP fluorescence after acceptor bleaching, whereas only a small increase was observed in the N/C interaction deficient

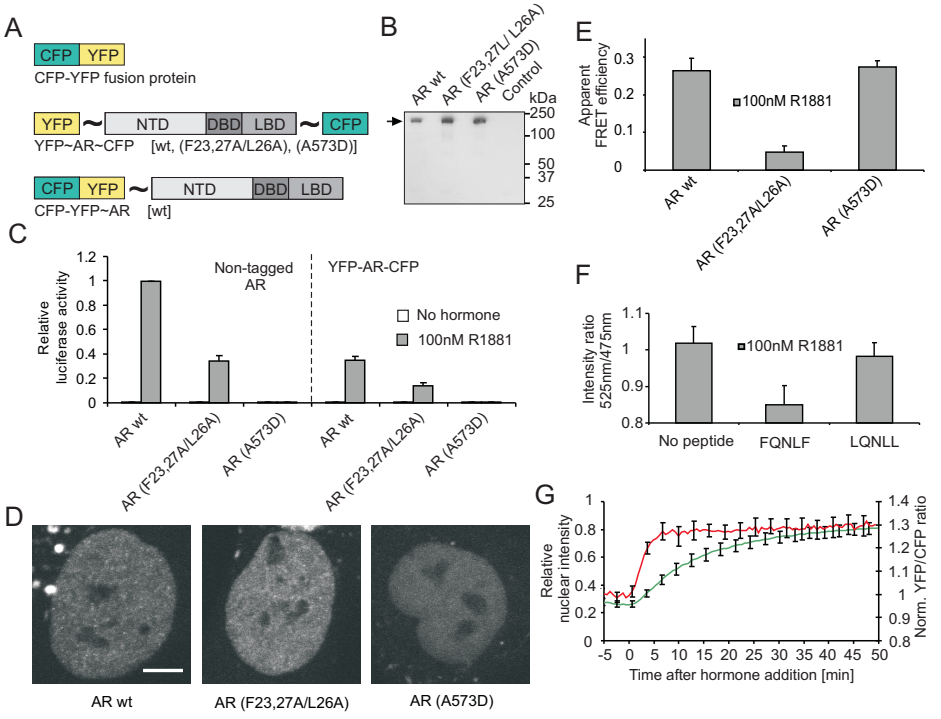

Figure 1 (A-D) Transactivating capacity and nuclear distribution of CFP and YFP tagged AR constructs are not affected by the (double) tags. (A) Schematic representation of the fusion proteins (~ represents a $(Gly\text{-}Ala)_6$ spacer). (B) Western blot of the fusion proteins expressed in Hep3B cells. (C) Transactivation activity of untagged and double tagged wild type and mutant ARs as measured on a (ARE)2-TATA Luc reporter. Averages +/- standard error of the mean (SEM) of five independent experiments are shown (D) Confocal images of nuclei of Hep3B cells stably expressing the indicated proteins in the presence of R1881. Bar represents 5 μm. (E-G) FRET of YFP-AR-CFP represents FQNLF mediated N/C interaction. (E) Acceptor photobleaching FRET (abFRET) (Fig. S2A) of the indicated proteins shows loss of N/C interaction in the AR(F23,27A/L26A) mutant, but not in the A573D mutant. Data shown are the mean +/- SEM of at least three independent experiments in which an average of 15 cells were measured. (F) Spectroscopic analysis of cell lysates of Hep3B cells expressing YFP-AR-CFP shows that FQNLF peptide motifs, but not LQNLL, inhibit interaction. Averages ± SEM of three independent experiments are shown. (G) Simultaneous detection of YFP and CFP signals (at 458nm excitation) shows a prompt increase of YFP/CFP ratio after R1881 addition at t = 0 min (red line) (n = 10). Translocation to the nucleus (green line) is much slower indicating that N/C interaction (red line) depends on hormone binding rather than cytoplasmic or nuclear localization (Schaufele et al., 2005). Error bars represent 2 x SEM.

mutant YFP-AR(F23,27A/L26A)-CFP (Fig. 1E). In addition, abFRET was not observed in the absence of agonistic ligand (Fig. S2B). These data indicate that the measured abFRET represents interaction of the FQNLF motif in the AR NTD with the ligand induced groove in the LBD. This was further corroborated by *in vitro* spectroscopy showing that FRET was strongly reduced by addition of FQNLF peptide motifs, which compete with the AR N-terminus for interaction with the C-terminal LBD, in lysates of cells expressing YFP-AR-CFP (Fig. 1F). This reduction in FRET signal was not observed when instead of FQNLF motifs non-competing LQNLL peptide motifs were added to the lysates (Fig. 1F), confirming that the observed FRET is due to N/C in-

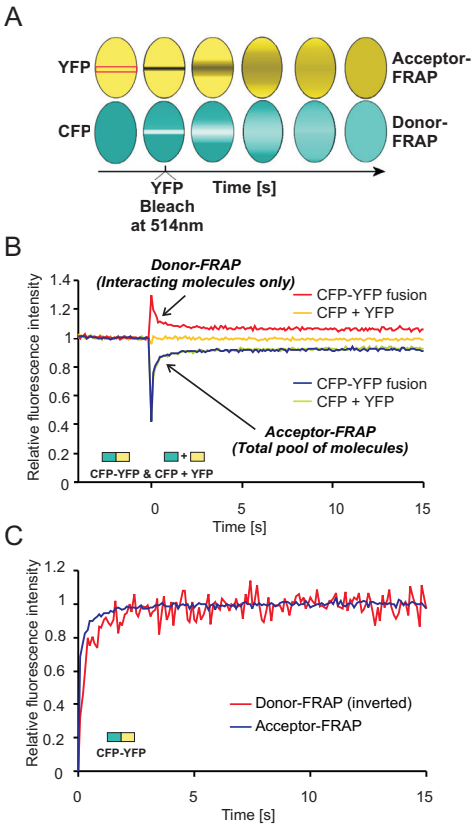

Figure 2 Simultaneous FRAP and FRET measurements to separately determine the mobility of interacting and non-interacting CFP- and YFP-tagged proteins in a single cell nucleus. (A) Schematic representation of the method. A 100 msec high intensity bleach pulse at 514 nm is applied to irreversibly photobleach YFPs in a narrow strip spanning the nucleus. Subsequently, redistribution of YFP and CFP fluorescence is recorded at 100 msec intervals (at 458 nm). Donor (CFP) emission (increased due to unquenching as a result of acceptor (YFP) bleaching) represents the mobility of interacting molecules only (donor-FRAP). Acceptor emission represents the total pool of YFP-tagged molecules irrespective of interaction (acceptor-FRAP). (B) Graph showing CFP and YFP fluorescence intensity in the bleached strip plotted against time. Experiments were performed in Hep3B cells expressing CFP-YFP fusions (red line: CFP fluorescence (donor-FRAP); blue line: YFP fluorescence (acceptor-FRAP)), or in Hep3B cells expressing separate CFPs and YFPs. (yellow line: CFP; green line: YFP). (n = 30) (C) Inverted donor-FRAP (red line) and acceptor-FRAP (blue line) plotted against time, showing similar kinetics. The curves were normalized by calculating $I_{norm} = (I_{raw} - I_0) / (I_{final} - I_0)$, where I_0 and I_{final} are the fluorescence intensities immediately after the bleach and after complete recovery, respectively.

teraction. Finally, extending previous data (Schaufele et al., 2005), confocal time lapse microscopy of living cells stably expressing YFP-AR-CFP showed that the YFP/CFP ratio significantly increased immediately after addition of hormone, followed by efficient translocation to the nucleus (Fig. 1G). In contrast, the N/C interaction deficient mutant YFP-AR(F23,27A/L26A)-CFP showed only a small increase in YFP/CFP ratio (Fig. S3). Based on this data it can be concluded that the FRET measured in the double-tagged YFP-AR-CFP represents N/C interaction.

Simultaneous FRAP and FRET enables analysis of the mobility of interacting molecules

We developed a method based on simultaneous measurement of FRAP and FRET to study the mobility of interacting molecules. In this method FRET-donor (CFP) and FRET-acceptor (YFP) fluorescence are simultaneously measured at regular time intervals after irreversibly photobleaching the acceptor in a defined sub-region of the nucleus. Donor fluorescence increase after acceptor photobleaching and subsequent decrease due to diffusion (donor-FRAP) reflects the mobility of only the interacting molecules (Fig. 2A). In contrast, acceptor fluorescence redistribution after acceptor bleaching (acceptor-FRAP) reveals the mobility of the total pool of both interacting and non-interacting molecules, similar to a conventional FRAP experiment (Houtsmuller et al., 1999; Houtsmuller and Vermeulen, 2001). Importantly, comparison of donor-FRAP and acceptor-FRAP curves allows to distinguish the mobility (and immobilization) of the sub-populations of interacting and non-interacting proteins.

First, the method was validated in Hep3B cells expressing either a CFP-YFP fusion protein or separate CFPs and YFPs (Fig. 2B,C). Briefly, a narrow strip spanning the nucleus was scanned at 458 nm excitation with short intervals (100 msec) at low laser power (YFP is sufficiently excited at this wavelength, Fig. S4A). Fluorescence intensities of the donor (CFP) and acceptor (YFP) were recorded simultaneously. After 40 scans, a high intensity, 100 msec bleach pulse at 514 nm was applied to specifically photobleach YFPs inside the strip (CFP was not bleached by the bleach pulse, Fig. S4B). Subsequently, scanning of the bleached strip was continued at 458 nm at low laser intensity. Acceptor (YFP) fluorescence in the strip was significantly reduced after bleaching and recovered at a velocity expected (*e.g.* Farla et al., 2005) for molecules of the size of the fusion proteins (Fig. 2B,C). In parallel, donor fluorescence in the bleached strip increased immediately after acceptor bleaching and decreased at a similar rate compared to the increase of YFP fluorescence (Fig. 2A-C). The observed CFP increase and subsequent decrease was not due to an artifact of YFP or CFP fluorescent properties since co-transfected separate YFPs and CFPs as well as ARs tagged with YFP or CFP only did not show a donor-FRAP signal (Fig. 2B, Fig. S4A, B).

AR N/C interactions are abolished when ARs are bound to DNA

We then performed simultaneous FRAP and FRET experiments to investigate AR N/C interaction. As a control experiment we first tested an AR tagged at the N-terminus with the CFP-YFP-fusion protein. FRET will occur in these fusion proteins independent of the N/C interaction, since CFP and YFP are always in close proximity. Donor-FRAP and acceptor-FRAP of CFP-YFP-AR both showed the same redistribution kinetics (Fig. 3A, B), which are slower then that of the CFP-YFP fusion alone (Fig. 2C) due to transient binding to DNA of wild type ARs (Farla et al., 2004; Farla et al., 2005) (Fig. 3A,B). In sharp contrast, donor-FRAP of the two-sided double-tagged YFP-AR-CFP (representing solely the mobility of N/C interacting ARs) was significantly faster than the corresponding acceptor-FRAP (representing the mobility of the total AR pool) (Fig. 3C). The difference between donor-FRAP and acceptor-FRAP was not

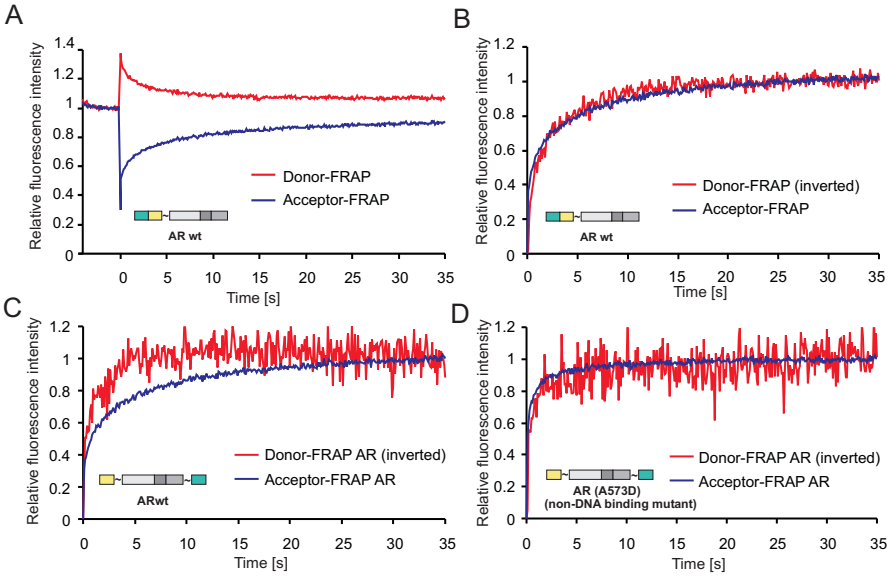

Figure 3 Simultaneous FRAP and FRET measurements in Hep3B cell expressing CFP-YFP-AR or wild type or mutant YFP-AR-CFP. (A and B) Donor-FRAP (red line) and acceptor-FRAP (blue line) curves of ARs tagged at the N-terminus with the CFP-YFP-fusion (CFP-YFP-AR) also show similar redistribution kinetics, but slower than the CFP-YFP fusion (Fig. 2) (n = 30). (C) Donor-FRAP (red line) and acceptor-FRAP (blue line) recorded in Hep3B cells expressing YFP-AR-CFP. The donor-FRAP curve (representing the mobility of N/C-interacting ARs only) shows faster recovery than the corresponding acceptor-FRAP curve (representing mobility of the total pool of AR) (n=45). (D) Donor-FRAP (red line) and acceptor-FRAP (blue line) curves of the non-DNA-binding YFP-AR(A573D)-CFP are rapid and similar to each other and to the donor-FRAP curve of YFP-AR-CFP (C), suggesting that N/C-interactions occur only when ARs are mobile (n=45). The curves in (B), (C) and (D) were normalized by calculating $I_{norm} = (I_{raw} - I_0) / (I_{final} - I_0)$, where I_0 and I_{final} are the fluorescence intensities immediately after the bleach and after complete recovery, respectively.

observed for the double-tagged non-DNA binding AR mutant (YFP-AR(A573D)-CFP) (Fig. 3D). Moreover, the YFP-AR-CFP donor-FRAP curve (Fig. 3C) showed similar fast kinetics as both donor-FRAP and acceptor-FRAP curves of the non-DNA binding AR mutant (Fig. 3D). These data strongly suggest that N/C interactions of the wild type AR occur mainly in the mobile pool and are abolished when ARs are transiently immobilized in a DNA-binding dependent fashion.

AR N/C interaction is reduced inside speckles

To further explore the observation that N/C interaction is reduced when ARs are transiently immobilized we determined the spatial distribution of N/C interacting and non-N/C-interacting ARs by high-resolution confocal ratio imaging of YFP-AR-CFP. Since YFP and CFP are present in the same quantity in cells expressing YFP-AR-CFP protein, these can be analyzed by straightforward ratio imaging. Briefly, ratio images of cells expressing either YFP-AR-CFP, CFP-YFP-AR and the non DNA-binding YFP-AR(A537D)-CFP were obtained by calculating for each pixel the ratio between the YFP and CFP emission intensity. Subsequently, the nuclei

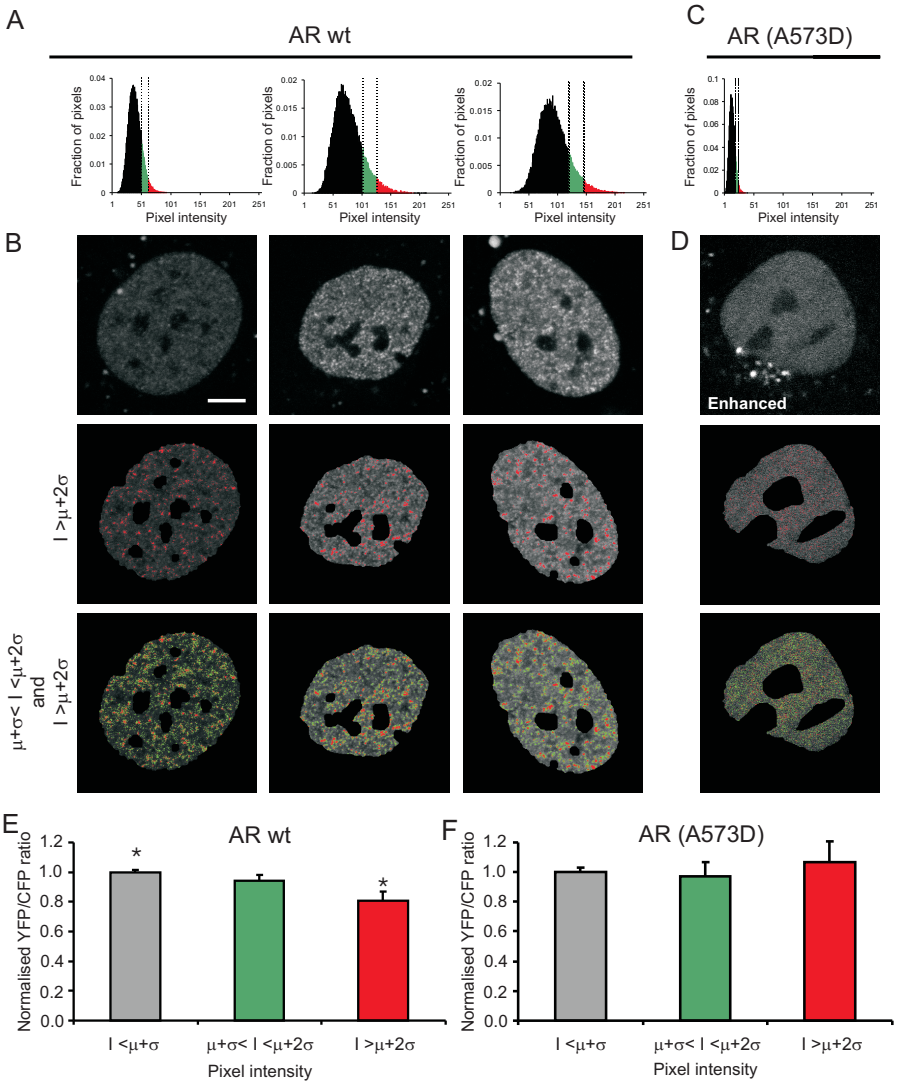

Figure 4 YFP-CFP ratio imaging on Hep3B cells expressing wild type or mutant YFP-AR-CFP. (A) Fluorescence intensity distributions of nuclei expressing wild type YFP-AR-CFP. For FRET analysis, the histograms were used to subdivide the nucleus in three areas based on mean intensity (μ) and standard deviation (σ): Pixel intensity $I < \mu + \sigma$ (black bars, 81.3% of total area), $\mu + \sigma < I < \mu + 2\sigma$ (green bars, 14.6%) and $I > \mu + 2\sigma$ (red bars, 4.1%). (B) Top panel: confocal images of the nuclei corresponding to the histograms in (a). Bar represents 5 μm. Middle panel: same nuclei (without background and regions with $I > \mu + 2\sigma$ indicated in red. Bottom panel: regions with $\mu + \sigma < I < \mu + 2\sigma$ indicated in green. Using the relative intensity threshold $> \mu + 2\sigma$ specifically selects high intensity regions that coincide largely with the well-described nuclear foci that give rise to a speckled pattern (e.g. Farla et al., 2005). (C and D) Intensity distribution and confocal image of a nucleus expressing non-DNA binding mutant AR(A573D). Although pixels with an intensity $> \mu + 2\sigma$ are present, these are randomly distributed throughout the nucleus and do not form aggregates or speckles. Contrast and brightness of the AR(A573D) images are digitally enhanced for visualization purposes, not for analysis. (E and F) YFP/CFP ratio of cells expressing wild type and non-DNA binding mutant YFP-AR(A573D)-CFP in the different relative pixel intensity categories (data shown are the mean +/- SEM of 100 and 20 cells respectively measured in 3 and 2 independent experiments respectively). Ratios in each category were normalized to corresponding categories measured in cells expressing CFP-YFP-AR with similar intensity. In wild type AR (E) a lower YFP/CFP ratio is observed in the regions with higher intensity indicating the loss of N/C-interaction in speckles (*$p=0.0002$). This is not found for the AR(A573D)(F).

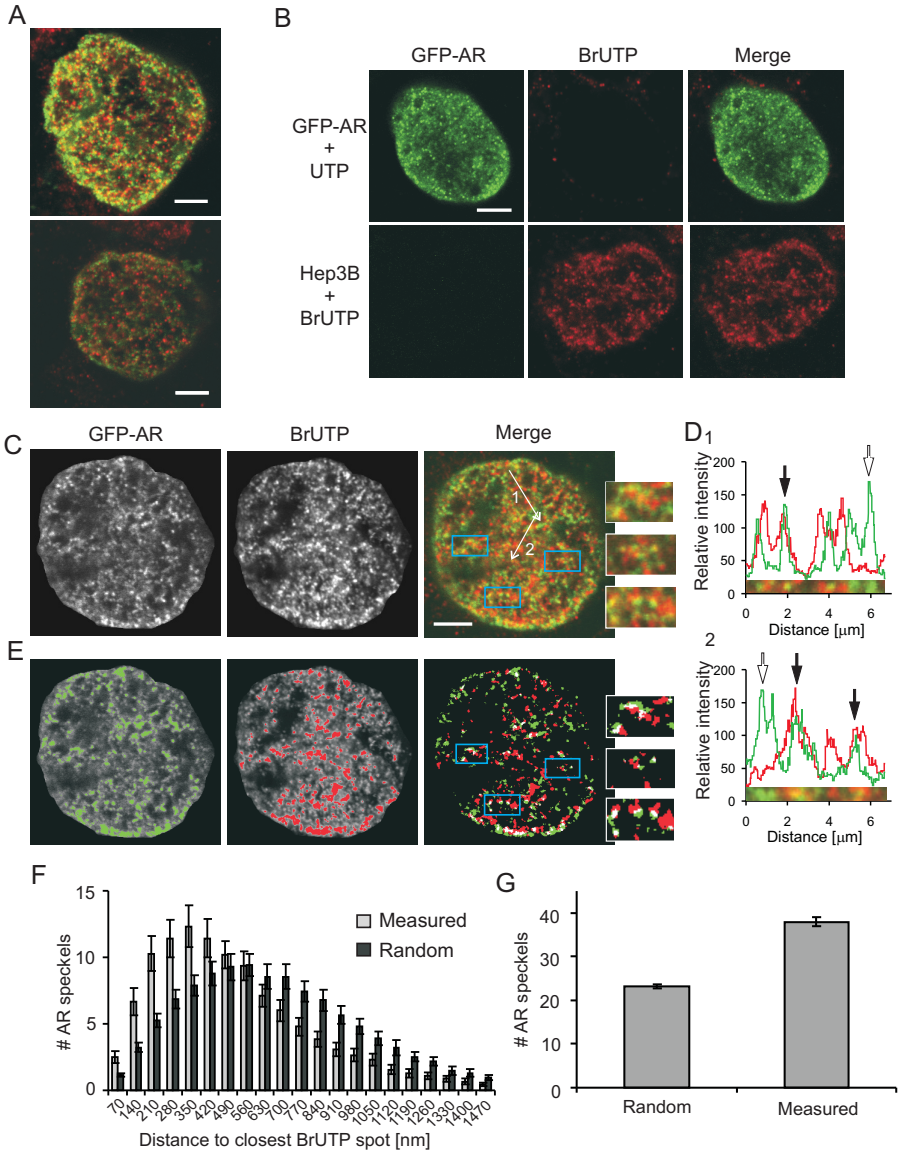

were divided into three areas based on the average fluorescence intensity of the entire nuclear area and corresponding standard deviation. In YFP-AR-CFP images, pixels with intensities higher than the mean plus two times the standard deviation (4.1% of total area, red bars in Fig. 4A) coincided largely with the area that is usually referred to as a speckled or focal pattern, whereas pixels with lower intensities coincided largely with the region outside the speckled pattern (Fig. 4A and B) (for image analysis see Materials and Methods). The average YFP/CFP ratio in each region was then calculated and expressed relative to the average ratio

Figure 5 AR speckles and hot spots of transcription. (A) Distribution of GFP-AR (green) and sites of BrUTP incorporation (red) in stably transfected Hep-3B cells (Farla et al., 2004). Sites of BrUTP incorporation were visualized by immunofluorescence. Bar represents 5 μm. (B) The fluorescent signals were monitored by sequential imaging of the GFP and Cy3 channels using confocal microscopy at a configuration at which no cross talk of signals occurred. Bar represents 5 μm. (C) Confocal images of a fixed Hep3B cell which stably expressed GFP-AR (green) and shows incorporated BrUTP staining (red). A partial overlap of the AR speckled pattern with sites of transcription can be seen (right panel and insets). White lines indicate the position of the line scans in (D). Bar represents 5 μm. (D) Line scans at the indicated position in Fig. 5C of the AR (green) and the BrUTP signal (red). Some but not all peaks coincided, indicating partial colocalization of some of the AR speckles with sites of transcription. Closed arrows indicate coinciding peaks, open arrows indicate AR speckles without a colocalized transcription site. (E) Images of AR and BrUTP thresholded similar to YFP-AR-CFP in Figure 4. In both the GFP-AR (GFP - green) and BrUTP (Cy3 - red) channels, regions with an intensity $I > \mu + 2\sigma$ and are indicated (two left panels). A merged image of the selected regions in both channels (right panel) shows the partial overlap (white) in the regions with an intensity $I > \mu + 2\sigma$. The insets represent the same regions as in (C). (F) Distribution of distances between AR speckles and the nearest BrUTP spot (light gray bars) or randomly distributed spots (dark gray bars) ($n = 68$). The number of AR speckles at relatively short distance (< 350 nm) to the nearest BrUTP spot was significantly higher compared to expected on the basis of random distribution ($p=0.00025$) and highest at the closest detectable distance. (G) Average number of AR speckles overlapping with the nearest UTP spot ($n = 68$). The number of AR speckles partially overlapping BrUTP spots is larger than expected on the basis of a random distribution ($p= 5.0 \times 10\text{-}8$).

in corresponding regions in CFP-YFP-AR with a similar intensity (see Materials and Methods). Cells expressing CFP-YFP-AR provide an ideal control to correct for potential imaging artifacts, because the ratio should be independent of AR folding and absolute fluorescence intensity. The wild type YFP-AR-CFP showed a significantly reduced YFP/CFP ratio in the speckles compared to the region outside the speckles (Fig. 4E) (*p=0.0002, see Materials and Methods), whereas no correlation is found for the non-DNA binding YFP-AR(A537D)-CFP which showed a homogeneous distribution (Fig. 4C, D and F). Apparently, the concentration of non-N/C interacting ARs is highest inside speckles.

AR speckles partially overlap sites of active transcription

The above results, suggesting that N/C interactions are abolished when AR is immobilized due to DNA-binding, and that N/C interactions are decreased inside speckles, prompted us to investigate whether the AR speckled pattern is correlated to the distribution of sites of active transcription. Previously, it was shown, using 5-bromo-uridine-5′-triphosphate (BrUTP) incorporation in nascent RNA and immunofluorescence (Jackson et al., 1993; Wansink et al., 1993), that progesterone receptor (Arnett-Mansfield et al., 2007), glucocorticoid receptors (Van Steensel et al., 1995), and several other transcription factors (BRG1, TFIIH, Oct1 and E2F-1) (Grande et al., 1997) do not show a complete, but rather a partial overlap with active sites of transcription (nascent RNA). Using the same approach (see Material and Methods) we were able to detect sites of transcription in Hep3B cells stably expressing GFP-AR at physiological levels (Farla et al., 2005). Newly incorporated BrUTP was detected by immunofluorescence using Cy3 which is excited at 543 nm excitation, GFP-AR was detected by 488 nm excitation. Sixty dual channel images were recorded at a configuration at which no cross talk occurred (Fig. 5A and B). Interestingly, visual analysis showed only a partial overlap between the AR

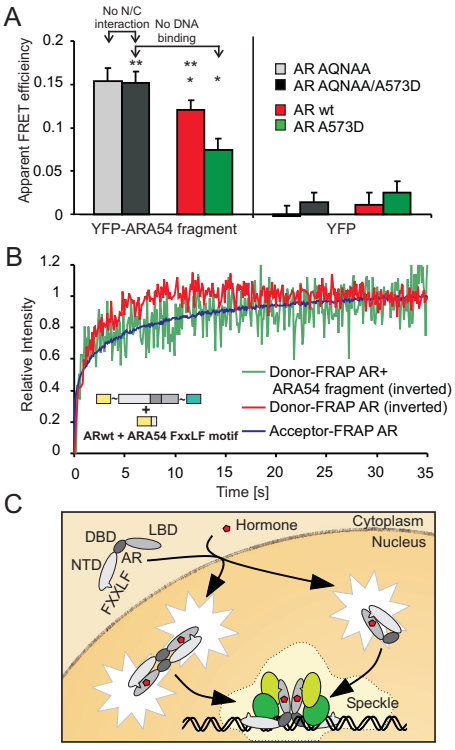

Figure 6 Interaction of ARA54 cofactor fragments with the AR. (A) AbFRET between YFP-tagged ARA54 fragments and CFP-tagged wild type AR (red bar) and three mutants: the non-DNA-binding mutant A573D (green bar), the N/C interaction deficient AR(F23,27A/L26A) (gray bar) and an AR carrying both mutations (black bar). Control experiments with free YFP are also shown. (data shown are the mean +/- SEM of four independent experiments in which 15 cells were measured. $^{*}p=0.003$; $^{**}p=0.042$). (B) Donor-FRAP curve of cells expressing YFP-AR-CFP and YFP-ARA54 fragments (green line) showing significantly retarded mobility compared to donor-FRAP of YFP-AR-CFP only (red line) and similar to the acceptor-FRAP of YFP-AR-CFP only (blue line), suggesting ARA54 fragments interact preferentially when ARs are transiently immobilized. (n = 45). The curves were normalized by calculating $I_{norm} = (I_{raw} - I_0) / (I_{final} - I_0)$, where I_0 and I_{final} are the fluorescence intensities immediately after the bleach and after complete recovery, respectively. (C) Model of N/C- and coregulator interactions of the androgen receptor. N/C-interactions may be either inter- or intramolecular (Schaufele et al., 2005), but are disrupted when AR is bound to DNA, allowing interactions with coregulators.

speckles and sites of active transcription (Fig. 5C, right panel and closed vs. open arrows in 5D). We quantified this observation by image analysis in which AR speckles and areas of active transcription were identified based on the average fluorescence intensity of the entire nuclear area and corresponding standard deviation. Similar to the ratio-imaging analysis (Fig. 4), where we used the same procedure to identify AR speckles (see above), pixels in the GFP-AR image with intensities higher than the mean plus two times the standard deviation coincided largely with AR speckles (Fig. 5E, left and right panel). In the Cy3-labeled BrUTP image, pixels with intensities higher than the mean plus two times the standard deviation were defined to be hot-spots of transcription (Fig. 5E, middle and right panel). The centers of on average 110 AR speckles and 130 hot-spots of transcription per nucleus were then determined

using the Zeiss KS-400 image analysis package (Zeiss). Subsequently the distances between each AR speckle and the closest hot-spot of transcription were determined and compared to a randomly distributed set consisting of an equal number of spots with the same size distribution as the measured hot-spots of transcription, taking care that the random spots were not in the nucleoli or outside the nucleus. The number of AR speckles at relatively short distance (< 350 nm, columns 1 to 5 in the histogram in Fig. 5F) to the nearest BrUTP spot was significantly higher compared to what is expected on the basis of a random distribution (43±5 spots measured versus 24±2 spots random (p=0.00025)(Fig. 5F). Moreover, the largest relative difference between measured and random was highest at the closest detectable distance. In addition, the number of AR speckles that showed overlap with the nearest hot spot of transcription was significantly higher than expected when there would be no correlation between AR and nascent RNA distributions ($p=5.0 \times 10^{-8}$)(Fig. 5G).

ARA54 cofactor fragments preferentially interact with DNA bound ARs

The strongly reduced N/C interaction in the transient immobile AR fraction lead us to hypothesize that AR coregulators containing FxxLF motifs may gain access more easily to this fraction, since no competition with the N-terminal AR FQNLF motif is expected to occur. We tested this hypothesis using YFP-tagged fragments of the cofactor ARA54, containing an FNRLF motif. ARA54 and ARA54-fragments containing the FNRLF-motif were previously shown to display a strong interaction with the AR LBD (Kang et al., 1999; He et al., 2002; Van de Wijngaart et al., 2006). In agreement with the above hypothesis, abFRET between the single-tagged wild type AR-CFP and YFP-ARA54 fragments was significantly higher ($^{*}p=0.003$, see Materials and Methods) than that of the non-DNA binding mutant AR(A573D)-CFP with YFP-ARA54, suggesting that interactions between AR and ARA54 fragments are significantly enhanced when ARs are bound to DNA (Fig. 6A, left panel). To further test the hypothesis that AR N/C interactions are responsible for blocking coregulator interactions we performed the same experiment using the N/C interaction deficient mutant AR(F23,27A/L26A)-CFP. In contrast to wild type AR, no difference in FRET with the ARA54 fragments was observed for the mutant and its non DNA binding variant AR(F23,27A/L26A/A573D)-CFP. Moreover, FRET was higher than that of the N/C interaction proficient wild type ARs ($^{**}p=0.042$) and much higher than the N/C interaction proficient non-DNA binding mutant (Fig. 6A, left panel). No FRET was found between any of the AR mutants and free YFP (Fig. 6A, right panel). These data are in agreement with a model in which YFP-ARA54 fragments bind preferentially to ARs lacking N/C interaction, i.e. either N/C interaction deficient AR(F23,27A/L26A) mutants or wild type ARs transiently immobilized as a result of DNA-binding.

To investigate this more extensively, we repeated the simultaneous FRAP and FRET measurements in living Hep3B cells expressing YFP-AR-CFP, now in the presence of co-transfected YFP-ARA54 fragments. Addition of YFP-ARA54 fragments significantly reduced the kinetics of the donor-FRAP curve compared to YFP-AR-CFP in absence of YFP-ARA54 fragments (Fig. 6B).

This is explained by the fact that in this experimental set-up not only the N/C interacting mobile ARs show FRET, but also the non-N/C interacting immobile ARs, now between AR C-terminal domain and the YFP-ARA54 fragments (which binds to the C-terminal domain instead of the YFP-tagged N-terminal domain of immobile YFP-AR-CFP). This indicates that the ARA54 fragments preferably interact with the C-terminus of the AR when it is transiently immobilized due to DNA-binding when the N-terminal FQNLF motif does not compete for interaction with the C-terminal domain.

Summarizing, the abFRET data (Fig. 6A) show that ARA54 fragments interact more frequently with wild type AR than with the non-DNA-binding mutant. The simultaneous FRAP and FRET analysis (Fig. 6B) suggests that this is because ARA54 fragments gain access more easily to the C-terminal LBD of the wild type ARs when there is no or less competition with the NTD. This occurs either when wild type ARs are transiently immobilized in a DNA-binding dependent manner (Fig. 3C) or when the N/C interaction is disrupted (Fig. 6A).

DISCUSSION

Activity of SRs is not only regulated by ligand binding but also by interacting cofactors. The best-described binding site for SR-coregulators is the hydrophobic cleft in the LBD to which LxxLL-motifs can bind. The AR LBD is unique in its preference for the interaction with cofactors carrying FxxLF-motifs rather than LxxLL-motifs (Dubbink et al., 2004; Hur et al., 2004). The AR itself also contains an FQNLF motif in the N-terminal domain enabling interaction with the LBD (N/C interaction) (Doesburg et al., 1997; He et al., 2000). The potential competition between the AR N-terminal FQNLF-motif and similar motifs in cofactors for interaction with the LBD raises questions regarding the role of the N/C interaction in orchestrating cofactor interactions. To study AR N/C interactions in living cells we tagged the AR at the N-terminus and C-terminus with YFP and CFP respectively or with CFP alone, and applied FRET and simultaneous FRET and FRAP experiments. In addition, to investigate cofactor interactions we tagged ARA54-fragments containing an FNRLF-motif with YFP. The presence of the tags had no effect on AR localization and hormone-induced nuclear translocation (Fig. 1D and G), and only limited effect on the transactivation function of the AR (Fig. 1C). Acceptor photobleaching FRET assays on living cells and *in vitro* competition experiments using FxxLF- and LxxLL-peptide motifs demonstrated that FRET represents N/C interaction (Fig. 1E and F).

Previously, utilizing FRAP assays we and others have shown that the mobility of ARs is reduced compared to the mobility of non-DNA-binding AR(A573D) mutants (Farla et al., 2004) as well as antagonist bound ARs (Farla et al., 2005). In addition, the observed hormone-induced slow-down of AR mobility was always accompanied by the formation of a speckled distribution pattern in the nucleus, suggesting that ARs transiently immobilize in speckles. We have now shown using combined FRET and FRAP analysis that, surprisingly, the mobility of the

pool of N/C-interacting ARs is not reduced in presence of hormone, and that, consequently, the pool of non-N/C-interacting ARs is responsible for the observed overall slow down of AR mobility. This suggests that the N/C interaction is largely lost when ARs are transiently immobilized, most likely due to DNA-binding (Fig. 3C). This was confirmed by high-resolution ratio-imaging showing that FRET is reduced inside speckles (Fig. 4E).

The loss of N/C interaction in immobilized ARs predicts that the C-terminal hydrophobic groove, to which FxxLF motifs can bind, is optimally accessible for coregulators when the ARs are bound to DNA. Our acceptor bleaching FRET experiments on YFP-tagged FNRLF-fragments of the AR cofactor ARA54 and AR-CFP provide evidence that strongly supports this view: first, the experiments indicate that ARA54-fragments interact more frequently with the wild type AR than with the non-DNA-binding AR mutants (A573D), whereas the non-N/C-interacting mutants of DNA-binding and non-DNA-binding ARs do not show this difference and interact more frequently than any of the N/C interaction proficient ARs (Fig. 6A). Moreover, when YFP-tagged ARA54 fragments are co-expressed with YFP-AR-CFP in a simultaneous FRET and FRAP assay, the mobility of the N/C-interacting pool is reduced (Fig. 6B). This indicates that on top of the mobile N/C-interacting ARs, also the immobile double-tagged ARs now show FRET due to their interaction with the YFP-tagged ARA54-fragments.

The observed loss of N/C interaction in immobile ARs and frequent interactions of cofactors fragments with immobile AR are in line with a scenario in which the AR itself dynamically regulates the time and place of interactions with coregulators by blocking the groove using its N-terminal FQNLF motif when not associated to DNA, and allowing access of coregulators only after DNA-binding (Fig. 6C).

As our data suggest that DNA-binding occurs in speckles, the question then arose whether these speckles also represent sites of active transcription. To investigate this we performed BrUTP incorporation experiments on Hep3B cells stably expressing AR-GFP. Interestingly, visual as well as statistical analysis showed that although speckles are closer to sites of active transcription than expected on the basis of a random distribution, AR and transcription hot-spots only partially overlap (Fig. 5), suggesting that DNA-binding of the AR does not always result in the formation of productive transcription complexes. Several lines of previous evidence are in agreement with these observations: first, it has been shown that progesterone receptor (Arnett-Mansfield et al., 2007), glucocorticoid receptors (Van Steensel et al., 1995), and several other transcription factors (BRG1, TFIIH, Oct1 and E2F-1) (Grande et al., 1997) showed only a partial correlation with active sites of transcription. Second, recent data on estrogen receptors (ER) using ChIP-on-chip assays suggested that SRs have many more binding sites (~3600) in the genome than expected on the basis of the estimated number of ER regulated genes, which probably is in the order of hundreds rather than thousands (Carroll et al., 2006). Third, it has been shown by ChIP that DNA-binding of the ER occurs in a cyclic pattern, and that an initial cycle of binding only prepares promoters for transcription but does not result in a productive transcription complex (reviewed in Métivier et al., 2006).

However, these non-productive cycles were observed in cells shortly after application of hormone. It remains questionable whether after longer exposure to hormone, as used in our experiments, promoters would be 'shut down' and reactivated.

If not all immobile ARs are involved in active transcription, the question remains what happens in speckles. It has frequently been suggested that many transcription factors, and other nuclear factors involved in DNA-metabolism, bind transiently to DNA also at non-specific sites, thereby scanning the DNA (Phair et al., 2004; Métivier et al., 2006). Possibly the majority of immobile ARs observed in our experiments are involved in such scanning activity. The interaction with cofactors may then play a role in identifying specific binding sites when encountered during scanning. In addition, it is not excluded that (part) of the speckles represent some sort of storage sites. However, since non-DNA-binding mutants do not form speckles, and move freely through the nucleus, such a model suggests that the DBD is also involved in storage.

In conclusion we have utilized a novel combination of FRAP and FRET to investigate interactions of the AR in living cells and provided evidence that AR N/C interactions are involved in the spatio-temporal regulation of interactions with coregulators. The FRET/FRAP-assay provides a novel tool to separately investigate the dynamics of interacting and non-interacting molecules. This opens up a multitude of possibilities to investigate the molecular mechanisms underlying not only the regulation of gene transcription but also that of other DNA-transacting systems such as DNA repair and replication.

MATERIALS AND METHODS

Constructs

The cDNA construct encoding N-terminally YFP-tagged AR was generated by replacing EGFP in pGFP-$(GA)_6$-AR (Farla et al., 2004) by EYFP-C1 (Clontech). The C-terminally CFP-tagged AR was generated by replacing EGFP by ECFP-N3 (Clontech) in pAR-$(GA)_6$-EGFP in which two AR fragments from respectively pcDNA-AR0mcs (lacking the AR stop codon) (Sui et al., 1999) and pAR0 (Brinkmann et al., 1989), where sequentially inserted in EGFP-N3 (Clontech) followed by the introduction of a spacer sequence coding for a $(Gly\text{-}Ala)_6$ stretch. The construct coding for double-tagged AR (pYFP-$(GA)_6$-AR-$(GA)_6$-CFP) was generated by combining a fragment of N-terminally YFP-tagged AR pYFP-$(GA)_6$-AR with a fragment of C-terminally CFP-tagged AR pAR-$(GA)_6$-CFP. The F23,27A/L26A variants were generated by QuikChange (Stratagene) mutagenesis using primers 5'-ACCTACCGAGGAGCTGCACAGAATGCTGCACAGAGCGTGCGC-GAA-3' and 5'-TTCGCGCACGCTCTGTGCAGCATTCTGTGCAGCTCCTCGGTAGGT-3'. To generate the A573D variants, the AR DBDs of pYFP-AR-CFP and pAR-$(GA)_6$–CFP were replaced by a pGFP-AR (A573D) (Farla et al., 2004) fragment containing the AR DBD (A573D) mutation. EYFP in pYFP-$(GA)_6$-AR was replaced by an ECFP-EYFP fusion to obtain pCFP-YFP-$(GA)_6$-AR. The

YFP tagged ARA54 peptide construct was obtained by annealing the primers 5'-GATCGAC-CCTGGTTCACCATGTTTTAACCGGCTGTTTTATGCTGTGGATGTTG-3' and 5'- AATTCAACATCCA-CAGCATAAAACAGCCGGTTAAAACATGGTGAACCAGGGTC-3' containing the FNRLF motif and inserting the fragment in pEYFP-C2 (Clontech). Structures of novel constructs were verified by appropriate restriction digestions and by sequencing. Sizes of expressed proteins were verified by Western blotting. pCYFP encoding the ECFP-EYFP fusion was kindly provided by Dr. Claude Gazin. The (ARE)2TATA Luciferase reporter was a gift from Dr. Guido Jenster.

Cell culture, transfections and luciferase assay

Two days before microscopic analyses Hep3B cells were grown on glass cover slips in 6 wells plates in α-MEM (Cambrex) supplemented with 5% fetal bovine serum (FBS) (HyClone), 2 mM L-glutamine, 100 units/mL penicillin, 100 μg/mL streptamycin. At least 4 h before transfection the medium was substituted by medium containing 5% dextran charcoal stripped FBS. Transfections were performed with 1 μg/well of AR or CFP-YFP expression constructs or 0.5 μg/well empty vector in FuGENE6 (Roche) transfection medium. In indicated experiments YFP-tagged ARA54 peptide expression constructs (0.5 μg/well) were added. Four hours after transfection the medium was replaced by medium with 5% dextran charcoal stripped FBS with or without 100 nM R1881. Hep3B cells stably expressing AR constructs were subjected to the same medium replacement schedule.

For the AR transactivation experiments Hep3B cells were cultured in 24-wells plates on α-MEM supplemented with 5% dextran charcoal stripped FBS in the presence or absence of 100 nM R1881 and transfected using 50 ng AR expression construct and 100 ng (ARE)2TATA Luc reporter. Twenty-four h after transfection cells were lysed and luciferase activity was measured in a Fluoroscan Ascent FL luminometer (Labsystems Oy). Light emission was recorded during 5 s after a delay of 2 s.

Western blot analysis

Hep3B cells were cultured and transfected in 6-wells plates. Twenty-four h after transfection cells were washed twice in ice-cold PBS and lysed in 200 μL Laemmli sample buffer (50 mM Tris-HCl pH 6.8, 10% glycerol, 2% SDS, 10 mM DTT and 0,001% Bromophenolblue). After boiling (5 min), 5 μL sample was separated on a 10% SDS-polyacrylamide gel and blotted to Nitrocellulose Transfer Membrane (Protran; Schleicher and Schuell). Blots were incubated with anti-AR (mouse monoclonal F34.4.1; 1:2000) or anti β-actin (mouse monoclonal anti-β-actin; 1:10000 (Sigma)) and subsequently incubated with horseradish peroxidase (HRP)-conjugated goat anti-mouse antibody (Dako). Proteins were visualized using Super Signal West Pico Luminol solution (Pierce), followed by exposure to X-ray film.

Confocal imaging and FRET acceptor photobleaching

Live cell and immunofluorescence imaging was performed using a Zeiss LSM510 confocal laser scanning microscope equipped with a Plan-Neofluar 40x/1.3 NA oil objective (Carl Zeiss) at a lateral resolution of 100 nm (FRET acceptor bleaching) or 70 nm (immunofluorescence). An argon laser was used for excitation of CFP, GFP and YFP at 458, 488 and, 514 nm, respectively, and a He/Ne laser was used to excite Cy3 at 543 nm.

Interactions between either the N- and C-terminal domain of the YFP-AR-CFP or between AR-CFP and YFP-ARA54 were assessed using acceptor photobleaching. For this, YFP and CFP images were collected sequentially prior to photobleaching of the acceptor. CFP was excited at 458 nm at moderate laser power and emission was detected using a 470-500 nm band pass emission filter. YFP was excited at 514 nm at moderate laser power and emission was detected using a 560 nm long pass emission filter. After image collection, YFP in the nucleus was bleached by scanning a nuclear region of ~100 μm^2 25 times at 514 nm at high laser power, covering the largest part of the nucleus. After photobleaching, a second YFP and CFP image pair was collected. Apparent FRET efficiency was estimated (correcting for the amount of YFP bleached) using the equation: $abFRET = ((CFP_{after} - CFP_{before}) \cdot YFP_{before}) / ((YFP_{before} - YFP_{after}) \cdot CFP_{after})$, where CFP_{before} and YFP_{before} are the average prebleach fluorescence intensities of CFP and YFP respectively in the area to be bleached (after background subtraction), and CFP_{after} and YFP_{after} are the average postbleach fluorescence intensities of CFP and YFP respectively in the bleached area. The apparent FRET efficiency was finally expressed relative to control measurements in cells expressing either free CFP and YFP ($abFRET_0$) or the CFP-YFP fusion protein ($abFRET_{CFP\text{-}YFP\ fusion}$): apparent FRET efficiency = $(abFRET - abFRET_0) / (abFRET_{CFP\text{-}YFP\ fusion} - abFRET_0)$. For statistical analysis, the abFRET data sets were tested for normality using the Kolmogorov-Smirnov test, and data sets were compared using the one-tailed Student's T-test.

For high-resolution immunofluorescent imaging of BrUTP incorporated into nascent RNA, Cy3 was excited at 543 nm at moderate laser power and emission was detected using a 560 nm long pass emission filter. GFP-AR was excited at 488 nm at moderate laser power and emission was detected using a 505-530 nm band pass emission filter. Cy3 and GFP images were recorded sequentially to avoid cross-talk.

FRET spectroscopy

Spectroscopic analysis of crude cell lysates of cells expressing YFP-AR-CFP was performed on a fluorescence spectrophotometer (Hitachi F-4500) by recording spectra at 425 nm excitation. The apparent FRET efficiency was calculated as the ratio of the emission intensities at 525 and 475 nm respectively. Background fluorescence of lysates of cells not expressing YFP-AR-CFP prepared in the same way was negligible. Spectra were recorded of lysates in absence and presence (300 mM) of synthesized peptides containing an FQNLF or LQNLL motif respectively.

Simultaneous FRAP and FRET

To study the mobility of interacting proteins a narrow strip spanning the nucleus was scanned at 458 nm excitation with short intervals (100 msec) at low laser power (YFP is sufficiently excited at this wavelength, Fig. S4A). Fluorescence intensities of the donor (CFP) and acceptor (YFP) were recorded simultaneously using 470-500 nm band pass and 560 nm long pass filters, respectively. After 40 scans, a high intensity, 100 msec bleach pulse at 514 nm was applied to specifically photobleach YFPs inside the strip (CFP was not bleached by the bleach pulse, Fig. S4B). Subsequently, scanning of the bleached strip was continued at 458 nm at low laser intensity. The curves are either normalized by calculating $I_{norm} = (I_{raw} - I_{bg}) / (I_{pre} - I_{bg})$ or to compare donor-FRAP and acceptor-FRAP curves by calculating Inorm = $(I_{raw} - I_0) / (I_{final} - I_0)$ where I_{pre}, I_0 and I_{final} are the fluorescent intensities before, immediately after the bleach and after complete recovery, respectively, and I_{bg} is the background intensity.

YFP/CFP ratio imaging

Since YFP and CFP are present in exactly the same quantity in cells expressing YFP-AR-CFP, ratio imaging can be applied to study the spatial distribution of ARs with and without N/C interaction. Local differences in YFP/CFP ratio within the nucleus of cells expressing YFP-AR-CFP will only be observed if the ratio between N/C interacting ARs, showing a relatively high YFP/CFP-ratio, and non-N/C interacting ARs, showing a relatively low YFP/CFP-ratio, are different. For high-resolution YFP/CFP ratio imaging YFP and CFP were imaged simultaneously using a moderate excitation at 458 nm and a 470-500 nm band pass emission filter for CFP and a 560 nm long pass emission filter for YFP. To reduce noise, eight times line averaging was used. Ratio images were obtained by calculating for each pixel $(I_{YFP} - I_{bg}) / (I_{CFP} - I_{bg})$, where I_{YFP} and I_{CFP} are the intensities of the YFP and CFP emission respectively, and I_{bg} is the background intensity. To obtain regions representing successive relative intensity ranges (see Fig. 4), the average of I_{YFP} and I_{CFP} was calculated for each pixel as Iaverage = $(I_{YFP} + I_{CFP}) / 2$. The mean $I_{average}$ of each nucleus (termed μ in Fig. 4) and the standard deviation σ were then calculated after (manual) selection of the nuclear area and exclusion of the nucleoli (Fig. 4B). The average ratio in areas with pixel intensities $I_{average} < \mu + \sigma$, $\mu + \sigma < I_{average} < \mu + 2\sigma$ and $I_{average} > \mu + 2\sigma$ were then first calculated for CFP-YFP-AR expressing cells. Since these molecules emit at a fixed YFP/CFP ratio irrespective of their conformation or local concentration, any difference in ratio in the three selected areas is due to imaging artifacts. Indeed CFP/YFP ratio increased in CFP-YFP-AR expressing cells with low intensity and decreased in cells with high intensities probably due to nonlinearity of the detectors (data not shown). Therefore, data obtained from each cell expressing YFP-AR-CFP and the non-DNA-binding mutant YFP-AR(A573D)-CFP were expressed relative to the average ratio measured in corresponding areas in 7 cells expressing CFP-YFP-AR with similar expression level. For statistical analysis, the YFP/CFP ratio imaging data sets were tested for normality using the Kolmogorov-Smirnov test, and data sets were compared using the Student's T-test.

Immunofluorescent labeling of nascent RNA

Nascent RNA was detected by BrUTP incorporation in permeabilized living Hep3B cells stably expressing GFP-AR (Farla et al., 2004) according to Wansink et al., 1993. Cells were grown overnight on coverslips in medium containing 5% dextran charcoal stripped FBS in the presence of 100 nM R1881. The procedure of BrUTP incorporation has been previously (Wansink et al., 1993). Cells were permeabilized in glycerolbuffer (20 mM Tris HCl, 0.5 mM MgCl2, 0.5 mM EGTA, 25% glycerol, 1 mM PMSF) supplemented with 0.05% Triton-X100 and 10 U/mL RNAsin for 3 min. To allow BrUTP incorporation, permeabilized cells were incubated for 30 min at RT in synthesis buffer (100 nM TrisHCl, 5 nM MgCl2, 0.5 mM EGTA, 200 mM KCl, 50% glycerol, 0.05 mM SAM, 20 U/ml RNAsin, 0.5 mM PMSF) supplemented with 0.5 mM ATP, CTP, GTP and BrUTP (or UTP as control)(Sigma, Chemical Co.). Next, cells were fixed in 2% formaldehyde in PBS, incubated in 0.5% Triton-X100/PBS for 5 min and in 100 nM glycin/PBS for 10 min, each step followed by two PBS washes. After blocking with PBG (0.05% gelatin, 0.5% BSA in PBS) incorporated BrUTP was immunolabelled overnight with a rat anti BrdU mAb (Seralab) diluted 1:500 in PBS at 4˚C. After 4 washes with PBG cells were incubated for 90 min at RT with biotin-conjugated sheep-anti-rat IgG (Jackson ImmunoResearch Laboratories Inc.) 1:200 in PBS followed by 4 washes with PBG. The biotinylated antibody was then visualized with Cy3-conjugated streptavidin (Jackson ImmunoResearch Laboratories Inc.) 1:250 in PBS for 30 min at room temperature. After extensive washing with PBG and PBS cells were embedded in Vectashield containing DAPI.

SUPPLEMENTAL MATERIAL

Fig. S1 YFP-AR-CFP expression analysis of cells used in the acceptor photobleaching FRET experiments and in the simultaneous FRAP and FRET measurements. YFP-AR-CFP expression levels are presented relative to endogenous AR in the VCaP prostate cancer cell line. Fig. S2 presents the validation of FRET measurements by acceptor photobleaching (abFRET) and shows the hormone dependency of FRET measured in cells expressing YFP-AR-CFP. Fig. S3 shows the minimal YFP/CFP ratio change after addition of R1881 in cells expressing YFP-AR(F23,27A/L26A)-CFP variant. Fig. S4 presents the control experiments for donor-FRAP and acceptor-FRAP on cells expressing YFP-AR (A) and AR-CFP (B).

ACKNOWLEDGEMENTS

We thank Drs J. Essers and R. Kanaar and for critically reading the manuscript. This work is supported by grant DDHK 2002-2679 of the Dutch Cancer Society (KWF) and VIDI grant 016.046.371 of the Dutch Organisation for Scientific Research (NWO).

REFERENCES

Agresti, A., P. Scaffidi, A. Riva, V.R. Caiolfa, and M.E. Bianchi. 2005. GR and HMGB1 interact only within chromatin and influence each other's residence time. *Mol Cell.* 18:109-121.

Arnett-Mansfield, R.L., J.D. Graham, A.R. Hanson, P.A. Mote, A. Gompel, L.L. Scurr, N. Gava, A. de Fazio, and C.L. Clarke. 2007. Focal Subnuclear Distribution of Progesterone Receptor Is Ligand Dependent and Associated with Transcriptional Activity. *Mol Endocrinol.* 21:14-29.

Bastiaens, P.I.H., and T.M. Jovin. 1996. Microspectroscopic imaging tracks the intracellular processing of a signal transduction protein: Fluorescent-labeled protein kinase C βI. *Proc Natl Acad Sci U S A.* 93:8407-8412.

Bastiaens, P.I.H., I.V. Majoul, P.J. Verveer, H.-D. Söling, and T.M. Jovin. 1996. Imaging the intracellular trafficking and state of the AB5 quaternary structure of cholera toxin. *EMBO J.* 15:4246-4253.

Brinkmann, A.O., P.W. Faber, H.C.J. van Rooij, G.G.J.M. Kuiper, C. Ris, P. Klaassen, J.A.G.M. van der Korput, M.M. Voorhorst, J.H. van Laar, E. Mulder, and J. Trapman. 1989. The human androgen receptor: domain structure, genomic organization and regulation of expression. *J Steroid Biochem.* 34:307-310.

Carroll, J.S., C.A. Meyer, J. Song, W. Li, T.R. Geistlinger, J. Eeckhoute, A.S. Brodsky, E.K. Keeton, K.C. Fertuck, G.F. Hall, Q. Wang, S. Bekiranov, V. Sementchenko, E.A. Fox, P.A. Silver, T.R. Gingeras, X.S. Liu, and M. Brown. 2006. Genome-wide analysis of estrogen receptor binding sites. *Nat Genet.* 38:1289-1297.

Claessens, F., G. Verrijdt, E. Schoenmakers, A. Haelens, B. Peeters, G. Verhoeven, and W. Rombauts. 2001. Selective DNA binding by the androgen receptor as a mechanism for hormone-specific gene regulation. *J Steroid Biochem Mol Biol.* 76:23-30.

Cleutjens, K.B.J.M., J.A.G.M. van der Korput, C.C.E.M. van Eekelen, H.C.J. van Rooij, P.W. Faber, and J. Trapman. 1997. An androgen response element in a far upstream enhancer region is essential for high, androgen-regulated activity of the prostate-specific antigen promoter. *Mol Endocrinol.* 11:148-161.

Doesburg, P., C.W. Kuil, C.A. Berrevoets, K. Steketee, P.W. Faber, E. Mulder, A.O. Brinkmann, and J. Trapman. 1997. Functional in vivo interaction between the amino-terminal, transactivation domain and the ligand binding domain of the androgen receptor. *Biochemistry.* 36:1052-1064.

Dubbink, H.J., R. Hersmus, C.S. Verma, J.A.G.M. van der Korput, C.A. Berrevoets, J. van Tol, A.C.J. Ziel-van der Made, A.O. Brinkmann, A.C.W. Pike, and J. Trapman. 2004. Distinct recognition modes of FXXLF and LXXLL motifs by the androgen receptor. *Mol Endocrinol.* 18:2132-2150.

Farla, P., R. Hersmus, B. Geverts, P.O. Mari, A.L. Nigg, H.J. Dubbink, J. Trapman, and A.B. Houtsmuller. 2004. The androgen receptor ligand-binding domain stabilizes DNA binding in living cells. *J Struct Biol.* 147:50-61.

Farla, P., R. Hersmus, J. Trapman, and A.B. Houtsmuller. 2005. Antiandrogens prevent stable DNA-binding of the androgen receptor. *J Cell Sci.* 118:4187-4198.

Georget, V., J.M. Lobaccaro, B. Terouanne, P. Mangeat, J.-C. Nicolas, and C. Sultan. 1997. Trafficking of the androgen receptor in living cells with fused green fluorescent protein-androgen receptor. *Mol Cell Endocrinol.* 129:17-26.

Grande, M., I. van der Kraan, L. de Jong, and R. van Driel. 1997. Nuclear distribution of transcription factors in relation to sites of transcription and RNA polymerase II. *J Cell Sci.* 110:1781-1791.

He, B., N.T. Bowen, J.T. Minges, and E.M. Wilson. 2001. Androgen-induced NH2- and COOH-terminal interaction inhibits p160 coactivator recruitment by activation function 2. *J Biol Chem.* 276:42293-42301.

He, B., J.A. Kemppainen, and E.M. Wilson. 2000. FXXLF and WXXLF sequences mediate the NH2-terminal interaction with the ligand binding domain of the androgen receptor. *J Biol Chem.* 275:22986-22994.

He, B., J.T. Minges, L.W. Lee, and E.M. Wilson. 2002. The FXXLF motif mediates androgen receptor-specific interactions with coregulators. *J Biol Chem.* 277:10226-10235.

Houtsmuller, A.B., S. Rademakers, A.L. Nigg, D. Hoogstraten, J.H.J. Hoeijmakers, and W. Vermeulen. 1999. Action of DNA repair endonuclease ERCC1/XPF in living cells. *Science.* 284:958-961.

Houtsmuller, A.B., and W. Vermeulen. 2001. Macromolecular dynamics in living cell nuclei revealed by fluorescence redistribution after photobleaching. *Histochem Cell Biol.* 115:13-21.

Hur, E., S.J. Pfaff, E.S. Payne, H. Gron, B.M. Buehrer, and R.J. Fletterick. 2004. Recognition and accommodation at the androgen receptor coactivator binding interface. *PLoS Biol.* 2:E274.

Jackson, D.A., A.B. Hassan, R.J. Errington, and P.R. Cook. 1993. Visualization of focal sites of transcription within human nuclei. *EMBO J.* 12:1059-1065.

Kang, H.-Y., S. Yeh, N. Fujimoto, and C. Chang. 1999. Cloning and characterization of human prostate coactivator ARA54, a novel protein that associates with the androgen receptor. *J Biol Chem.* 274:8570-8576.

Kenworthy, A.K. 2001. Imaging protein-protein interactions using fluorescence resonance energy transfer microscopy. *Methods.* 24:289-296.

Korenchuk, S., J. Lehr, L. McLean, Y. Lee, S. Whitney, R. Vessella, D. Lin, and K. Pienta. 2001. VCaP, a cell-based model system of human prostate cancer. *In Vivo.* 15:163-168.

Marcelli, M., D.L. Stenoien, A.T. Szafran, S. Simeoni, I.U. Agoulnik, N.L. Weigel, T. Moran, I. Mikic, J.H. Price, and M.A. Mancini. 2006. Quantifying effects of ligands on androgen receptor nuclear translocation, intranuclear dynamics, and solubility. *J Cell Biochem.* 98:770-788.

McNally, J.G., W.G. Müller, D. Walker, R. Wolford, and G.L. Hager. 2000. The glucocorticoid receptor: rapid exchange with regulatory sites in living cells. *Science.* 287:1262-1265.

Métivier, R., G. Reid, and F. Gannon. 2006. Transcription in four dimensions: nuclear receptor-directed initiation of gene expression. *EMBO Rep.* 7:161-167.

Michalides, R., A. Griekspoor, A. Balkenende, D. Verwoerd, L. Janssen, K. Jalink, A. Floore, A. Velds, L. van 't Veer, and J. Neefjes. 2004. Tamoxifen resistance by a conformational arrest of the estrogen receptor-α PKA activation in breast cancer. *Cancer Cell.* 5:597-605.

Rayasam, G.V., C. Elbi, D.A. Walker, R. Wolford, T.M. Fletcher, D.P. Edwards, and G.L. Hager. 2005. Ligand-specific dynamics of the progesterone receptor in living cells and during chromatin remodeling in vitro. *Mol Cell Biol.* 25:2406-2418.

Rosenfeld, M.G., V.V. Lunyak, and C.K. Glass. 2006. Sensors and signals: a coactivator/corepressor/epigenetic code for integrating signal-dependent programs of transcriptional response. *Genes Dev.* 20:1405-1428.

Schaaf, M.J., and J.A. Cidlowski. 2003. Molecular determinants of glucocorticoid receptor mobility in living cells: the importance of ligand affinity. *Mol Cell Biol.* 23:1922-1934.

Schaufele, F., X. Carbonell, M. Guerbadot, S. Borngraeber, M.S. Chapman, A.A.K. Ma, J.N. Miner, and M.I. Diamond. 2005. The structural basis of androgen receptor activation: Intramolecular and intermolecular amino-carboxy interactions. *Proc Natl Acad Sci U S A.* 102:9802-9807.

Stenoien, D.L., K. Patel, M.G. Mancini, M. Dutertre, C.L. Smith, B.W. O'Malley, and M.A. Mancini. 2001. FRAP reveals that mobility of oestrogen receptor-alpha is ligand- and proteasome-dependent. *Nat Cell Biol.* 3:15-23.

Sui, X., K.S. Bramlett, M.C. Jorge, D.A. Swanson, A.C. von Eschenbach, and G. Jenster. 1999. Specific androgen receptor activation by an artificial coactivator. *J Biol Chem.* 274:9449-9454.

Van de Wijngaart, D.J., M.E. van Royen, R. Hersmus, A.C.W. Pike, A.B. Houtsmuller, G. Jenster, J. Trapman, and H.J. Dubbink. 2006. Novel FXXFF and FXXMF Motifs in Androgen Receptor Cofactors Mediate High Affinity and Specific Interactions with the Ligand-binding Domain. *J Biol Chem.* 281:19407-19416.

Van Steensel, B., M. Brink, K. Van der Meulen, E. Van Binnendijk, D. Wansink, L. De Jong, E. De Kloet, and R. Van Driel. 1995. Localization of the glucocorticoid receptor in discrete clusters in the cell nucleus. *J Cell Sci.* 108:3003-3011.

Wansink, D., W. Schul, I. Van der Kraan, B. Van Steensel, R. Van Driel, and L. De Jong. 1993. Fluorescent labeling of nascent RNA reveals transcription by RNA polymerase II in domains scattered throughout the nucleus. *J Cell Biol.* 122:283-293.

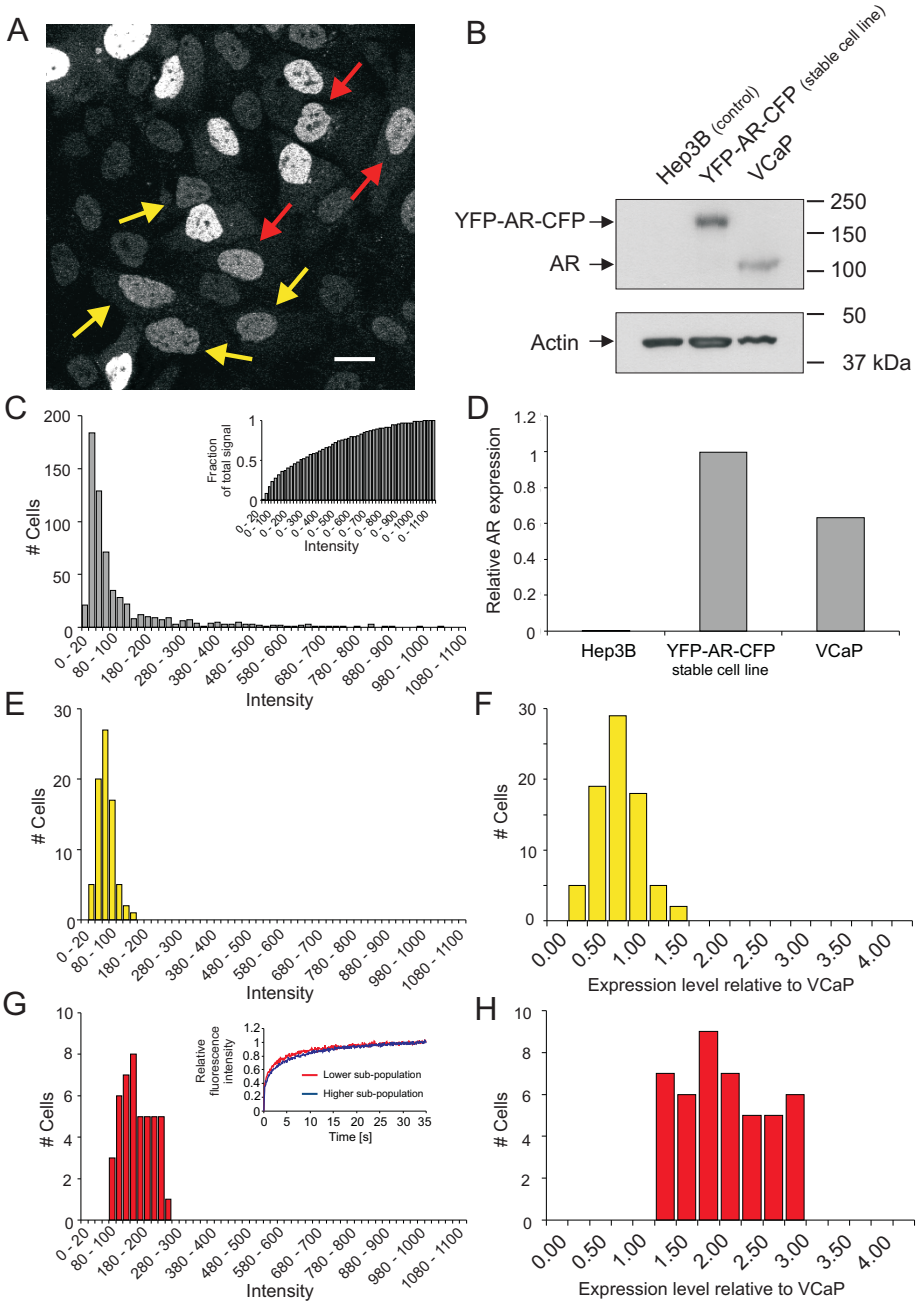
A
B
Hep3B (control)
YFP-AR-CFP (stable cell line)
VCaP
YFP-AR-CFP
AR
Actin
250
150
100
50
37 kDa
C
Cells
Intensity
Fraction of total signal
D
Relative AR expression
Hep3B
YFP-AR-CFP
VCaP
stable cell line
E
Cells
Intensity
F
Cells
Expression level relative to VCaP
G
Cells
Intensity
Relative fluorescence intensity
Lower sub-population
Higher sub-population
Time [s]
H
Cells
Expression level relative to VCaP

Figure S1 Expression levels of YFP-AR-CFP cells used for abFRET and simultaneous FRET and FRAP measurements. (A) Confocal image of Hep3B cells stably expressing YFP-AR-CFP. Arrows indicate cells within the intensity range that was used for abFRET (yellow) or simultaneous FRET and FRAP measurements (red). Scale bar represents 20 mm. (B) Western blot analysis of tagged (165 kDa) and untagged (110 kDa) AR in Hep3B cells stably expressing YFP-AR-CFP and a VCaP prostate cancer cell line endogenously expressing AR (Korenchuk et al., 2001). The Hep3B cells that stably express YFP-AR-CFP do not have endogenous AR expression. β-Actin was used as a loading control. (C) Intensity distribution of YFP emission in Hep3B cells stably expressing YFP-AR-CFP (inset shows the cumulative distribution of the same data multiplied by the intensity) ($n = 620$). (D) Quantification of AR expression in Hep3B cells stably expressing YFP-AR-CFP and the VCaP prostate cancer cell line. (E and G) Intensity distribution of YFP emission in Hep3B cells expressing YFP-AR-CFP used for abFRET (E) ($n = 77$) and simultaneous FRET and FRAP measurements (G) ($n = 45$). Due to the necessity of lower excitation power to avoid monitor bleaching we used cells with somewhat higher YFP-AR-CFP expression for simultaneous FRET and FRAP measurements. Because high expression levels tend to influence the AR mobility (Marcelli et al., 2006) we compared the AR FRAP curves in the higher and lower AR expressing subpopulation (50%) of cells (inset in G). The highest AR expressing 50% of the cells show a similar (transient) immobilization of the AR compared to the lowest expressing cells, thus the AR expression levels within the range of expressions chosen do not influence the AR mobility. (F and H) The intensity distribution and Western blot analysis of the Hep3B cell line stably expressing YFP-AR-CFP is used to calculate the expression level of the cells used in our abFRET experiments (F) and simultaneous FRET and FRAP measurements (H) relative to the AR expression in VCaP cells.

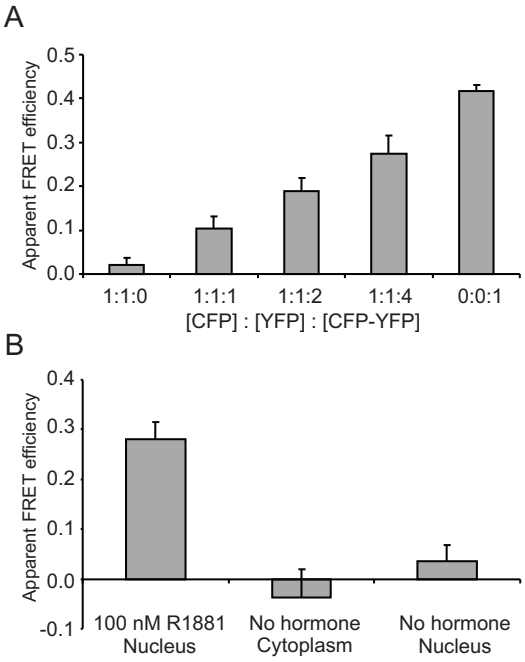

Figure S2 Validation of FRET measurement by acceptor photobleaching (abFRET). (A) abFRET on Hep3B cells co-transfected with plasmids containing CFP, YFP or CFP-YFP fusion constructs at different ratios as indicated, showing increasing abFRET with increasing relative concentration of CFP-YFP fusion constructs. (B) abFRET on double-tagged YFP-AR-CFP showed only FRET in the presence of hormone (100 nM R1881), when the AR is predominantly present in the nucleus (n = 30). No FRET was observed in the absence of hormone, neither in the cytoplasm nor in the smaller nuclear fraction (n = 30), indicating that the observed FRET is due to N/C interaction (see also Fig. 1E-G).

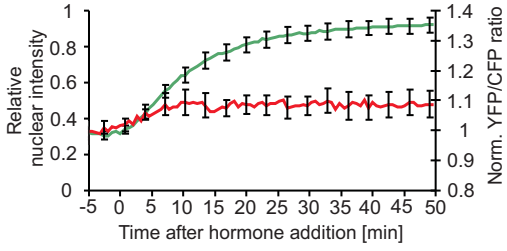

Figure S3 Simultaneous detection of YFP and CFP signals at 458 nm excitation on Hep3B cells expressing the double tagged N/C-interaction deficient mutant YFP-AR(F23,27A/L26A)-CFP showed an immediate but very small YFP/CFP ratio change after hormone addition (t = 0) (compare with Fig. 1E, G) (n = 8).

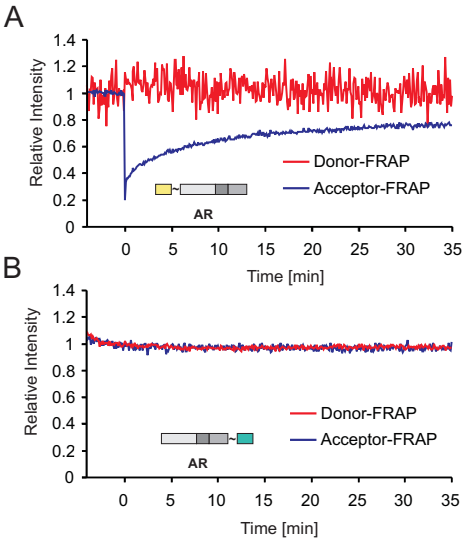

Figure S4 Control experiments for donor-FRAP and acceptor-FRAP analysis. (A) Simultaneous FRAP and FRET measurements in Hep3B cells expressing ARs tagged with YFP only. 458 nm excitation at low laser power for monitoring is sufficient to excite YFP and enables FRAP analysis of ARs tagged with YFP. In addition, after application of the 514 nm bleach pulse at high intensity the (low) signal in the CFP channel did not significantly change. These experiments show that neither monitoring at 458 nm nor applying the bleach pulse at 514 nm leads to detectable photo-conversion or other aberrant behavior of YFP (n = 10). (B) Simultaneous FRAP and FRET measurements in Hep3B cells expressing ARs tagged with CFP only. The high intensity bleach pulse at 514 nm does not bleach CFP (n = 10).

Chapter 6

A Two-step Model for Androgen Receptor Dimerization in Living Cells

Van Royen, M.E., A.B. Houtsmuller,
and J. Trapman.

Manuscript in preparation.

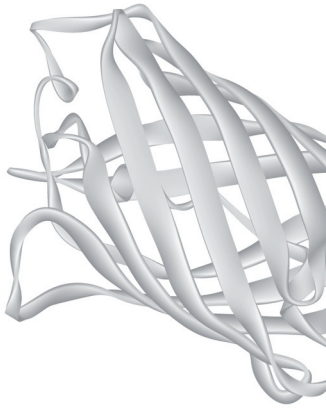

ABSTRACT

Transcription regulation by the androgen receptor (AR) is not only mediated by ligand-binding and DNA-binding, but also by protein-protein interactions. Protein-protein interactions include DBD-DBD interactions, mediated by the D-box, and N/C interactions, mediated by the FxxLF motif in the N-terminal domain of AR, and interactions of AR with cofactors. Here we studied the roles of DBD-DBD interaction and N/C interaction in AR dimerization using confocal microscopy and quantitative imaging techniques. We show that the rapidly initiated intramolecular AR N/C interaction after ligand-binding in the cytoplasm is followed by AR nuclear translocation and a D-box dimerization dependent transition to intermolecular N/C interaction. These subsequent domain interactions leading to AR dimerization are initiated before DNA-binding. Together, this study elucidates important steps in the spatio-temporal relationship of the consecutive AR intramolecular and intermolecular domain interactions in living cells.

INTRODUCTION

The androgen receptor (AR) is a ligand-activated transcription factor and a member of the steroid receptor (SR) subfamily of nuclear receptors (NRs). Like all SRs, the AR has a modular structure composed of an N-terminal domain (NTD), a conserved DNA-binding domain (DBD) and a C-terminal ligand-binding domain (LBD) (Brinkmann et al., 1989). Activated ARs regulate genes involved in the development and maintenance of the male phenotype. AR is also a key factor in prostate cancer. AR activity is not only regulated by ligand-binding and DNA-binding but also by intramolecular interactions between functional domains, by homodimerization and by interactions with cofactors. The best characterized interactions between AR functional domains are the intra- and intermolecular NTD-LBD interaction (N/C interaction), which is mediated by the FQNLF motif in the NTD and the coactivator groove in the LBD, and the intermolecular DBD-DBD interaction, mediated by the D-box (Centenera et al., 2008).

In recent years confocal microscopy and quantitative microscopic techniques such as fluorescence recovery after photobleaching (FRAP) revealed a dynamic behavior of factors involved in chromatin-associated processes. Using FRAP analysis based on computer modelling we and others have shown that binding of agonistic ligands lead in the nucleus to freely mobile SRs, which are only transiently immobilised (McNally et al., 2000; Stenoien et al., 2001; Farla et al., 2004; Farla et al., 2005; Houtsmuller, 2005; Rayasam et al., 2005; Marcelli et al., 2006; Van Royen et al., 2007; reviewed in Van Royen et al., 2009b). The transient immobilisation is most likely caused by DNA-binding, because specific DNA-binding deficient mutants did not contain a detectable immobile fraction (Farla et al., 2004; Farla et al., 2005).

Using fluorescence resonance energy transfer (FRET) and combined FRAP and FRET analysis, initial studies on the spatio-temporal organisation of AR protein-protein interactions were presented (Schaufele et al., 2005; Van Royen et al., 2007). FRET showed that in the cytoplasm the N/C interaction is in an intramolecular conformation that is initiated directly after ligand binding and prior to translocation to the nucleus (Schaufele et al., 2005; Van Royen et al., 2007). In the nucleus, the intramolecular N/C interaction is followed by an intermolecular N/C interaction (Schaufele et al., 2005). We showed that the N/C interaction preferentially occurs in the mobile AR and is lost when the AR is bound to DNA (Van Royen et al., 2007). These observations indicate that the AR itself regulates the time and place of interactions with coregulators by preventing untimely protein interactions when the AR is mobile and allowing coregulator binding when the AR is bound to DNA (He et al., 2001; Dubbink et al., 2004; Van Royen et al., 2007).

The intra- and intermolecular N/C interaction is mediated by binding of the FxxLF peptide motif (FQNLF) in the AR NTD to the ligand-induced cofactor binding groove in AR LBD. The phenylalanine residues bind deep into the coactivator groove with van der Waals interactions, the leucine residue in the peptide motif lies in a shallow ridge on the surface of the LBD,

the other two amino acid residues are solvent exposed (Hur et al., 2004). In a homodimer, ARs also interact via their dimerization boxes (D-boxes) in the second zinc-finger of the DBD. SR D-box interactions consist of a network of hydrogen bonds between D-box amino acid residues and by an extensive complementary surface. In the AR DBD, a serine residue at position 597 (S597), which is not present in the D-boxes of other SRs, forms an extra hydrogen bond and makes extra Van der Waals contacts with its counterpart in the opposing D-box in an AR homodimer. An additional pair of symmetrical hydrogen bonds is formed between an alanine at position 596 (A596) and a threonine at position 602 (T602) in the opposing AR DBD and vice versa, resulting in the relative strong AR dimerization interface compared to other SRs (Shaffer et al., 2004). The importance of the D-box in AR function is highlighted by the relative large number of mutations in this domain found in partial androgen insensitivity syndrome (PAIS) patients (Centenera et al., 2008: http://androgendb.mcgill.ca/).

To study the relevance of D-box interactions and N/C interactions in AR dimerization and to investigate when these interaction take place, we applied confocal microscopy and quantitative microscopic techniques on Hep3B cells expressing functional, single and double YFP- and CFP-tagged wild type ARs and appropriate AR mutants.

RESULTS

Interactions of functional domains of single- and double YFP, CFP tagged ARs

We tagged the fluorescent proteins YFP and CFP to the N- and C- terminus of a single AR (YFP-AR-CFP) or separate ARs (YFP-AR and AR-CFP) (Fig. 1 A) to study by FRET and FRAP AR domain interactions and mobility in living Hep3B cells. Western blot analysis showed that all tagged ARs were of the expected size (Fig. 1 B). All tagged ARs were able to induce transcription of a luciferase reporter gene driven by an androgen-regulated promoter ((ARE)2-TATA Luc). The different N- and, or C-terminal tags reduced the transcriptional activity of the wild type AR (50 - 70% reduction) (Fig. S1), but mutations in tagged ARs influence the transcriptional activity similarly to untagged ARs (Van Royen et al., 2007). In the absence of hormone, double-tagged YFP-AR-CFP and single-tagged YFP-AR and AR-CFP were mainly located in the cytoplasm (Fig. 1 C, D and E respectively, left panels). Upon hormone addition single- and double-tagged ARs rapidly translocated to the nucleus (Fig S2). In the nucleus the ARs were distributed in a typical punctate distribution pattern (Fig. 1 C, D and E respectively, right panels). This punctate distribution pattern correlates with a transient immobilisation of the AR and partially overlaps with sites of active transcription (Farla et al., 2005; Van Royen et al., 2007).

We then applied acceptor bleaching FRET (abFRET) analysis on cells expressing either double-tagged or single-tagged ARs (Fig. 1 F). In abFRET, the relative increase of the donor emission after photobleaching the acceptor is a measure for the interaction between tagged

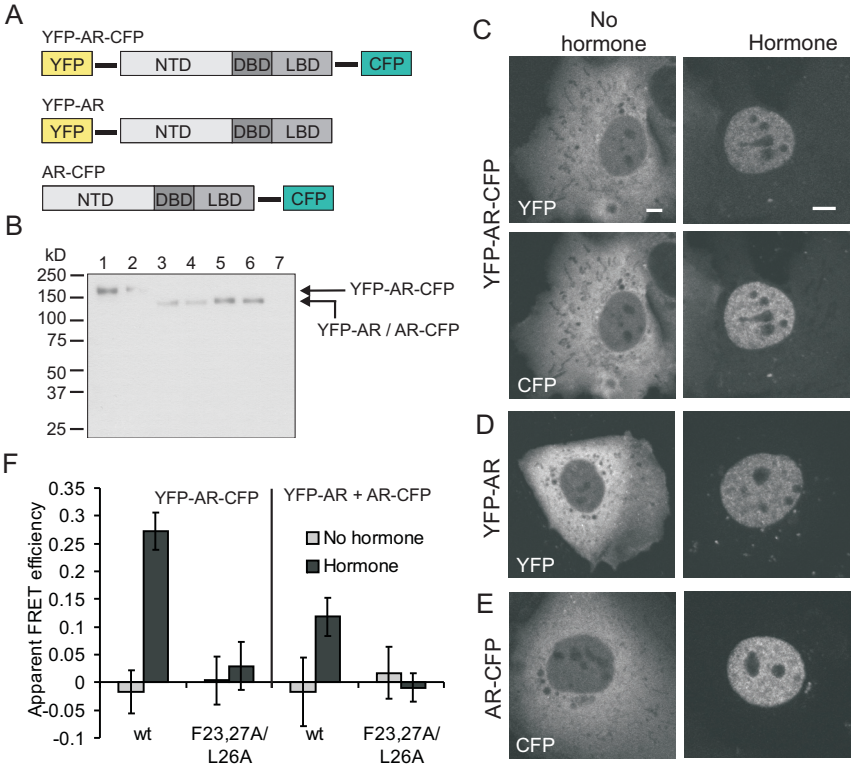

Figure 1. Properties of double- and single-tagged ARs. (A) Schematic representation of YFP-AR-CFP, YFP-AR and AR-CFP (horizontal bars represent a [Gly-Ala]6 spacer). (B) Western blot of the fusion proteins expressed in Hep3B cells. Lane 1: YFP-AR-CFP; lane 2: YFP-AR (F23,27A/L26A)-CFP: lane 3: YFP-AR; lane 4: YFP-AR (F23,27A/L26A), lane 5: AR-CFP; lane 6: AR (F23,27A/L26A)-CFP; lane 7: non-transfected cells. AR was detected using a mouse AR monoclonal antibody (F39.4.1). (C - E) Confocal images of Hep3B cells expressing double- and single-tagged AR (YFP-AR-CFP, YFP-AR and AR-CFP) in the absence (left panels) and presence (right panels) of 100 nM R1881. Bars represent 5 mm. (F) Acceptor photobleaching FRET (abFRET) shows an interaction between the N-terminal FQNLF motif and the AR-LBD (N/C interaction) in YFP-AR-CFP and between YFP-AR and AR-CFP. The N/C interaction is hormone (100 nM R1881) induced and dependent on the N-terminal FQNLF-motif. Data shown are mean +/- 2*SEM of at least 25 cells measured in two independent experiments.

molecules under surveillance (Bastiaens and Jovin, 1996; Bastiaens et al., 1996; Kenworthy, 2001; Karpova et al., 2003; Van Royen et al., 2009a). In the presence of hormone, both cells expressing double-tagged AR and cells expressing a combination of single-tagged YFP-AR and AR-CFP showed abFRET. AbFRET was strongly reduced in double-tagged N/C interaction deficient mutant ARs, in which the N-terminal FQNLF motif was mutated to AQNAA (AR F23,27A/L26A), and completely lost in single-tagged N/C interaction deficient AR mutants (Fig. 1 F). These results indicate that abFRET allows to quantitatively studying inter- or intramolecular N/C interaction in double-tagged ARs and intermolecular N/C interaction in single-tagged ARs.

The AR N/C interaction is predominantly intermolecular

Previously, confocal time-lapse microscopy has shown that the YFP/CFP ratio in YFP-AR-CFP expressing cells increased rapidly after hormone addition, prior to translocation to the nucleus (Fig. S2 A). In contrast, in cells expressing YFP-AR and AR-CFP the YFP/CFP ratio only occurred after translocation to the nucleus (Fig. S2 B), indicating that the intramolecular N/C interactions were initiated rapidly after hormone binding, followed by nuclear translocation and initiation of intermolecular N/C interactions (see also Schaufele et al., 2005). Coexpressed single-tagged YFP-AR and AR-CFP showed FRET only in the case of an intermolecular N/C interaction, whereas FRET in YFP-AR-CFP did not distinguish between inter- and intramolecular N/C interactions.

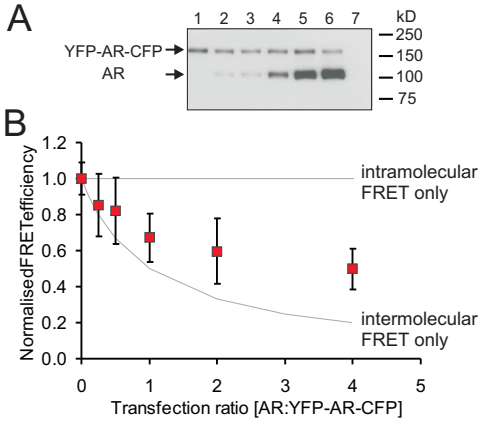

Figure 2. AR N/C interaction in the nucleus is mainly intermolecular. (A) Western blot analysis of lysates of Hep3B cells cotransfected with a construct expressing YFP-AR-CFP and increasing amounts of constructs coding for untagged AR in the transfection ratios 1:0, 4:1, 2:1, 1:1, 1:2 and 1:4 (YFP-AR-CFP : AR) lane 1-6 respectively. Lane 7 contains a lysate of control cells not expressing ARs. Plasmid samples were corrected for the total DNA content and total CMV-promoter content. AR was detected using a mouse AR monoclonal antibody (F39.4.1). (B) Acceptor bleaching FRET analysis on Hep3B cells coexpressing YFP-AR-CFP and increasing amounts of untagged AR (see A). Increasing quantities of untagged AR results in a lower FRET efficiency in cells expressing YFP-AR-CFP. Grey lines indicate the stochastic FRET efficiencies if only intermolecular N/C interaction (100% intermolecular N/C interaction, lower line) up to 100% intramolecular N/C interaction (0% intermolecular N/C interaction, top line) would occur in YFP-AR-CFP. Data shown are mean +/- 2*SEM of at least 60 cells measured in four independent experiments.

To determine the relative contribution of intermolecular versus intramolecular interactions in nuclear ARs we cotransfected an YFP-AR-CFP expression vector with increasing amounts of a vector expressing untagged AR (Fig. 2 A). In this setting, untagged AR competes with YFP-AR-CFP for intermolecular, and not intramolecular, N/C interaction with a double-tagged AR, but will not contribute to FRET. Indeed, with an increased expression of untagged ARs the abFRET of YFP-AR-CFP decreased proportionally (red squares in Fig. 2 B). Comparing the decrease of the experimental FRET data with theoretical FRET efficiencies based on intramolecular or intermolecular N/C interaction only (grey curves in Fig. 2 B), indicated that in steady state AR N/C interactions were mostly intermolecular, although a clearly measurable AR fraction showed intramolecular N/C interaction.

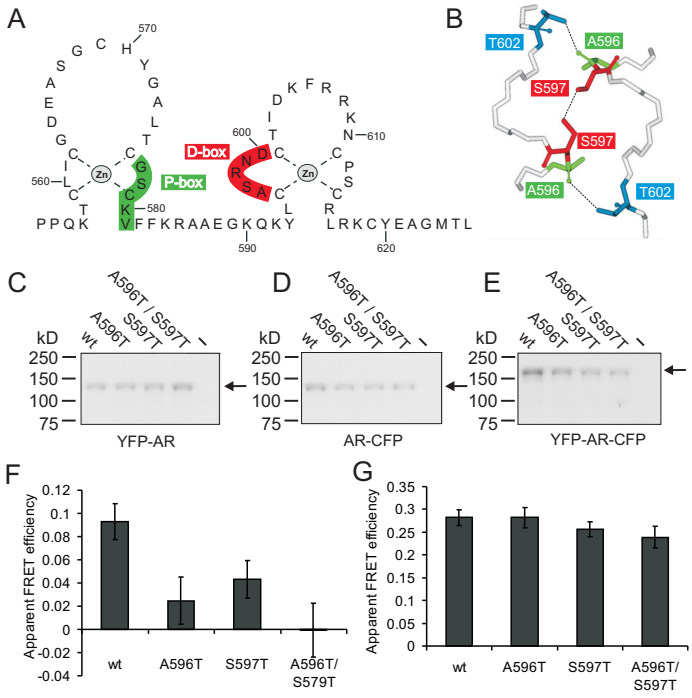

Figure 3. Mutations in the AR D-box inhibit the intermolecular but not the intramolecular N/C interaction. (A) Schematic representation of the AR DBD. The DBD consists of two zinc-fingers. The amino acid residues in the D-box (red) and the residues in the P-box (green), responsible for the interaction with DNA, are indicated. (B) Structure of the dimer-interface (D-box) in a fragment of the second zinc-finger of the DBD. Major interactions between the two AR D-boxes are indicated (A596 – T602, S597 – S597 and T602 – A596). The structure was modified from PBD-file 1R4I (www.pdb.org) (Shaffer et al., 2004). (C – E) Western blot analysis of YFP / CFP single- and double-tagged wild type AR and D-box mutants. AR was detected using a mouse AR monoclonal antibody (F39.4.1). Single- and double-tagged wild type ARs and D-box mutants were expressed in Hep3B cells. All fusion proteins had the expected size. (F) Acceptor bleaching FRET analysis on Hep3B cells coexpressing single-tagged wild type YFP-AR and AR-CFP and the D-box mutants. AR D-box mutants (A596T), (S597T) and (A596T S597T) show a lower or complete lack of FRET efficiency in the presence of 100 nM R1881, indicating partial and complete loss of the intermolecular N/C interaction, respectively. Data shown are mean +/- 2*SEM of at least 40 cells measured in minimally 3 independent experiments. (G) Acceptor bleaching FRET on Hep3B cells expressing YFP and CFP double-tagged wild type AR and AR D-box mutants in the presence of 100 nM R1881. None of the D-box mutations result in a lower FRET efficiency in the double-tagged ARs, indicating that lower intermolecular N/C interaction is compensated by higher intramolecular N/C interaction. Data shown are mean +/- 2*SEM of at least 30 cells measured in at least 2 independent experiments.

The intermolecular N/C interaction is driven by the AR D-box interaction

A second domain enabling an intermolecular interaction between two ARs is the dimerization box (D-box) in the second zinc-finger of the AR DBD (Fig. 3 A). Three residues in the D-box interact with their counterpart in the corresponding AR DBD in an AR dimer (A596-T602, S597-S597 and T602-A596) (Fig. 3 B). We introduced two functional mutations, found in PAIS, A596T and S597T, and a combination of the two, in single- and double-tagged ARs to study the role of the D-box in AR dimerization in living cells and in N/C interaction. Western blot analysis showed that the expressed fusion proteins were all of the expected sizes (Fig. 3 C - E).

Mutating either one (S597T or A596T) of these amino acid residues abolished one (in S597T) or two (in A596T) hydrogen bonds between the D-boxes. Mutating either one of these residues in YFP- and CFP- single-tagged ARs resulted in a partial loss of intermolecular N/C interaction. Importantly, mutating both residues, thereby abolishing all three hydrogen bonds resulted in a complete loss of FRET efficiency, indicating absence of N/C interaction (Fig. 3 F). The absence of N/C interaction in this complete D-box mutant strongly suggests that the AR DBD-DBD interaction drives the N/C interaction, or in other words: although the N/C interaction needs binding of the FQNLF motif in the AR NTD to the coactivator groove in the LBD, the D-box interaction is essential for intermolecular N/C interaction.

Substitution of the same D-box amino acid residues in YFP-AR-CFP hardly affected the FRET efficiency (Fig. 3 G). As shown above, in wild type YFP-AR-CFP most N/C interactions in steady state are intermolecular (Fig. 2). So, our observation indicates that an expected drop in FRET in double-tagged D-box mutants, because of the loss of intermolecular N/C interaction, was compensated by intramolecular N/C interaction. In conclusion, the intramolecular N/C interaction is independent on D-box dimerization, and more importantly, D-box dimerization is an essential step in intermolecular N/C interaction, possibly because of a conformational change in the AR induced by DBD-DBD interaction.

Stable DNA binding is not essential for AR dimerization

To study the role of DNA binding in AR dimerization we introduced a mutation in the α-helix in the first zinc-finger that binds in the major groove of ARE half-sites. The arginine residue at position 585 (R585) within this helix and directly flanking the defined P-box makes additional base-specific Van der Waals contacts with the thymine residue in the consensus ARE (Shaffer et al., 2004). Western blot analysis of double- and single-tagged ARs in which the arginine is mutated to either a lysine (R585K) as is found in CAIS (Sultan et al., 1993) or more subtle to alanine (R585A) that probably retains the tertiary structure of the DBD, showed that the expressed YFP-AR-CFP, YFP-AR and AR-CFP mutants were all of the expected size (Fig. 4 A – C, respectively). High resolution imaging of Hep3B cells expressing the AR mutants showed a homogeneous nuclear distribution unlike the speckled pattern found for wild type AR (Fig. 4 D) and very similar to a previously published AR mutant known to be DNA-binding deficient (A573D) (Farla et al., 2004). Moreover, FRAP analysis of both AR mutants (R585K and R585A) showed a mobility very similar to AR (A573D), lacking the transient immobilisation of wild type AR (Fig. 4 E and F). As expected of DNA binding deficient AR mutants, the AR mutants (R585K and R585A) were unable to induce transcription on a transiently transfected reporter gene driven by a minimal promoter containing two consensus AREs ((ARE)2TATA-Luc) (Fig. S3) (Sultan et al., 1993).

Next, the AR R585K and R585A mutants were used to study the effect of absence of DNA binding on AR dimerization. AbFRET analysis of single YFP- and CFP-tagged DNA binding deficient AR mutants showed that loss of DNA binding did not abolish the intermolecular N/C

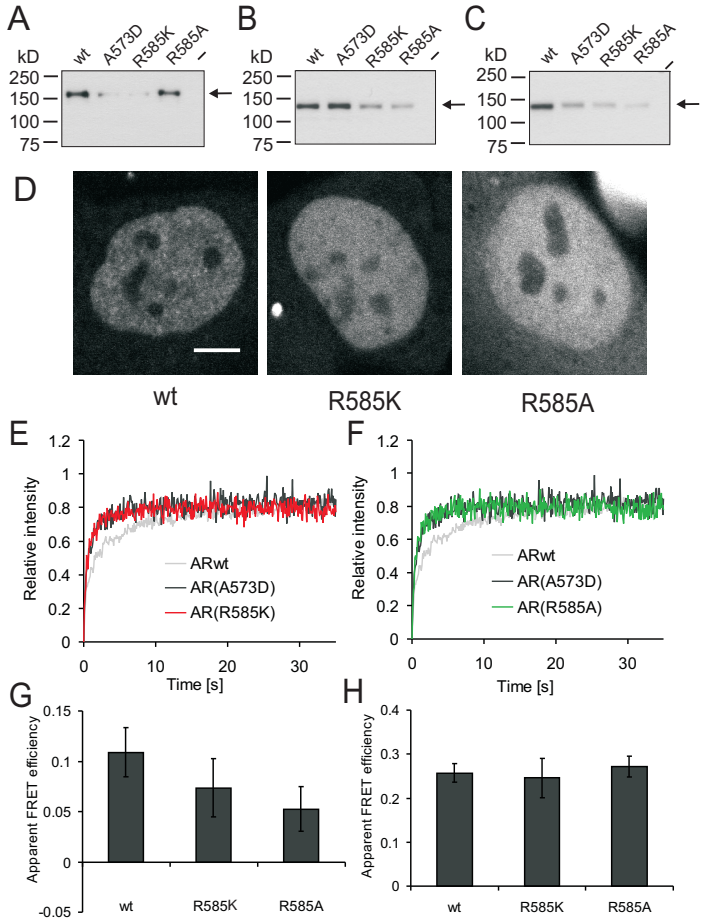

Figure 4. DNA-binding deficient AR mutants show inter- and intramolecular N/C interaction (A - C) Western blot analysis of YFP / CFP single- and double-tagged wild type AR and DNA binding deficient mutants. AR was detected with antibody F39.4.1. Single- and double-tagged wild type and DNA binding mutant ARs were expressed in Hep3B cells. All fusion proteins had the expected size. (D) High resolution confocal images of Hep3B cells expressing YFP/CFP double-tagged wild type AR and DNA-binding deficient mutants. The AR mutants (R585K) and (R585A) show a homogeneous distribution. Bars represent 5 mm. (E and F) Strip-FRAP analysis on YFP emission of YFP/CFP double-tagged AR DNA binding mutants in the presence of 100 nM R1881. The AR mutants (R585K) and (R585A) showed a rapid recovery similar to the DNA-binding deficient mutant AR (A573D). Curves shown are mean +/- 2*SEM of at least 25 cells. (G) Acceptor bleaching FRET analysis on cotransfected wild type YFP-AR and AR-CFP and DNA-binding deficient mutants. AR (R585K) and (R585A) retain most of the intermolecular N/C interaction. Data shown are mean +/- 2*SEM of at least 30 cells measured in minimally 2 independent experiments. (H) Acceptor bleaching FRET analysis on Hep3B cells expressing wild type YFP-AR-CFP and the DNA-binding deficient mutants in the presence of 100 nM R1881. None of the DNA-binding deficient mutants is disabled in N/C interaction. Data shown are mean +/- 2*SEM of at least 30 cells measured in minimally 2 independent experiments.

interaction although the FRET value for the mutants was somewhat lower than that of wild type AR (Fig. 4 G). This observation supports our previous findings shown in Fig. 3 and described above that D-box interactions occur prior to DNA binding of AR homodimers. AbFRET analysis of double-tagged ARs showed that the DNA binding deficient AR mutants were not

diminished in their total intra- and intermolecular N/C interactions (Fig. 4 H). Summarising, transcriptionally inactive, DNA binding deficient AR mutants, mutated in an amino acid residue directly involved in AR-DNA contact, are able to show both intra- and more importantly intermolecular N/C interaction, the latter involves also the D-box interaction.

Transactivation capacity of AR dimerization mutants is promoter dependent

High-resolution confocal images of Hep3B cells expressing wild type and mutant ARs showed a typical speckled pattern for the wild type AR whereas a more homogeneous pattern is found in AR D-box mutants (Fig. 5 A). As we previously showed using FRAP, this speckled pattern always is accompanied by a reduced mobility of the AR due to transient immobilisation (Farla et al., 2005). Here we applied the strip FRAP procedure to study the mobility of the D-box mutants (Houtsmuller, 2005; Van Royen et al., 2009b). All three D-box mutants (A596T; red curve in Fig. 5 B, S597T; green curve in Fig. 5 C and A596T/S597T; blue curve in Fig. 5 D) showed a rapid redistribution, similar to the DNA binding deficient mutant AR A573D (black curve in Fig 5 B, C and D), indicating that these AR D-box mutants are much more mobile than wild type AR and lack the relatively long transient immobilisation of wild type AR (grey curve in Fig 5 B, C and D).

To explore the role of the D-box dimerization in AR regulated transcription, we studied first the activity of the double-tagged AR mutants on two transiently transfected luciferase reporter genes driven by minimal promoters containing different types of AREs. Mutating the D-box amino acid residues differentially affected AR transactivation capacity on the different promoters in overexpression systems (Fig. 5 E, F). Where the double mutant AR (A596T/S597T) showed no change in transcriptional activity on a minimal promoter composed of two consensus AREs ((ARE)2TATA-luciferase; ARE sequence: 5'-TGTACAnnnTGTTCT-3') (Fig. 5E), it almost completely abolished the activity on a minimal promoter driven by two probasin AREIIs (sequence: 5'-AGTACTnnnAGAACC-3') (Fig. 5F). AR mutated in either one of the two residues (A596T or S597T) surprisingly showed an increased hormone dependent transcription activity on the first promoter, whereas there was a slightly lower activity on the latter (Fig. 5 E and F). Again different effects were found on a transiently transfected reporter driven by a natural promoter, the mouse mammary tumour virus LTR (MMTV-LTR). Complete lack of D-box interaction did not substantially affect AR activity on the MMTV LTR promoter. AR S597T, but not AR A596T showed a strongly increased ligand dependent transcription activity on this promoter (Fig. 5 G). To study the transcriptional activity of the AR mutants on a chromatin based reporter, we also tested the AR mutants on an stably integrated (ARE)2TATA-luc reporter. Results were essentially identical to those of the same reporter if transiently transfected (compare Fig. 5H and E). In summary, complete loss of D-box interactions leads to lower AR activity or has no effect on activity. Diminished D-box interactions lead to increased or slightly decreased AR activity. The differential effects are ARE dependent.

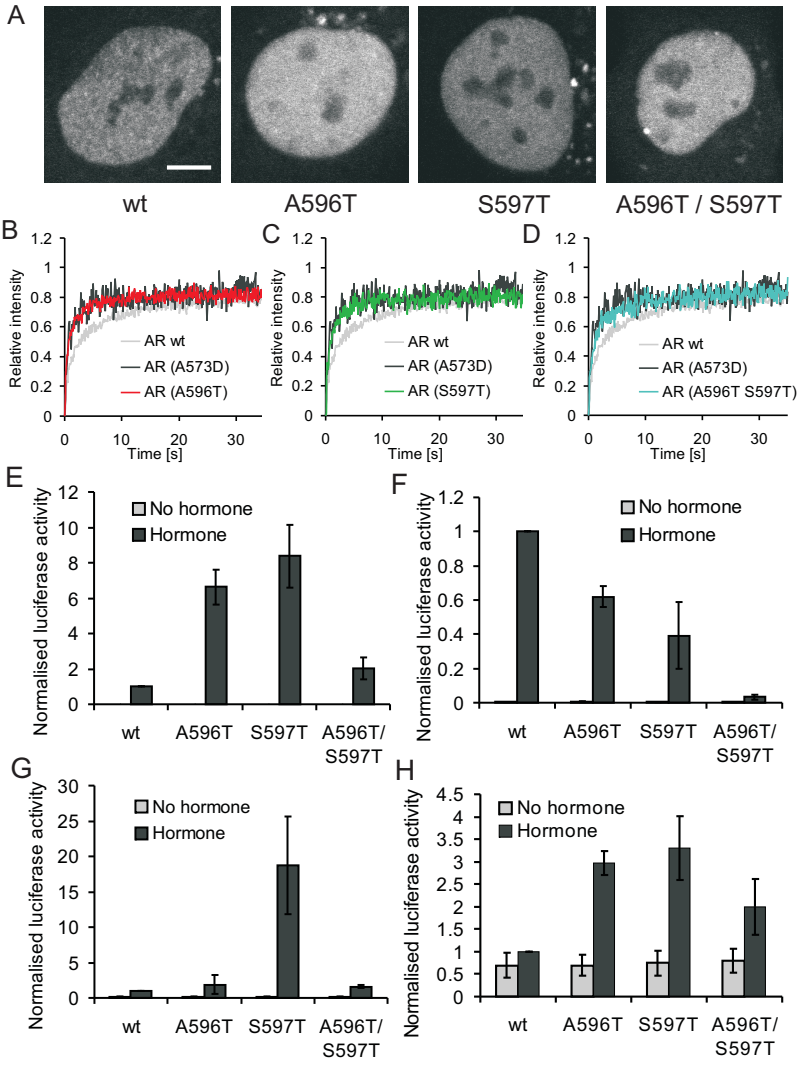

Figure 5. Loss of stable DNA binding of AR D-box mutants and differential effects on different types of AR regulated reporter genes. (A) High resolution confocal images of Hep3B cells expressing YFP and CFP double-tagged wild type and mutant ARs. All AR D-box mutants showed a more homogeneous fluorescence. Bars represent 5 mm. (B - D) Strip-FRAP analysis on YFP emission of YFP/CFP double-tagged AR D-box mutants in the presence of 100 nM R1881. Loss of the ability to dimerize results in a rapid recovery of fluorescence similar to the DNA-binding deficient mutant (AR (A573D)) indicating the loss of stable DNA binding of the AR (A596T), AR (S597T) and AR (A596T / S597T) mutants. Curves shown are mean +/- 2*SEM of at least 25 cells. (E - H) Normalized transcription activity of wild type AR and D-box AR mutants in the presence of 100 nM R1881 measured on different luciferase reporters driven by; a transiently transfected minimal promoter containing two high-affinity AREs ((ARE)2-TATA Luc) (E), two probasin AREIIs ((PB-AREII)2-TATA Luc) (F), the complex MMTV promoter (MMTV Luc) (G) or the ((ARE)2-TATA-luciferase) reporter stably integrated in genomic DNA (H). Means +/- 2*SEM of at least 3 independent experiments are shown.

DISCUSSION

Transcription activity of SRs is not only regulated by ligand-binding and DNA-binding but also by multiple protein-protein interactions including homodimerization and interactions with transcriptional coregulators (reviewed in Rosenfeld et al., 2006). A subgroup of SR coregulators interacts with a hydrophobic cleft in the LBD via LxxLL-like motifs (Dubbink et al., 2004; Hur et al., 2004). Unlike other SRs, the deep cofactor groove of AR preferentially binds bulky FxxLF motifs, enabling interactions with cofactors containing FxxLF-like motifs. The D-box in the second zinc-finger of the DBD is a well-characterized dimerization interface of all SRs bound to DNA (Dahlman-Wright et al., 1991). The AR contains as a second homodimerization motif the unique FQNLF-sequence in the NTD that can bind to the coactivator groove. However, AR N/C interaction not only occurs intermolecular, but also intramolecular so either between an FQNLF motif and a cofactor groove in the same AR molecule or between two ARs (Schaufele et al., 2005). In the present study we investigated the spatio-temporal relation between the D-box interaction and the N/C interaction in AR dimerization, by applying confocal microscopy and quantitative microscopic techniques on Hep3B cells expressing YFP- and CFP- single- and double-tagged wild type and mutant ARs (Fig. 1 A). Moreover, we investigated the role of dimerization in DNA binding. Based on our findings we propose a novel model of dynamics of AR protein-protein interactions (Fig. 6). In the model, AR D-box interaction is positioned as an essential step between intra- and intermolecular AR N/C interaction.

Previously, we and others found that the intramolecular N/C interaction, but not the intermolecular N/C interaction is initiated rapidly after hormone binding before the AR translocates to the nucleus (Schaufele et al., 2005; Van Royen et al., 2007). Only after nuclear translocation the intramolecular N/C interaction is followed by an intermolecular N/C interaction (Fig. S2) (Schaufele et al., 2005). In the *in vivo* abFRET based competition assay where we added increasing amounts of untagged AR to YFP-AR-CFP, we showed here that in steady state the majority of FRET in YFP-AR-CFP is by this intermolecular N/C interaction (Fig. 2). This finding implicates that AR homodimers are the preferred conformation of AR in the nucleus.

Based on crystal structures of DBDs complexed with DNA, DBD-DBD dimerization via the D-box has been established as an important protein-protein interaction interface of SRs (Luisi et al., 1991; Schwabe et al., 1993a; Shaffer et al., 2004; Roemer et al., 2006). The most prominent amino acid residues involved in the AR dimerization in this complex are A596, S597 and T602 (Fig. 3 B) (Shaffer et al., 2004). We showed here that mutation of these three amino acid residues completely abolished intermolecular N/C interaction, most likely due to complete absence of the D-box interaction. The mutations had no effect on intramolecular N/C interaction. In fact, in the absence of intermolecular N/C interaction more intramolecular N/C interaction was observed. These findings strongly suggest that the D-box drives the

transition from intramolecular AR N/C interaction to intermolecular N/C interaction following translocation of AR to the nucleus upon ligand binding.

It has long been a matter of dispute whether AR dimerization occurs prior to or following DNA binding (Centenera et al., 2008). We showed that the N/C interaction occurs predominantly when the ARs are mobile and is lost when the ARs are bound to chromatin (Van Royen et al., 2007). Combined with the observation that D-box interaction drives N/C interaction this implicates that D-box interaction must occur in full length AR prior to DNA-binding. This was confirmed by experiments carried out with the DNA-binding deficient mutants (Fig. 4). These findings contrast ideas based on crystallographic studies that the DBDs of SRs are monomeric in solution, as was suggested for ER, GR and AR, and show only cooperative dimerization when bound to DNA (Freedman et al., 1988; Härd et al., 1990a; Härd et al., 1990b; Luisi et al., 1991; Schwabe et al., 1993a; Schwabe et al., 1993b; Shaffer et al., 2004).

It is at present unknown whether domain-interactions other than D-box interaction and N/C interaction can play a prominent role in AR dimerization. For AR the evidence for LBD-LBD interaction, as documented for other SRs, is limited. In LBD crystals, the AR is present as a monomer, in contrast to GR, PR and ER LBD crystals (Tanenbaum et al., 1998; Williams and Sigler, 1998; Matias et al., 2000; Sack et al., 2001; Bledsoe et al., 2002). However, amino acid residues involved in GR LBD-LBD dimerization are conserved in AR (Centenera et al., 2008). A dimerization function might also be present in the hinge region as suggested for GR, or in the C-terminal extension (CTE) of the AR DBD (Savory et al., 2001; Haelens et al., 2003; Centenera et al., 2008).

Although most ARs in the nucleus are present as homodimers with intermolecular N/C interaction, the fraction of ARs with intramolecular N/C interaction is still estimated as 30-40% of the total nuclear AR. This can hardly be explained as a transient intermediate population prior to AR intermolecular N/C interaction. Our AR N/C and D-box mutant analyses suggest a dynamic equilibrium in mobile AR between intra- and intermolecular N/C interaction. This raises the question whether ARs with intramolecular N/C interaction are homodimers that are hold together by D-box interaction or other less well-defined homodimerization functions, or, alternatively that intramolecular N/C interaction represents AR monomers. Because stable AR D-box interaction has never been observed in AR DBDs in solution (see above) we favor the explanation that the intramolecular N/C interaction in nuclear ARs represents a stable monomer population.

Unlike wild type AR, ARs with D box mutations do not stably bind to DNA (Fig. 5 B). Interestingly, the loss of stable DNA binding of these AR mutants cannot be extrapolated to transcriptionally inactive ARs (Fig. 5). A similar observation has been found in other AR mutants, including a constitutively active AR lacking the LBD (Farla et al., 2004 and data not shown).

In luciferase reporter gene assays, the relative strong dimerization of the AR enables activation of promoters containing different types of AREs, including those consisting of one

high affinity and one low affinity ARE half-site as present in probasin AREII (Fig. 5 F) (Shaffer et al., 2004; and reviewed in Centenera et al., 2008; Claessens et al., 2008). ARs without appropriate D-box interaction cannot activate a promoter driven by probasin AREII, although a promoter with high affinity AREs can be stimulated (Fig. 5). Based on our findings it is tempting to speculate that promoters with high affinity AREs can be activated both by ARs binding in a dimer configuration and by consecutive binding of AR monomers, which subsequently dimerize on the DNA. Promoters with weaker AREs are preferentially activated by binding of AR dimers. This would indicate that AR monomers in the nucleus are of functional importance. If ARs with different configurations and different ARE affinity indeed occur in the nuclei of target cells, the monomer to dimer ratio is a novel mechanism of regulation of gene expression. Obviously, such a hypothesis could be extended with cofactors that differentially interact with monomers and dimers. Recently, evidence has been provided that the genome contains in promoters and enhancers many functional AR binding sites that are composed of ARE half sites or ARE half sites with suboptimal spacing (Bolton et al., 2007; Massie et al., 2007; So et al., 2007; Wang et al., 2007). No doubt AR complexes with different binding affinities will also differentially affect expression of these target genes. Our finding that AR mutants with weakened D-box interaction are more active on some promoters than wild type AR confirms and extends a previous study (Geserick et al., 2003). Possibly, this observation might be explained by a more flexible AR dimer configuration, allowing improved interaction with the particular ARE.

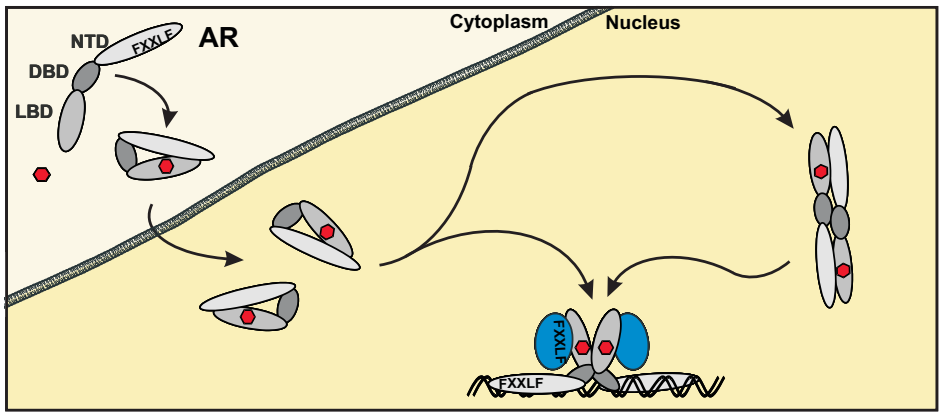

Figure 6. Model of spatio-temporal organization of consecutive AR domain interactions. Rapidly after ligand binding the intramolecular N/C interaction is initiated. Nuclear translocation is accompanied with a D-box interaction. The D-box interaction drives the transition to intermolecular N/C interaction. Next, the AR homodimer binds an ARE, looses its N/C interaction and allows cofactor binding.

In summary, previous data on the AR intra and intermolecular N/C interaction lead to a model in which the intramolecular N/C interaction is initiated in the cytoplasm directly after hormone binding followed by intermolecular N/C interaction in the nucleus (Schaufele et al.,

2005). Using quantitative imaging techniques, we elucidated the essential role of the D-box dimerization in the transition from intramolecular to intermolecular N/C interaction (Fig. 6). The D-box dimerization and the shift from intramolecular to intermolecular N/C interaction might occur as one event, but are both independent of DNA binding. Together with our recent study showing that the AR N/C interaction is lost in DNA bound AR enabling cofactor interactions (Van Royen et al., 2007) data in the present study elucidated the spatio-temporal relationship of the consecutive AR intra- and intermolecular domain interactions in living cells (Fig. 6). Moreover, we propose in the nucleus a dynamic equilibrium of AR homodimers and monomers, which can be an important mechanism of AR regulated gene expression.

MATERIALS AND METHODS

Constructs

In all constructs expressing AR fusion proteins the AR was separated from the fluorescent tag by a flexible $(GlyAla)_6$ spacer (Farla et al., 2004). The $(GlyAla)_6$ spacer will be referred to as a single dash. Constructs coding for wild type and (A573D) variants of YFP-AR-CFP and AR-CFP were generated as previously described (Van Royen et al., 2007). The construct expressing N-terminally YFP-tagged AR was generated by replacing EGFP in pGFP-AR (Farla et al., 2004) by EYFP-C1 (CLONTECH Laboratories, Inc.). The construct expressing untagged AR was obtained by inserting the AR cDNA from pAR0 (Brinkmann et al., 1989) into pEGFP-C1 from which EGFP was deleted. The F23,27A/L26A mutation was introduced by Quik Change mutagenesis (Stratagene) of YFP-AR-CFP, AR-CFP and untagged AR. In YFP-AR-CFP an LBD-CFP fragment was replaced by an AR LBD fragment from YFP-AR to obtain YFP-AR (F23,27A/L26A). The DBD mutations R585K, R585A, A596T, S597T and A596T/S597T were introduced by QuikChange mutagenesis in pYFP-AR-CFP. The LBD mutation E897A in untagged AR was also generated with QuikChange mutagenesis. For mutagenesis primers see Table S1. To generate the single-tagged DBD mutant ARs, the AR DBDs of pYFP-AR and pAR-CFP were replaced by a pYFP-AR-CFP fragment containing the mutant DBD.

The (ARE)2-TATA Luc reporter, containing two high-affinity AREs (CCGGGAGCTTGTACAGGATGTTCTGCATGCTCTAGATGTACAGGATGTTCTGGTA) was a gift from G. Jenster (Rotterdam, Netherlands). The probasin AREII driven Luc reporter ((PB-AREII)2-TATA Luc) was generated by swapping the ARE fragment in (ARE)2-TATA Luc by fragment containing two probasin AREIIs (5'-CCGGGAGCTAGTACTGGAAGAACCGCATGCTCTAGAAGTACTGGAAGAACCGGTA-3') after inserting suitable restriction sites flanking the AREs. The MMTV-Luciferase reporter construct was described previously (De Ruiter et al., 1995). All new constructs were verified by sequencing. Sizes of expressed ARs were verified by Western blotting.

Cell culture, transfection, and luciferase assay

Two days before microscopic analyses, Hep3B cells, lacking endogenous AR expression, were grown on glass coverslips in 6-well plates in α-MEM (Cambrex) supplemented with 5% FBS (HyClone), 2 mM L-glutamine, 100 U/mL penicillin, and 100 μg/mL streptomycin. At least 4 h before transfection, the medium was substituted by medium containing 5% dextran charcoal stripped FBS (DCC-FBS). Transfections were performed with 1 μg/well AR expression constructs or 0.5 μg/well empty YFP or CFP expression vector in FuGENE6 (Roche) transfection medium. Four hours after transfection, the medium was replaced by medium with 5% DCC-FBS with or without 100 nM R1881. In the abFRET competition experiments 1 μg YFP-AR-CFP was cotransfected with increasing amounts of untagged AR (ratio YFP-AR-CFP : AR 1:0, 4:1, 2:1, 1:1, 1:2 and 1:4). Different vector sizes were taken into account. The amounts of CMV promoters and total transfected DNA were corrected by cotransfecting pcDNA3 (CMV) and pTZ19 vectors.

For the AR transactivation experiments, Hep3B cells were cultured in 24-well plates in α-MEM supplemented with 5% DCC-FBS in the presence or absence of 100 nM R1881 and transfected using 50 ng AR expression construct and 100 ng luciferase reporter construct. After 24 h, cells were lysed and luciferase activity was measured in a luminometer (GloMax Microplate luminometer; Promega). The Hep3B cell line with stably transfected (ARE)2-TATA Luc reporter was generated by cotransfection with pGKneo in medium containing 0.4 mg/mL G418 (Invitrogen). Next, a clone with appropriate luciferase activity after transfection with AR and stimulation with R1881 was selected and further propagated.

Western blot analysis

Hep3B cells were cultured and transfected in 6-well plates. After 24 h, cells were washed twice in ice-cold PBS and lysed in 200 μL Laemmli sample buffer (50 mM Tris-HCl, pH 6.8, 10% glycerol, 2% SDS, 10 mM DTT, and 0.001% Bromophenol blue). After boiling for 5 min, a 5 μL sample was separated on a 10% SDS-polyacrylamide gel and blotted to Immobilon-P Transfer Membrane (Millipore). Blots were incubated with anti-AR (1:2,000; mouse monoclonal antibody F39.4.1) and subsequently incubated with HRP-conjugated goat anti–mouse antibody (DakoCytomation). Protein bands were visualized using Super Signal West Pico Luminol solution (Pierce Chemical Co.), followed by exposure to x-ray film.

Confocal imaging, YFP/CFP ratio imaging and acceptor photobleaching FRET analysis

Immunofluorescence imaging of Hep3B cells expressing tagged-Ars was performed using a confocal laser-scanning microscope (LSM510; Carl Zeiss MicroImaging, Inc.) equipped with a Plan-Neofluar 40×/1.3 NA oil objective (Carl Zeiss MicroImaging, Inc.) at a lateral resolution of 100 nm. An argon laser was used for excitation of CFP and YFP at 458 and 514 nm, respectively.

In all quantitative imaging experiments cells with a physiological relevant expression level of tagged ARs were selected for analysis (Van Royen et al., 2007; Van Royen et al., 2009a).

N/C interactions of double-tagged YFP-AR-FP, or cotransfected YFP-AR and AR-CFP were assessed using YFP/CFP ratio imaging and acceptor photobleaching FRET (abFRET) (Van Royen et al., 2009a and references therein). In YFP/CFP ratio imaging cells expressing YFP/CFP double-tagged AR or a combination of YFP-AR and AR-CFP with initially similar signal ratios to YFP-AR-CFP were imaged with an interval of 30 sec. using a 458 nm excitation at low laser power to avoid monitor bleaching. YFP and CFP emissions were detected using a 560-nm longpass emission filter and a 470–500 nm bandpass emission filter, respectively. The AR N/C interaction was initiated by adding R1881 to the cell culture. After background subtraction FRET was calculated as: I_{YFP} / I_{CFP}. The relative nuclear intensity was determined simultaneously using the YFP emission and was calculated as $I_{nucleus} / (I_{nucleus} + I_{cytoplasm})$.

In abFRET, YFP and CFP images were collected sequentially before photobleaching of the acceptor. CFP was excited at 458 nm at moderate laser power, and emission was detected using a 470–500 nm bandpass emission filter. YFP was excited at 514 nm at moderate laser power, and emission was detected using a 560-nm longpass emission filter. After image collection, YFP in the nucleus was bleached by scanning a nuclear region of ~100 μm^2 25 times at 514 nm at high laser power, covering the largest part of the nucleus. After photobleaching, a second YFP and CFP image pair was collected. Apparent FRET efficiency was estimated (correcting for the amount of YFP bleached) using the equation abFRET = $((CFP_{after} - CFP_{before}) \times YFP_{before}) \times ((CFP_{after} \times YFP_{before}) - (CFP_{before} \times YFP_{after}))^{-1}$, where CFP_{before} and YFP_{before} are the mean prebleach fluorescence intensities of CFP and YFP, respectively, in the area to be bleached (after background subtraction), and CFP_{after} and YFP_{after} are the mean postbleach fluorescence intensities of CFP and YFP, respectively, in the bleached area (Dinant et al., 2008). The apparent FRET efficiency was finally expressed relative to control measurements in cells expressing either free CFP and YFP ($abFRET_0$) or the CFP-YFP fusion protein ($abFRET_{CFP\text{-}YFP\ fusion}$): apparent FRET efficiency = $(abFRET - abFRET_0) \times (abFRET_{CFP\text{-}YFP\ fusion} - abFRET_0)^{-1}$.

FRAP

The mobility of interacting proteins was studied using FRAP (Van Royen et al., 2009b). A narrow strip spanning the nucleus was scanned at 458 nm excitation (because of simultaneous CFP recording in FRET FRAP (Van Royen et al., 2007)) with short intervals (100 msec) at low laser power (YFP is sufficiently excited at this wavelength (Van Royen et al., 2007)). Fluorescence intensity of YFP was recorded using a 560-nm longpass filter. After 40 scans, a high-intensity, 100-msec bleach pulse at 514 nm was applied photobleach YFP inside the strip. Subsequently, scanning of the bleached strip was continued at 458 nm at low laser intensity. The curves are either normalized by calculating $I_{norm} = (I_{raw} - I_{bg})/(I_{pre} - I_{bg})$ or to compare donor-FRAP and acceptor-FRAP curves by calculating Inorm = $(I_{raw} - I_0)/(I_{final} - I_0)$, where I_{pre}, I_0, and

I_{final} are the fluorescent intensities before, immediately after, the bleach and after complete recovery, respectively, and I_{bg} is the background intensity.

ACKNOWLEDGEMENTS

The authors would like to thank Michel Molier for generating the Hep3B cell line with the integrated expressing (ARE)2TATA luciferase reporter. This work is supported by grant DDHK 2002-2679 from the Dutch Cancer Society (KWF) and grant 03-DYNA-F-18 of the European Science Foundation (ESF).

REFERENCES

Bastiaens, P.I.H., and T.M. Jovin. 1996. Microspectroscopic imaging tracks the intracellular processing of a signal transduction protein: Fluorescent-labeled protein kinase C βI. *Proc Natl Acad Sci U S A.* 93:8407-8412.

Bastiaens, P.I.H., I.V. Majoul, P.J. Verveer, H.-D. Söling, and T.M. Jovin. 1996. Imaging the intracellular trafficking and state of the AB5 quaternary structure of cholera toxin. *EMBO J.* 15:4246-4253.

Bledsoe, R.K., V.G. Montana, T.B. Stanley, C.J. Delves, C.J. Apolito, D.D. McKee, T.G. Consler, D.J. Parks, E.L. Stewart, and T.M. Willson. 2002. Crystal Structure of the Glucocorticoid Receptor Ligand Binding Domain Reveals a Novel Mode of Receptor Dimerization and Coactivator Recognition. *Cell.* 110:93-105.

Bolton, E.C., A.Y. So, C. Chaivorapol, C.M. Haqq, H. Li, and K.R. Yamamoto. 2007. Cell- and gene-specific regulation of primary target genes by the androgen receptor. *Genes Dev.* 21:2005-2017.

Brinkmann, A.O., P.W. Faber, H.C.J. van Rooij, G.G.J.M. Kuiper, C. Ris, P. Klaassen, J.A.G.M. van der Korput, M.M. Voorhorst, J.H. van Laar, E. Mulder, and J. Trapman. 1989. The human androgen receptor: domain structure, genomic organization and regulation of expression. *J Steroid Biochem.* 34:307-310.

Centenera, M.M., J.M. Harris, W.D. Tilley, and L.M. Butler. 2008. The Contribution of Different Androgen Receptor Domains to Receptor Dimerization and Signaling. *Mol Endocrinol.* (in press)

Claessens, F., S. Denayer, N. Van Tilborgh, S. Kerkhofs, C. Helsen, and A. Haelens. 2008. Diverse roles of androgen receptor (AR) domains in AR-mediated signaling. *Nucl Recept Signal.* 6:e008.

Dahlman-Wright, K., A. Wright, J. Gustafsson, and J. Carlstedt-Duke. 1991. Interaction of the glucocorticoid receptor DNA-binding domain with DNA as a dimer is mediated by a short segment of five amino acids. *J Biol Chem.* 266:3107-3112.

De Ruiter, P.E., R. Teuwen, J. Trapman, R. Dijkema, and A.O. Brinkmann. 1995. Synergism between androgens and protein kinase-C on androgen-regulated gene expression. *Mol Cell Endocrinol.* 110:R1-R6.

Dinant, C., M. van Royen, W. Vermeulen, and A. Houtsmuller. 2008. Fluorescence resonance energy transfer of GFP and YFP by spectral imaging and quantitative acceptor photobleaching. *J Micros.* 231:97-104.

Dubbink, H.J., R. Hersmus, C.S. Verma, J.A.G.M. van der Korput, C.A. Berrevoets, J. van Tol, A.C.J. Ziel-van der Made, A.O. Brinkmann, A.C.W. Pike, and J. Trapman. 2004. Distinct recognition modes of FXXLF and LXXLL motifs by the androgen receptor. *Mol Endocrinol.* 18:2132-2150.

Farla, P., R. Hersmus, B. Geverts, P.O. Mari, A.L. Nigg, H.J. Dubbink, J. Trapman, and A.B. Houtsmuller. 2004. The androgen receptor ligand-binding domain stabilizes DNA binding in living cells. *J Struct Biol.* 147:50-61.

Farla, P., R. Hersmus, J. Trapman, and A.B. Houtsmuller. 2005. Antiandrogens prevent stable DNA-binding of the androgen receptor. *J Cell Sci.* 118:4187-4198.

Freedman, L.P., K.R. Yamamoto, B.F. Luisi, and P.B. Sigler. 1988. More fingers in hand. *Cell.* 54:444.

Geserick, C., H.A. Meyer, K. Barbulescu, and B. Haendler. 2003. Differential modulation of androgen receptor action by deoxyribonucleic acid response elements. *Mol Endocrinol.* 17:1738-1750.

Haelens, A., G. Verrijdt, L. Callewaert, V. Christiaens, K. Schauwaers, B. Peeters, W. Rombauts, and F. Claessens. 2003. DNA recognition by the androgen receptor: evidence for an alternative DNA-dependent dimerization, and an active role of sequences flanking the response element on transactivation. *Biochem J.* 369:141-151.

Härd, T., K. Dahlman, J. Carlstedt-Duke, J.A. Gustafsson, and R. Rigler. 1990a. Cooperativity and specificity in the interactions between DNA and the glucocorticoid receptor DNA-binding domain. *Biochemistry.* 29:5358-5364.

Härd, T., E. Kellenbach, R. Boelens, B. Maler, K. Dahlman, L. Freedman, J. Carlstedt-Duke, K. Yamamoto, J. Gustafsson, and R. Kaptein. 1990b. Solution structure of the glucocorticoid receptor DNA-binding domain. *Science.* 249:157-160.

He, B., N.T. Bowen, J.T. Minges, and E.M. Wilson. 2001. Androgen-induced NH2- and COOH-terminal interaction inhibits p160 coactivator recruitment by activation function 2. *J Biol Chem.* 276:42293-42301.

Houtsmuller, A.B. 2005. Fluorescence recovery after photobleaching: application to nuclear proteins. *In* Adv Biochem Eng Biotechnol. Vol. 95. J. Rietdorf, editor. Springer-Verlag GmbH, Berlin. 177-199.

Hur, E., S.J. Pfaff, E.S. Payne, H. Gron, B.M. Buehrer, and R.J. Fletterick. 2004. Recognition and accommodation at the androgen receptor coactivator binding interface. *PLoS Biol.* 2:E274.

Karpova, T., C. Baumann, L. He, X. Wu, A. Grammer, P. Lipsky, G. Hager, and J. McNally. 2003. Fluorescence resonance energy transfer from cyan to yellow fluorescent protein detected by acceptor photobleaching using confocal microscopy and a single laser. *J Microsc.* Vol. 209:56-70.

Kenworthy, A.K. 2001. Imaging protein-protein interactions using fluorescence resonance energy transfer microscopy. *Methods.* 24:289-296.

Luisi, B.F., W.X. Xu, Z. Otwinowski, L.P. Freedman, K.R. Yamamoto, and P.B. Sigler. 1991. Crystallographic analysis of the interaction of the glucocorticoid receptor with DNA. *Nature.* 352:497-505.

Marcelli, M., D.L. Stenoien, A.T. Szafran, S. Simeoni, I.U. Agoulnik, N.L. Weigel, T. Moran, I. Mikic, J.H. Price, and M.A. Mancini. 2006. Quantifying effects of ligands on androgen receptor nuclear translocation, intranuclear dynamics, and solubility. *J Cell Biochem.* 98:770-788.

Massie, C.E., B. Adryan, N.L. Barbosa-Morais, A.G. Lynch, M.G. Tran, D.E. Neal, and I.G. Mills. 2007. New androgen receptor genomic targets show an interaction with the ETS1 transcription factor. *EMBO Rep.* 8:871-878.

Matias, P.M., P. Donner, R. Coelho, M. Thomaz, C. Peixoto, S. Macedo, N. Otto, S. Joschko, P. Scholz, A. Wegg, S. Basler, M. Schafer, U. Egner, and M.A. Carrondo. 2000. Structural Evidence for Ligand Specificity in the Binding Domain of the Human Androgen Receptor. Implications for pathogenic gene mutations. *J Biol Chem.* 275:26164-26171.

McNally, J.G., W.G. Müller, D. Walker, R. Wolford, and G.L. Hager. 2000. The glucocorticoid receptor: rapid exchange with regulatory sites in living cells. *Science.* 287:1262-1265.

Rayasam, G.V., C. Elbi, D.A. Walker, R. Wolford, T.M. Fletcher, D.P. Edwards, and G.L. Hager. 2005. Ligand-specific dynamics of the progesterone receptor in living cells and during chromatin remodeling in vitro. *Mol Cell Biol.* 25:2406-2418.

Roemer, S.C., D.C. Donham, L. Sherman, V.H. Pon, D.P. Edwards, and M.E.A. Churchill. 2006. Structure of the Progesterone Receptor-Deoxyribonucleic Acid Complex: Novel Interactions Required for Binding to Half-Site Response Elements. *Mol Endocrinol.* 20:3042-3052.

Rosenfeld, M.G., V.V. Lunyak, and C.K. Glass. 2006. Sensors and signals: a coactivator/corepressor/epigenetic code for integrating signal-dependent programs of transcriptional response. *Genes Dev.* 20:1405-1428.

Sack, J.S., K.F. Kish, C. Wang, R.M. Attar, S.E. Kiefer, Y. An, G.Y. Wu, J.E. Scheffler, M.E. Salvati, S.R. Krystek, R. Weinmann, and H.M. Einspahr. 2001. Crystallographic structures of the ligand-binding domains of the androgen receptor and its T877A mutant complexed with the natural agonist dihydrotestosterone. *Proc Natl Acad Sci U S A.* 98:4904-4909.

Savory, J.G.A., G.G. Prefontaine, C. Lamprecht, M. Liao, R.F. Walther, Y.A. Lefebvre, and R.J.G. Hache. 2001. Glucocorticoid Receptor Homodimers and Glucocorticoid-Mineralocorticoid Receptor Heterodimers Form in the Cytoplasm through Alternative Dimerization Interfaces. *Mol Cell Biol.* 21:781-793.

Schaufele, F., X. Carbonell, M. Guerbadot, S. Borngraeber, M.S. Chapman, A.A.K. Ma, J.N. Miner, and M.I. Diamond. 2005. The structural basis of androgen receptor activation: Intramolecular and intermolecular amino-carboxy interactions. *Proc Natl Acad Sci U S A.* 102:9802-9807.

Schwabe, J.W., L. Chapman, J.T. Finch, and D. Rhodes. 1993a. The crystal structure of the estrogen receptor DNA-binding domain bound to DNA: how receptors discriminate between their response elements. *Cell.* 75:567-578.

Schwabe, J.W., L. Chapman, J.T. Finch, D. Rhodes, and D. Neuhaus. 1993b. DNA recognition by the oestrogen receptor: from solution to the crystal. *Structure.* 1:187-204.

Shaffer, P.L., A. Jivan, D.E. Dollins, F. Claessens, and D.T. Gewirth. 2004. Structural basis of androgen receptor binding to selective androgen response elements. *Proc Natl Acad Sci U S A.* 101:4758-4763.

So, A.Y., C. Chaivorapol, E.C. Bolton, H. Li, and K.R. Yamamoto. 2007. Determinants of cell- and gene-specific transcriptional regulation by the glucocorticoid receptor. *PLoS Genet.* 3:e94.

Stenoien, D.L., K. Patel, M.G. Mancini, M. Dutertre, C.L. Smith, B.W. O'Malley, and M.A. Mancini. 2001. FRAP reveals that mobility of oestrogen receptor-alpha is ligand- and proteasome-dependent. *Nat Cell Biol.* 3:15-23.

Sultan, C., S. Lumbroso, N. Poujol, C. Belon, C. Boudon, and J. Lobaccaro. 1993. Mutations of androgen receptor gene in androgen insensitivity syndromes. *J Steroid Biochem Mol Biol.* 46:519-530.

Tanenbaum, D.M., Y. Wang, S.P. Williams, and P.B. Sigler. 1998. Crystallographic comparison of the estrogen and progesterone receptors ligand binding domains. *Proc Natl Acad Sci U S A.* 95:5998-6003.

Van Royen, M.E., S.M. Cunha, M.C. Brink, K.A. Mattern, A.L. Nigg, H.J. Dubbink, P.J. Verschure, J. Trapman, and A.B. Houtsmuller. 2007. Compartmentalization of androgen receptor protein-protein interactions in living cells. *J Cell Biol.* 177:63-72.

Van Royen, M.E., C. Dinant, P. Farla, J. Trapman, and A.B. Houtsmuller. 2009a. FRAP and FRET methods to study nuclear receptors in living cells. *In* The Nuclear Receptor superfamily. Vol. 505. I.J. McEwan, editor. Humana Press / Springer, in press.

Van Royen, M.E., P. Farla, K.A. Mattern, B. Geverts, J. Trapman, and A.B. Houtsmuller. 2009b. FRAP to study nuclear protein dynamics in living cells. *In* The Nucleus. Vol. 464. R. Hancock, editor. Humana Press / Springer, Totowa. 363-385.

Wang, Q., W. Li, X.S. Liu, J.S. Carroll, O.A. Jänne, E.K. Keeton, A.M. Chinnaiyan, K.J. Pienta, and M. Brown. 2007. A hierarchical network of transcription factors governs androgen receptor-dependent prostate cancer growth. *Mol Cell.* 27:380-392.

Williams, S.P., and P.B. Sigler. 1998. Atomic structure of progesterone complexed with its receptor. *Nature.* 393:392-396.

Table S1. Primers used in Quik Change mutagenesis to introduce mutations in tagged and untagged ARs.

AR mutation	Primers	
F23,27A/L26A	Forw.	5′-ACCTACCGAGGAGCTGCACAGAATGCTGCACAGAGCGTGCGCGAA-3′
	Rev.	5′-TTCGCGCACGCTCTGTGCAGCATTCTGTGCAGCTCCTCGGTAGGT-3′
R585K	Forw.	5′-GTCTTCTTCAAAAAAGCCGCTGAAGGG-3′
	Rev.	5′-CCCTTCAGCGGCTTTTTTGAAGAAGAC-3′
R585A	Forw.	5′-GTCTTCTTCAAAGCAGCCGCTGAAGGG-3′
	Rev.	5′-CCCTTCAGCGGCTGCTTTGAAGAAGAC-3′
A596T	Forw.	5′-GTACCTGTGCACCAGCAGAAATGATTGC-3′
	Rev.	5′-GCAATCATTTCTGCTGGTGCACAGGTAC-3′
S597T	Forw.	5′-GTACCTGTGCGCCACCAGAAATGATTGC-3′
	Rev.	5′-GCAATCATTTCTGGTGGCGCACAGGTAC-3′
A596T/S597T	Forw.	5′-GTACCTGTGCACCACCAGAAATGATTGC-3′
	Rev.	5′-GCAATCATTTCTGGTGGTGCACAGGTAC-3′
E897A	Forw.	5′-CCGGAAATGATGGCAGCGATCATCTCTGTGCAA-3′
	Rev.	5′-TTGCACAGAGATGATCGCTGCCATCATTTCCGG-3′

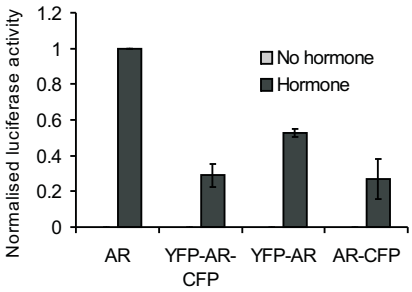

Figure S1. Normalized transactivation activity of untagged wild type AR and double- and single-tagged variants as measured on an (ARE)2-TATA Luc reporter in transiently transfected Hep3B cells. Means +/- 2*SEM of two independent experiments are shown.

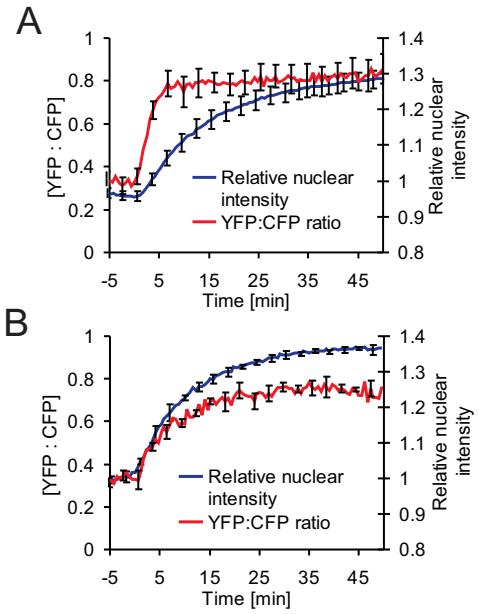

Figure S2. (A) YFP-AR-CFP translocates to the nucleus within 30-40 min. after addition of hormone (100 nM R1881) (blue curve). The AR N/C interaction is indicated by an YFP/CFP ratio change (red curve). The N/C interaction precedes the nuclear translocation and occurs within 5-10 min. after hormone addition. Curves shown are mean +/- 2*SEM of 15 cells measured in three independent experiments. (B) In contrast to the YFP/CFP double-tagged AR, the N/C interaction follows the nuclear translocation in Hep3B cells coexpressing YFP- and CFP- single-tagged ARs (YFP-AR and AR-CFP). Data shown are mean +/- 2*SEM of 7 cells measured in two independent experiments.

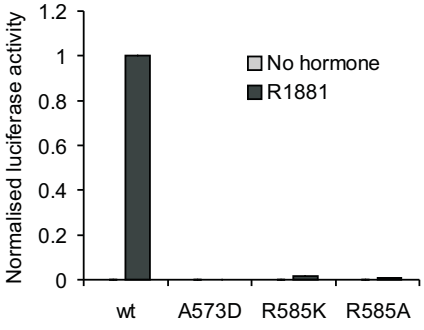

Figure S3. Normalized transactivation function of DNA-binding deficient AR mutants on a luciferase reporter gene driven by a minimal promoter containing two AREs ((ARE)2-TATA Luc). None of the DNA-binding deficient AR mutants is able to activate the reporter gene in the presence of 100 nM R1881. Means +/- 2*SEM of two independent experiments are shown.

Chapter 7

A FRET-based Assay to Study Ligand Induced Androgen Receptor Activation

Van Royen, M.E., D.J. van de Wijngaart,
S.M. Cuhna, J. Trapman,
and A.B. Houtsmuller.

Manuscript in preparation.

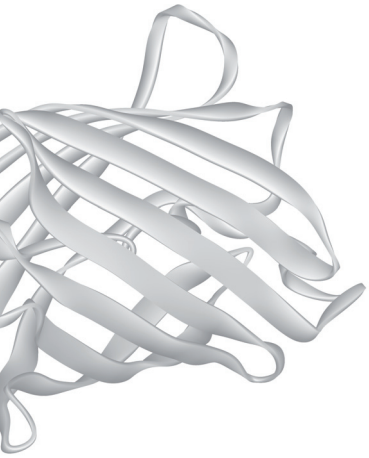

ABSTRACT

Androgens exert their key function in development and maintenance of the male phenotype via the androgen receptor. Ligand activated ARs also play a role in prostate cancer. Despite initial success of treatment by testosterone depletion or blocking of androgen binding to the AR using anti-androgens, eventually all tumors escape to a therapy resistant stage. Development of novel therapies by other antagonistic ligands or compounds that target events subsequent to ligand binding is very important. Here we validated a FRET assay for ligand induced AR activity, based on the conformational change in the AR caused by interaction between the FQNLF motif in the N-terminal domain and the cofactor binding groove in the ligand binding domain (N/C interaction). We tested the assay using known agonistic and antagonistic ligands on wild type AR and specific AR mutants. Our data shows a strong correlation between the ligand induced AR N/C interaction and transcriptional activity in wild type AR, but also in AR mutants with broadened ligand responsiveness. Moreover, we explored additional readouts of this assay that contribute to the understanding of the working mechanism of the ligands. Together, we present a sensitive assay that can be used to quantitatively assess the activity of agonistic and antagonistic AR ligands.

INTRODUCTION

The androgen receptor (AR) is a ligand-dependent transcription factor and member of the steroid receptor (SR) subfamily of nuclear receptors (NRs). Like all SRs, the AR is composed of a central DNA binding domain (DBD), an N-terminal transactivating domain (NTD) and a C-terminal ligand binding domain (LBD) (Brinkmann et al., 1989). In the absence of ligand the AR is mainly localised in the cytoplasm, but AR translocates rapidly to the nucleus after ligand binding (Georget et al., 1997). In the nucleus ARs interact in a highly dynamic manner with promoters and enhancers of target genes, and recruit transcriptional coregulators to regulate gene expression (Cleutjens et al., 1997; Claessens et al., 2001; Farla et al., 2004; Rosenfeld et al., 2006). Ligand binding of SRs induces repositioning of helix 12 in the SR LBD resulting in the formation of a hydrophobic pocket on the surface. Many cofactors, like the p160 family, can bind to this groove via LxxLL like motifs (Heery et al., 1997). The AR LBD preferentially with FxxLF motifs (Dubbink et al., 2004; Hur et al., 2004). This preference for FxxLF motifs enables an extra level of AR regulation via a ligand induced interaction with the FQNLF motif in the AR NTD (the AR N/C interaction) (Doesburg et al., 1997; He et al., 2000). It has been suggested that the AR N/C interaction plays a role in the stability of ligand binding and also protects the cofactor groove for untimely and unfavorable protein-protein interactions (He et al., 2001; Dubbink et al., 2004; Van Royen et al., 2007).

Activated ARs regulate genes involved in the development and maintenance of the male phenotype (Brinkmann et al., 1999). The AR is also a key factor in prostate cancer (reviewed in Feldman and Feldman, 2001; Trapman, 2001; Heinlein and Chang, 2004; Taplin and Balk, 2004). Therapy of metastasised prostate cancers aims at testosterone depletion by chemical or surgical castration or at blocking of androgen binding to the AR using anti-androgens. Despite initial success of these treatments, eventually all tumors escape to a therapy resistant stage (Trapman, 2001). Importantly, endocrine therapy resistant (hormone refractory) prostate cancer remains dependent on a functionally active AR. Therapy resistance can be caused by several mechanisms, including AR mutations resulting in inappropriate activation by anti-androgens and low affinity agonists, ligand independent activation of the AR and aberrant expression or properties of cofactors (reviewed in Taplin et al., 1999; Heinlein and Chang, 2004; Rahman et al., 2004; Taplin and Balk, 2004; Edwards and Bartlett, 2005). Recently, it has been shown that in prostate cancer the expression of enzymes needed for DHT synthesis are increased (Mostaghel and Nelson, 2008).

Most of the AR mutations found in prostate cancer so far are localised in the AR LBD, where the threonine at position 877 is a mutational hot-spot mostly mutated to an alanine (AR T877A) (Veldscholte et al., 1990). The T877A mutation decreases the AR ligand specificity and allows other steroids like estrogens, progestrogens and adrenal androgens, but also anti-androgens like OH-flutamide to act as agonists (Veldscholte et al., 1992; Steketee et al., 2002; Farla et al., 2005). Similarly, in patients treated with the anti-androgen bicalutamide a trypto-

phan to cysteine substitution (W741C) can be found (Haapala et al., 2001; Taplin et al., 2003), which leads to AR activation by bicalutamide (Hara et al., 2003; Farla et al., 2005; Urushibara et al., 2007). A third prostate cancer AR mutation affecting its ligand specificity, a leucine - histidine substitution at position 701 (L701H), was found in two independent patients and the MDA PCa 2A prostate cancer cell line (Suzuki et al., 1993; Watanabe et al., 1997; Zhao et al., 1999). The L701H mutation makes the AR highly sensitive to the glucocorticoids cortisol and cortisone (Brinkmann and Trapman, 2000; Zhao et al., 2000; Krishnan et al., 2002). In the MDA PCa prostate cancer cell line the L701H mutation was accompanied with the T877A LNCaP mutation, combining the ligand binding characteristics of the two single mutants (Zhao et al., 1999; Brinkmann and Trapman, 2000; Zhao et al., 2000; Matias et al., 2002). Research on new steroid based therapies and therapies based on AR inhibitors that target the AR activity in another way is therefore of great relevance.

Historically, most screening approaches for activating SR ligands or SR inhibitory compounds use target promoter driven reporter genes as assays. Although these assays do quantitatively assess SR transcriptional activity, these measurements do not provide mechanistical details on which of the consecutive steps, from ligand binding to transcriptional activity is inhibited. More recently, a number of fluorescent indicators have been designed for ligand-mediated responses of SRs. Some of these quantify ligand-induced activity by nuclear translocation or nuclear mobility of fluorescently labeled receptors or receptor chimeras (Martinez et al., 2005; Marcelli et al., 2006; Agler et al., 2007; Nakauchi et al., 2007). Others make use of ligand induced conformational changes in the SR LBDs. A very elegant system directly uses the ligand induced repositioning of helix 12 in the estrogen receptor LBD (ER LBD) to sense ER – ligand interactions (Paulmurugan and Gambhir, 2006). A whole set of indicators has been designed to detect ligands for the estrogen receptor (ER), glucocorticoid receptor (GR), progesterone receptor (PR), and AR, but also the orphan receptor peroxisome proliferator-activated receptor γ (PPAR-γ) (Awais et al., 2004; Awais et al., 2006; Awais et al., 2007b; Awais et al., 2007a; Awais M, 2007). These indicators make use of the conformational change in the LBD that leads to cofactor recruitment to the cofactor groove in the SR LBD. The conformational change of YFP- and CFP-, double tagged SR LBD – cofactor peptide chimeras, due to the peptide interaction with the cofactor groove in the ligand activated LBD, was detected by fluorescence resonance energy transfer (FRET).

A similar principle was used on full length ER and AR, tagged with YFP and CFP at both termini (Michalides et al., 2004; Schaufele et al., 2005; Griekspoor et al., 2007; Van Royen et al., 2007). In the AR the conformational change is a direct result of the ligand induced AR N/C interaction (Schaufele et al., 2005; Van Royen et al., 2007). Applying FRET on these double tagged ARs showed that the intra-molecular AR N/C interaction was initiated rapidly after ligand binding, followed by an inter-molecular N/C interaction (Schaufele et al., 2005). Very recently the FRET approach on YFP-and CFP- double-tagged ARs, was presented in a high throughput cellular conformation-based screening setting. This assay was used in a screen

of FDA-approved drugs and natural products and identified compounds with previously unidentified anti-androgen activity (Jones and Diamond, 2008). Comparing FRET results from a compound screening of double tagged ARs in two different cell lines with a traditional transcription reporter assay indicated that the FRET assay is less sensitive to nonspecific cellular variation than a typical promoter-reporter assay. Therefore, the authors suggest that this FRET based assays are expected to give a higher specificity of the AR function, less noise and similar sensitivity in compound detection in larger screens (Jones and Diamond, 2008).

We generated a similar FRET assay based on the AR N/C interaction (Van Royen et al., 2007). Here we examined, and validated activation of wild type AR and specific AR mutants bound with activating and inactivating ligands with this assay. Furthermore we extended the use of tagged AR and identify different potential readouts of this assay in a microscope-based setting enabling the extraction of additional mechanistical details of AR activity inhibition.

RESULTS

Acceptor bleaching FRET on functionally active YFP-AR-CFP represents AR N/C interaction in living cells

The molecular basis of the AR N/C interaction is the interaction of the ^{23}FQNLF^{27} motif in the AR NTD with the cofactor groove in the AR LBD. To be able to utilise the AR N/C interaction in a FRET based assay for ligand induced AR activation we tagged wild type and mutant ARs with the fluorescent protein YFP at the N-terminus and CFP at the C-terminus and transiently expressed them in Hep3B cells lacking endogenous SRs (Fig. 1A). Previously we and others showed that similar double tagged ARs are applicable in studies on AR function (Schaufele et al., 2005; Van Royen et al., 2007). To determine whether FRET observed in double tagged wt-AR (Fig. 1A) was caused by N/C interaction, we mutated the FQNLF motif to LQNLL and AQNAA in YFP-AR-CFP (YFP-AR(F23,27L)-CFP and YFP-AR(F23,27A/L26A)-CFP, respectively. In addition, we deleted the FQNLF motif (YFP-AR(ΔFQNLF)-CFP). Western blot analysis showed that all expressed AR fusion proteins have the expected size (Fig. 1B). Mutating the FQNLF motif in the AR NTD does not change the speckled distribution of the AR (Fig. 1C) indicating that AR FQNLF mutants are still able to stably bind DNA (Farla et al., 2004). We applied acceptor photobleaching FRET (abFRET) to these cells where the readout was based on confocal images taken before and after photobleaching the acceptor (YFP) in which the subsequential increase of the donor (CFP) is measured (Bastiaens and Jovin, 1996; Bastiaens et al., 1996; Kenworthy, 2001; Karpova et al., 2003; Van Royen et al., 2007). Weakening the N/C interaction in YFP-AR-CFP by mutating the FQNLF motif indeed proportionally lowered the FRET signal (Fig. 1D). Furthermore, in similar proportions the AR transcriptional activity on a transiently transfected luciferase reporter gene driven by an androgen regulated promoter ((ARE)2TATA-luciferase) drops (Fig. 1E). This data indicates that the FRET measured on YFP-AR-CFP repre-

sents the AR N/C interaction and that loss of N/C interaction by mutating the FQNLF motif results in the loss of AR transcriptional activity.

AR N/C interaction based FRET is hormone dose dependent

The dependency of the N/C interaction on hormone concentration was compared with the efficiency of AR nuclear translocation and AR transcriptional activity. In the absence of hormone the AR was mainly localised in the cytoplasm and translocated to the nucleus only after incubation with a sufficient dose of R1881 (Georget et al., 1997) (Fig. 2A). The Hep3B cells stably expressing YFP-AR-CFP were treated for minimally 12 hours to allow AR distribution to reach steady state. Without hormone the AR shows a 30% nuclear fraction (Fig. 2B). The minimal R1881 concentration necessary to induce the nuclear translocation was 0.1 nM (~60% nuclear fraction). A plateau in relative nuclear fraction (~80% nuclear fraction) was reached by culturing the cells in medium containing at least 1 nM R1881 (Fig. 2B). Acceptor bleaching FRET applied to these cells showed a very similar pattern where no N/C interaction was detected in the absence of hormone, 0.1 nM R1881 induced a substantial FRET signal, but already 0.01 nM R1881 induces some N/C- interaction (Fig. 2C). Also for initiating transcriptional activity on a transiently transfected luciferase reporter gene driven by a minimal promoter ((ARE)2TATA-luciferase) minimally 0.1 nM R1881 is necessary to induce transcriptional activity of the YFP- and CFP- double tagged AR (Fig. 2D).

Comparing the hormone dose dependency of YFP-AR-CFP with untagged ARs indicate that both were activated at the same minimal concentration of R1881 (0.1 nM), but that YFP-AR-CFP had a lower maximal activity, indicating that the tags on YFP-AR-CFP do not interfere with hormone binding efficiency but rather affect the maximal activity of the AR (data not shown). Furthermore, the absence of N/C interaction, transcriptional activity but also diminished of nuclear translocation in the presence of low concentrations of R1881 suggests an insufficient ligand binding efficiency by the AR LBD at these concentrations. We can conclude from this data that the FRET detected N/C interaction is a bonafide measure for ligand induced activity of wild type AR.

Agonist and antagonist action assessed by FRET

Next to AR agonists and AR antagonists, a third class of AR ligands is that of the partial antagonists. These ligands are able to activate the AR at high concentration whereas at lower concentrations these ligands function as antagonist. To investigate whether the partial antagonists are able to induce the AR N/C interaction in living cells we applied abFRET on Hep3B cells stably expressing YFP-AR-CFP in the presence of 1 μM CPA or RU486. Similar to R1881, DHT bound AR is distributed in the typical nuclear speckled pattern, not seen for antagonist (bicalutamide and OH-flutamide) bound AR. A very similar speckled distribution pattern is found for the partial antagonist RU486, but CPA showed a weaker, less prominent, speckled pattern (Fig. 3A). Confirming previous data, the three classes of ligands; agonists, partial

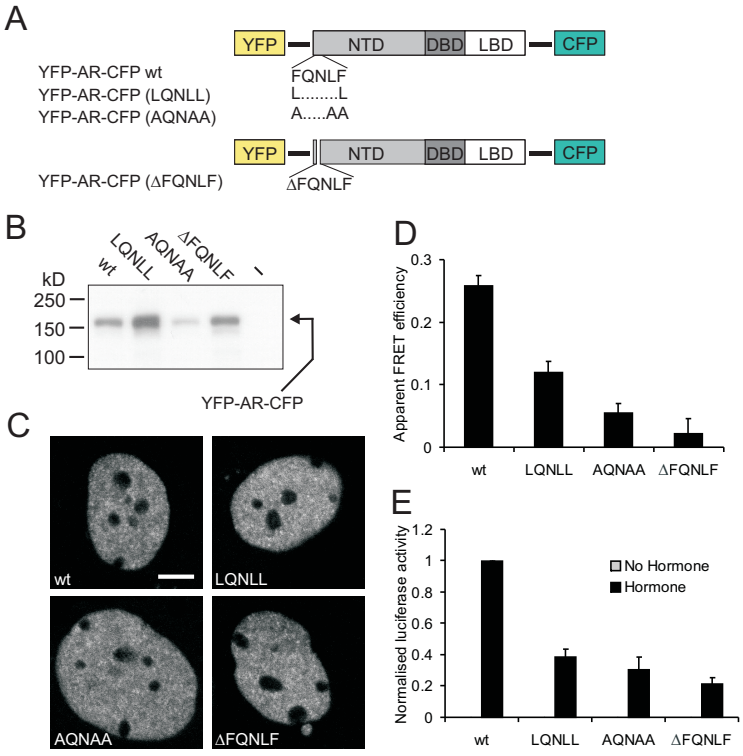

Figure 1. FRET on YFP-AR-CFP indicates AR N/C interaction in living cells. (A) Schematic representation of the YFP-, CFP- double tagged AR (YFP-AR-CFP), and the positioning of the FQNLF mutations. (B) Western analysis of wild type YFP-AR-CFP and FQNLF motif mutants. AR was detected using a mouse AR monoclonal antibody (F39.3.1). (C) High resolution confocal images of cells expressing wild type YFP-AR-CFP or ARs with mutated FQNLF motifs. Loss of N/C interaction does not interfere with the speckled nuclear AR distribution. Bars represent 5 μm. Brightness and contrast of the images was enhanced for presentation only. (D) Acceptor bleaching FRET on YFP-AR-CFP and the FQNLF mutants. Mutating the N-terminal FQNLF to LQNLL or AQNAA, or deletion of the FQNLF motif results in the loss of FRET efficiency indicating that the FRET represents the AR N/C interaction. Means +/- 2*SEM of minimally 50 cells measured in 2 independent experiments are shown. (E) Weakening or loss of AR N/C interaction results in a less transcriptionally active AR on transiently transfected (ARE)2TATA Luc reporter gene. Means +/- 2*SEM of 2 independent experiments are shown.

antagonists and full antagonists, indeed showed three levels of transcription activation of the AR on a transiently transfected ARE driven luciferase reporter gene. Where both agonists (R1881 and DHT) were able to activate the AR and both full antagonists (bicalutamide and OH-flutamide) were not, both partial antagonists (CPA and RU486) showed a minimal activation of the AR on this reporter gene (Fig. 3B) (Berrevoets et al., 2002).

Both agonists (DHT and R1881), but not the full antagonists (OH-flutamide and bicalutamide), were able to induce the AR N/C interaction. In contrast to in vitro pull-down and mammalian two-hybrid assays, both partial antagonists (CPA and RU486) showed a detectable, although moderate, FRET efficiency, indicating that these partial antagonists did induce the AR N/C interaction (Fig. 3C) (Kuil and Mulder, 1994; Kuil et al., 1995; Song et al., 2004).

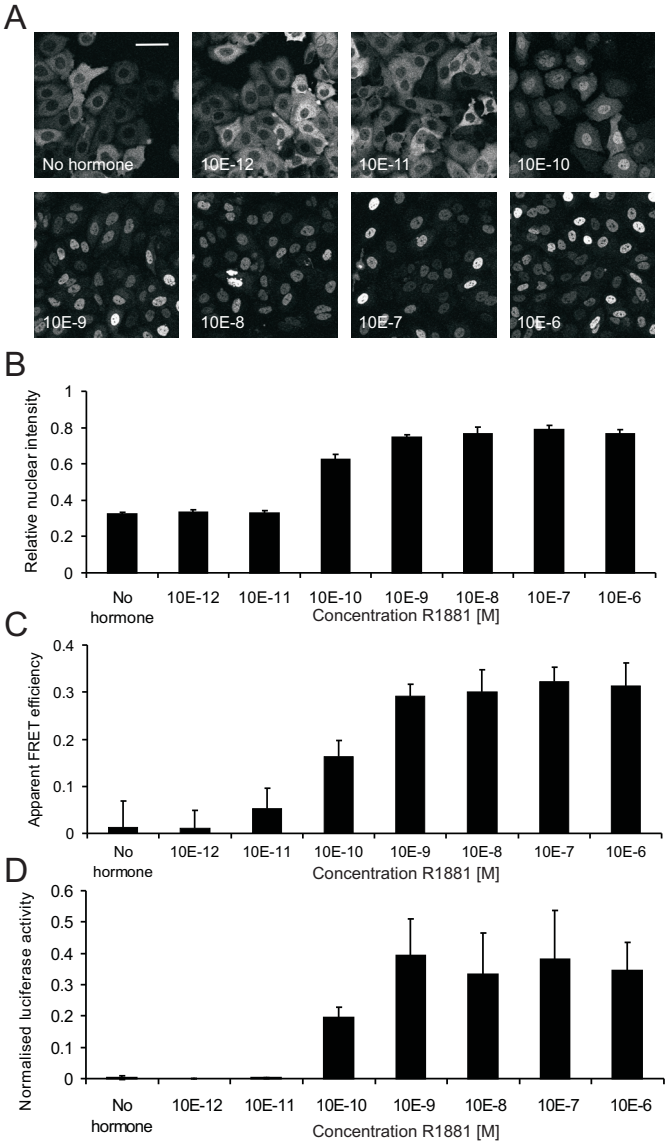

Figure 2. The AR N/C interaction based FRET efficiency is hormone dose dependent. (A) Overview images of cells stably expressing YFP-AR-CFP in the absence and presence (minimally 12 hours) of increasing quantities of R1881 (1 pM – 1 μM). In the absence of R1881 YFP-AR-CFP is predominantly localized in the cytoplasm. Only with minimally 0.1 nM R1881 the AR efficiently translocates to the nucleus. Bars represent 50 μm. Brightness and contrast of the images was enhanced for presentation only. (B) Quantitative analysis of the nuclear translocation of YFP-AR-CFP in the presence of increasing amounts of R1881. In the absence of R1881 about 30% of the ARs is present in the nucleus. In the presence of a high dose of R1881 the nuclear fraction increases to ~80%. Means +/- 2*SEM of 10 cells measured are shown. (C) Acceptor bleaching FRET on YFP-AR-CFP with increasing quantities of R1881 indicate a dose dependency of the AR N/C interaction. The minimal dose of necessary to induce the AR N/C interaction is 0.01 nM R1881 and FRET reaches a plateau with 1 nM R1881. Means +/- 2*SEM of 20 cells measured in minimally 2 independent experiments are shown. (D) Normalized transcription activity of both untagged AR and YFP-AR-CFP with increasing doses of R1881. The transcriptional activity of the double tagged YFP-AR-CFP is about 30% of the untagged variant. The minimal dose of R1881 to induce transcription is the same for untagged and double tagged ARs (0.1 nM) indicating that the dose dependency of AR activity is not changed by the two tags on YFP-AR-CFP. Means +/- 2*SEM of 2 independent experiments are shown.

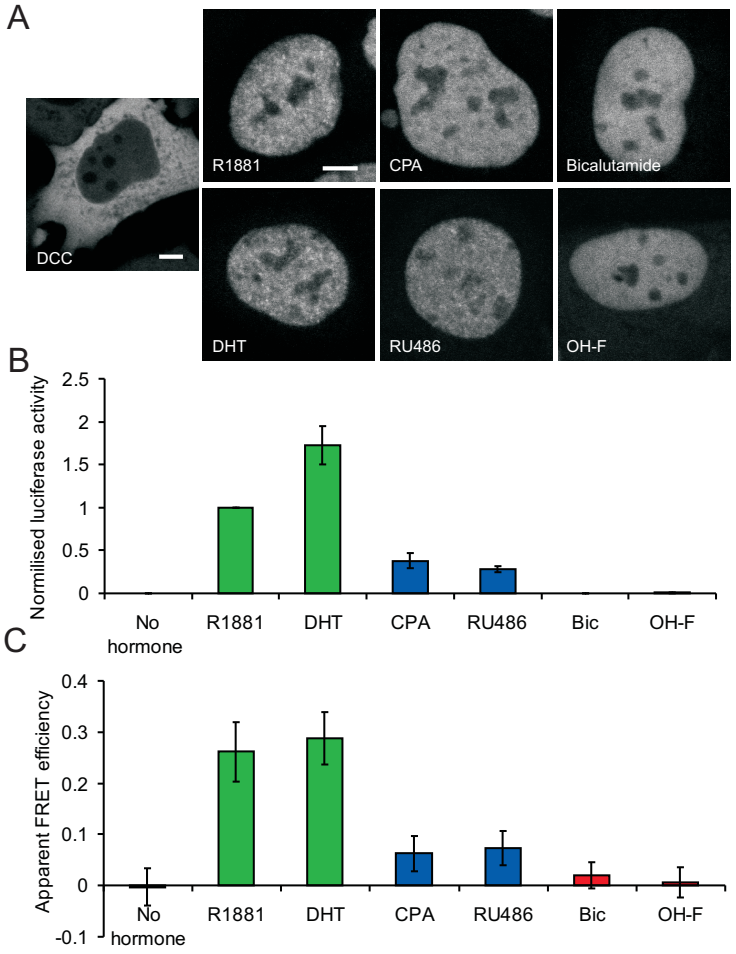

Figure 3. Agonist and antagonist action on wild type AR detected with abFRET. (A) High resolution confocal images of Hep3B cells stably expressing YFP-AR-CFP in the presence of different hormones; the agonists R1881 and DHT, partial antagonists CPA and RU486, and the full antagonists bicalutamide and OH-flutamide. Agonists bound ARs are distributed in a typical speckled pattern, which is not present in antagonist bound ARs. Partial antagonist RU486 is also able to induce the AR speckled pattern, whereas partial antagonist CPA bound AR only shows a weak speckled pattern. Bars represent 5 μm. Brightness and contrast of the images was enhanced for presentation only. (B) Normalized transactivation activity on a transiently transfected (ARE)2TATA-luciferase reporter gene of ARs bound with the different AR ligands. Identical to results of the FRET assay, only pure agonists (R1881 and DHT; green bars) are able to induce a strong AR transcription activity. Partial antagonists (CPA and RU486; blue bars) only minimally activate the AR, whereas pure antagonists (bicalutamide and OH-flutamide; red bars) do not induce AR activity. (C) AbFRET on YFP-AR-CFP in the presence of the different AR ligands. Both pure agonists (R1881 and DHT; green bars) are able to induce the AR N/C interaction, whereas both partial antagonists (CPA and RU486; blue bars) only show a weak FRET signal.

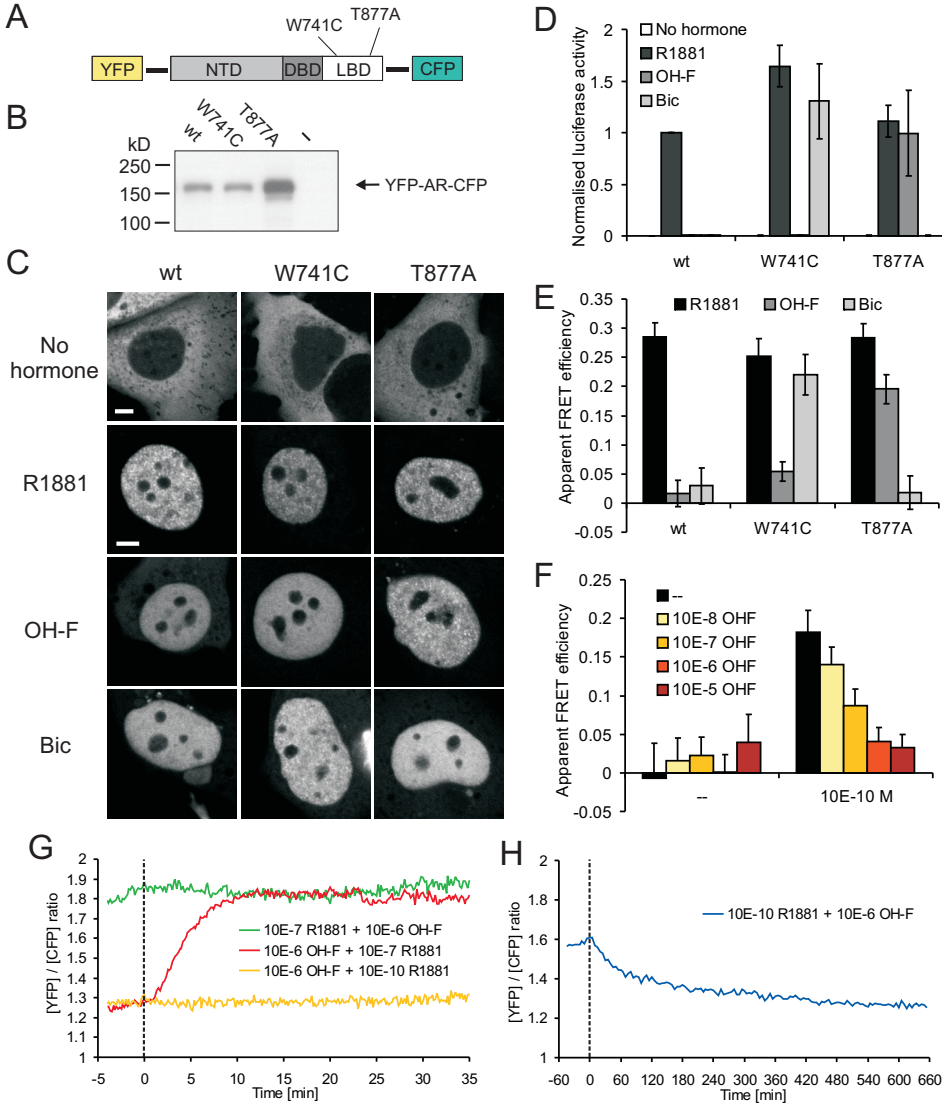

This apparent discrepancy suggests a higher sensitivity of the FRET assay compared to the previously used assays, enabling the detection of short and possibly weak interactions.

In conclusion, the FRET based AR ligand assay identified the three classes of AR ligands on the basis of the induction of the N/C interaction. Furthermore, the FRET data on the N/C interaction status of ARs bound with partial and full antagonists and agonists, correlates very well with the transcriptional activity of the AR.

Figure 4. FRET identifies agonist and antagonist action and ligand competition on wild type and mutant ARs. (A) Schematic representation of the YFP-, CFP- double tagged AR (YFP-AR-CFP), and the positioning of the LBD mutations. (B) Western blot analysis of YFP- and CFP- double tagged wild type AR and AR mutants W741C and T877A. AR was detected using a mouse AR monoclonal antibody (F39.3.1). (C) High resolution confocal images on cells expressing wild type YFP-AR-CFP or its prostate cancer variants AR W741C and AR T877A. Both antagonists, 1 μM OH-flutamide or 1 μM Bicalutamide, induce a homogeneous wild type AR distribution lacking the typical AR speckles. In contrast, AR mutants W741C and T877A mutants treated with respectively bicalutamide or OH-flutamide, and not vice versa, show a typical speckled AR distribution. Bars represent 5 μm. Brightness and contrast of the images was enhanced for presentation only. (D) Normalized transactivation activity of wild type and mutant YFP-AR-CFP. AR agonist R1881 (0.1 μM) is able to activate wild type AR and AR mutants W741C and T877A, but not DNA-binding deficient AR mutant A573D. Prostate cancer AR mutations W741C and T877A enable AR activation by the antagonists bicalutamide and OH-flutamide (1 μM), respectively. (E) AbFRET efficiency of YFP-AR-CFP in the presence of an agonist (0.1 mM R1881) or an antagonist (1 μM Bicalutamide or OH-flutamide). In concurrence with the transactivation assay (see D) AR prostate cancer mutants W741C and T877A show an AR N/C interaction in the presence of the antagonists bicalutamide or OH-flutamide, respectively and not vice versa. (F) AbFRET efficiency of YFP-AR-CFP treated with both R1881 and OH-flutamide. Only a higher dose of OH-flutamide (0.01 mM) is able to minimally induce the AR N/C interaction. Simultaneous treatment of 0.1 nM R1881 with increasing quantities of OH-flutamide (0.01 μM to 0.01 mM) result in the inhibition of R1881 induced AR N/C interaction. (G) Time laps *[YFP] / [CFP]* ratio imaging of cells expressing wild type YFP-AR-CFP. Cells were treaded for minimally 12 h with either 0.1 μM R1881 (green curve), or 1 μM OH-flutamide (red and yellow curves). At t = 0 minutes a second hormone was added. The addition of a high dose of OH-flutamide (1 μM) to 0.1 μM R1881, nor a low dose of R1881 (0.1 nM) to 1 μM OH-flutamide result in a change of the YFP / CFP ratio. Only 0.1 μM R1881 was able to compete with 1 μM OH-flutamide and induce the AR N/C interaction. (H) Time laps *[YFP] / [CFP]* ratio imaging of cells expressing wild type YFP-AR-CFP. Similarly to Fig. 3F, cells expressing YFP-AR-CFP were first treated with R1881 (0.1 nM). Whereas a high dose of OH-flutamide does not compete with 0.1 μM R1881, with ARs first treated with a low dose of R1881 (0.1 nM) lose their N/C interaction in a period of about 10 hours after addition of 1 μM OH-flutamide.

FRET reveals agonist and antagonist activity and ligand competition on wild type and mutant AR

To further explore the FRET based assay two AR LBD mutations; W741C (Haapala et al., 2001) and T877A (Veldscholte et al., 1990) found in prostate cancer from patients treated with bicalutamide and OH-flutamide, respectively, were introduced in YFP-AR-CFP (Fig. 4A). Western blot analysis showed that all fusion proteins were of the expected size (Fig. 4B). Previously, it has been show that these mutations enable antagonists to act as agonists by restoring the coactivator groove in antagonist bound AR (Hara et al., 2003; Urushibara et al., 2007). Corroborating previous data, both AR antagonists do not induce a speckled AR distribution in Hep3B cells transiently expressing wild type YFP-AR-CFP, as is found for R1881, but rather show a homogeneous distribution in like is previously shown in DNA binding deficient mutants *e.g.* A573D (Fig. 4C) (Farla et al., 2004). In contrast, anti-androgen (bicalutamide and OH-flutamide) bound double tagged AR W741C and AR T877A, respectively, do show the typical speckled pattern (Fig. 4C). As shown before, the nuclear distribution of wild type AR and these AR mutants bound with R1881 and these anti-androgens is correlated with nuclear mobility and transcriptional activity (Farla et al., 2005). Indeed, transcriptional activity shows a very similar effect of R1881 activation of wild type AR and both mutants, and activation by bicalutamide of only AR W741C and by OH-flutamide of AR T877A (Fig. 4D). The same effect is found in the N/C interaction status of these ARs (Fig. 4E). Again, R1881 induces the N/C interaction in wild type AR and both W741C and T877A mutants, as shown by abFRET. Anti-androgens bicalutamide and OH-flutamide induce the N/C interaction only in the mutants

W741C and T877A, respectively. This data shows that also for anti-androgens and ARs with mutations in the ligand binding pocket the degree to which N/C interaction occur is strongly correlated to the transcriptional activity of the AR mutants and their ligands.

The antagonistic effect of anti-androgens is only detectible in competition with an agonist. Cells expressing YFP-AR-CFP simultaneously treaded with a low concentration of the agonist R1881 (0.1 nM) and increasing concentrations of OH-flutamide. AbFRET analysis showed the proportional loss of the N/C interaction with increasing amounts of the antagonist OH-flutamide (Fig. 4F). The addition of 10 μM OH-flutamide together with 0.1 nM R1881 resulted in an identical FRET efficiency to cells treated with 10 μM OH-flutamide only (Fig. 4F).

The competition between agonists and antagonist was studied in more detail by time lapse YFP / CFP ratio imaging, monitoring the effect of adding an antagonist or agonist to cells expressing YFP-AR-CFP, primarily treated with either an agonist or an antagonist, respectively. In this assay, instead of abFRET we used (increase of) YFP / CFP ratio as a measure for the induction of the AR N/C interaction. A low concentration of R1881 (0.1 nM) was not sufficient to induce the N/C interaction if cells were already treated with a high dose of OH-flutamide (1 μM) (Fig. 4G, yellow curve), nor was a concentration of 1 μM OH-flutamide sufficient to compete with a relative high dose of R1881 (0.1 μM) and N/C interaction therefore was not abolished (Fig. 4G, green curve). In contrast, addition of this same dose of R1881 (0.1 μM) at t = 0 minutes, to YFP-AR-CFP treated for minimally 12 h with a high dose of OH-flutamide resulted in a rapid increase in YFP / CFP ratio from ~1.3 to ~ 1.8, indicating a rapid induction of the AR N/C interaction (Fig. 4G, red curve). In the opposite set-up, initial treatment of cells expressing YFP-AR-CFP with 0.1 nM R1881 moderately induced the AR N/C interaction (see also Fig. 4C). Adding 1 μM OH-flutamide (at t = 0 minutes) to these cells, showed a decrease of YFP/CFP ratio. The latter (red curve in Fig. 4F) took about 10 h to reach the new steady state at the YFP / CFP ratio level similar to the initial level of 1 μM OH-flutamide treatment (Fig. 4H, blue curve).

Together this data shows that this FRET based assay on cells expressing YFP-AR-CFP is applicable for the detection of agonistic and antagonistic activities of ligands. These types of analysis can provide relative binding efficiencies of different ligands in living cells.

FRET detection of broadened ligand responsiveness of AR L701 mutants

A third type of AR mutant found in prostate cancer (Suzuki et al., 1993; Watanabe et al., 1997) is a mutation at position 701 in the AR LBD (L701H), which results in a broadened ligand responsiveness of the AR to corticosteroids (Zhao et al., 2000). This mutant and a variant (L701M) were transiently expressed in Hep3B cells and tested for their ability to induce the AR N/C interaction (Fig. 5A). Western blot analysis showed that all fusion proteins were of the expected size (Fig. 5B). AbFRET analysis of wild type YFP-AR-CFP, both mutants (L701H and L701M) and also a double mutant (L701H/T877A) (Zhao et al., 1999), found in the prostate cancer cell line MDA PCa, showed that the agonist R1881 was able to induce the N/C interac-

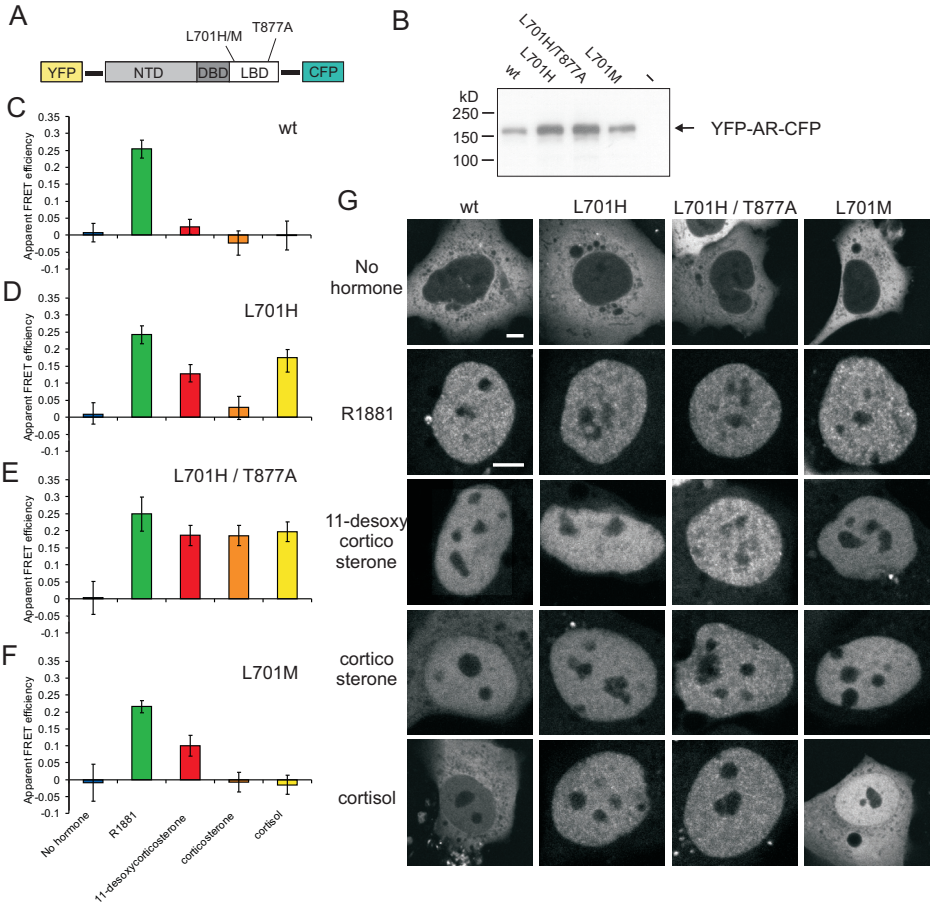

Figure 5. FRET detection of broadened ligand responsiveness of AR L701 prostate cancer mutants. (A) Schematic representation of the YFP-, CFP- double tagged AR (YFP-AR-CFP), and the positioning of the LBD mutations. (B) Western blot analysis of YFP- and CFP- double tagged wild type AR and AR L701 mutants. AR was detected using a mouse AR monoclonal antibody (F39.3.1). (C - F) AbFRET on wild type YFP-AR-CFP or AR LBD mutants (L701H, L701H/T877A and L701M). AbFRET shows differential ability of the corticosteroids; 11-desoxycorticosterone, corticosterone and cortisol, to induce FRET in cells expressing YFP-AR-CFP. (G) High resolution confocal images of Hep3B cells expressing wild type YFP-AR-CFP of its AR L701H, L701H/T877A and L701M variants in the presents of R1881 or the corticosteroids; 11-desoxycorticosterone, corticosterone and cortisol. Most hormones translocated the AR to the nucleus with exception of wild type AR and, in a lesser degree, AR L701M in the presence of cortisol. Bars represent 5 μm. Brightness and contrast of the images was enhanced for presentation only.

tion in all AR variants (Fig 5C - F, green bars). 11-desoxycorticosterone was able to induce the N/C interaction in all three AR mutants (Fig. 5D – F, red bars) but not wild type AR (Fig. 5C, red bar). Similarly, cortisol induced the N/C interaction in two AR mutants (L701H and L701H/T877A) (Fig. 5D and E, yellow bars) and corticosterone in the AR L701/T877A double mutant only (Fig. 5E, orange bar). Strikingly, the ability of most of these hormones to induce the N/C interaction in the different ARs correlated with the subnuclear speckled distribution

of these ARs in the presence of these ligands (Fig 5G). The remaining combinations of ligand bound ARs (11-desoxycorticosterone bound wild type AR, corticosterone bound wild type AR, AR L701H and AR L701M) do not show the AR N/C interaction and the typical speckled pattern but a more homogeneous distribution. Two of the four exceptions in this are 11-desoxycorticosterone-bound AR L701H, which shows a less pronounced speckled pattern and AR L701M, of which no speckled pattern can be detected. More importantly, two other exceptions, wild type AR and AR L701M in the presence of cortisol, show complete lack of, or limited nuclear translocation (Fig. 5G). In conclusion, most data obtained with this FRET assay correlates well with the AR subnuclear distribution. Moreover, the FRET data highly correlates with previously described AR activity on an ARE driven lucifererase reporter gene (van de Wijngaart et al., manuscript in preparation).

DISCUSSION

In recent years, a number of fluorescent indicators have been developed to study ligand or compound mediated responses of SRs. Most of these fluorescent indicators report on consecutive steps during SR transcription activation, including hormone induced conformational changes and dimerisation (FRET), translocation to the nucleus (time lapse imaging), interactions with cofactors (FRET) and DNA binding (FRAP) (reviewed in Griekspoor et al., 2007; Van Royen et al., 2009a). For the AR, two early events induced by ligand binding are the formation of a groove in the C-terminal LBD and subsequent interaction of the N-terminal FQNLF motif with the groove (N/C interaction) (Doesburg et al., 1997; He et al., 2000; Steketee et al., 2002; Dubbink et al., 2004; Schaufele et al., 2005). Here we validated a FRET based assay for ligand induced AR activity that quantitatively detects the N/C interaction using cells expressing YFP-AR-CFP.

The AR N/C interaction in wild type and mutant ARs reflects transcriptional activity

Mutational analysis of the FQNLF motif showed that FRET efficiency of YFP-AR-CFP is a measure for the N/C interaction (Fig. 1 D and E). Hormone dose responsiveness of the FRET based detection of the N/C interaction was very similar compared to transcriptional activity of the AR (Fig. 2). Furthermore, the N/C interaction status in wild type AR and a set of specific cancer derived AR mutants with a broadened ligand responsiveness (T877A, W741C, L701H/T877A, L701H and a variant L701M) bound with a variety of hormones very well reflected the AR transcriptional activity (Fig. 3, 4 and 5) (Veldscholte et al., 1990; Zhao et al., 2000; Krishnan et al., 2002; Steketee et al., 2002; Hara et al., 2003; Farla et al., 2005; van de Wijngaart et al., manuscript in preparation).

The correlation between transcriptional activity and the N/C interaction status in antagonist bound ARs can be explained by the formation of a functional coactivator binding groove

in the LBD. Binding of antagonist but possibly also non-androgenic ligands displaces helix 12 over the coactivator binding groove, as is show for other antagonist bound NRs (Brzozowski et al., 1997; Moras and Gronemeyer, 1998; Pike et al., 1999; Kauppi et al., 2003). This displacement results in a non-functional coactivator groove and, as a consequence, lack of N/C interaction and transcriptional activity due to loss of coactivator binding either directly to the groove or indirectly via the N/C interaction to the NTD. AR mutations L701H, L701M, W741C and T877A results in broadened ligand responsiveness by providing a different set of pocket-ligand interactions or by avoiding sterical hindrance for ligand binding. The overall conformation of these AR LBD mutants bound to their cognate antagonists and possibly also non-androgenic ligands is very similar to that of agonist bound wild type AR LBD (Sack et al., 2001; Matias et al., 2002; Bohl et al., 2005; Urushibara et al., 2007). These mutations restore the coactivator groove in antagonist or non-androgenic ligand bound AR enabling N/C interaction and transcriptional activity (Fig 4 and 5) (Veldscholte et al., 1990; Steketee et al., 2002; Hara et al., 2003; Urushibara et al., 2007).

In total, the strong correlation between the N/C interaction and transcriptional activity qualifies the FRET assay as a bonafide ligand induced AR activation assay.

Role of AR N/C interaction in transcriptional activity

The strong correlation between the N/C interaction and transcriptional activity contrasts the lack of known direct functional role for the N/C interaction in transcription activation. Moreover, it is generally accepted that, in contrast to other SRs, the transactivation function in the AR LBD (AF-2) is poorly active and that the major transactivation function of the AR is localized in the AR NTD (AF-1), raising questions on the role of the AR LBD coactivator groove. Therefore it is surprising that the N/C interaction status reflects so well the transcriptional activity on a transiently transfected reporter driven by a minimal promoter. The most likely explanation is that the N/C interaction has a function in facilitating cofactor binding to the AR NTD, by exposing regions in the NTD. If so, mutations in the FQNLF motif disabling the N/C interaction, possibly results in less efficient binding of coactivators to the NTD. Alternatively, the N/C interaction may regulate cofactor binding to the coactivator groove in the AR LBD by blocking the groove when interactions are not required (Van Royen et al., 2007). Loss of N/C interaction then disables regulation of coactivator binding which may result in unfavorable protein interactions and inefficient coactivator binding to the coactivator binding groove. This is possibly reflected by the remaining transcriptional activity in N/C interaction deficient mutants (Fig 1).

Limitations of the FRET based assay for ligand induced activity

It is important to note that the correlation between the AR N/C interaction and transcriptional activity does not necessary point to a causal relationship, but rather that the N/C interaction reflects an individual step leading to a functionally active AR. The N/C interaction can there-

fore be used to identify initial activating or repressing activity of AR ligands, but additional functional steps, like DNA binding and cofactor recruitment could be disabled resulting in aberrant activity of the AR or total lack of AR activity, without any affect on the N/C interaction. For example, we have shown that aberrant AR activity of *e.g.* AR DNA binding deficient or dimerization mutants is not necessarily reflected by the N/C interactions status (Van Royen et al., 2007; Van Royen et al., manuscript in preparation). As a result, it is conceivable that compounds that do not act like ligands, are able to efficiently inhibit the AR activity, but do not interfere with the N/C interaction and therefore will not be detected in this assay.

Moreover, the causal relationship between the N/C interaction and transcriptional activity is blurred, because the requirement for the N/C interaction is suggested to be promoter specific, implicating that the choice of promoter could important (He et al., 2002). In addition, ChIP data indicated that N/C interaction deficient AR mutants were able to bind to plasmid based AREs but not chromatin, but this could not be confirmed by FRAP (data not shown) (Li et al., 2006).

FRET based detection of antagonist activity

Antagonist activity of wild type YFP-AR-CFP was detected in a ligand competition setting. OH-flutamide was able to inhibit an R1881 induced N/C interaction in a dose dependent manner (Fig. 4 F). A more detailed analysis of ligand competition showed a rapid (< 10 minutes) replacement of OH-flutamide by a sufficient dose of R1881, and very slow (> 10 hours), complete replacement of a low dose of R1881 by a high dose of OH-flutamide in reverse set-up (Fig. 4 G and H). This type of analysis enables the detection of relative ligand binding efficiencies for agonists versus antagonists.

A quantitative microscopy approach of this assay provides additional mechanistical data on ligand activity

The quantitative microscopic approach, as used here, not only enables single cell selection to allow the analysis of cells with physiological relevant AR expression levels, but also provides additional relevant parameters together with the AR N/C interaction, including nuclear translocation, and sub-nuclear distribution. These parameters provide extra information of the mechanism of inhibition of anti-androgens or other antagonistic compounds. The speckled distribution of DHT, R1881 and RU486 bound AR, the less pronounced speckled pattern of CPA bound AR and the lack of speckles in OH-flutamide and bicalutamide bound AR, reflect the DNA binding characteristics of ARs bound with these ligands as previously found with FRAP (Fig. 3A) (Farla et al., 2005; Klokk et al., 2007).

In general, the N/C interaction status in wild type AR and AR LBD mutants correlated to their speckled nuclear distribution (Fig. 3, 4 and 5). The only exceptions are the 11-desoxycorticosterone-bound AR L701H, which shows a less pronounced speckled pattern and AR L701M, of which no speckled pattern can be detected (Fig. 5 G). Exactly these combinations

show relative lower FRET efficiency comparable to their transcriptional activity, suggesting that the FRET based detections of ligand induced activation is more sensitive than speckle detection (Fig. 5 D and F, red bars). Importantly, most used ligands induced nuclear translocation of the ARs, and thus bind the AR, independent of their ability to induce N/C interaction. In contrast, the strongly inhibited nuclear translocation in wild type AR and AR L701M in the presence of cortisol indicated that these ARs probably had a low affinity for cortisol (Fig. 3, 4 and 5).

In conclusion, this FRET based assay using double tagged ARs provides a sensitive application in screens for both agonistic and antagonistic AR ligands or other compounds. Because the N/C interaction initiation is one of the first transitions following ligand binding, this assay could very well be used as surrogate assay for ligand induced AR activation. Although it was not shown here, in larger screening programs, FRET based techniques (*e.g.* YFP/CFP ratio imaging or sensitised emission) in general are especially applicable in high-throughput settings (Jones and Diamond, 2008).

MATERIALS AND METHODS

Constructs

The cDNA construct encoding for double tagged AR (pYFP-AR-CFP) was generated as described (Van Royen et al., 2007; Van Royen et al., 2009a). In all AR fusion constructs the AR was separated from the fluorescent tag by a flexible $(GlyAla)_6$ spacer (Farla et al., 2004). In this article the $(GlyAla)_6$ spacer will be referred to as a single dash. The F23,27A/L26A and F23,27L mutations were introduced by Quik Change mutagenesis (Stratagene) in YFP-AR-CFP. The FQNLF deletion mutant was generated by creating appropiate restriction sites by introducing silent mutations in the N-terminus and replacing a 53 bp fragment by a linker coding for this fragment with deleted FQNLF. The LBD mutation T877A was introduced in pYFP-AR-CFP by QuikChange mutagenesis. To generate the other LBD mutants, W741C, L701H, L701H/T877A and L701M, the AR LBDs of pYFP-AR-CFP or pYFP-AR(T877A)-CFP in the case of the double mutant, were replaced by a pGFP-AR or pSVAR0 fragment containing the mutant LBD (Farla et al., 2005; van de Wijngaart et al., manuscript in preparation). All new constructs were verified by appropriate restriction digestions and sequencing. Sizes of expressed AR (-fusions) were verified by Western blotting.

The (ARE)2-TATA Luc reporter was a gift from G. Jenster (Josephine Nefkens Institute, Rotterdam, Netherlands). The positive FRET control, pCYFP encoding the ECFP-EYFP fusion was provided by C. Gazin (Hôpital Saint-Louis, Paris, France).

Cell culture, transfection, and luciferase assay

Two days before microscopic analyses, Hep3B cells, lacking endogenous SR expression, were grown on glass coverslips in 6-well plates in α-MEM (Cambrex) supplemented with 5% FBS (HyClone), 2 mM L-glutamine, 100 U/mL penicillin, and 100 μg/mL streptomycin. At least 4 h before transfection, the medium was substituted by medium containing 5% dextran charcoal stripped FBS. Transfections were performed with 1 μg/well AR or CFP-YFP expression constructs or 0.5 μg/well empty YFP or CFP expression vector in FuGENE6 (Roche) transfection medium. 4 h after transfection, the medium was replaced by medium with 5% dextran charcoal stripped FBS with or without hormone.

For the AR transactivation experiments, Hep3B cells were cultured in 24-well plates on α-MEM supplemented with 5% dextran charcoal stripped FBS in the presence or absence of hormone and transfected using 50 ng AR expression construct and 100 ng luciferase reporter construct. 24 h after transfection, cells were lysed and luciferase activity was measured in a luminometer (GloMax Microplate luminometer; Promega). Hep3B stably expressing wild type YFP-AR-CFP was generated as previously described (Van Royen et al., 2009b).

Western blot analysis

Hep3B cells were cultured and transfected in 6-well plates. 24 h after transfection, cells were washed twice in ice-cold PBS and lysed in 200 μL Laemmli sample buffer (50 mM Tris-HCl, pH 6.8, 10% glycerol, 2% SDS, 10 mM DTT, and 0.001% Bromophenol blue). After boiling for 5 min, a 5 μL sample was separated on a 10% SDS-polyacrylamide gel and blotted to Immobilon-P Transfer Membrane (Millipore). Blots were incubated with an antibody agains AR (1 : 2,000; mouse monoclonal F34.4.1) and subsequently incubated with HRP-conjugated goat anti–mouse antibody (DakoCytomation). Proteins were visualized using Super Signal West Pico Luminol solution (Pierce Chemical Co.), followed by exposure to x-ray film.

Confocal imaging, YFP/CFP ratio imaging and acceptor photobleaching FRET analysis

Live-cell and immunofluorescence imaging was performed using a confocal laser-scanning microscope (LSM510; Carl Zeiss MicroImaging, Inc.) equipped with a Plan-Neofluar 40×/1.3 NA oil objective (Carl Zeiss MicroImaging, Inc.) at a lateral resolution of 100 nm. An argon laser was used for excitation of CFP and YFP at 458 and 514 nm, respectively. In all quantitative live cell imaging experiments cells with a physiological relevant expression level of tagged ARs were selected for analysis (Van Royen et al., 2007; Van Royen et al., 2009a).

N/C interactions in YFP-AR-FP was assessed using YFP/CFP ratio imaging and acceptor photobleaching FRET (abFRET) (Van Royen et al., 2009a and references therein). In YFP/CFP ratio imaging cells expressing YFP/CFP double tagged AR or a combination of YFP-AR and AR-CFP with initially similar signal ratio's to YFP-AR-CFP were imaged with an interval of 30 seconds using a 458 nm excitation at low laser power to avoid monitorbleaching. YFP and

CFP emissions were detected using a 560-nm longpass emission filter and a 470-500 nm bandpass emission filter, respectively. The AR N/C interaction is initiated after adding R1881. After background subtraction FRET is simply calculated as: I_{YFP} / I_{CFP}. The relative nuclear intensity is determined simultaneously using the YFP emission and is calculated as $I_{nucleus} / (I_{nucleus} + I_{cytoplasm})$.

In abFRET, YFP and CFP images were collected sequentially before photobleaching of the acceptor. CFP was excited at 458 nm at moderate laser power, and emission was detected using a 470-500 nm bandpass emission filter. YFP was excited at 514 nm at moderate laser power, and emission was detected using a 560 nm longpass emission filter. After image collection, YFP in the nucleus was bleached by scanning a nuclear region of ~100 μm^2 25 times at 514 nm at high laser power, covering the largest part of the nucleus. After photobleaching, a second YFP and CFP image pair was collected. Apparent FRET efficiency was estimated (correcting for the amount of YFP bleached) using the equation abFRET = $((CFP_{after} - CFP_{before}) \times YFP_{before}) \times ((CFP_{after} \times YFP_{before}) - (CFP_{before} \times YFP_{after}))^{-1}$, where CFP_{before} and YFP_{before} are the mean prebleach fluorescence intensities of CFP and YFP, respectively, in the area to be bleached (after background subtraction), and CFP_{after} and YFP_{after} are the mean postbleach fluorescence intensities of CFP and YFP, respectively, in the bleached area. The apparent FRET efficiency was finally expressed relative to control measurements in cells expressing either free CFP and YFP ($abFRET_0$) or the CFP-YFP fusion protein ($abFRET_{CFP\text{-}YFP\ fusion}$): apparent FRET efficiency = $(abFRET - abFRET_0) \times (abFRET_{CFP\text{-}YFP\ fusion} - abFRET_0)^{-1}$.

ACKNOWLEDGEMENT

This work is supported by grant DDHK 2002-2679 from the Dutch Cancer Society (KWF) and grant 03-DYNA-F-18 of the European Science Foundation (ESF).

REFERENCES

Agler, M., M. Prack, Yingjie Zhu, J. Kolb, K. Nowak, R. Ryseck, Ding Shen, M.E. Cvijic, J. Somerville, S. Nadler, and Taosheng Chen. 2007. A High-Content Glucocorticoid Receptor Translocation Assay for Compound Mechanism-of-Action Evaluation. *J Biomol Screen.* 12:1029-1041.

Awais M, M.S., Yoshio Umezawa,. 2007. Imaging of Selective Nuclear Receptor Modulator-Induced Conformational Changes in the Nuclear Receptor to Allow Interaction with Coactivator and Corepressor Proteins in Living Cells. *ChemBioChem.* 8:737-743.

Awais, M., M. Sato, X. Lee, and Y. Umezawa. 2006. A fluorescent indicator to visualize activities of the androgen receptor ligands in single living cells. *Angew Chem Int Ed.* 45:2707-2712.

Awais, M., M. Sato, K. Sasaki, and Y. Umezawa. 2004. A Genetically Encoded Fluorescent Indicator Capable of Discriminating Estrogen Agonists from Antagonists in Living Cells. *Anal Chem.* 76:2181-2186.

Awais, M., M. Sato, and Y. Umezawa. 2007a. A fluorescent indicator to visualize ligand-induced receptor/coactivator interactions for screening of peroxisome proliferator-activated receptor γ ligands in living cells. *Biosens Bioelectron.* 22:2564-2569.

Awais, M., M. Sato, and Y. Umezawa. 2007b. Optical probes to identify the glucocorticoid receptor ligands in living cells. *Steroids.* 72:949-954.

Bastiaens, P.I.H., and T.M. Jovin. 1996. Microspectroscopic imaging tracks the intracellular processing of a signal transduction protein: Fluorescent-labeled protein kinase C βI. *Proc Natl Acad Sci U S A.* 93:8407-8412.

Bastiaens, P.I.H., I.V. Majoul, P.J. Verveer, H.-D. Söling, and T.M. Jovin. 1996. Imaging the intracellular trafficking and state of the AB5 quaternary structure of cholera toxin. *EMBO J.* 15:4246-4253.

Berrevoets, C.A., A. Umar, and A.O. Brinkmann. 2002. Antiandrogens: selective androgen receptor modulators. *Mol Cell Endocrinol.* 198:97-103.

Bohl, C.E., W. Gao, D.D. Miller, C.E. Bell, and J.T. Dalton. 2005. Structural basis for antagonism and resistance of bicalutamide in prostate cancer. *Proc Natl Acad Sci U S A.* 102:6201-6206.

Brinkmann, A.O., L.J. Blok, P.E. de Ruiter, P. Doesburg, K. Steketee, C.A. Berrevoets, and J. Trapman. 1999. Mechanisms of androgen receptor activation and function. *J Steroid Biochem Mol Biol.* 69:307-313.

Brinkmann, A.O., P.W. Faber, H.C.J. van Rooij, G.G.J.M. Kuiper, C. Ris, P. Klaassen, J.A.G.M. van der Korput, M.M. Voorhorst, J.H. van Laar, E. Mulder, and J. Trapman. 1989. The human androgen receptor: domain structure, genomic organization and regulation of expression. *J Steroid Biochem.* 34:307-310.

Brinkmann, A.O., and J. Trapman. 2000. Prostate cancer schemes for androgen escape. *Nat Med.* 6:628-629.

Brzozowski, A.M., A.C.W. Pike, Z. Dauter, R.E. Hubbard, T. Bonn, O. Engstrom, L. Ohman, G.L. Greene, J.-A. Gustafsson, and M. Carlquist. 1997. Molecular basis of agonism and antagonism in the oestrogen receptor. *Nature.* 389:753-758.

Claessens, F., G. Verrijdt, E. Schoenmakers, A. Haelens, B. Peeters, G. Verhoeven, and W. Rombauts. 2001. Selective DNA binding by the androgen receptor as a mechanism for hormone-specific gene regulation. *J Steroid Biochem Mol Biol.* 76:23-30.

Cleutjens, K.B.J.M., J.A.G.M. van der Korput, C.C.E.M. van Eekelen, H.C.J. van Rooij, P.W. Faber, and J. Trapman. 1997. An androgen response element in a far upstream enhancer region is essential for high, androgen-regulated activity of the prostate-specific antigen promoter. *Mol Endocrinol.* 11:148-161.

Doesburg, P., C.W. Kuil, C.A. Berrevoets, K. Steketee, P.W. Faber, E. Mulder, A.O. Brinkmann, and J. Trapman. 1997. Functional in vivo interaction between the amino-terminal, transactivation domain and the ligand binding domain of the androgen receptor. *Biochemistry.* 36:1052-1064.

Dubbink, H.J., R. Hersmus, C.S. Verma, J.A.G.M. van der Korput, C.A. Berrevoets, J. van Tol, A.C.J. Ziel-van der Made, A.O. Brinkmann, A.C.W. Pike, and J. Trapman. 2004. Distinct recognition modes of FXXLF and LXXLL motifs by the androgen receptor. *Mol Endocrinol.* 18:2132-2150.

Edwards, J., and J. Bartlett. 2005. The androgen receptor and signal-transduction pathways in hormone-refractory prostate cancer. Part 2: androgen-receptor cofactors and bypass pathways. *BJU Int.* 95:1327-1335.

Farla, P., R. Hersmus, B. Geverts, P.O. Mari, A.L. Nigg, H.J. Dubbink, J. Trapman, and A.B. Houtsmuller. 2004. The androgen receptor ligand-binding domain stabilizes DNA binding in living cells. *J Struct Biol.* 147:50-61.

Farla, P., R. Hersmus, J. Trapman, and A.B. Houtsmuller. 2005. Antiandrogens prevent stable DNA-binding of the androgen receptor. *J Cell Sci.* 118:4187-4198.

Feldman, B.J., and D. Feldman. 2001. The development of androgen-independent prostate cancer. *Nat Rev Cancer.* 1:34-45.

Georget, V., J.M. Lobaccaro, B. Terouanne, P. Mangeat, J.-C. Nicolas, and C. Sultan. 1997. Trafficking of the androgen receptor in living cells with fused green fluorescent protein-androgen receptor. *Mol Cell Endocrinol.* 129:17-26.

Griekspoor, A., W. Zwart, J. Neefjes, and R. Michalides. 2007. Visualizing the action of steroid hormone receptors in living cells. *Nucl Recept Signal.* 5:e003.

Haapala, K., E.-R. Hyytinen, M. Roiha, M. Laurila, I. Rantala, H.J. Helin, and P.A. Koivisto. 2001. Androgen Receptor Alterations in Prostate Cancer Relapsed during a Combined Androgen Blockade by Orchiectomy and Bicalutamide. *Lab Invest.* 81:1647-1651.

Hara, T., J. Miyazaki, H. Araki, M. Yamaoka, N. Kanzaki, M. Kusaka, and M. Miyamoto. 2003. Novel Mutations of Androgen Receptor: A Possible Mechanism of Bicalutamide Withdrawal Syndrome. *Cancer Res.* 63:149-153.

He, B., N.T. Bowen, J.T. Minges, and E.M. Wilson. 2001. Androgen-induced NH2- and COOH-terminal interaction inhibits p160 coactivator recruitment by activation function 2. *J Biol Chem.* 276:42293-42301.

He, B., J.A. Kemppainen, and E.M. Wilson. 2000. FXXLF and WXXLF sequences mediate the NH2-terminal interaction with the ligand binding domain of the androgen receptor. *J Biol Chem.* 275:22986-22994.

He, B., L.W. Lee, J.T. Minges, and E.M. Wilson. 2002. Dependence of Selective Gene Activation on the Androgen Receptor NH2- and COOH-terminal Interaction. *J Biol Chem.* 277:25631-25639.

Heery, D., E. Kalkhoven, S. Hoare, and M. Parker. 1997. A signature motif in transcriptional co-activators mediates binding to nuclear receptors. *Nature.* 387:733-736.

Heinlein, C.A., and C. Chang. 2004. Androgen Receptor in Prostate Cancer. *Endocr Rev.* 25:276-308.

Hur, E., S.J. Pfaff, E.S. Payne, H. Gron, B.M. Buehrer, and R.J. Fletterick. 2004. Recognition and accommodation at the androgen receptor coactivator binding interface. *PLoS Biol.* 2:E274.

Jones, J.O., and M.I. Diamond. 2008. A Cellular Conformation-Based Screen for Androgen Receptor Inhibitors. *ACS Chem Biol.* 3:412-418.

Karpova, T., C. Baumann, L. He, X. Wu, A. Grammer, P. Lipsky, G. Hager, and J. McNally. 2003. Fluorescence resonance energy transfer from cyan to yellow fluorescent protein detected by acceptor photobleaching using confocal microscopy and a single laser. *J Microsc.* 209:56-70.

Kauppi, B., C. Jakob, M. Farnegardh, J. Yang, H. Ahola, M. Alarcon, K. Calles, O. Engstrom, J. Harlan, S. Muchmore, A.-K. Ramqvist, S. Thorell, L. Ohman, J. Greer, J.-A. Gustafsson, J. Carlstedt-Duke, and M. Carlquist. 2003. The Three-dimensional Structures of Antagonistic and Agonistic Forms of the Glucocorticoid Receptor Ligand-binding Domain: RU-486 induces a Transconformation that leads to active Antagonism. *J Biol Chem.* 278:22748-22754.

Kenworthy, A.K. 2001. Imaging protein-protein interactions using fluorescence resonance energy transfer microscopy. *Methods.* 24:289-296.

Klokk, T.I., P. Kurys, C. Elbi, A.K. Nagaich, A. Hendarwanto, T. Slagsvold, C.-Y. Chang, G.L. Hager, and F. Saatcioglu. 2007. Ligand-Specific Dynamics of the Androgen Receptor at Its Response Element in Living Cells. *Mol Cell Biol.* 27:1823-1843.

Krishnan, A.V., X.-Y. Zhao, S. Swami, L. Brive, D.M. Peehl, K.R. Ely, and D. Feldman. 2002. A Glucocorticoid-Responsive Mutant Androgen Receptor Exhibits Unique Ligand Specificity: Therapeutic Implications for Androgen-Independent Prostate Cancer. *Endocrinology.* 143:1889-1900.

Kuil, C.W., C.A. Berrevoets, and E. Mulder. 1995. Ligand-induced Conformational Alterations of the Androgen Receptor Analyzed by Limited Trypsinization. *J Biol Chem.* 270:27569-27576.

Kuil, C.W., and E. Mulder. 1994. Mechanism of antiandrogen action: Conformational changes of the receptor. *Mol Cell Endocrinol.* 102:R1-R5.

Li, J., J. Fu, C. Toumazou, H.-G. Yoon, and J. Wong. 2006. A Role of the Amino-Terminal (N) and Carboxyl-Terminal (C) Interaction in Binding of Androgen Receptor to Chromatin. *Mol Endocrinol.* 20:776-785.

Marcelli, M., D.L. Stenoien, A.T. Szafran, S. Simeoni, I.U. Agoulnik, N.L. Weigel, T. Moran, I. Mikic, J.H. Price, and M.A. Mancini. 2006. Quantifying effects of ligands on androgen receptor nuclear translocation, intranuclear dynamics, and solubility. *J Cell Biochem.* 98:770-788.

Martinez, E.D., G.V. Rayasam, A.B. Dull, D.A. Walker, and G.L. Hager. 2005. An estrogen receptor chimera senses ligands by nuclear translocation. *J Steroid Biochem Mol Biol.* 97:307-321.

Matias, P.M., M.A. Carrondo, R. Coelho, M. Thomaz, X.-Y. Zhao, A. Wegg, K. Crusius, U. Egner, and P. Donner. 2002. Structural Basis for the Glucocorticoid Response in a Mutant Human Androgen Receptor (ARccr) Derived from an Androgen-Independent Prostate Cancer. *J. Med. Chem.* 45:1439-1446.

Michalides, R., A. Griekspoor, A. Balkenende, D. Verwoerd, L. Janssen, K. Jalink, A. Floore, A. Velds, L. van 't Veer, and J. Neefjes. 2004. Tamoxifen resistance by a conformational arrest of the estrogen receptor-α PKA activation in breast cancer. *Cancer Cell.* 5:597-605.

Moras, D., and H. Gronemeyer. 1998. The nuclear receptor ligand-binding domain: structure and function. *Curr. Opin. Cell Biol.* 10:384-391.

Mostaghel, E.A., and P.S. Nelson. 2008. Intracrine androgen metabolism in prostate cancer progression: mechanisms of castration resistance and therapeutic implications. *Best Pract Res Clin Endocrinol Metab.* 22:243-258.

Nakauchi, H., K. Matsuda, I. Ochiai, A. Kawauchi, Y. Mizutani, T. Miki, and M. Kawata. 2007. A Differential Ligand-mediated Response of Green Fluorescent Protein-tagged Androgen Receptor in Living Prostate Cancer and Non-prostate Cancer Cell Lines. *J Histochem Cytochem.* 55:535-544.

Paulmurugan, R., and S.S. Gambhir. 2006. An intramolecular folding sensor for imaging estrogen receptor-ligand interactions. *Proc Natl Acad Sci U S A.* 103:15883-15888.

Pike A.C., R.E. Hubbard, T. Bonn, A.G. Thorsell, O. Engstrom, J. Ljunggren, J.-A. Gustafsson, M. Carlquist. Structure of the ligand-binding domain of oestrogen receptor-β in the presence of a partial agonist and a full antagonist. *EMBO J.* 18:4608-4618.

Rahman, M., H. Miyamoto, and C. Chang. 2004. Androgen Receptor Coregulators in Prostate Cancer: Mechanisms and Clinical Implications. *Clin Cancer Res.* 10:2208-2219.

Rosenfeld, M.G., V.V. Lunyak, and C.K. Glass. 2006. Sensors and signals: a coactivator/corepressor/epigenetic code for integrating signal-dependent programs of transcriptional response. *Genes Dev.* 20:1405-1428.

Sack, J.S., K.F. Kish, C. Wang, R.M. Attar, S.E. Kiefer, Y. An, G.Y. Wu, J.E. Scheffler, M.E. Salvati, S.R. Krystek, R. Weinmann, and H.M. Einspahr. 2001. Crystallographic structures of the ligand-binding domains of the androgen receptor and its T877A mutant complexed with the natural agonist dihydrotestosterone. *Proc Natl Acad Sci U S A.* 98:4904-4909.

Schaufele, F., X. Carbonell, M. Guerbadot, S. Borngraeber, M.S. Chapman, A.A.K. Ma, J.N. Miner, and M.I. Diamond. 2005. The structural basis of androgen receptor activation: Intramolecular and intermolecular amino-carboxy interactions. *Proc Natl Acad Sci U S A.* 102:9802-9807.

Song, L.-N., M. Coghlan, and E.P. Gelmann. 2004. Antiandrogen Effects of Mifepristone on Coactivator and Corepressor Interactions with the Androgen Receptor. *Mol Endocrinol.* 18:70-85.

Steketee, K., L. Timmerman, A. Ziel-van der Made, P. Doesburg, A. Brinkmann, and J. Trapman. 2002. Broadened ligand responsiveness of androgen receptor mutants obtained by random amino acid substitution of H874 and mutation hot spot T877 in prostate cancer. *Int J Cancer.* 100:309-317.

Suzuki, H., N. Sato, Y. Watabe, M. Masai, S. Seino, and J. Shimazaki. 1993. Androgen receptor gene mutations in human prostate cancer. *J Steroid Biochem Mol Biol.* 46:759-765.

Taplin, M.-E., and S. Balk. 2004. Androgen receptor: A key molecule in the progression of prostate cancer to hormone independence. *J Cell Biochem.* 91:483-190.

Taplin, M.-E., G.J. Bubley, Y.-J. Ko, E.J. Small, M. Upton, B. Rajeshkumar, and S.P. Balk. 1999. Selection for Androgen Receptor Mutations in Prostate Cancers Treated with Androgen Antagonist. *Cancer Res.* 59:2511-2515.

Taplin, M.-E., B. Rajeshkumar, S. Halabi, C.P. Werner, B.A. Woda, J. Picus, W. Stadler, D.F. Hayes, P.W. Kantoff, N.J. Vogelzang, and E.J. Small. 2003. Androgen Receptor Mutations in Androgen-Independent Prostate Cancer: Cancer and Leukemia Group B Study 9663. *J Clin Oncol.* 21:2673-2678.

Trapman, J. 2001. Molecular mechanisms of prostate cancer. *Eur J Cancer.* 37:S119-125.

Urushibara, M., J. Ishioka, N. Hyochi, K. Kihara, S. Hara, P. Singh, J. Isaacs, and Y. Kageyama. 2007. Effects of steroidal and non-steroidal antiandrogens on wild-type and mutant androgen receptors. *Prostate.* 67:799-807.

van de Wijngaart, D.J., M. Molier, S.J. Lusher, R. Hersmus, G. Jenster, J. Trapman, and H.J. Dubbink. 2008. Differential ligand-responsiveness of androgen receptor L701 mutants. (manuscript in preparation).

Van Royen, M.E., A.B. Houtsmuller, and T. Trapman. 2009 A two-step model for androgen receptor domain interactions in living cells. (manuscript in preparation)

Van Royen, M.E., S.M. Cunha, M.C. Brink, K.A. Mattern, A.L. Nigg, H.J. Dubbink, P.J. Verschure, J. Trapman, and A.B. Houtsmuller. 2007. Compartmentalization of androgen receptor protein-protein interactions in living cells. *J Cell Biol.* 177:63-72.

Van Royen, M.E., C. Dinant, P. Farla, J. Trapman, and A.B. Houtsmuller. 2009a. FRAP and FRET methods to study nuclear receptors in living cells. *In* The Nuclear Receptor superfamily. Vol. 505. I.J. McEwan, editor. Humana Press / Springer, in press.

Van Royen, M.E., P. Farla, K.A. Mattern, B. Geverts, J. Trapman, and A.B. Houtsmuller. 2009b. FRAP to study nuclear protein dynamics in living cells. *In* The Nucleus. Vol. 464. R. Hancock, editor. Humana Press / Springer, Totowa. 363-385.

Veldscholte, J., C.A. Berrevoets, C. Ris-Stalpers, G.G.J.M. Kuiper, G. Jenster, J. Trapman, A.O. Brinkmann, and E. Mulder. 1992. The androgen receptor in LNCaP cells contains a mutation in the ligand binding domain which affects steroid binding characteristics and response to antiandrogens. *J Steroid Biochem Mol Biol.* 41:665-669.

Veldscholte, J., C. Ris-Stalpers, G.G.J.M. Kuiper, G. Jenster, C. Berrevoets, E. Claassen, H.C. van Rooij, J. Trapman, A.O. Brinkmann, and E. Mulder. 1990. A mutation in the ligand binding domain of the androgen receptor of human LNCaP cells affects steroid binding characteristics and response to anti-androgens. *Biochem Biophys Res Commun.* 173:534-540.

Watanabe, M., T. Ushijima, T. Shiraishi, R. Yatani, J. Shimazaki, T. Kotake, T. Sugimura, and M. Nagao. 1997. Genetic alterations of androgen receptor gene in Japanese human prostate cancer. *Jpn J Clin Oncol.* 27:389-393.

Zhao, X., B. Boyle, A. Krishnan, N. Navone, D. Peehl, and D. Feldman. 1999. Two mutations identified in the androgen receptor of the new human prostate cancer cell line MDA PCa 2a. *J Urol.* 162:2192-2199.

Zhao, X., P. Malloy, A. Krishnan, S. Swami, N. Navone, D. Peehl, and D. Feldman. 2000. Glucocorticoids can promote androgen-independent growth of prostate cancer cells through a mutated androgen receptor. *Nat Med.* 6:703-706.

Chapter 8

General Discussion

The AR transcriptional activity is regulated by ligand binding, by binding to AREs in enhancer and promoter regions of target genes, and by multiple protein-protein interactions, including interactions with cofactors and homodimerization. The best studied AR protein interactions are those with cofactors via LxxLL or FxxLF-like motifs with the cofactor groove in the AR LBD (He et al., 2002; Dubbink et al., 2004; Van de Wijngaart et al., 2006). An FQNLF motif in the AR NTD also interacts with the cofactor groove in the AR LBD, the N/C interaction (He et al., 2000; Steketee et al., 2002). This N/C interaction can be intramolecular but also intermolecular in AR homodimers (Langley et al., 1995; Shaffer et al., 2004; Schaufele et al., 2005). A second well-defined dimerization domain is present in the D-box of the AR DBD. Next to its role in dimerization, the N/C interaction competes with cofactors for binding with the AR LBD

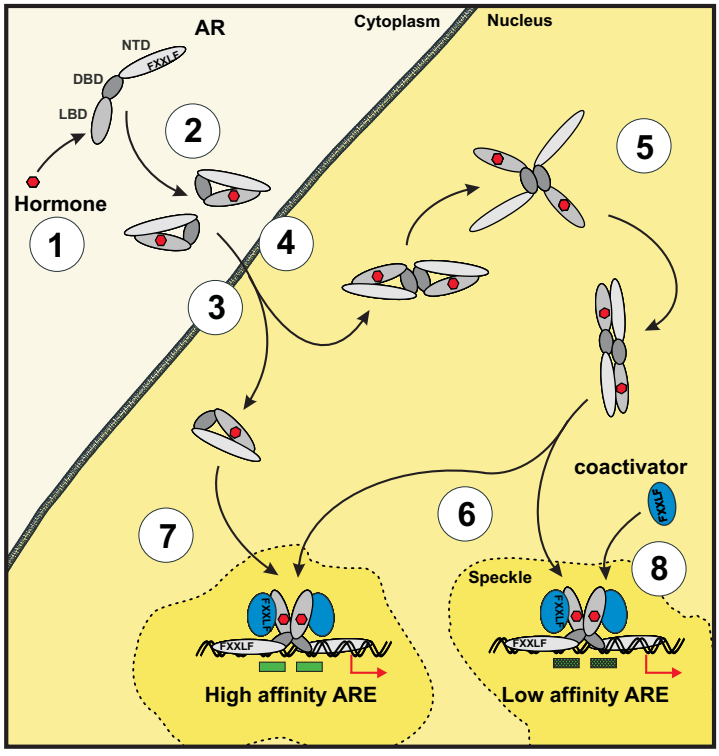

Figure 1: Schematic representation of the spatiotemporal organization of domain interactions in AR function. In the absence of hormone the AR is predominantly localized in the cytoplasm. Hormone binding by the AR (**1**) results in a rapid initiation of the intramolecular N/C interaction (**2**) followed by nuclear translocation of the AR (**3**). In the nucleus the AR dimerizes via the D-box interaction (**4**) that drives a transition from intra- to intermolecular N/C interaction (**5**). It is unclear whether the indicated intermediate conformations, the AR homodimer with intramolecular N/C interaction or without the N/C interaction, exists as stable configurations. The AR dimer is able to stably bind to either a high affinity ARE or a more selective low affinity ARE in promoter or enhancer regions of target genes which are then clustered in local accumulations (speckles) (**6**), which possibly represent transcription factories. Alternatively, AR monomers only very transiently bind consecutively to a high affinity ARE, where they possibly dimerize on the DNA (**7**). In the DNA bound AR the N/C interaction is lost, allowing interactions with coactivators to initiate transcription (**8**).

(He et al., 2001). In this thesis the spatial and temporal organization of AR protein interactions in living cells as studied by confocal microscopy and quantitative imaging approaches is described. The results are summarized in a model (Fig. 1). Moreover, the presented data accumulates in a novel model of androgen regulated gene expression. In this chapter the findings presented in previous chapters are discussed in more detail and directions of future research are suggested.

1 AR activation in the cytoplasm

In the absence of a ligand, the AR is preferentially localized in the cytoplasm in complex with protein chaperones (reviewed in Prescott and Coetzee, 2006). The chaperone complex keeps the AR in such a conformation that transport to the nucleus is inhibited, possibly by shielding the bipartite nuclear localization signal (NLS) (Zhou et al., 1994; reviewed in Pratt and Toft, 1997; Heinlein and Chang, 2001). Unliganded AR is in an inactive conformation without a structured coactivator groove in its LBD and as a consequence without interactions with coactivators or the AR N/C interaction (Moras and Gronemeyer, 1998). Like other SRs inactive, cytoplasmic AR is in a monomer configuration.

Ligand binding triggers important structural and functional changes in the AR. Initiated by the binding of an agonistic ligand, helix 12 in the AR LBD is repositioned. This conformational change seals the ligand-binding pocket, and also results in the formation of the cofactor binding groove (Darimont et al., 1998; Moras and Gronemeyer, 1998; Nolte et al., 1998; Shiau et al., 1998; Bledsoe et al., 2002; Li et al., 2003; Hur et al., 2004). In contrast to other SRs, the AR cofactor groove preferentially binds FxxLF-like motifs as present in some cofactors and AR NTD (He et al., 2000; He et al., 2002; Steketee et al., 2002; Dubbink et al., 2004). Previous data and results presented in this study clearly show that as a result of ligand binding cytoplastic AR rapidly adopts a novel conformation based on intramolecular N/C interaction (Fig. 1) (Chapter 6, Schaufele et al., 2005; Van Royen et al., 2007). Why intramolecular N/C interaction is preferred above intermolecular N/C interaction might simply be an effect of local concentration. The clear intramolecular N/C configuration of cytoplasmic AR seems different from that of other SRs, for which such a configuration has never been described.

AR N/C interaction is thought to play a role in ligand stabilization in the ligand binding pocket, although its effect on ligand dissociation rate is limited (Zhou et al., 1995; He et al., 2000). However, nuclear translocation is not delayed in ARs with an inactivated N/C interaction, as might have been expected if ligand dissociation is an important limiting factor in functioning of these AR mutants (Chapter 5).

A specific function of the intramolecular N/C configuration in cytoplasmic AR is essentially unknown. Intramolecular N/C interaction might be functionally identical to intermolecular N/C interaction or might be different, including induction of different protein interaction platforms.

An interesting hypothesis that can be derived from the results described in Chapter 6 is that the intramolecular N/C interaction blocks unfavorable binding of cytoplasmic proteins

to the active cofactor-binding groove. These interactions with cytoplasmic proteins with AR FQNLF mutants deficient in N/C interaction might be reflected by the reduced transcriptional activity of these mutants (Chapter 7).

Another attractive hypothesis is that the initial intramolecular N/C interaction in AR monomers may add to conformational changes of the monomer exposing the D-box in the centrally located DBD, thereby enabling the AR dimerization through the D-box. In the AR dimer, the D-box interaction in its turn, drives a transition from intra- to intermolecular N/C interaction (see below) (Schaufele et al., 2005, and Chapter 6).

2 Nuclear translocation and ARs in the nucleoplasm

Following ligand binding and intramolecular N/C interaction, the AR translocates to the nucleus (Prescott and Coetzee, 2006). Direct after this nuclear translocation the majority of ARs shifts from a monomer to a homodimer conformation (Schaufele et al., 2005, and Chapter 6). According to the results presented in this thesis AR dimerization is initiated via the D-box interaction in the second zinc finger of the AR DBD, followed by intermolecular N/C interaction (Fig. 1) (Chapter 6). Without D-box interaction the shift to intermolecular N/C interaction does not take place. The intermolecular N/C interaction on its turn might stabilize the D-box interaction. It is unclear whether the intermediate AR homodimer with intramolecular N/C interaction, exists as a stable configuration (Fig. 1).

Importantly, AR dimerization can already be found in the soluble AR fraction prior to DNA binding (Chapter 6). Therefore, the majority of androgen-regulated gene expression seems mediated by direct binding of AR dimers to AREs in target genes. This hypothesis based on findings described in this thesis is an important contribution to the longstanding debate whether ARs bind to AREs as dimers or whether dimers are formed following sequential binding of AR monomers. It should be noted, however, that indirect evidence indicates also that a stable AR fraction remains in the nucleus in a monomeric configuration (Chapter 6). Monomeric AR might also regulate AR target gene expression. Possibly, there is a dynamic balance between monomeric and dimeric AR in the nucleus. An important question that should be further addressed concerns the size of the monomeric nuclear fraction, which conditions influence this size and what the differences are between AR dimer and monomer regulated gene expression (see also below).

3 Selective trancription activation

It is generally accepted that ARs exert their function in transcription activation by AR dimers that bind to AREs, composed of two AR binding half-sites. The AR D-box dimerization is very important for stable ARE binding of AR dimers (Shaffer et al., 2004). The strong D-box interaction of ARs enables binding to AREs with one high affinity ARE half site and one low affinity half site, and could explain very well the loss of transcriptional activity on these AREs if the D-box is inactivated. Intriguingly, ARs without clear D-box interaction are still able to

activate genes that are driven by high affinity AREs (Fig. 1). These findings suggest that there can be an important regulatory mechanism of differential gene expression by influencing the equilibrium between monomeric and dimeric ARs in the nucleoplasmic AR population. To address this question, reporter experiments as presented in this thesis should be extended by studies on the effects of various (PAIS) mutant ARs on endogenous gene expression.

The increased activity of AR mutants with partially mutated D-box on high affinity AREs is surprising (Chapter 7). The data suggests that weakening, but not abolishing the D-box dimerization results in a more flexible AR dimer that induces a better fit to these AREs. Alternatively, loss of stable DNA binding of these mutants results in a highly dynamic 'hit-and-run' transcription initiation, as also is suggested for truncated ARs lacking the LBD, that might lead to multiple rapid transcription initiation events (Farla et al., 2004).

ChIP analysis showed that AR mutants deficient in N/C interaction are impaired in chromatin binding, but this could not be confirmed by FRAP analysis of these mutants (Li et al., 2007, and Chapter 5). This apparent discrepancy might be explained by loss of chromatin binding in a small subset of promoters, undetectable in FRAP. Alternatively, it cannot be excluded that the transient immobilization observed in FRAP does not detect the functional AR binding to AREs, but another process, like DNA scanning of the genome for binding sites, which is not seen in ChIP (Phair et al., 2004).

4 Cofactor recruitment by the AR

The best-studied cofactor binding site in the AR is the cofactor groove in the LBD (He et al., 2004; Hur et al., 2004). Binding of the AR FQNLF motif in the NTD to the cofactor groove raises questions regarding competition with cofactors for binding with the LBD and the role of the cofactor groove in AR function (He et al., 2000; Steketee et al., 2002). It is indeed suggested that the AR N/C interaction limits the recruitment of coactivators by the AR LBD (He et al., 2001; Toumazou et al., 2007 in press). In chapter 5, we propose a model in which the AR N/C interaction is lost when the AR is bound to DNA, enabling cofactor binding to the LBD (Fig. 1) (Van Royen et al., 2007). It is unclear what regulates the loss of N/C interaction in DNA bound AR. Possibly DNA binding itself changes AR structure and thereby disrupts its N/C interaction. Alternatively, a cofactor or set of cofactors bind to DNA bound AR and disrupts the N/C interaction. A candidate AR cofactor with such a function is MAGE11, that binds to a region in AR NTD overlapping the FQNLF motif (Bai et al., 2005). It is not determined whether this occurs preferentially in DNA bound AR.

The spatiotemporal organisation of AR domain interactions contributes to the ordered recruitment of cofactors and transcriptional activity. In the nucleus, the competing N/C interaction could serve as a blockade for premature interaction with specific cofactors. (He et al., 2002; Van Royen et al., 2007, Chapter 5). Loss of the N/C interaction in the DNA bound AR makes the cofactor groove in the AR LBD available for cofactor interactions (Fig. 1) (Chapter 5), not only with cofactors via strong interacting FxxLF-like motifs but possibly even for weaker

interactions with cofactors bearing LxxLL-like motifs as found in the p160 family of cofactors (McInerney et al., 1998; He et al., 2002; Xu and Li, 2003; Dubbink et al., 2004 and Chapter 5).

The AR N/C interaction is unique for the AR, and although similar interactions have been suggested for other SRs, no clear molecular mechanism for these SRs has been shown (Kraus et al., 1995; Rogerson and Fuller, 2003; Dong et al., 2004). Not only for cytoplasmic AR, but also for nuclear AR the question why only the AR has this regulatory interaction is unanswered. Possibly, the uncharacteristic structure of the AR LBD cofactor groove compared to other SR LBDs explains the need for the N/C interaction as an additional regulatory unit (Dubbink et al., 2004; Hur et al., 2004).

In total, the spatio-temporal regulation of cofactor recruitment to the coactivator groove by the AR N/C interaction will contribute to the optimal regulated AR function. Most likely the complexity of the recruitment of multiple coactivators includes significant redundancy. Loss of either one of the regulatory mechanisms, apart from ligand binding and DNA binding, will therefore not result in complete inactive ARs but rather in less efficient regulated AR function, as probably is the case for N/C interaction deficient ARs (Chapter 7).

5 Transient immobilization of ARs

FRAP analysis of fluorescently tagged ligand-activated ARs shows a delayed mobility compared to DNA-binding deficient AR mutants or wild type AR inactivated by antagonists. These observations suggest that the transient immobilization is due to binding to DNA, most likely to cognate sequences in androgen regulated genes (Farla et al., 2004). Computer aided quantitative analysis of FRAP data showed a binding time of the AR to the DNA in the range of 30-60 seconds (Farla et al., 2005). This dynamic behavior seems to be in disagreement with ChIP data showing a cyclic pattern of AR-promoter interaction and subsequent recruitment of other transcription factors on response elements with a cycle time of 20 to 40 minutes (Shang et al., 2000; Metivier et al., 2003; Reid et al., 2003; Métivier et al., 2006). However, a comparative study on binding of transcriptional activator Ace1 on the endogenous *CUP1* promoter array recently showed both rapid turnover (similarly to our AR FRAP data) and slow cycling on the yeast endogenous *CUP1* gene array. It was concluded that the rapid turnover reflected the transcriptional initiation and on top of that a slow cycling of availability of the promoter for transcription factor binding regulates the quantity of mRNA produced (Karpova et al., 2008).

Surprisingly, two types of transcriptionally active AR mutants, the truncated AR lacking the LBD and most likely also the AR D-box dimerization mutants are immobilized for much shorter times in the order of seconds or hundreds of milliseconds. This may be explained by a model in which longer chromatin binding times are not essential for global transcription initiation, but rather are required to modulate expression levels (Farla et al., 2004 and Chapter 6). In conclusion, the exact role of the transient immobilization in transcription initiation is not fully understood and requires further investigation.

Transient AR immobilization is always observed together with a speckled nuclear distribution (Farla et al., 2004; Farla et al., 2005). Similar findings have been described for other NRs (Htun et al., 1999; Schaaf et al., 2005; Sunn et al., 2005; Arnett-Mansfield et al., 2007). Moreover, it has been found that AR speckles and ERα speckles partially colocalize although they bind to very different sequences (Ochiai et al., 2004). We estimated that the number of AR speckles in the nucleus is in the order of hundreds rather than thousands. Based on fluorescence data, a single cell expresses 10^4-10^5 ARs, of which 10-20% is bound to DNA (FRAP data). This indicates that thousands ARs are bound and that each speckle should contain 10-100 ARs. From these calculations it can be estimated that the genomic DNA of one cell contains a few thousand AR binding sites. This number is in agreement with global genomic ChIP analysis that estimated around 4500 unique AR binding sites binding sites across the entire genome. Surprisingly, many of these are not in the core of promoters, but more distant from the target genes (Carroll et al., 2006; Wang et al., 2007). Although, it has been suggested that most AR binding sites identified by ChIP act as transcriptional enhancers of neighboring genes, experimental data on the functionality of many of the binding sites is far from complete.

It is very unlikely if not impossible, that a speckle represents ARs binding to one single gene. Therefore, speckles might represent local accumulations of DNA bound ARs present in multiple target genes. This would fit into the hypothesis that transcription factors like AR bound to regulatory units in promoter and enhances regions of active genes dynamically colocalize to preassembled transcription sites or transcription factories (Osborne et al., 2004; Carter et al., 2008).

The situation, however, is more complex than described above. In Chapter 5 we showed that, although AR speckles were often located in close vicinity of the sites of BrUTP incorporation, only a part of the AR speckles overlap with sites of active transcription, This is also found for other SRs, and suggests that DNA binding and speckle formation not always results in transcriptional activity (Arnett-Mansfield et al., 2007). Similar findings have been described for the distribution of GR and several other transcription factors (Van Steensel et al., 1995; Grande et al., 1997). Recently, it has been determined that the sites of promoter accumulation (supposedly transcription factories) are specialized in the production of particular types of transcripts determined by the need for specific transcription factors and splicing factors (Xu and Cook, 2008). It is therefore not inconceivable that the transcriptional activity in a part of the AR driven genes are cell type or cell cycle dependent, although they accumulated into speckles (Wang et al., 2007).

Together the data described above suggests that at least a subset of nuclear speckles play a functional role in transcription. In total, the numbers of AR binding sites correlate reasonably well to the speckle density in the nucleus, but the calculations are largely based on rough estimations of the number of speckles in a nucleus and number of ARs per speckle. Further detailed analysis of the AR speckles is required for a better understanding of their role in transcription.

REFERENCES

Arnett-Mansfield, R.L., J.D. Graham, A.R. Hanson, P.A. Mote, A. Gompel, L.L. Scurr, N. Gava, A. de Fazio, and C.L. Clarke. 2007. Focal Subnuclear Distribution of Progesterone Receptor Is Ligand Dependent and Associated with Transcriptional Activity. *Mol Endocrinol.* 21:14-29.

Bai, S., B. He, and E.M. Wilson. 2005. Melanoma Antigen Gene Protein MAGE-11 Regulates Androgen Receptor Function by Modulating the Interdomain Interaction. *Mol Cell Biol.* 25:1238-1257.

Bledsoe, R.K., V.G. Montana, T.B. Stanley, C.J. Delves, C.J. Apolito, D.D. McKee, T.G. Consler, D.J. Parks, E.L. Stewart, and T.M. Willson. 2002. Crystal Structure of the Glucocorticoid Receptor Ligand Binding Domain Reveals a Novel Mode of Receptor Dimerization and Coactivator Recognition. *Cell.* 110:93-105.

Carroll, J.S., C.A. Meyer, J. Song, W. Li, T.R. Geistlinger, J. Eeckhoute, A.S. Brodsky, E.K. Keeton, K.C. Fertuck, G.F. Hall, Q. Wang, S. Bekiranov, V. Sementchenko, E.A. Fox, P.A. Silver, T.R. Gingeras, X.S. Liu, and M. Brown. 2006. Genome-wide analysis of estrogen receptor binding sites. *Nat Genet.* 38:1289-1297.

Carter, D.R., C. Eskiw, and P.R. Cook. 2008. Transcription factories. *Biochem Soc Trans.* 36:585-589.

Darimont, B.D., R.L. Wagner, J.W. Apriletti, M.R. Stallcup, P.J. Kushner, J.D. Baxter, R.J. Fletterick, and K.R. Yamamoto. 1998. Structure and specificity of nuclear receptor-coactivator interactions. *Genes Dev.* 12:3343-3356.

Dong, X., Challis, JR, and S. Lye. 2004. Intramolecular interactions between the AF3 domain and the C-terminus of the human progesterone receptor are mediated through two LXXLL motifs. *J Mol Endocrinol.* 32:843-857.

Dubbink, H.J., R. Hersmus, C.S. Verma, J.A.G.M. van der Korput, C.A. Berrevoets, J. van Tol, A.C.J. Ziel-van der Made, A.O. Brinkmann, A.C.W. Pike, and J. Trapman. 2004. Distinct recognition modes of FXXLF and LXXLL motifs by the androgen receptor. *Mol Endocrinol.* 18:2132-2150.

Farla, P., R. Hersmus, B. Geverts, P.O. Mari, A.L. Nigg, H.J. Dubbink, J. Trapman, and A.B. Houtsmuller. 2004. The androgen receptor ligand-binding domain stabilizes DNA binding in living cells. *J Struct Biol.* 147:50-61.

Farla, P., R. Hersmus, J. Trapman, and A.B. Houtsmuller. 2005. Antiandrogens prevent stable DNA-binding of the androgen receptor. *J Cell Sci.* 118:4187-4198.

Grande, M., I. van der Kraan, L. de Jong, and R. van Driel. 1997. Nuclear distribution of transcription factors in relation to sites of transcription and RNA polymerase II. *J Cell Sci.* 110:1781-1791.

He, B., N.T. Bowen, J.T. Minges, and E.M. Wilson. 2001. Androgen-induced NH2- and COOH-terminal interaction inhibits p160 coactivator recruitment by activation function 2. *J Biol Chem.* 276:42293-42301.

He, B., J. Gampe, Robert T., A.J. Kole, A.T. Hnat, T.B. Stanley, G. An, E.L. Stewart, R.I. Kalman, J.T. Minges, and E.M. Wilson. 2004. Structural Basis for Androgen Receptor Interdomain and Coactivator Interactions Suggests a Transition in Nuclear Receptor Activation Function Dominance. *Mol Cell.* 16:425-438.

He, B., J.A. Kemppainen, and E.M. Wilson. 2000. FXXLF and WXXLF sequences mediate the NH2-terminal interaction with the ligand binding domain of the androgen receptor. *J Biol Chem.* 275:22986-22994.

He, B., J.T. Minges, L.W. Lee, and E.M. Wilson. 2002. The FXXLF motif mediates androgen receptor-specific interactions with coregulators. *J Biol Chem.* 277:10226-10235.

Heinlein, C., and C. Chang. 2001. Role of chaperones in nuclear translocation and transactivation of steroid receptors. *Endocrine.* 14:143-149.

Htun, H., L.T. Holth, D. Walker, J.R. Davie, and G.L. Hager. 1999. Direct Visualization of the Human Estrogen Receptor alpha Reveals a Role for Ligand in the Nuclear Distribution of the Receptor. *Mol Biol Cell.* 10:471-486.

Hur, E., S.J. Pfaff, E.S. Payne, H. Gron, B.M. Buehrer, and R.J. Fletterick. 2004. Recognition and accommodation at the androgen receptor coactivator binding interface. *PLoS Biol.* 2:E274.

Karpova, T.S., M.J. Kim, C. Spriet, K. Nalley, T.J. Stasevich, Z. Kherrouche, L. Heliot, and J.G. McNally. 2008. Concurrent Fast and Slow Cycling of a Transcriptional Activator at an Endogenous Promoter. *Science.* 319:466-469.

Kraus, W.L., E.M. McInerney, and B.S. Katzenellenbogen. 1995. Ligand-dependent, transcriptionally productive association of the amino- and carboxyl-terminal regions of a steroid hormone nuclear receptor *Proc Natl Acad Sci U S A.* 92:12314-12318.

Langley, E., Z.-x. Zhou, and E.M. Wilson. 1995. Evidence for an Anti-parallel Orientation of the Ligand-activated Human Androgen Receptor Dimer. *J Biol Chem.* 270:29983-29990.

Li, J., D. Zhang, J. Fu, Z. Huang, and J. Wong. 2007. Structural and Functional Analysis of Androgen Receptor in Chromatin. *Mol Endocrinol.* (in press).

Li, Y., M.H. Lambert, and H.E. Xu. 2003. Activation of Nuclear Receptors: A Perspective from Structural Genomics. *Structure.* 11:741-746.

McInerney, E.M., D.W. Rose, S.E. Flynn, S. Westin, T.-M. Mullen, A. Krones, J. Inostroza, J. Torchia, R.T. Nolte, N. Assa-Munt, M.V. Milburn, C.K. Glass, and M.G. Rosenfeld. 1998. Determinants of coactivator LXXLL motif specificity in nuclear receptor transcriptional activation. *Genes Dev.* 12:3357-3368.

Métivier, R., G. Penot, M. Hubner, G. Reid, H. Brand, M. Kos, and F. Gannon. 2003. Estrogen receptor-alpha directs ordered, cyclical, and combinatorial recruitment of cofactors on a natural target promoter. *Cell.* 115:751-763.

Métivier, R., G. Reid, and F. Gannon. 2006. Transcription in four dimensions: nuclear receptor-directed initiation of gene expression. *EMBO Rep.* 7:161-167.

Moras, D., and H. Gronemeyer. 1998. The nuclear receptor ligand-binding domain: structure and function. *Curr. Opin. Cell Biol.* 10:384-391.

Nolte, R.T., G.B. Wisely, S. Westin, J.E. Cobb, M.H. Lambert, R. Kurokawa, M.G. Rosenfeld, T.M. Willson, C.K. Glass, and M.V. Milburn. 1998. Ligand binding and co-activator assembly of the peroxisome proliferator-activated receptor-γ. *Nature.* 395:137-143.

Ochiai, I., K.-i. Matsuda, M. Nishi, H. Ozawa, and M. Kawata. 2004. Imaging Analysis of Subcellular Correlation of Androgen Receptor and Estrogen Receptor-α in Single Living Cells Using Green Fluorescent Protein Color Variants. *Mol Endocrinol.* 18:26-42.

Osborne, C.S., L. Chakalova, K.E. Brown, D. Carter, A. Horton, E. Debrand, B. Goyenechea, J.A. Mitchell, S. Lopes, W. Reik, and P. Fraser. 2004. Active genes dynamically colocalize to shared sites of ongoing transcription. *Nat Genet.* 36:1065-1071.

Phair, R.D., P. Scaffidi, C. Elbi, J. Vecerova, A. Dey, K. Ozato, D.T. Brown, G. Hager, M. Bustin, and T. Misteli. 2004. Global Nature of Dynamic Protein-Chromatin Interactions In Vivo: Three-Dimensional Genome Scanning and Dynamic Interaction Networks of Chromatin Proteins. *Mol Cell Biol.* 24:6393-6402.

Pratt, W.B., and D.O. Toft. 1997. Steroid Receptor Interactions with Heat Shock Protein and Immunophilin Chaperones. *Endocr Rev.* 18:306-360.

Prescott, J., and G.A. Coetzee. 2006. Molecular chaperones throughout the life cycle of the androgen receptor. *Cancer Lett.* 231:12-19.

Reid, G., M.R. Hubner, R. Metivier, H. Brand, S. Denger, D. Manu, J. Beaudouin, J. Ellenberg, and F. Gannon. 2003. Cyclic, Proteasome-Mediated Turnover of Unliganded and Liganded ER-α on Responsive Promoters Is an Integral Feature of Estrogen Signaling. *Mol Cell.* 11:695-707.

Rogerson, F.M., and P.J. Fuller. 2003. Interdomain interactions in the mineralocorticoid receptor. *Mol Cell Endocrinol.* 200:45-55.

Schaaf, M.J.M., L.J. Lewis-Tuffin, and J.A. Cidlowski. 2005. Ligand-selective targeting of the glucocorticoid receptor to nuclear subdomains is associated with decreased receptor mobility. *Mol Endocrinol.* 19:1501-1515.

Schaufele, F., X. Carbonell, M. Guerbadot, S. Borngraeber, M.S. Chapman, A.A.K. Ma, J.N. Miner, and M.I. Diamond. 2005. The structural basis of androgen receptor activation: Intramolecular and intermolecular amino-carboxy interactions. *Proc Natl Acad Sci U S A.* 102:9802-9807.

Shaffer, P.L., A. Jivan, D.E. Dollins, F. Claessens, and D.T. Gewirth. 2004. Structural basis of androgen receptor binding to selective androgen response elements. *Proc Natl Acad Sci U S A.* 101:4758-4763.

Shang, Y., X. Hu, J. DiRenzo, M.A. Lazar, and M. Brown. 2000. Cofactor Dynamics and Sufficiency in Estrogen Receptor-Regulated Transcription. *Cell.* 103:843-852.

Shiau, A.K., D. Barstad, P.M. Loria, L. Cheng, P.J. Kushner, D.A. Agard, and G.L. Greene. 1998. The Structural Basis of Estrogen Receptor/Coactivator Recognition and the Antagonism of This Interaction by Tamoxifen. *Cell.* 95:927-937.

Steketee, K., C.A. Berrevoets, H.J. Dubbink, P. Doesburg, R. Hersmus, A.O. Brinkmann, and J. Trapman. 2002. Amino acids 3-13 and amino acids in and flanking the 23 FxxLF 27 motif modulate the interaction between the N-terminal and ligand-binding domain of the androgen receptor. *Eur J Biochem.* 269:5780-5791.

Sunn, K.L., J.A. Eisman, E.M. Gardiner, and D.A. Jans. 2005. FRAP analysis of nucleocytoplasmic dynamics of the vitamin D receptor splice variant VDRB1: preferential targeting to nuclear speckles. *Biochem J.* 388:509-514.

Toumazou, C., J. Li, and J. Wong. 2007. Cofactor Restriction by Androgen Receptor N-terminal and C-terminal Interaction. *Mol Endocrinol.* (in press).

Van de Wijngaart, D.J., M.E. van Royen, R. Hersmus, A.C.W. Pike, A.B. Houtsmuller, G. Jenster, J. Trapman, and H.J. Dubbink. 2006. Novel FxxFF and FxxMF motifs in androgen receptor cofactors mediate high affinity and specific interactions with the ligand-binding domain. *J Biol Chem.* 281:19407-19416

Van Royen, M.E., S.M. Cunha, M.C. Brink, K.A. Mattern, A.L. Nigg, H.J. Dubbink, P.J. Verschure, J. Trapman, and A.B. Houtsmuller. 2007. Compartmentalization of androgen receptor protein-protein interactions in living cells. *J Cell Biol.* 177:63-72.

Van Steensel, B., M. Brink, K. Van der Meulen, E. Van Binnendijk, D. Wansink, L. De Jong, E. De Kloet, and R. Van Driel. 1995. Localization of the glucocorticoid receptor in discrete clusters in the cell nucleus. *J Cell Sci.* 108:3003-3011.

Wang, Q., W. Li, X.S. Liu, J.S. Carroll, O.A. Jänne, E.K. Keeton, A.M. Chinnaiyan, K.J. Pienta, and M. Brown. 2007. A hierarchical network of transcription factors governs androgen receptor-dependent prostate cancer growth. *Mol Cell.* 27:380-392.

Xu, J., and Q. Li. 2003. Review of the in Vivo Functions of the p160 Steroid Receptor Coactivator Family. *Mol Endocrinol.* 17:1681-1692.

Xu, M., and P.R. Cook. 2008. Similar active genes cluster in specialized transcription factories. *J Cell Biol.* 181:615-623.

Zhou, Z., M. Lane, J. Kemppainen, F. French, and E. Wilson. 1995. Specificity of ligand-dependent androgen receptor stabilization: receptor domain interactions influence ligand dissociation and receptor stability. *Mol Endocrinol.* 9:208-218.

Zhou, Z., M. Sar, J. Simental, M. Lane, and E. Wilson. 1994. A ligand-dependent bipartite nuclear targeting signal in the human androgen receptor. Requirement for the DNA-binding domain and modulation by NH2-terminal and carboxyl-terminal sequences. *J Biol Chem.* 269:13115-13123.

Summary & Samenvatting

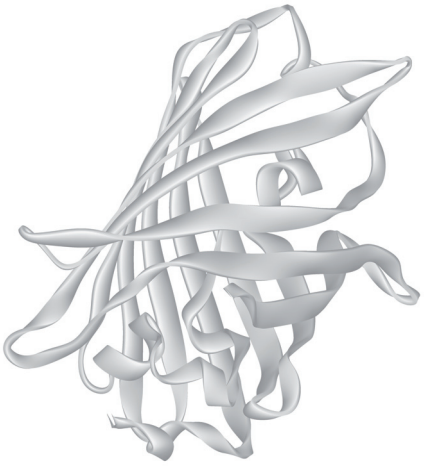

SUMMARY

Androgens are essential in the development and maintenance of the male phenotype. These steroids exert their function via the androgen receptor (AR), a ligand dependent transcription factor that also plays an important role in prostate cancer. AR activity is not only regulated by ligand binding but also by homodimerization and protein-protein interactions with cofactors. In this thesis the role of AR protein-protein interactions in living cells is investigated.

Chapter 1 describes an overview of AR structure and function. Like all nuclear receptors (NRs) the AR consists of three functional domains; the N-terminal domain (NTD), the centrally located DNA binding domain (DBD), and the C-terminal ligand binding domain (LBD). The role of these different functional domains and the two main AR domain interactions, the D-box interaction and the N/C interaction, in AR regulated transcription are introduced. Briefly, the roles of AR in androgen insensitivity syndromes (AIS) and prostate cancer are described.

The use of confocal microscopy and quantitative imaging techniques, like *fluorescence recovery after photobleaching* (FRAP) and *fluorescence resonance energy transfer* (FRET) enable the study of the dynamics and spatio-temporal distribution of AR protein-protein interactions in living cells. **Chapter 2 and 3** describe the background and application of the imaging techniques that were used throughout this thesis. In FRAP, fluorescently tagged proteins in a small, defined region within a larger volume are rapidly bleached. The kinetics of redistribution of the tagged proteins provides information on speed of diffusion and on stable or transient immobilisation. Previously, agonist bound AR was found to be highly mobile and was only transiently immobilized due to DNA binding. A powerful technique to study protein-protein interactions in living cells is FRET. In FRET, excitation of the donor fluorophore (e.g. CFP) results in a nonradiative energy transfer to the acceptor fluorophore (e.g. YFP) brought in close proximity by interaction between two fluorescently tagged proteins. Because these distances are in the range of protein sizes, FRET can be used to detect protein-protein interactions. Some approaches to measure FRET, like YFP/CFP ratio imaging and acceptor photobleaching FRET, have been described. In addition, to study specifically the mobility of interacting proteins a new technology, combining FRAP and FRET was developed.

One of the best-described sites of protein interactions of the AR is the cofactor groove in the AR LBD to which cofactors can bind via FxxLF-like motifs. In **Chapter 4** two novel FxxLF like motifs are identified in cofactors that interact with the AR LBD. Mutational analysis of the leucine at position +4 (L+4) in the FxxLF motifs of the AR NTD, and the cofactors ARA54 and ARA70 identified phenylalanine (F) and methionine (M) as potential substitutions for leucine without loss of specific interaction with the AR LBD, as was determined by yeast-two-hybrid and mammalian-one-hybrid screening approaches. Using similar approaches, but also by FRET analysis, it was shown that peptides and large fragments of two potential cofactors, Gelsolin and PAK6, specifically interact with the AR LBD via these FxxFF and FxxMF motifs.

The cofactor groove in the AR LBD not only enables the interaction with cofactors bearing FxxLF-like motifs but also facilitates an interaction with the FQNLF motif in the AR NTD, the N/C interaction. The potential competition between the AR FQNLF motif in the AR NTD and similar motifs in cofactors for interaction with the LBD raises questions regarding the role of the N/C interaction in orchestrating cofactor interactions. In **Chapter 5**, FRET analysis and a newly developed combined technique of FRET and FRAP showed that the AR N/C interactions predominantly occurs in mobile ARs and that the N/C interaction is lost when the AR is bound to DNA in a typical speckled distribution, allowing interactions with cofactors via FxxLF like motifs. The N/C interaction occurs in an intra- and intermolecular conformation. Previously it was shown that ligand-binding rapidly initiated intramolecular AR N/C interaction and that it was followed by a nuclear translocation of the AR. In **Chapter 6**, FRET analysis on cells coexpressing YFP- and CFP- single tagged ARs shows that this translocation is accompanied by a transition from intra- to intermolecular N/C interaction driven by the AR D-box dimerization. This AR dimerization is independent of DNA binding. The occurrence of both intra- and intermolecular N/C interaction strongly suggests the presence of both AR dimers and AR monomers. Both these AR configurations can activate transcription of genes driven by different types of androgen response elements (AREs). Together the studies described in **Chapter 5 and 6** elucidated the spatio-temporal relationship of the consecutive AR domain interactions in living cells.

In **Chapter 7**, a strong correlation is shown between the AR N/C interaction and transcriptional activity of wild type AR and AR mutants bound with different agonists and antagonists. This strong correlation possibly reflects the requirement of a functional cofactor groove in the AR LBD for transcriptional activity of the AR. Alternatively, the AR N/C interaction itself is important for the activation of transcription. The strong correlation between the AR N/C interaction and transcriptional activity qualifies the use of a FRET based assay on YFP- and CFP- double tagged ARs as a *bona fide* ligand induced AR activation assay.

In the general discussion in **Chapter 8**, the findings of the studies described in this thesis are implemented in a discussion on AR-DNA interactions and the spatio-temporal organization of AR protein-protein interactions. The findings in this thesis contribute to the understanding of the role of the different protein-protein interactions in AR function and may be useful for the development of new therapeutic strategies in prostate cancer.

SAMENVATTING

Androgenen zijn cruciaal voor de ontwikkeling en het in stand houden van de mannelijke geslachtskenmerken. Deze steroïden vervullen hun functie via de androgeenreceptor (AR), een ligand afhankelijke transcriptiefactor, die ook een belangrijke rol speelt bij de groei van prostaatkanker. De activiteit van de AR is niet alleen gereguleerd door binden van het ligand, maar ook door homodimerisatie en eiwit-eiwit interacties met cofactoren. In dit proefschrift wordt de rol van eiwit-eiwit interacties van de AR in levende cellen bestudeerd.

Hoofdstuk 1 geeft een overzicht van de structuur en functie van de AR. Zoals alle kernreceptoren (NRs) bestaat de AR uit drie functionele domeinen; het N-terminale domein (NTD), het centraal gelegen DNA bindend domein (DBD), en het C-terminaal gelegen ligand bindend domein (LBD). De rol van deze verschillende functionele domeinen en de twee belangrijkste AR eiwit interactiedomeinen, de D-box interactie en the N/C interactie, in door AR gereguleerde transcriptie worden geïntroduceerd. Daarnaast wordt kort de rol van de AR in androgeen ongevoeligheidssyndromen (AIS) en prostaatkanker beschreven.

Het gebruik van confocale microscopie en kwantitatieve beeldanalyse technieken, zoals *fluorescence recovery after photobleaching* (FRAP) en *fluorescence resonance energy transfer* (FRET) maken het bestuderen van de dynamiek en in tijd en in plaats verdeling van AR eiwit-eiwit interacties in levende cellen mogelijk. De **Hoofdstukken 2 en 3** beschrijven de achtergrond en toepassing van de microscopische technieken die werden gebruik in dit proefschrift. In FRAP worden de fluorescerende labels van eiwitten, in een klein gedefinieerd gebied binnen een groter volume, snel gebleekt. De kinetiek van de herverdeling van de gelabelde eiwitten verschaft informatie over diffusiesnelheid en over stabiele en tijdelijke immobilisatie. Eerdere studies lieten zien dat ARs, die geactiveerd zijn door binden van een agonist, erg mobiel zijn en slechts kort geïmmobiliseerd worden door binden aan DNA. Een krachtige techniek voor het bestuderen van eiwit-eiwit interacties is FRET. In FRET, excitatie van de donor-fluorofoor (b.v. CFP) resulteert in een stralingsvrije energie-overdracht naar de acceptor-fluorofoor (b.v. YFP), die in elkaars nabijheid zijn gebracht door een interactie tussen de twee gelabelde eiwitten. Omdat de afstanden tussen donor- en acceptor-fluoroforen ongeveer even groot zijn als de grootte van eiwitten, kan FRET gebruikt worden om eiwit-eiwit interacties te detecteren. Enkele van de methoden om FRET te meten, zoals YFP/CFP *ratio imaging* en *acceptor photobleaching* FRET, zijn beschreven. Daarnaast is een nieuwe technologie ontwikkeld waarin FRAP en FRET werden gecombineerd, om specifiek de mobiliteit van interacterende eiwitten te bestuderen.

Een van de best beschreven gebieden van eiwit-eiwit interacties van de AR is de cofactor groef in de AR LBD, waaraan cofactoren kunnen binden via FxxLF-achtige motieven. In **Hoofdstuk 4** zijn twee nieuwe FxxLF-achtige motieven geïdentificeerd in cofactoren, die interacteren met de AR LBD. Mutatie-analyse van de leucine op positie +4 (L+4) in de FxxLF motieven van de AR NTD, en de cofactoren ARA54 en ARA70 en *yeast-two-hybrid* en *mamma-*

lian-one-hybrid screenings methodieken, identificeerden phenylalanine (F) en methionine (M) als mogelijke vervangingen voor leucine, zonder dat daarbij de specifieke interactie met de AR LBD verloren gaat. Door middel van een vergelijkbare aanpak, maar ook met FRET analyse, is aangetoond dat peptiden en grotere fragmenten van twee mogelijke cofactoren (Gelsolin en PAK6) specifiek met de AR LBD interacteren via deze FxxFF en FxxMF motieven.

De cofactor groef in de AR LBD maakt niet alleen de interactie met cofactoren met FxxLF-motieven mogelijk, maar faciliteert ook een interactie met het FQNLF motief in de AR NTD, de N/C interactie. De mogelijke competitie tussen het AR FQNLF motief in de AR NTD en vergelijkbare motieven in cofactoren voor interactie met de LBD roept vragen op over de rol van de N/C interactie in het orkestreren van interacties met cofactoren. In **Hoofdstuk 5** laten FRET analyse en een nieuw ontworpen gecombineerde methode van FRET en FRAP zien dat de AR N/C interactie voornamelijk voorkomt in de mobiele ARs en dat de N/C interactie verloren is gegaan als de AR aan DNA gebonden is in een typisch granulair patroon, waardoor interacties met cofactoren via FxxLF-achtige motieven worden toegestaan. De N/C interactie komt zowel in een intra- als in een intermoleculaire conformatie voor. Eerder was aangetoond dat binden van ligand snel de intramoleculaire AR N/C interactie initieert, gevolgd door een translocatie van de AR naar de kern. In **Hoofdstuk 6**, laat FRET analyse van cellen die een combinatie van met YFP of CFP gemerkte ARs tot expressie brengen zien dat deze translocatie samen gaat met een overgang van intra- naar intermoleculaire N/C interactie. Deze overgang wordt aangedreven door de AR D-box dimerisatie. Deze AR dimerisatie is onafhankelijk van DNA binding. Het bestaan van zowel intra- als intermoleculaire N/C interactie suggereert sterk de aanwezigheid van en AR dimeren en AR monomeren. Beide AR configuraties kunnen transcriptie activeren van genen die aangestuurd worden door verschillende typen van androgeen responsieve elementen (AREs). Tezamen geven de studies beschreven in **Hoofdstuk 5 en 6** de relatie in ruimte en tijd weer tussen de opvolgende interacties van AR domeinen in levende cellen.

In **hoofdstuk 7** wordt een sterke correlatie aangetoond tussen de AR N/C interactie en activering van transcriptie door wild type AR en AR mutanten gebonden met verschillende agonisten en antagonisten. Deze sterke correlatie reflecteert mogelijk de behoefte aan een functionele cofactor groef in de AR LBD voor transcriptie activiteit van de AR. Als alternatief kan de AR N/C interactie zelf mogelijk van direct belang zijn voor de activering van transcriptie. De sterke correlatie tussen de AR N/C interactie en activiteit kwalificeert het gebruik van een op FRET gebaseerde methode met YFP- en CFP- dubbel gelabelde ARs, als bonafide test voor ligand geïnduceerde AR activering.

In de algemene discussie in **Hoofdstuk 8**, zijn de bevinding van de studies in dit proefschrift opgenomen in een discussie over AR-DNA interacties en de organisatie van AR eiwit-eiwit interacties in ruimte en tijd. De bevindingen in dit proefschrift dragen bij aan het inzicht in de rollen van de verschillende eiwit-eiwit interacties in de functie van de AR en kunnen van belang zijn in de ontwikkeling van nieuwe therapeutische strategieën in de strijd tegen prostaatkanker.

List of abbreviations

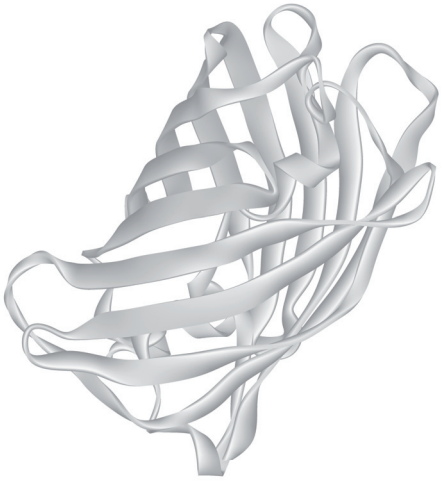

LIST OF ABBREVIATIONS:

aa	amino acid
abFRET	Acceptor photobleaching FRET
AF-1/2	Activation function 1/2
AIS	Androgen insensitivity syndrome
Ala	Alanine
AOTF	Acousto-Optic Tunable Filter
AR	Androgen receptor
ARA	Androgen receptor associated protein
ARE	Androgen response element
ATP	Adenosine triphosphate
BAF	BRM/BRG associated factor
BF-3	Binding Function-3
BRG	Brahma related factor
BRM	Brahma
Br-UTP	Broom-Uridine-tri-phosphate
CAIS	Complete androgen insensitivity syndrome
cAMP	Cyclic adenosine monophosphate
CARM1	Coactivator-associated arginine methyltransferase 1
CBP	CREB-binding protein
cdc37	Cell division cycle 37 homolog
cdk	Cyclin depandent kinase
CFP	Cyan fluorescent protein
CHD	Chromodomain
ChIP	Chromatin immuno precipitation
CLSM	Confocal Laser Scanning Microscope
CPA	Cyproterone acetate
CREB	cAMP response element binding protein
CTD	C-terminal domain
CTE	Carboxy-terminal extension
Da	Dalton
DBD	DNA-binding domain
D-box	Distal-box
DHT	5alfa-dihydrotestosterone
DNA	Deoxyribonucleic acid
E2	Estradiol
E6-AP	E6-associated protein
ECFP	Enhanced CFP

EGFP	Enhanced GFP
ER	Estrogen receptor-alfa/beta
ERCC	Excision repair cross complementation
ERR	Estrogen receptor related receptor
EYFP	Enhanced YFP
FKBP	FK506 binding protein
FLIP	Fluorescence loss in photobleaching
FRAP	Fluorescence recovery after photobleaching
FRET	Fluorescence resonance energy transfer
Gal4	Galactosidase 4
GFP	Green fluorescent protein
Gln	Glutamine
Gly	Glycine
GR	Glucocorticoid receptor
GRIP1	Glucocorticoid receptor interacting protein 1
GTF	General (or basal) transcription factors
HAT	Histone acetyltransferase
HDAC	Histone deacetylase
HMT	Histone methyl transferase
Hsp	Heat shock protein
iFRAP	Inverted FRAP
ISWI	Imitation switch
kDa	kiloDalton
LBD	Ligand-binding domain
LNCaP	Lymph node cancer of the prostate
LSD1	lysine-specific demethylase 1
LTR	long terminal repeat
Luc	Luciferase
MAGE11	Melanoma antigen gene protein 11
MAIS	Mild androgen insensitivity syndrome
MAPK	Mitogen activated protein kinase
Mdm2	Murine double minute
MED	Mediator
MMTV	Mouse mammary tumor virus
MR	Mineralocorticoid receptor
mRNA	Messenger RNA
MT	Microtubule
N/C interaction	N-terminal/C-terminal interaction
NcoA	Nuclear receptor coactivator

NCoR	Nuclear receptor corepressor
NER	Nucleotide excission repair
NER	Nucleotide Excision Repair
NLS	Nuclear localization signal
NR	Nuclear receptor
NTD	Amino (NH2)-terminal domain
NuRD	Nucleosome remodeling and deacetylation
Oct1	organic cation transporter 1
OH-F	OH-flutamide
P/CAF	p300/CBP-associated factor
p/CIP	p300/CBP interacting protein
PAIS	Partial androgen insensitivity syndrome
PAK6	P21(CDKN1A)-activated kinase 6
PB	Probasin
P-box	proximal box
PCa	Prostate cancer
PCAF	p300/CBP-associated factor
PCNA	Proliferating Cell Nuclear Antigen
PCR	Polymerase chain reaction
PGC1	PPAR-coactivator-1
PMRT1/5	protein arginine methyltransferase 1/5
pol II	RNA-polymerase II
PPAR	Peroxisome proliferator-activated receptor
PR	Progesterone receptor
PSA	Prostate specific antigen
R1881	Methyltrienolone, synthetic androgen
Rac3	RAS-related C3 botulinum substrate 3
RAD9	RADiation sensitivity abnormal/yeast RAD-related homolog 9
RAP250	Nuclear receptor-activating protein 250
RAR	Retinoic acid receptor
RIP140	Receptor-interacting protein 140
RNA	Ribonucleic acid
RNAP	RNA-polymerase
ROI	Region of interest
RSC	(Complex with capacity to) remodel the (-complex) structure of chromatin
RU486	Mifeprisone
RXR	Retinoic X receptor
SARM	Selective Androgen Receptor Modulator

SBMA	Spinal bulbar muscular atrophy
SCFP3A	Super CFP 3A
SIRT1 = Sirtuin 1	Silent mating type information regulation 2 homolog 1
SMRT	Silencing mediator of retinoid and thyroid receptors
SNF	Sucrose non-fermenting
SR	Steroid receptor
SRC	Steroid receptor coactivator
SRE	Steroid response element
STAT	Signal transducers and activators of transcription
SUMO	Small Ubiquitin-like Modifier
SWI	Switch
T	Testosterone
TAF	TBP associated factor
TAU	Transactivation unit
TBP	TATA-box binding protein
TF	Transcription factor (as in TFIIH)
TIF2	Transcription intermediary factor 2
Tip60	Tat interactive protein-60
TMPRSS2	Transmembrane protease, serine 2
TR	Thyroid hormone receptor
TRAM1	Translocation Associated Membrane Protein 1
TRAP, as in TRAP220	Thyroid Hormone Receptor-Associated Protein
TRBP	Transactivation-Responsive RNA-Binding Protein
TRF1/2	TTAGGG repeat binding factor 1/2
Ubc9	Ubiquitin-like protein SUMO-1 conjugating enzyme
VCaP	Vertebral-Cancer of the Prostate
VDR	Vitamin D receptor
XP	Xeroderma Pigmentosum (as in XPA)
YFP	Yellow Fluorescent Protein

Curriculum Vitae

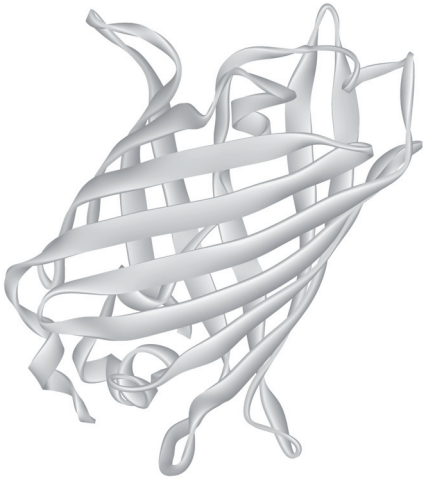

CURRICULUM VITAE

Martin E. van Royen was born on the 24th of September 1971 in Utrecht. After secondary school (M.A.V.O.) he started his study on Chemistry at the secondary vocational school (M.L.O.) in Utrecht (Dr. Ir. W. L. Ghijsen Institute). After two years he changed his study to Technical Microbiology at the Reynevelt College in Delft of which he received his diploma in 1993. After obtaining his propaedeutics on Biochemistry at the professional school (H.L.O.) in Delft (Hogeschool Rotterdam & Omstreken) in 1995 he studied Molecular Biology at Leiden University. In 1998 he started his first of two graduation projects entitled 'Chromosomal Aberrations in Chondrosarcoma' at the department of Pathology at the Leiden University Medical Center (L.U.M.C.) under supervision of Prof. dr. P.C.W. Hogendoorn and Dr. J.V.M.G. Bovée. His second graduation project in 1999 was performed at the Department of Biochemistry and Molecular Biology of the University of Barcelona under the supervision of Prof. dr. J.M. Argilés on Cancer induced Cachexia. Specializing in Medical Biology he graduated in Biology in 2001. In 2002 he started his PhD project on Protein-protein Interactions of the Androgen Receptor in Living Cells at the Department of Pathology (Josephine Nefkens Institute) of the Erasmus MC at the Erasmus University Rotterdam, under supervision of Prof. dr. J. Trapman and Dr. A.B. Houtmuller. Currently, Martin focuses on chromatin in nuclear receptor induced transcription, in addition he is studying the effects of DNA damage on AR regulated transcription, under supervision of Dr. A. B. Houtsmuller in collaboration with Prof. dr. R. Kanaar.

LIST OF PUBLICATIONS:

Van Royen ME, Van de Wijngaart DJ, Cunha SM, Trapman J and Houtsmuller AB. A FRET-based assay to study ligand induced androgen receptor activation., *manuscript in preparation*.

Van Royen ME, Houtsmuller AB, Trapman J. A two-step model for androgen receptor dimerization in living cells., *manuscript in preparation*.

Elfferich P, Juniarto Z, Dubbink HJ, **van Royen ME**, Molier M, Hoogerbrugge J, Houtsmuller AB, Trapman J, Drop SLS, Faradz SMH, Brüggenwirth H and Brinkmann AO. Functional analysis of novel androgen receptor mutations in a unique cohort of Indonesian DSD patients., s*ubmitted for publication*.

Van Royen ME, Dinant C, Farla P, Trapman J, and Houtsmuller AB. FRAP and FRET methods to study nuclear receptors in living cells. in "*Nuclear Receptor Superfamily*" (McEwan, IJ., ed.), Meth Mol Biol, 2009. Vol. 505, Humana Press / Springer, Totowa, *in press*.

Van Royen ME, Farla P, Mattern KA, Geverts B, Trapman J., and Houtsmuller AB. FRAP to study nuclear protein dynamics in living cells. in "*The Nucleus, Volume 2: Chromatin, Transcription, Envelope, Proteins, Dynamics, and Imaging*" (Hancock, R., ed.), Meth Mol Biol, 2009. Vol. 464, Humana Press / Springer, Totowa. 363-385.

Wong HY, Hoogerbrugge JW, Pang KL, van Leeuwen M, **van Royen ME**, Molier M, Berrevoets CA, Dooijes D, Dubbink HJ, van de Wijngaart DJ, Wolffenbuttel KP, Trapman J, Kleijer WJ, Drop SLS, Grootegoed JA, Brinkmann AO. A novel mutation F826L in the human androgen receptor results in increased NH2-/COOH-terminal domain interaction and TIF2 co-activation.Mol Cell Endocrinol, 2008; 292(1-2):69-78.

Dinant C, **van Royen ME**, Vermeulen W, and Houtsmuller AB, Fluorescence resonance energy transfer of GFP and YFP by spectral imaging and quantitative acceptor photobleaching. J Microscopy, 2008; 231(Pt 1):97-104.

Smal I, Meijering E, Draegestein K, Galjart N, Grigoriev I, Akhmanova A, **van Royen ME**, Houtsmuller AB, Niessen W. Multiple object tracking in molecular bioimaging by Rao-Blackwellized marginal particle filtering. Med Image Anal. 2008, *in press*

Van Royen ME, Cunha SM, Brink MC, Mattern KA, Nigg AL, Dubbink HJ, Verschure PJ, Trapman J, Houtsmuller AB. Compartmentalization of androgen receptor protein-protein interactions in living cells. J Cell Biol. 2007; 177(1):63-72.

Van de Wijngaart DJ, **van Royen ME**, Hersmus R, Pike AC, Houtsmuller AB, Jenster G, Trapman J, Dubbink HJ. Novel FXXFF and FXXMF motifs in androgen receptor cofactors mediate high affinity and specific interactions with the ligand-binding domain. J Biol Chem. 2006; 281(28):19407-19416.

Carbó N, Busquets S, **van Royen M**, Alvarez B, López-Soriano FJ, Argilés JM. TNF-alpha is involved in activating DNA fragmentation in skeletal muscle. Br J Cancer. 2002; 86(6):1012-1016.

Busquets S, Alvarez B, **Van Royen M**, Figueras MT, López-Soriano FJ, Argilés JM. Increased uncoupling protein-2 gene expression in brain of lipopolysaccharide-injected mice: role of tumour necrosis factor-alpha? Biochim Biophys Acta. 2001; 1499(3):249-256.

Van Royen M, Carbó N, Busquets S, Alvarez B, Quinn LS, López-Soriano FJ, Argilés JM. DNA fragmentation occurs in skeletal muscle during tumor growth: A link with cancer cachexia? Biochem Biophys Res Commun. 2000; 270(2):533-537.

Argilés JM, Alvarez B, Carbó N, Busquets S, **Van Royen M**, López-Soriano FJ. The divergent effects of tumour necrosis factor-alpha on skeletal muscle: implications in wasting. Eur Cytokine Netw. 2000; 11(4):552-559.

Bovée JV, **van Royen M**, Bardoel AF, Rosenberg C, Cornelisse CJ, Cleton-Jansen AM, Hogendoorn PC. Near-haploidy and subsequent polyploidization characterize the progression of peripheral chondrosarcoma. Am J Pathol. 2000; 157(5):1587-1595.

Busquets S, Alvarez B, **van Royen M**, Carbó N, López-Soriano FJ, Argilés JM. Lack of effect of the cytokine suppressive agent FR167653 on tumour growth and cachexia in rats bearing the Yoshida AH-130 ascites hepatoma. Cancer Lett. 2000 Aug 31;157(1):99-103.

DANKWOORD

Nou, dit zijn ze dan,....de laatste woorden van dit proefschrift. Dit is het moment om even stil te staan bij het feit dat je een promotieonderzoek niet alleen doet. Het is dan ook een goed gebruik om kort de mensen te bedanken die op enigerlei wijze zijn betrokken bij dit werk. Het meest in het oog springend zijn mijn promotor en copromotor. Jan en Adriaan, als mijn begeleiders waren jullie beiden nauw betrokken bij dit werk en, ondanks dat jullie soms op verschillende koers lagen (of misschien wel juist omdat), hebben jullie zeker een grote rol gespeeld in de vernieuwende inzichten die dit werk hebben opgeleverd.

Adriaan, wij hebben vele discussies gevoerd waarbij we het niet altijd eens waren, maar juist dat bracht ons vaak net die stap verder. Jouw enthousiasme, inzichten in dynamiek van moleculaire processen en soms oneindig optimisme hebben onder andere geleid tot een mooi artikel, beschreven in hoofdstuk 6, waarbij ik een door jouw bedachte techniek gebruikt heb voor het bestuderen van de mobiliteit van interacterende eiwitten. Bedankt dat ik gebruik heb mogen maken van jouw ideeën. Ik hoop daar nog even mee door te kunnen gaan.

Jan, je hebt mij vaak met beide benen op de grond gezet. Jouw zorgvuldigheid en kennis op het gebied van de androgeenreceptor hebben vaak geleid tot het doen van de juiste experimenten en het verkrijgen van nieuwe inzichten in de werkingsmechanismen van de receptor. In het onderzoek beschreven in hoofdstuk 7 heeft dit geleid tot een mooi model van opvolgende androgeenreceptor domein interacties, dat misschien met nog wat aanvullende experimenten nogmaals kan leiden tot een mooi artikel. Laten we het proberen. De laatste maanden heb je me veel geholpen met het schrijven van dit proefschrift, al ging dat niet altijd gemakkelijk. Ik wil je bedanken voor je hulp en hoop dat je er snel weer helemaal bovenop komt.

De mensen van de Houtsmuller onderzoeksgroep; Sonia, Bart, Petra (de R.) en Martijn en Hedy, maar ook de mensen die al weer vertrokken zijn; Eddy, Renate, Karin (M), Maartje, Pascal en Chris. Bedankt voor jullie hulp en gezelschap in de afgelopen jaren. Shehu, P.O. and Giri, thanks for your help and company. Helaas zijn de werkbesprekingen en (misschien wel erger) de donderdagmiddagborrels met de groep in verval geraakt, laten we die draad maar weer eens oppakken. Pascal, wij waren het niet altijd eens en onze samenwerking is niet echt van de grond gekomen, maar ik realiseer me zeker dat jouw initiërende werk het mij mogelijk gemaakt heeft om de extra stappen te zetten in het onderzoek. Bedankt daarvoor. Sonia, Petra en Bart, bedankt voor jullie huidige samenwerking aan de visuele kant van het androgeenreceptor onderzoek. Ik geloof zeker dat onze samenwerking nog tot mooie bevindingen kan leiden.

Dit werk zou niet mogelijk geweest zijn zonder goed functionerende microscopen. In de loop der jaren zijn we nog al wat problemen tegengekomen. Gelukkig stonden vanuit het OIC Alex en Gert altijd klaar om te helpen achterhalen waar de fouten zaten en hadden ze het telefoonnummer van Zeiss onder de sneltoets zitten. En al hebben die problemen bij elkaar

veel tijd gekost, ze hebben ook zeker bijgedragen aan mijn kennis van de ins en outs van de confocale microscoop. Ik wil jullie nogmaals bedanken voor de hulp bij het oplossen van de problemen met de microscoop en bij het opzetten van nieuwe experimenten.

De tweede groep waar ik onderdeel van uit gemaakt heb, is het Trapman-lab. Hetty, Karin (H.), Angelique, Xiaoqian, Binha, Joost, Delila, Remko, Erik Jan, Dennis, Michel, Hanneke, Petra (van D.), Wendy, Anke, Ellen en Carola, bedankt voor jullie gastvrijheid en de leuke werksfeer op het lab. Toen ik bij jullie begon heeft Remko me ingewerkt op het lab. Na een paar weken stoomcursus kon ik het wel alleen,.....dacht ik. Die AIO's ook altijd..... Bedankt dat ik jou en ook Hetty telkens weer mocht gebruiken als vraagbaak. Hetty, de kaartjespost heeft mijn verhuizing naar een andere kamer niet overleefd. Ik mis onze 'steuntjes in de rug' wel een beetje. Erik Jan, wij hebben vaak gesproken over eiwit-eiwit interacties en de androgeenreceptor structuur. Inmiddels werk je niet meer aan de androgeenreceptor, maar gelukkig besloot je in de buurt te blijven waardoor ik je nog regelmatig op kan zoeken …….met weer een volgende vraag. Karin, jij besloot je plek als analist in te ruilen voor een AIO positie, en zeker niet zonder succes. Maar ook in jouw geval, die AIO's ook altijd..... Nu sta jij ook op het punt te promoveren. Inmiddels ben je de grote plas overgestoken. Je hebt groot gelijk, het lijkt me een mooi avontuur waar je nooit slechter van zal worden. Alvast succes met de laatste fase van je promotie en met je nieuwe werk in Toronto. Dennis en Michel, ik hoop dat onze huidige samenwerking nog zal leiden tot mooie resultaten. In ieder geval alvast bedankt voor jullie hulp in deze en eerdere experimenten. Dennis, ook voor jou zit het er bijna op. Ook jij succes met het afronden van je proefschrift. Geen stress (of in ieder geval niet te veel), het komt goed. Ik ben blij dat jij en Robin bereid zijn mij bij te staan bij in de laatste fase van mijn promotie. Bedankt voor jullie hulp als paranimfen.

Natuurlijk wil ik ook de mensen van buiten onze eigen groepen waarmee ik heb samengewerkt bedanken. Maartje en Pernette, bedankt voor jullie hulp bij de *BrUTP incorporation* experimenten zoals beschreven in hoofdstuk 5. En Hao Yun, Albert, Peter, Ihor, en Eric, bedankt voor het mij betrekken bij jullie (aanstaande) publicaties.

Natuurlijk bestaat de afdeling uit meer dan deze twee groepen, maar het is ondoenlijk hier ieder persoonlijk te bedanken. Ik heb het de afgelopen jaren erg naar mijn zin gehad op de 3e verdieping van het JNI en hopelijk zijn jullie voorlopig nog niet van mij af. Angelique (van R.), na jouw vertrek een paar weken geleden is het kweken zo mogelijk nog saaier geworden. Zal ik niet een paar cellijnen voor je uitzetten? En Flip, wanneer ga je nou eens inzien dat telkens mazzelen in de laatste minuten echt niet iets is om trots op te zijn?

Het werk heeft niet altijd alleen maar bestaan uit experimenten. Via de AIO-commissie van de Molecular Medicine Postgraduate School ben ik o.a. betrokken geweest bij de organisatie van de Biomedical Research Technique cursussen en de 2004 editie van de jaarlijkse Molecular Medicine dag. Ik wil graag Frank en Joris alsmede alle leden van de AIO-commissie bedanken voor hun samenwerking. Elk jaar lijken de cursussen wel een groter succes te worden.

De laatste maanden hebben naast dit proefschrift, ook in het teken gestaan van de organisatie van Androgens 2008. Vele uren voorbereiding hebben geresulteerd in een zeer succesvol congres. Jan, Albert, Adriaan, Guido, Ellen, Margot, Dennis en Theo, bedankt voor de mooie ervaring van het organiseren van een internationaal congres. En al heb ik een paar keer geroepen dat ik dit nooit meer zou doen, ik ben blij en trots dat ik heb mogen meewerken aan dit succes.

Bij promotie onderzoek is het niet te voorkomen dat je werk mee naar huis neemt. In de hele periode, maar ook zeker deze laatste paar maanden hebben ouders, schoonouders, broer, zussen en vrienden, meegeleefd met dit proces. Bedankt voor jullie interesse en betrokkenheid. Pa en ma, bedankt voor de kansen die jullie mij hebben gegeven. Zonder jullie steun zou dit nooit mogelijk geweest zijn. Heel erg bedankt dat jullie er in zijn blijven geloven. En inderdaad, ...het gaat lukken, …stap voor stap. En natuurlijk Helen en Kim. Lieve Kim, jouw tederheid, plezier en enthousiasme maken het soms erg moeilijk om weer luiers te gaan verdienen, maar maken het ook extra fijn om weer thuis te komen. Helen, jouw geduld is vaak flink op de proef gesteld. Ik weet dat werk vaak voorrang kreeg. Dank je wel voor je begrip en de steun die je me gegeven hebt. Zonder jou had ik het niet kunnen afmaken. Ik wil jullie beiden bedanken voor het thuis dat jullie me geven. Ik hou van jullie.

Allen bedankt!

Martin